

AFFDL-TR-76-6

(12)
B-5.

ADA 029345

DESIGN AND ANALYSIS OF WINGLETS FOR MILITARY AIRCRAFT

*BOEING COMMERCIAL AIRPLANE COMPANY
P.O. BOX 3707
SEATTLE, WASHINGTON 98124*

FEBRUARY 1976

DDC
RECEIVED
SEP 8 1976
REGULATED
B

TECHNICAL REPORT AFFDL-TR-76-6
FINAL REPORT FOR PERIOD JUNE 1975 - NOVEMBER 1975

Approved for public release; distribution unlimited

Prepared for
AIR FORCE FLIGHT DYNAMICS LABORATORY
AIR FORCE WRIGHT AERONAUTICAL LABORATORIES
AIR FORCE SYSTEMS COMMAND
WRIGHT-PATTERSON AIR FORCE BASE, OHIO 45433

NOTICE

When Government drawings, specifications, or other data are used for any purpose other than in connection with a definitely related Government procurement operation, the United States Government thereby incurs no responsibility nor any obligation whatsoever; and the fact that the government may have formulated, furnished, or in any way supplied the said drawings, specifications, or other data, is not to be regarded by implication or otherwise as in any manner licensing the holder or any other person or corporation, or conveying any rights or permission to manufacture, use, or sell any patented invention that may in any way be related thereto.

This report has been reviewed by the Information Office (OI) and is releasable to the National Technical Information Service (NTIS). At NTIS, it will be available to the general public, including foreign nations.

This technical report has been reviewed and is approved for publication.

George W. Loptien
George W. Loptien
Project Engineer

Alfred C. Draper
Alfred C. Draper
Assistant for Research and Technology
Aeromechanics Division

Copies of this report should not be returned unless return is required by security considerations, contractual obligations, or notice on a specific document.

AIR FORCE - 27 AUGUST 76 - 125

ACCESSION for	
NTIS	White Section <input checked="" type="checkbox"/>
GCC	Buff Section <input type="checkbox"/>
UNANNOUNCED	<input type="checkbox"/>
JUSTIFICATION
BY
DISTRIBUTION/AVAILABILITY CODES	
Dist.	Avail. or Sec. Status
A	

Unclassified

SECURITY CLASSIFICATION OF THIS PAGE (When Data Entered)

19 REPORT DOCUMENTATION PAGE		READ INSTRUCTIONS BEFORE COMPLETING FORM	
1. REPORT NUMBER AFFDL TR-76-6	2. GOVT ACCESSION NO.	3. RECIPIENT'S CATALOG NUMBER	
4. TITLE (and Subtitle) DESIGN AND ANALYSIS OF WINGLETS FOR MILITARY AIRCRAFT		5. TYPE OF REPORT & PERIOD COVERED Final 16 June 1975 to 25 Nov 1975	
7. AUTHOR(s) K. K. Ishimitsu, N. VanDevender, R. Dodson, etc. P. C. Brault B. A. Byers		14. PERFORMING ORG. REPORT NUMBER D6-41799	8. CONTRACT OR GRANT NUMBER(s) F33615-75-C-3123
9. PERFORMING ORGANIZATION NAME AND ADDRESS Boeing Commercial Airplane Company P.O. Box 3707 Seattle, Washington 98124		10. PROGRAM ELEMENT, PROJECT, TASK AREA & WORK UNIT NUMBERS Program Element 62201F Project 1431, Task 143101 Work Unit 14310125	
11. CONTROLLING OFFICE NAME AND ADDRESS Aeromechanics Division (FX) Air Force Flight Dynamics Laboratory Wright-Patterson AFB, Ohio 45433		12. REPORT DATE 3 Feb 1976	13. NUMBER OF PAGES 191
14. MONITORING AGENCY NAME & ADDRESS (if different from Controlling Office)		15. SECURITY CLASS. (of this report) Unclassified	
16. DISTRIBUTION STATEMENT (of this Report) Approved for public release Distribution Unlimited		15a. DECLASSIFICATION/DOWNGRADING SCHEDULE	
17. DISTRIBUTION STATEMENT (of the abstract entered in Block 20, if different from Report)			
18. SUPPLEMENTARY NOTES			
19. KEY WORDS (Continue on reverse side if necessary and identify by block number) KC-135, C-141, Winglets, Tip Extensions, Induced Drag, Drag Reduciton, Fuel Savings, Wing-Root Bending Moment, Advanced Composites Design, Advanced Metallic Design			
20. ABSTRACT (Continue on reverse side if necessary and identify by block number) A study of the design and analysis of winglets for Military Aircraft has been completed. The program consisted of investigating analytically winglet concepts for application to the KC-135 and C-141, designing and building winglets for an 0.035 and 0.070 scale model KC-135, and conducting a structural feasibility investigation of the winglet installation on the KC-135.			

DD FORM 1 JAN 73 1473 EDITION OF 1 NOV 65 IS OBSOLETE

Unclassified
SECURITY CLASSIFICATION OF THIS PAGE (When Data Entered)

390145

JB

Unclassified

SECURITY CLASSIFICATION OF THIS PAGE(When Data Entered)

20. Continued

The analysis of the winglets showed a 14% reduction in induced drag for the KC-135 and a 11% reduction for the C-141. The structural design study of the KC-135A winglet installation estimated a 592 lb weight increase. An 8.4% improvement was estimated in $M(L/D)_{MAX}$ and an 8.1% improvement in range factor for the KC-135A. ^{sub}

An 0.070 scale half span KC-135 wind tunnel model has been tested in the NASA 8 Ft Transonic Tunnel. Preliminary unpublished test data have substantiated the analytical procedures used by The Boeing Company to determine the aerodynamic characteristics and performance benefits from winglets on the KC-135 aircraft.

Unclassified

SECURITY CLASSIFICATION OF THIS PAGE(When Data Entered)

FOREWORD

This is the final report on the design and analysis of winglets for Military Aircraft. This report has been assigned Boeing document number D6-41799 for internal use and covers work performed by the Boeing Commercial Airplane Company, Seattle, Washington and Boeing Wichita Division, Wichita, Kansas. This work was performed under the technical direction of George W. Loptien, Air Force Flight Dynamics Laboratory/FXS, Air Force Systems Command, Wright-Patterson Air Force Base, Ohio.

Mr. A. L. daCosta was the Program Manager and K. K. Ishimitsu was the Technical Leader. Others supporting the effort were N. VanDevender, R. O. Dodson, P. C. Brault, B. A. Byers, R. P. Johnson, R. P. Syring, M. P. Schaefer, D. R. Endorf, C. McGinnis, N. E. Conley, and M. Grant.

The work was performed under contract F33615-75-C-3123.

CONTENTS

	Page
I INTRODUCTION	1
II ANALYSIS OF WINGLETS	3
A Aerodynamic Improvement of KC-135 and C-141 with Winglets	3
B Structural Load Analysis	5
C Stress Analysis	5
D Weight Estimates	6
E Flutter Analysis	7
F Structural Design and Layout (Conventional)	9
1 Outboard Wing Modification	10
2 Winglet Assembly	11
3 Winglet Installation	12
G Advanced Composite Winglet Structural Design	13
1 Design/Analysis	13
2 Fabrication Concept	14
H Advanced Metallic Winglet Structural Design	15
1 Design/Analysis	15
2 Fabrication Concept	16
I Cost and Weight Comparisons of Winglet Structural Design	16
J Airplane Performance Estimation	17
III WINGLET PARAMETER STUDY	19
A Winglet Chordwise Location Study	20
B Winglet Sweep Study	20
C Winglet Taper Ratio Study	21
D Winglet Area Study	21
E Winglet Length Study	22
F Winglet Cant Study-Constant Span	23
G Winglet Cant Study-Variable Span	24
IV EQUAL AREA TIP EXTENSION	26
A Geometry Variations	26
B Aerodynamic Performance	26
C Comparison with Winglets	26
V DESIGN OF WINGLET FOR THE KC/135 AIRCRAFT	29
A Final Design	30
B Analysis of Design	31
VI CONCLUSIONS	32

CONTENTS (Concluded)

	Page
APPENDIX A-Computer Programs Used for Analysis and Design of Winglets	186
APPENDIX B-Material Costs	190
REFERENCES	191

ILLUSTRATIONS

No.	Page
1 Typical Winglet Application	35
2 Wind Tunnel Model Winglet Design	36
3 KC-135 Winglet Planform	37
4 Effect of 0.135 b/2 Winglets on KC-135	38
5 C-141 Winglet Planform	41
6 Effect of 0.135 b/2 Winglet on C-141	42
7 Symmetric Maneuver Conditions	45
8 Overyaw Conditions	46
9 KC-135A Winglet Load Reference Axis	47
10 Ultimate Chordwise Pressure Distribution for Symmetric Flight Conditions	48
11 Ultimate Chordwise Pressure Distribution for Unsymmetric Flight Conditions	49
12 Winglet Geometry	50
13 Nastran Model, Winglet to Wingtip Detail	51
14 Flutter Analysis Conditions	52
15 Nominal KC-135A Winglet	53
16 Vibration Model	54
17 Aerodynamic Panels in the X-Y and Y-Z Planes	55
18 Symmetric Baseline	56
19 Symmetric With Nominal Winglet	57
20 Antisymmetric Baseline	58
21 Antisymmetric With Nominal Winglet	59
22 Antisymmetric With 300 Lb Winglet	60
23 Antisymmetric Flutter Boundary Versus Winglet Weight	61
24 Antisymmetric Flutter Boundary Versus Winglet c.g. Position	62
25 Antisymmetric Flutter Boundary Versus Winglet Frequency	63
26 Centerline Diagram-Winglet, KC-135A Airplane (Preliminary)	65
27 Winglet Installation KC-135A Airplane (Preliminary)	67
28 Wing Modification-Winglet Provisions (Preliminary)	69
29 Wing Modification-Winglet Provisions (Preliminary)	71
30 Wing Modification-Winglet Provisions (Preliminary)	73
31 Winglet Assembly Drawing-KC-135A Airplane (Preliminary)	75
32 Winglet Assembly-KC-135A Airplane (Advanced Composite Structural Concept)	77
33 Winglet Attachment-KC-135A Airplane (Advanced Composite Structural Concept)	79
34 Preliminary Torsional Stiffness Distribution of Winglet Designs	81
35 Preliminary Maximum Bending Stress of Winglet Concepts	82
36 Winglet Assembly KC-135A Airplane (Advanced Metallic Structural Concept)	83
37 Winglet Attachment KC-135A Airplane (Advanced Metallic Structural Concept)	85

ILLUSTRATIONS (Concluded)

No.	Page
38	Effect of Winglets on Range Performance (Ferry Mission) 87
39	Winglet Parameters Analyzed on KC-135A 88
40	Baseline Winglet Planform for the First 5 Parameters Studies 89
41	Winglets for Chordwise Location Study 90
42	Effect of Winglet Chordwise Location 91
43	Winglets for Sweep Study 96
44	Effect of Winglet Sweep 97
45	Winglets for Taper Ratio Study 102
46	Effect of Winglet Taper Ratio 103
47	Winglets for Area Study 108
48	Effect on Winglet Area 109
49	Winglets for Length Study 114
50	Effect of Winglet Length 115
51	Winglet Length Study at 0° Cant, $C_{L_{config}} = 0.426$ 120
52	Winglets for Constant Span Cant Study 121
53	Effect of Winglet Cant 122
54	Winglet Cant Study with Constant Span, $C_{L_{config}} = 0.426$ 127
55	Winglets for Variable Span Cant Study 128
56	Effect of Winglet Cant 129
57	Winglet Cant Study With Variable Span, $C_{L_{config}} = 0.426$ 134
58	Equal Area Tip Extension Geometry Variations 135
59	Effect of Tip Extension 136
60	Comparison of Induced Drag and Wing-Root Bending Moment Increments Between Winglets and Tip Extensions 141
61	Comparison of Pitching Moment Increment Between Winglets and Tip Extensions 142
62	Upper and Lower Winglets Analyzed in TEA-230 143
63	TEA-230 Modeling of Winglet and Outboard Portion of Wing 144
64	Effect of Cant and Lower Winglet on Wing Pressure Distribution 146
65	Effect of Cant and Lower Winglet on Upper Winglet Pressure Distribution 147
66	Final Selected KC-135 Winglet Planform 148
67	Streamwise Airfoil Sections of Winglet Designed for KC-135 149
68	Twist Distribution of KC-135 Winglet 150
69	Outboard Wing Pressure Distributions on KC-135 With Designed Winglet Installed 151
70	Pressure Distributions on Winglet Designed for KC-135 Wing 156

TABLES

No.		Page
1	Summary of Winglet Effects on the KC-135 and C-141	162
2	Wing and Winglet Design Conditions	163
3	Ultimate Load Factors	164
4	KC-135A Winglet Spanwise Loads-Condition 1	164
	KC-135A Winglet Spanwise Loads-Condition 2	165
6	KC-135A Winglet Spanwise Combined Loads-Condition 3	166
7	KC-135A Winglet Spanwise Combined Loads-Condition 4	167
8	KC-135A Winglet Spanwise Combined Loads-Condition 5	168
9	KC-135A Winglet Spanwise Combined Loads-Condition 6	169
10	Wing-Root Bending Moments (Ultimate)	170
11	Wing Loads and Deflections-Condition 1	171
12	Wing Loads and Deflections-Condition 2	172
13	Wing Loads and Deflections-Condition 3	173
14	Winglet to Wingtip Loading	174
15	Model Constrained Reactions at W.S. 948.744	175
16	Model Nodal Deflections	176
17	Model Chord Loads and Stresses	177
18	Model Panel Maximum Shear Stresses and Shear Flows	178
19	Weight Summary	179
20	Weights Breakdown of Production Winglet Modification	180
21	Weights Breakdown of Prototype Winglet Modification	181
22	Fuel Condition	182
23	Analysis Configurations	182
24	Weight Comparison of Three (3) Winglet Design Concepts	183
25	Relative Cost of Winglet Design Concepts	183
26	KC-135A Performance Improvement for Installing Winglets	184
27	Summary of Equal Area Tip Extension Geometry Variations	184
28	Summary of Tip Extension to Winglet Performance Comparisons	185

NOMENCLATURE

b	Wing span
B.S.	Body station
C	Section chord length
C_{ave}	Average chord of the wing alone
\bar{C} , MAC	Mean aerodynamic chord
C_D	Drag coefficient
C_{D_i}	Induced drag coefficient
C_l	Section lift coefficient
C_L	Lift coefficient
$C_{M_{.25\bar{c}}}$	Pitching moment coefficient about the quarter chord of the mac
C_{m_x}	Rolling moment of the right half of the configuration
C_p	Pressure coefficient
c.g.	Center of gravity
D	Drag
h	Altitude
l	Winglet length
L	Lift
M	Mach number
$M_{.25\bar{c}}$	Pitching moment about quarter chord of mac
n	Load factor

P	Pressure
q	Dynamic pressure
S	Wing area
S _{REF}	Wing reference area
V _e	Equivalent airspeed
W	Weight of airplane
WBL	Wing buttock line
W.S.	Wing station
α_w	Wing angle of attack
β	Winglet incidence angle, toe in direction is positive direction
Δ	Increment
Λ	Winglet leading-edge sweep angle
η	Nondimensional spanwise location
ψ	Yaw angle
ϕ	Winglet cant angle, angle of winglet plane from X-Z with positive direction being clockwise as viewed from rear of airplane of the right-hand side
λ	Taper ratio

REFERENCE DIMENSIONS

Item	KC-135	C-141
Wing Span, b	130.7 Ft.	159.8 Ft.
Mean Aerodynamic Chord, \bar{c}	241.9 In.	266.5 In.
Wing Reference Area, S	2433 Ft. ²	3228 Ft. ²

SUMMARY

An investigation has been conducted to determine analytically the potential performance improvement of winglet for military aircraft. This investigation used a conventional design for the winglet structure. As a complementary study, an advanced composite and an advanced metallic design winglet structural concept was laid out. The costs and weights of these designs were estimated and compared to the conventional design.

The aerodynamic shape of the winglet was designed for the KC-135 and this design was then used to fabricate winglets for existing 0.035 and 0.070 scale wind tunnel models.

The conventional design winglets were estimated to provide a 8.4% improvement in the cruise $M(L/D)$, a net improvement in range factor of 8.1%, and an increase in OEW of 592 lb. reduced the range factor by 0.6%. The net effect of winglets on the ferry range of the KC-135A amounted to a 7.5% improvement.

The advanced metallic design winglet weighed 73% of the conventional design and cost 27% less to manufacture. The advanced composite winglet weighed 76% of the conventional design and cost 18% less to manufacture.

The winglets designed for the KC-135A and fabricated for the 0.035 and 0.070 scale wind tunnel model are aerodynamic surfaces which have a leading-edge sweep of 37° , a basic trapezoid with aspect ratio of 2.33 and taper ratio of 0.338 and a length of 106 in. or $0.135 b/2$. The winglet is blended into the wingtip with a leading-edge strake. The winglet planform is canted outboard 20° from the vertical.

The winglet has been cambered and twisted to provide the optimum induced drag configuration with low interference drag.

The C-141 was analyzed to determine the potential induced drag reduction due to winglets. For a 130 in. long ($0.135b/2$) winglet and at a representative cruise condition, $C_L = 0.55$ at $M_\infty = 0.76$, an induced drag reduction of 11% was estimated for the C-141 with winglets. This compares to a 14% reduction in induced drag for a KC-135 with winglets at a $C_L = 0.426$ and $M_\infty = 0.77$.

I INTRODUCTION

The recent escalation of fuel costs and the threat of future increases have quickly brought to the forefront the need to improve aircraft efficiency. Various ideas are being presented to improve aerodynamic and propulsion system efficiency and to lower structural weight through the use of composites. One aerodynamic concept which has recently been reviewed by Dr. Whitcomb at NASA-Langley is the use of winglets. Winglets are aerodynamic surfaces placed on a wing to reduce the induced drag. A typical application of a winglet is shown in figure 1. Dr. Whitcomb has demonstrated the aerodynamic improvement of these devices in the transonic wind tunnel. Subsequent analytical and experimental work at Boeing have shown that a 3% drag reduction can be achieved with winglets on the 747 at a typical cruise condition.

The primary effect of winglets is to reduce the induced drag. There are several other concomitant changes which affect the net drag improvement. First and most obvious, the profile drag of the winglet itself negates some of the induced drag reduction. Second, for most wing/winglet configurations the required airplane lift coefficient will be reached at a lower angle of attack than for the wing alone. As a result, the parasite drag of the wing is decreased. Third, the interference effect on drag due to the intersection of the wing and winglet is of concern. However, steps can be taken to minimize and/or eliminate this interference. These will be discussed later in the report, where thickness effects on the winglet design are presented.

The objective of this program was to analytically determine the potential performance improvements from winglets and to design and fabricate winglets for existing wind tunnel models. Recent investigations of winglets have given primary consideration to their effect on lift and drag. Little has been done to assess the total impact of winglets on the performance of a particular airplane. In this feasibility investigation an attempt was made to study the winglet structure, its effect on airplane weight, and its effect on flutter. The weight of the winglets themselves and their attachment structure to the wing will obviously cancel some of the aerodynamic benefit. In addition, both the local wing bending moments near the tip and the wing-root bending moment will increase. The wing weight will likely have to increase to carry these moments. With this impact on structures in mind, the root bending moment was monitored throughout the aerodynamic analysis portion of this study. Load distributions on the wing and winglet were provided to the structures group to determine the weight penalty. As a portion of the structures study, cost and weight comparisons were made of three (3) different winglet structural design concepts. These concepts were identified as the conventional, advanced composite, and advanced metallic designs. The aerodynamic study is comprised of three parts. Analytical investigations were first made on the KC-135 and C-141 to determine if winglets can provide a significant drag reduction. The winglets selected for these two analyses are based on a winglet designed for the 747.

A parameter study was then conducted on the KC-135 to determine the effects of winglet chordwise position, leading-edge sweep, taper ratio, area, length, and cant on drag. Induced drag reductions were obtained from a potential flow vortex-lattice program, and the winglet profile drag was estimated for a cruise flight condition.

Following the parameter study, one winglet was designed for subsequent wind tunnel testing on the KC-135, see figure 2. A three-dimensional, potential flow analysis with thickness was made on this final wing/winglet configuration to obtain detailed pressure data. The boundary-layer development was analyzed using two-dimensional methods on several spanwise strips of the winglet.

The performance improvement was estimated for the KC-135 with the final winglet configuration. The drag estimation of this configuration was made using the KC-135A flight test data as the base. The conventional structural concept, winglet weights estimation were used for this performance calculation. Several equal area wing-tip extensions were analyzed and their performance compared to winglets. This study was conducted to determine which wing-tip device, extensions or winglets, is more effective in improving airplane performance.

II ANALYSIS OF WINGLETS

To determine the potential performance improvement of winglets for military aircraft, a representative, multiengine, jet aircraft was selected for the application of winglets. The KC-135A was selected as this representative aircraft.

A representative winglet geometry was then selected in order to estimate the aerodynamic loads and a preliminary structural layout. Using the spanload changes measured in the wind tunnel for a similar winglet, the spanloads for the KC-135A were estimated. These loads and winglet geometry were used to determine the winglet structure, wing attachment structure, and the modification required to the KC-135A wing structure. A stress and flutter analysis was made of the KC-135A with the winglet. The weights of the winglet structure, attachment, and wing modifications were estimated.

With the estimated aerodynamic change and increase in operating empty weight (OEW), the performance improvement for the KC-135A with winglets was calculated.

In addition to this winglet study, the potential aerodynamic performance improvement due to the incorporation of winglets to the C-141 was determined analytically.

II.A AERODYNAMIC IMPROVEMENT OF KC-135 AND C-141 WITH WINGLETS

The first task of this study was to determine the potential aerodynamic improvement of the KC-135 and C-141 with typically configured winglets. The procedure followed was the same for each airplane. A cruise flight condition was selected and the corresponding lift coefficient calculated. The wing alone was analyzed in a vortex-lattice, digital computer program (appendix A) to obtain a baseline induced drag at this lift coefficient. A winglet of typical planform was then placed vertically at the wingtip, and an analysis was made to obtain the induced drag increment due to the winglet. Note that in this step the program optimized the winglet twist with the wing geometry fixed and at the lift coefficient of interest. The profile drag increment of the winglet was estimated at the full-scale cruise flight condition. Finally, the net drag reduction was calculated as the sum of the induced and parasite drag increments.

The winglets selected for the KC-135 and C-141 were based on previous Boeing experience in winglet design for the 747. Their sizing is also compatible with winglets previously tested by Dr. Whitcomb. Geometric parameters common to both the KC-135 and C-141 winglets are as follows: (1) the root chord is about 60% of the wing-tip chord; (2) the taper ratio is 0.338; (3) the leading-edge sweep is 37°, and (4) the height is 13.5% of wing semispan. In addition, the winglet is positioned chordwise so that the trailing edge of its root section is at the wing trailing edge.

The flight condition selected for the KC-135 was $M = 0.77$, $W = 270\,000$ lb., and $h = 30\,000$ ft.. The lift coefficient for this flight condition is 0.426. Figure 3 shows the KC-135 winglet planform. Its root and tip chords are 68 and 23 in., respectively, and it is 106 in. high.

Aerodynamic coefficients for the KC-135 baseline and the optimized wing/winglet configuration are presented in figures 4a-4c. With the winglet on, the desired lift coefficient was reached at 0.15° angle of attack less than with the winglet off. The pitching moment became more negative, as would be expected with the more highly loaded wingtip. This change would result in a higher trim drag penalty. The induced drag reduction at $C_L = 0.426$ is 11 drag counts, where one drag count equal $\Delta C_D = 0.0001$, nearly 14% of baseline induced drag. Note that this KC-135 winglet configuration is not the same as the final winglet design which is described in section V.A ; therefore, the estimated drag change does not agree with that which is shown. The estimated profile drag for two winglets at cruise is two drag counts and the estimated change in wing drag due to parasite and compressibility affects is 3.4 counts. The net drag reduction for the KC-135 with the winglets specified in this section is 12.4 counts and this is 5.1% of airplane drag.

Winglet effects on the C-141 were studied at a flight condition of $M = 0.756$, $W = 265\ 000$ lb., and $h = 41\ 000$ ft. The corresponding cruise lift coefficient is 0.55. Figure 5 shows the winglet planform selected for the C-141. The root and tip chords are 80 and 27 in., respectively and the winglet height is 130 in.

The results of the C-141 winglet study are shown in figures 6a-6c. A 0.15° angle of attack reduction at cruise lift coefficient is again evident with winglets. The change in pitching moment is about -0.01 , somewhat less than was observed for the KC-135. A 13.5 count reduction in induced drag was obtained at $C_L = 0.55$. This represents an 11% improvement over the baseline induced drag.

Note that the percent improvement is 3% below what was achieved for the KC-135, even though the cruise lift is considerably higher. This result is believed primarily due to the fact that the KC-135 wing has dihedral while the C-141 wing has anhedral. The benefit of an upper surface winglet is not as large for a wing with anhedral (C-141) as for a wing with dihedral (KC-135). For a C-141 winglet of given height, more aerodynamic improvement would be realized by putting the winglet on the lower surface. However, such a location would probably be impractical.

The estimated profile drag of the winglets is 2 counts and estimated change in wing drag due to parasite and compressibility effects is 4.4 counts. These drag changes plus the induced drag change result in a net drag reduction of 15.9 counts for the C-141 with winglets at its cruise condition. This is a 5.6% change in airplane drag.

A summary of the data obtained in this particular study is tabulated in table 1. The drag improvements are certainly significant enough to warrant a more detailed study of the total impact of winglets on airplane performance and stability and control.

II.B STRUCTURAL LOADS ANALYSIS (KC-135 ONLY)

Several design flight conditions were investigated for structural design purposes. The flight conditions analyzed are illustrated in figures 7 and 8 and listed in table 2. The symmetric maneuver conditions are presented in figure 7. Note that both the tanker and tanker/transport V-n flight envelopes are presented. The one corner of the KC-135A tanker/transport V-n diagram at $n = 2.5$ g's was analyzed to define any potential problems with this configuration. Conditions studied for critical wing loads and critical winglet loads are designated in the figure. Winglet over yaw design conditions are presented in figure 8. Note that condition no. 3 was analyzed at $n = 1.0$ g for the winglet design loads as opposed to $n = 2.0$ g for the wing design loads as shown in figure 7. Note also that at 250 kn the KC-135A powered rudder actuator is pressure limited. The hydraulic pressure is reduced from the nominal system pressure of 3,000 psi to 1,000 psi to reduce the authority at high speeds.

Wind tunnel data obtained for a 747 winglet design were utilized to determine the wing and winglet aerodynamic load distributions for the KC-135. For the antisymmetric overyaw condition no. 3, wind tunnel data did not exist at the extreme 14.4 deg. yaw angle so that the available data had to be extrapolated.

The winglet to wing attachment ultimate design load factor criteria are shown in table 3. These ultimate load factors are the load factors used in designing external store to wing attachments for inertia loads. The design load factor criteria are based on a linear extrapolation of the KC-135A nacelle load factors to account for positioning on the wingspan. The KC-135A nacelle ultimate load factors are also listed in table 3 for comparison purposes.

The KC-135A winglet reference system and sign convention used in the loads analysis is presented in figure 9 and the winglet spanwise ultimate loads for the six flight conditions studied are presented in tables 4-9. Conditions no. 1 through 4 were analyzed to obtain the ultimate chordwise pressure distributions and are presented in figures 10 and 11.

Ultimate wing-root bending moments are compared for the basic airplane and the airplane with winglets in table 10 for the more critical higher g flight conditions. The table shows the highest increase in ultimate wing-root bending moment was about 2% for condition no. 1. The loads and wing deflections along the wingspan for the same three flight conditions are presented in tables 11-13 for the basic airplane and the airplane with winglets. Note with the winglets on, the wingtip deflection is greater and the wing is slightly more washed out, both of which will tend to relieve the wing-root bending moment compared to a rigid analysis.

II.C STRESS ANALYSIS

The baseline winglet configuration was analyzed to evaluate its structural feasibility by determining the adequacy of the internal load paths for the winglet and its attachment to the basic wing. Critical winglet-to-wingtip loading was obtained from the structural

loads analysis discussed in section II.B and internal loads, deflections and stresses were obtained from a NASTRAN (ref. 1) model of the winglet to wingtip detail design as defined in section II.F.

For the winglet-to-wingtip loading, the stresses due to beam bending moments and shear loads are affected by the sweepback of the winglet. Near the root portion of a swept winglet the load path at the rear spar is shorter than the load path at the front spar. This causes the structure near the rear spar to be relatively more effective in bending. Since the shear flow depends upon the rate of change of segment end load, it is also affected by sweepback. Comparisons of this effectiveness factor, as used in references 2 and 3, to the winglet structure as defined by the layout drawings resulted in the following assumption of load distribution:

1. The winglet spars react the root shear and bending moment by a 40% front spar and an 80% aft spar overlapping load distribution.
2. The torsion in the winglet is reacted equally by the winglet front and rear spars.

The critical wing up-bending and down-bending loads are given in table 14 for the winglet geometry shown in figure 12.

Figure 13 shows the elemental model used to obtain internal loads, deflections and stresses of the winglet-to-wingtip design as given by the layout drawings. Since the load path inboard of the auxiliary spar of the wing is soft, the model assumes no structure effective at that location. Properties for elements 28, 29, 128, and 129 at $\eta = 0.91$ were taken from the KC-135 wing stress analysis in reference 2. Critical wing up-bending (condition no. 4) and down-bending (condition no 3A) loads, as noted in table 14, were applied to the model. These loads were applied perpendicular and parallel to the WBL 780 wingtip rib. The NASTRAN model nodal deflections, chord loads and stresses, and panel maximum shear stresses and shear flows are presented in tables 15-18.

In conclusion, the stress levels obtained from the NASTRAN model analysis in the area of existing wing structure exceed the allowables as given by the KC-135 wing stress analysis in reference 1 at $\eta = 0.91$. Therefore, structural modification of the outboard section of the wing would be necessary to accomplish the installation of winglets. Tension allowable, based on static requirements, in the upper and lower spar chords per (ref. 2) is 66 000 psi. Compression allowable for the front and rear spar lower chords is 25 000 psi; for the rear spar upper it is 40 000 psi; and for the front spar upper it is 39 000 psi.

II.D WEIGHT ESTIMATES

An initial weight estimate of the wing modification, winglet to wing attachment and winglet structure was made so that preliminary flutter analyses could be made. The initial estimate for the winglet weight was 141.3 lb. and 50.1 lb. of weight associated with the wingtip modification. This initial weight estimate was considered as the nominal winglet configuration in the flutter analysis discussed in section II.E.

Following the completion of the structural design and layout drawings, the initial estimates were updated with a more detailed and refined estimate. A summary of the weight estimate obtained is presented in table 19. Both an incremental airplane weight and a kit weight is presented. The kit weight includes all the new structure and reworked structure in the area of modification. This was required for preliminary fabrication and installation cost estimates. The incremental weight was used in the aerodynamic performance analysis. A more detailed weight breakdown is tabulated in tables 20 and 21.

II.E FLUTTER ANALYSIS

Preliminary flutter analyses of the KC-135A equipped with a winglet at each wingtip (WBL ± 780) were accomplished. This limited study was undertaken to obtain preliminary analytical data on the sensitivity of the airplane flutter boundary to the inclusion of the winglets.

Symmetric and antisymmetric analyses were conducted for one gross weight configuration (245.3 kips) which is representative of the KC-135A immediately prior to the initial cruise phase of the 5.10 hr composite mission. This configuration was chosen for analysis since past flight flutter testing has indicated that aeroelastic damping is lowest when wing tanks are full or nearly full.

Analysis conditions included altitudes of 21 500 ft and 29 000 ft as illustrated in figure 14. The nominal winglet, which is illustrated in figure 15 weighed 141.3 lb and was assumed to be rigid. The nominal winglet center of gravity was located at BS 1234, WBL ± 780 , and BWL 300.926 (i.e., 39.0 in. above the wing chord plane at WBL ± 780). In addition to the winglet weight, 50.1 lb of weight associated with the wingtip modification was included in the analysis.

Table 22 illustrates the fuel condition that was utilized, and table 23 describes the complete set of configurations that were analyzed including variations in winglet weight, winglet c.g. position, winglet frequency, and airplane altitude.

Determination of normal modes of vibration for the basic airplane configuration was accomplished by representing the airplane as an assemblage of interconnected components, each of which, with the exception of the nacelles, is described by an elastic axis lumped parameter system as shown in figure 16. An uncoupled vibration analysis was performed for the forward body, aft body, horizontal tail, wing, and fin. The wingtip stiffness (outboard of WBL 740) was increased 15% to account for the wing modification. Empirical frequencies and mode shapes obtained through previous ground vibration testing were used to describe the uncoupled modes of the inboard and outboard nacelles.

Symmetric and antisymmetric equations representing free vibration of the entire airplane were formulated using rigid body freedoms and selected uncoupled component modes as generalized coordinates. Coupled vibration equations were solved to obtain 24 symmetric elastic modes (symmetric analyses) and 27 antisymmetric modes (antisymmetric analyses) for use with the appropriate airplane center of gravity freedoms in formulating the flutter equations.

In addition, flutter analyses of the KC-135A with winglet root flexibility were accomplished by augmenting the airplane flutter equations with an equation representing the vibratory mode of the given winglet configuration.

Unsteady aerodynamic forces on the wing, horizontal stabilizer, vertical tail, forward body, aft body, and winglets were generated using a three-dimensional doublet-lattice computer program. The doublet-lattice theory accounts for Mach number and finite span effects and includes aerodynamic coupling among all airplane components. The following well known integral equation relating unknown pressure to known downwash is solved:

$$w(x, y, t) = e^{i\omega t} \iint \Delta P(\xi, \eta) K(x - \xi, y - \eta, M, K) d\xi d\eta$$

where $\Delta P(\xi, \eta)$ unknown pressure distribution

$K(x - \xi, y - \eta, M, K)$ kernel influence function

$e^{i\omega t}$ time dependence relation

The downwash is defined as follows:

$$w(x, y, t) = - \left[\frac{\partial z(x, y)}{\partial x} + ik_r \frac{z(x, y)}{b_r} \right] e^{i\omega t}$$

where $z(x, y)$ surface deflection

b_r reference length

k_r reference reduced frequency

The lifting surfaces are divided into small trapezoidal elements (aerodynamic panels) arranged in strips parallel to the free stream, as illustrated in figure 17. The unknown pressure distribution is determined for each airplane mode by considering pressure to be constant over a given aerodynamic panel and solving the above equations (one equation for each panel) based on a specified reduced frequency and Mach number. Generalized aerodynamic forces are finally determined by calculating virtual work associated with aerodynamic panel pressure forces and modal deflections.

Results of the preliminary flutter analysis are summarized in figures 18-25. Figures 18 and 19 illustrate results of the symmetric analysis, whereas figures 20-25 are associated with the antisymmetric analysis.

Figures 18 and 19 indicate damping and frequency of elastic modes versus airplane velocity for the symmetric baseline configuration as well as the symmetric configuration equipped with a nominal weight winglet. These results, together with results for winglet weight, cg position, and frequency variations, as well as airplane altitude variations, indicate that the KC-135A symmetric flutter boundary is not significantly influenced by the winglet variations that were considered in this study

Figures 20-22 illustrate damping and frequency versus airplane velocity (airplane altitude = 21 500 ft) for the antisymmetric baseline configuration as well as the antisymmetric configurations equipped with a nominal weight (141.3 lb) winglet and a 300 lb winglet, respectively. These figures indicate that one elastic mode is degraded due to the installation of the winglet. For clarity, this mode is identified with an asterisk at the extreme ends of the velocity range. As indicated by the plots of frequency versus velocity, the mode exhibits a frequency of approximately 2.5 cps at low speeds and increases to a frequency of approximately 2.85 cps at flutter. Results indicate the mode to be primarily wing bending and torsion; however, significant coupling of aft body and fin lateral bending is apparent.

Figure 23 is a plot of flutter velocity versus winglet weight for the elastic mode described above. Data are shown for both altitudes that were considered in this study. Also shown in this figure is the speed corresponding to $1.15 V_D$ (1.15 times design velocity), which is approximately the same in terms of true airspeed for both altitudes. As indicated in this figure, no structural damping is reflected in the results shown. Inclusion of a nominal amount of structural damping ($g = 0.015$) would raise the flutter speeds approximately 25 kn. Figure 23 indicates that increased weight at the wingtips is degrading; however, the airplane is flutter free below $1.15 V_D$.

Figure 24 is similar to figure 23 except that flutter velocity is plotted versus winglet cg position for a nominal weight winglet (141.3 lb). This figure indicates that the antisymmetric flutter boundary is not significantly influenced by the winglet cg positions that were analyzed.

Figure 25 illustrates flutter velocity versus winglet frequency for an airplane altitude of 21 500 ft. Results obtained from analyzing winglet frequencies of 5.0 cps, 10.0 cps, and rigid winglets indicate that flutter velocity is not strongly influenced by these variations in winglet frequency. It is anticipated that the actual winglet frequency will be greater than 5.0 cps.

In summary, preliminary flutter results associated with the limited number of configurations that were considered in this study indicate that the KC-135A would be flutter free up to and including $1.15 V_D$. However, more detailed flutter analyses, considering a variety of fuel loadings, need to be accomplished in future studies of the KC-135A winglet. In addition, flight flutter testing will be required to demonstrate an adequate flutter boundary.

II.F STRUCTURAL DESIGN AND LAYOUT

Preliminary design layouts for the winglet structure, wingtip structure and winglet attachments were prepared. The layouts included consideration of the basic wing modifications and the structural load paths for the wing to winglet interface. The layout drawings of the wing modification and the conventional structure winglet design are presented in figures 26-31. The winglet structure design shown in these figures considered only an experimental flight demonstration winglet. Figure 26 is the centerline diagram of the winglet for the conventional structure design. The winglet has

zero degree cant (vertical), capability for ± 2 degrees incidence rigging, and 2 degrees of wash out from the winglet root to tip. Figure 31 is the winglet assembly drawing. The structural loads shown in this drawing are initial load estimates and do not reflect the results of the stress analysis discussed in section II.C. The details of the winglet interface structure to the wing is shown in figure 27 and the structural modifications to the wingtip area are shown in figures 28-31.

A description of the work involved in the outboard wing modification, winglet assembly and installation is as follows:

II.F.1 OUTBOARD WING MODIFICATION

Modify the outboard wing as follows:

1. Jack the airplane per applicable T.O. and install pogo sticks at front and rear spar near the wingtips.
2. Perform an alignment check of the wing. Establish transit and level points on the hangar floor as required to facilitate subsequent alignment checking of the wing modification. Adjust pogos as required. Furnish a copy of all results to Engineering.
3. Remove the existing wingtips, fuel vent tubes and flux gate transmitter. Disconnect and roll back wiring.
4. Replace the W.S. 960 tank end rib with a similar assembly which is 24% heavier in construction. The rib will be divided into 3 parts by the front and rear spars.
5. Fabricate and install a front spar assembly consisting of upper and lower machined extruded chords, sheet metal web and a machined outboard end terminal fitting. The spar assembly will extend inboard to approximately W.S. 950 and will overlap the existing front spar. See figure 30, zone A9. Rework the existing leading edge as required to clear the spar assembly.
6. Fabricate and install a rear spar assembly consisting of upper and lower machined extruded chords, sheet metal web and doubler and a machined outboard end terminal fitting. The spar assembly will extend inboard to approximately W.S. 940 and will overlap the existing rear spar. Rework the existing trailing edge as required to clear the spar assembly. See figure 30, zone A3.
7. Fabricate and install a tip auxiliary spar assembly consisting of upper and lower machined extruded chords, sheet metal web and doublers and a machined outboard end terminal fitting. This spar will extend from W.S. 960 to WBL 780. Nonmagnetic fasteners will be used because of the proximity of the flux gate transmitter. See figure 29, zone B4.
8. Replace the WBL 780 rib with a similar assembly of heavier construction. The rib will be divided into 4 parts by the front, rear, and auxiliary spars. A shop aid tool

will be required to insure the correct spacing and alignment of the fin attach bolt holes in the spar terminal fittings. Verify position by an alignment check during installation. Furnish a copy of data to Engineering. See figure 29, zone A9.

9. Fabricate and install a rib at WBL 765.6 from the auxiliary spar forward. The rib will have machined extruded chords and a sheet metal web.
10. Fabricate a new fuel vent scoop similar to Canadian Tanker scoop 65-81020. This is a 6061 weld assembly.
11. Fabricate and install heavy skins from front spar to auxiliary spar and from W.S. 960 to WBL 780 on upper and lower surface. Two rows of closely spaced screws will be required along the edges of each skin panel.
12. Roll electrical wiring back into the rework area and connect. Install a connector on the navigation light wires at WBL 780. Install salvaged fuel vent elbows.
13. Down jack airplane.

II.F.2 WINGLET ASSEMBLY

Fabricate the left and right-hand winglets as follows:

1. Machine a front-and a rear-spar fitting each from a 7075- F block specially hand forged to shape. Heattreat to T- 73 before finish machining. Use machine tools capable of cutting compound contours. See drawing figure 27 and 31.
2. Machine root and tip ribs from 7075-T73 plate. Use machine tools capable of cutting compound contours. Assemble these ribs with the spars. Jig bore the winglet attach bolt holes in the spar fittings. See figure 27.
3. Fabricate and install 10 sheet metal rib assemblies. These ribs have separate chords so contour payoff may be accomplished with simple contour bars. See figure 31, section 4-A.
4. Fabricate and install inspar skins of 0.040 clad 2024-T3 sheet. All fasteners will install in dimpled holes. Blind bolts will be used on the outboard face. See figure 31.
5. Machine one leading-edge rib and one trailing-edge rib from 2 in 7075-T73 plate, and install on inspar box.
6. Fabricate a tip rib assembly 92 in long with stretched extruded chords and sheet metal webs. This rib will extend from the wing front spar to the wing trailing edge. The rib will be divided into three parts by the winglet front and rear spar. At the wing front spar install a machined fitting to transmit winglet loads to the wing. See figure 27.

7. Using polyester/glass laminate per BAC 5426 fabricate a one-piece leading-edge 0.250 thick. Fabricate inboard and outboard T.E. skins of the same material except 0.090 thick. Attach the T.E. skins to each other with 1 x 2 in. foam block ribs and a machined T.E. strip. Attach the leading- and trailing-edges to the winglet inspar box with screws and nutplates. See figure 31.
8. Using polyester/glass laminate per BAC 5426. fabricate a three-piece wingtip cap approximately 0.250 thick which extends the full length of the tip rib assembly. Install the salvaged wingtip navigation light in the center piece of the cap. Fabricate a dorsal fin of 0.250 polyester/glass laminate and attach to the forward section of the wingtip cap. A severely formed 6061 skate angle is riveted to the cap and the dorsal is attached with screws and nutplates. Apply aerodynamic smoother all around the dorsal to wingtip cap joint. See figure 27.
9. Fabricate 5 pairs of incidence blocks for each wing. Each pair consists of two 7075-T6 blocks approx. 6 x 6 in. with 1 large face machined flat and the opposite face machined to the exact required incidence angle using a sine table or equivalent. Incidence angles of +2°, +1°, 0°, -1°, and -2° will be required. Each block will be bored with clearance holes for the winglet attach bolts. See figure 27 rigging program.
10. Fabricate winglet root fillets of polyester/glass laminate approximately 0.060 thick and attach to the winglet with screws and clinch nuts.
11. Fabricate a winglet tip assembly by molding laminated polyester/glass in two half molds. Join the two halves at the chord plane and bond in two phenolic blocks to form attach hard points. Install with screws and nutplates. See figure 31.

II.F.3 WINGLET INSTALLATION

With the airplane hangared and ballasted to the correct c.g., install the winglets as follows:

1. Select the correct incidence blocks for the required test condition and attach to the wingtip rib with bolts and nutplates. Insure any previous wing-to-winglet gap covers are removed and systems lines are clear of the tips. See figure 26 and 27 for diagram and rigging.
2. Attach the lifting sling to the inboard side of the winglet. Lift the winglet clear of the floor and shorten the upper wire of the sling rotating the winglet to a nearly upright position. Move the winglet to approximately the correct position at the wingtip. Using a drift pin, line up winglet attach holes one at a time and install winglet attach bolts. When all bolts are installed, torque and retorqued all bolts. Putty all bolts. See figure 27.
3. Connect systems, such as navigation light.

4. Fabricate and install winglet to wingtip gap covers of clad 2024-T3 sheet 0.050 thick and attached with screws and nutplates. Hand form as required.

II.G ADVANCED COMPOSITE WINGLET STRUCTURAL DESIGN

As a possible alternative to the winglet structure which uses conventional materials and designs, an advanced composite and an advanced metallic design concepts were laid out. These design alternatives were investigated for the possible weights and cost savings. The advanced composite winglet structural design is discussed in this Section and the advanced metallic design concept in section II.H.

II.G.1 DESIGN AND ANALYSIS

The design concept is shown in figures 32 and 33. The approach is to use full-depth honeycomb to reduce part count and increase the effectiveness of the skin in providing bending and torsional stiffness.

3.1 PCF nomex is used as the honeycomb core material in all areas where the core shear requirements allow. Eight to twelve PCF fiberglass core provides the higher shear requirements at the front spar, rear spar and root rib. These core materials are inexpensive, easy to machine, and can be formed to contour. Their formability enables the core assembly to be made by machining one side and forming the other as a cost saving method.

The spar caps and root rib caps are made primarily of 0° intermediate strength graphite epoxy tape. This provides the bending stiffness and strength at a minimum weight. The cap strip/honeycomb spar and rib construction is less expensive than a laid up I-section spar or channel rib. The tooling costs are greatly reduced. The honeycomb to spar fitup problems are eliminated.

The inboard and outboard skins are made of laid up reinforced fiberglass. The fiberglass skins are cost effective but not as weight effective as either ±45 graphite/epoxy skin or aluminum skins due to the lower stiffness/weight ratio. Graphite skins were eliminated due to material costs and additional layup expense. Aluminum skins were eliminated due to the expense of stretch forming the skins to the compound contour. The minimum skin gage in the leading edge is 0.063 to resist hail damage. A rubber boot is sprayed on the same area to protect against rain erosion. The entire fiberglass skin is covered with conductive paint for lightning strike and static discharge.

Bending stiffness is provided primarily by the graphite/epoxy spars. The addition of full-depth honeycomb core and the elimination of chordwise mechanical splices makes the entire air foil section effective in providing torsional stiffness. Full-depth core in the leading- and trailing-edge eliminates the requirement for the thick leading- and trailing-edge fiberglass skins of the baseline configuration. Beam shear in the cover is significantly reduced in the composite design due to the multicell shear load paths provided by the honeycomb core. Finite element modeling of the winglet root area and wingtip will be required to evaluate the load distribution in this area. Preliminary

stress and stiffness analysis of the fully effective section using a multicell composite wing box computer program have confirmed the structural feasibility of the concept. The bending stress and stiffness distribution are shown on figures 34 and 35.

The winglet assembly is attached to the wing structure in the same manner as the conventional design. The rear spar fitting is machined from a titanium block with tabs welded on to pickup the spar caps. The front spar fitting is larger and is fabricated by welding titanium plates together. The fittings are split to obtain good bonding pressure between the fittings and the rib cap. Titanium is utilized because its coefficient of thermal expansion is compatible with the coefficient of thermal expansion of graphite/epoxy. This minimizes the thermal stresses induced in the cap strip/titanium fitting joint during the bond operation. The titanium fittings also splice the root rib cap strips and transfer the spar kick loads into them.

A potential problem area is the thermal mismatch between the composite winglet and the aluminum wing. A temperature change results in thermal loads being introduced into the closure rib chord. Initial bond areas of graphite to titanium have been sized using a shear allowable of 200 PSI. Preliminary structural analysis of the complex load distribution from the titanium fittings to the composite winglet was evaluated.

II.G.2 FABRICATION-ADVANCED COMPOSITE WINGLET

The advanced composite final assembly will be a mechanical assembly consisting of the bonded assembly, machined and/or welded fittings, leading-edge cap, tip cap and loose attached cover fairing. The bonded assembly will consist of the outboard side skin-core assembly and the inboard side skin assembly bonded together in a lay-up mandrel.

The outboard side skin-core assembly will be a assembly of the outboard side skin, precured graphite/epoxy details, precured fiberglass attachment strips and the titanium straps bonded together.

The fiberglass honeycomb core to be formed to a layup mandrel surface. The core is to be made in segments and will include excess thickness for final machining. The core segments under the graphite epoxy cap strips are to be 0.02 to 0.03 inches under thickness. The graphite/epoxy cap strips (inboard side) will include (three) plies of type 181 epoxy preimpregnated to allow for final machining without degrading the requirements of the graphite/epoxy cap strip. The core segments under the root rib and attachment angle are to be net (any mismatch in this area can be adjusted by sanding or adding additional plies of preimpregnated type 181 epoxy on the final bond).

The inboard side of this assembly will be numerical control machined to contour by a vendor or by converting inplant equipment by adding duct shrouds and oil collectors. The layup mandrel used for the layup can be used as a base for machining.

The inboard side skin assembly will consist of a precured skin.

The leading-edge cap assembly will consist of a precured plastic glass reinforced epoxy skin. The leading-edge cap assembly will be bonded to the bonded assembly with splice plate reinforcement. The cavity between the leading-edge cap assembly and the bonded assembly will be injected with structural foam.

The tip cap assembly will consist of a precured plastic glass reinforced epoxy skin. This assembly will be bonded to the bonded assembly.

The tapered titanium straps will be machined using conventional machining tools.

The aft titanium fitting is a bath tub type titanium fitting which will be machined using conventional machining tools. The forward fitting will be made of welded titanium plates. The mating surface of the forward fitting will be machined using conventional machining tools.

II.H ADVANCED METALLIC

II.H.1 DESIGN/ANALYSIS

The advanced metallic design concept is shown in Figures 36 and 37. The concept is to use full-depth honeycomb to reduce part count and make the skin fully effective in providing bending and torsional stiffness.

3.1 PCF aluminum core is used in all areas where the core shear permitables allow. 8.1 PCF aluminum core is used in the front spar, rear spar and root rib areas. The core, which is machined to contour on both sides, eliminates the large amount of tooling required to fabricate the baseline structure of multiple ribs.

With the full-depth honeycomb core combined with the aluminum skins makes the entire shell work in torsion and in bending. This allows use of skin gages one half of the baseline gages. The (0.020 in.) gage results in a slightly lower torsional stiffness in the upper third of the winglet. The addition of doublers in the lower section results in greater torsional stiffness than the baseline design. Bending stress and stiffness distributions are shown in figures 34 and 35. Doublers are used to provide bending stiffness in the lower two thirds of the winglet. A 0.063 leading-edge cover is used to join the inboard and outboard skins and to protect the winglet from hail damage.

The loads in the shell are transferred to the winglet attachment fittings through stub spars. The spar caps are bonded to the shell and bolted to the attachment fittings. This cap strip/honeycomb core spar concept offers a cost and weight advantage over the full length hogged out aluminum spars in the conventional design.

The kick loads produced by the kink in the spars at the winglet root are reacted by an aluminum cap strip/honeycomb core rib. The cap strips are spliced at each spar.

The winglet assembly is attached to the wing structure in the same manner as the conventional design. The fittings are hogged out of an aluminum block.

II.H.2 FABRICATION CONCEPT-ADVANCED METALLIC WINGLET

The advanced metallic winglet final assembly will be a mechanical assembly consisting of the bonded assembly, machined fittings, leading-edge cap, tip cap and loose attached cover fairing. The bonded assembly will consist of the outboard side skin, core assembly and the inboard side skin assembly bonded together in a layup mandrel.

The 8.1 P.C.F. and 3.10 P.C.F. aluminum honeycomb core will be spliced together. The core will be milled to contour and steps milled in core to net configuration. Bond aluminum spar caps to core. Bond stretch formed aluminum doublers and stretchformed outboard and inboard aluminum skin to core assembly.

The leading-edge assembly will be made from a laminated aluminum sheet .040/.020 inches thick. The sheet will be stretchformed to the leading-edge contour. The leading-edge assembly will be bonded to the bonded assembly and the cavity in the leading-edge assembly will be filled with a structural foam.

The tip cap will be made of plastic fiberglass reinforced epoxy materials. The fiberglass will be molded to contour in a layup mandrel. The tip cap will be bonded to the bonded assembly.

The forward and aft fittings will be made of aluminum. These fittings will be machined using conventional machining tools. The fittings will be fastened to the bonded assembly with 3/8 in. dia. huck blind bolts.

III.I COST AND WEIGHT COMPARISONS OF WINGLET STRUCTURAL DESIGNS

The weight estimates are based on the prototype concepts. A summary of the weight breakdown is shown in table 24. The lightest design is the advanced metallic followed by the composite and baseline design. In the baseline design a large portion of the cover weight is associated with the heavy polyester leading and trailing edge. The cover weight of the advanced metallic is lighter than the advanced composites due to the higher shear stiffness/weight ratio of aluminum to fiberglass* The combined weight of the spars and terminal fitting is close in the three designs. The weight of the integral spar/fitting of the baseline is comparable to the combined weight of the short stub spar, terminal fitting and dense core of the all metallic design. For the advanced composite design the weight efficiency of the graphite spars is lowered when the dense honeycomb spar web and titanium terminal fitting are included. The weight of the rib assemblies of the baseline design have been compared with the weight of the full-depth honeycomb core. These are comparable due to their similar functions of stabilizing the skin panels, and carrying chordwise shear.

* An advanced composite material like graphite epoxy was not selected for the winglet skin because of the high cost. Although the graphite epoxy has a higher shear stiffness/weight ratio than the fiberglass, the substantially higher cost of the graphite epoxy lead to the use of fiberglass with its higher weight.

The cost of the three winglet structural design concepts was estimated on a prototype basis and on the basis of a hundred sets of production winglets. The fabrication concepts described in sections II.F.2, II.G.2 and II.H.2, and the material costs listed in appendix B were used to estimate the winglet construction costs. A summary of the relative costs (the cost of the conventional design winglet as the comparative base) of the structural design concepts is shown in table 25. For the prototype winglet, the cost of the advanced composite winglets was substantially lower than the conventional design and advanced metallic design. The conventional design was penalized from the cost standpoint by both part count and tooling. The metallic design required more expensive tooling costs.

For the production winglets, the nonrecurring tooling costs when spread over 100 sets, tend to even out. The part count, the manufacturing process and material costs become the major factors. As shown in table 25, for the production winglet, the advanced metallic design becomes the least costly design of the three. The more expensive materials and more manufacturing manhours required for the advanced composite design causes the switch in position (relative to cost) of the advanced metallic design with the advanced composite design. The material and labor costs are about 13% greater for the advanced composite design.

For all three designs, the structural design and manufacturing processes could be changed to reduce the cost of constructing these winglets; however, the relative positions of the designs with respect to cost, most likely will not change. Based on this assumption, if only a flight demonstration program for a single set of winglets is planned, the advanced composite design appears to be the most cost effective. If a production program is envisioned for the winglets, the advanced metallic design would be the choice.

II. J AIRPLANE PERFORMANCE ESTIMATION

The KC-135A performance improvement for installing winglets was based on the addition of 0.135b/2 long, winglets to the KC-135A wingtips. The effect of the winglets on KC-135A drag is given in section V.B.

The winglet drag was added to the basic KC-135A drag polar and the cruise conditions were reoptimized. L/D and ML/D were calculated for both the basic KC-135A and the KC-135A with winglets for a 210 000 lb. gross weight. $TSFC/\sqrt{\theta}$ corrected for a 1.25% bleed and power extraction factor was also computed for a 210 000 lb. gross weight. The KC-135A performance improvements obtained with the winglets are summarized in table 26 and figure 38. The range factors shown are an average value for weights between the maximum weight to the operating empty weight. The range factors include 5% fuel flow service tolerance, 99% maximum range and climbing cruise corrections in addition to the bleed and power extraction factor. The net improvement in range factor is 8.1%. The increase in OEW reduced the factor by 0.6% and the net effect of the

winglets on ferry range is a 7.5% improvement. The conditions should be noted for these performance improvements. The KC-135A with winglets cruises at an average altitude which is 3.4% higher than the basic KC-135A. As shown in table 26, the KC-135A with winglets cruises 0.51% faster at a 4.9% higher lift coefficient, 7.8% greater lift to drag ratio and a 0.3% greater thrust specific fuel consumption.

III WINGLET PARAMETER STUDY ON THE KC-135 WING

The following winglet parameters were studied to determine the effects on the potential aerodynamic improvement of the KC-135: (1) chordwise location; (2) leading-edge sweep angle; (3) taper ratio; (4) area; (5) length; (6) cant, while holding the configuration span constant; and (7) cant, while allowing the configuration span to increase. These parameters investigated are illustrated in figure 39. In general it was not possible to vary just one parameter while holding all others constant. When possible the implication of varying more than one parameter will be discussed on the basis of linear superposition based on the previously obtained results. In all cases the winglets were located on the upper surface at the wingtip. The first four parameters were investigated with a winglet length of $0.141 b/2$. The last two were investigated using a winglet length of $0.135 b/2$. The KC-135 cruise flight condition selected for the parameter study was $M = 0.77$ and $W/\delta = 0.91 \times 10^6$. The corresponding lift coefficient is 0.426.

A vortex-lattice computer program TEA-372 (see appendix A for description of program) was used throughout this portion of the study. An analysis run was first made for the wing alone. A design run was then made for each wing/winglet configuration at $C_L = 0.426$. In this run the wing twist distribution was fixed, but the winglet twist distribution was allowed to be optimized for minimum C_{D_i} of the total configuration. Finally, an analysis run was made for each optimized configuration over a C_L range from 0.15 to 0.75. Note that the winglet was not optimized for minimum C_{D_i} at each C_L , only at $C_L = 0.426$.

The aerodynamic plots which will be presented for each parameter study include the lift coefficient, induced drag, pitching moment, bending moment, sectional lift coefficient, and span loading. The force coefficients are based on $S_{REF} = 2433 \text{ ft}^2$, and the pitching moment coefficient is based on $S_{REF} = 2433 \text{ ft}^2$ and $c = 241.88 \text{ in.}$ C_{m_x} is the moment generated by the right half of the configuration about the axis of symmetry. For this study, changes in C_{m_x} are viewed as indicative of changes in wing-root bending moment. C_{m_x} is based on $S_{REF}/2 = 1216.5 \text{ ft}^2$ and $c = 241.88 \text{ in.}$

The planform of the baseline winglet for the first five parameters (location, sweep, taper ratio, area, and length) studied is shown in figure 40. Its root section is about 60% of the wing tip chord and it is positioned on the wing such that its trailing edge intersects the wing trailing-edge. The winglet has a taper ratio of 0.338, a leading-edge sweep of 37° , and a length of about 110.5 in., about 14.1% of wing semispan. Winglet length is the true distance from the wing trailing-edge to the winglet tip trailing edge along a line perpendicular to the wing tip chord line. The first five parameter studies were made with 0° winglet cant.

III.A WINGLET CHORDWISE LOCATION STUDY

The effect of winglet chordwise location was investigated with the three winglets shown in figure 41. $(x/c)_{LE}$ denotes the point at which the winglet leading-edge intersects the wing chord plane. The baseline winglet was just shifted forward to obtain the cases for $(x/c)_{LE} = 0$, and 0.20. All three winglets thus have the same leading-edge sweep, taper ratio, and length. For practical purposes, they also have the same area.

The results of the chordwise location study are presented in figure 42a - 42e. There is an increase in lift curve slope (fig. 42a) due to the higher effective aspect ratio created by the winglet. The slope improves slightly as the winglet is moved forward. As would be expected, the winglet increases nosedown pitching moment (fig. 42a) because the wingtip is more highly loaded. This would generally increase trim drag. The pitching moment increment increases a small amount as the winglet moves forward. Note that the winglet improves static longitudinal stability somewhat.

Induced drag (fig. 42b) is reduced about 11 counts at $C_L = 0.426$ for the baseline winglet. This reduction decreases slightly as the winglet is moved forward. Wing-root bending moment (fig. 42c) naturally increases as the load shifts outboard on the wing. It is not heavily dependent on winglet location, with the forward location just slightly increasing the moment over the baseline. Figure 42e shows that the wing loading shifts outboard as the winglet moves forward. This result is consistent with the increases in pitching moment and wing-root bending moment. The winglet becomes more highly loaded over its entire span as it moves forward.

In summary, the chordwise location of the winglet does not significantly affect lift, induced drag, pitching moment, or wing-root bending moment. The trends however, would make an aft location slightly preferable.

III.B WINGLET SWEEP STUDY

Five different winglets are analyzed in the sweep study. They are shown in figure 43. The leading-edge sweep angles are -30° , -8° , 14° , 37° (baseline), and 60° . All winglets intersect the wing at the same chordwise position, $(x/c)_{LE} = 0.40$. They also have the same taper ratio, area, and vertical length.

The effects of winglet sweep are shown in figures 44a-44e. Sweep has no effect on the aircraft lift curve slope (fig. 44a) over the range $\Lambda_{LE} = -30^\circ$ to 37° . At the extreme value of $\Lambda_{LE} = 60^\circ$, a slight deterioration in lift does appear. The change in pitching moment with winglet sweep is essentially a rotation of the curve about $C_L = 0.55$. The rotation results in a small, gradual increase in stability as the sweep varies from -30° to 60° . In practical terms, though, the changes in magnitude of the pitching moment itself and the stability are not significant.

The effect of winglet sweep on induced drag (fig. 44b) or wing-root bending moment (fig. 44c) is minimal until the sweep angle reaches 60° . At this sweep angle the induced drag shows some increase at lift coefficients above 0.55. However, these high C_L 's would not ordinarily be reached during cruise flight. The wing-root bending moment at $\Lambda_{LE} = 60^\circ$ shows a small reduction from the other winglet cases.

Figures 44d and 44e show that the wingtip and the winglet are most highly loaded when the winglet is swept to the forward most position $\Lambda_{LE} = -30^\circ$. As the winglet is swept back from this position, the wingtip and winglet are gradually unloaded to achieve the condition for minimum induced drag.

III.C WINGLET TAPER RATIO STUDY

In this parameter study, the taper ratio was adjusted by changing the winglet tip chord as shown in figure 45. The three winglets have taper ratios of 0.15, 0.338 (baseline), and 0.68. They have the same chordwise location ($(x/c)_{LE} = 0.40$) and the same length ($0.141 b/2$), but they do not have the same leading-edge sweep angles or the same areas. The leading-edge sweep angles are 41° , 37° , and 28° . From the results of the previous parameter study, the sweep has a negligible effect on lift, induced drag, pitching moment, and wing-root bending moment over this range of sweep angles. Thus the sweep difference of the taper ratio study winglets can be neglected. It will be shown in the area parameter study that the area variation of the winglets in figure 45 can also be neglected for purposes of the taper ratio study.

The winglet taper ratio effects are presented in figures 46a-46e. The lift and pitching moment curves (fig. 46a) are the same for taper ratios of 0.15 and 0.338. When the taper ratio is increased to 0.68, the lift curve slope shows a small additional improvement, while the pitching moment becomes more nosedown.

The induced drag polar (fig. 46b) shows no change as the taper ratio is reduced from the baseline value of 0.338 to the relatively small value of 0.15. When the taper ratio is increased to .68, the polar shows a small amount of improvement at C_L 's much higher than usable cruise values. The wing-root bending moment (fig. 46c), likewise, shows no change when the winglet taper ratio is reduced to 0.15. The taper ratio of 0.68 results in a small increase in bending moment.

Figure 46d shows an important consequence of reducing the winglet taper ratio. The sectional lift coefficients on the outboard portion of the winglet are driven to high values which might precipitate flow separation. The optimum loading on the winglet (fig. 46e) decreases a small amount as taper ratio is decreased. At the same time, the wing loading shifts inboard.

III.D WINGLET AREA STUDY

The area of a winglet has an obvious effect on skin friction drag. From this standpoint it would be desirable to have a winglet with the smallest possible area which could still be loaded up satisfactorily. The limiting factor as winglet area is reduced is the lift

coefficient at which the winglet must operate. To determine what implications winglet area might have the three winglet geometries shown in figure 47 were studied.

Winglet area was increased by simply moving the leading edge of the baseline winglet forward. The $(x/c)_{LE}$ location of the three winglets are 0., 0.20, and 0.40 (baseline). All winglets have a common trailing edge. Their respective areas, nondimensionalized by the baseline winglet area, are 2.00, 1.49 and 1.0. The winglets have the same leading-edge sweep angle and the same length. It was determined from the chordwise location study that the effects of leading-edge location are small. The taper ratio varies from 0.61 for $(x/c)_{LE} = 0.$ to 0.338 for the baseline winglet, but this change is being neglected on the basis of the results of the taper ratio study.

Figures 48a-48e show the results of the winglet area study. There are small but discernable changes in both lift and pitching moment (fig. 48a) with area. The lift curve slope improves slightly as the area is increased, and the pitching moment becomes more negative due to a rotation of the curve in the direction of increased stability.

The changes in induced drag with area (fig. 48b) are negligible around the lift coefficient at which the winglets were optimized. At higher and lower C_L 's, there is a small drag reduction with increasing area. Wing root bending moment (fig. 48c) increases a small amount as winglet area is increased.

Figure 48d shows the expected reduction in the winglet sectional lift distribution as the winglet area grows. The optimized winglet loadings, however, do not change significantly with area, as can be seen in figure 48e, and the loading on the wing shifts outboard as the area of the winglet increases.

The winglet parameters investigated thus far include chordwise location, sweep, taper ratio, and area. (Note that winglet length was always held constant.) It was found that variations in these parameters do not significantly affect the configuration lift, induced drag, pitching moment, or wing-root bending moment. These results were obtained on the KC-135 with winglets optimized at $C_L = 0.426$. When designing winglets for another airplane and flight condition, it would naturally be best to investigate the effects of these same parameters. However, if time and/or budget do not permit, it seems acceptable to assume that results similar to those above would be obtained. The values which the winglet designer selects for these parameters could thus be based only on other factors such as, (1) cruise Mach number and associated compressibility problem, (2) wetted area, (3) sectional lift coefficient distribution across the winglet, (4) weight, and (5) flutter.

III.E WINGLET LENGTH STUDY

Winglet length has a very important effect on the potential benefit which can be realized from winglets. The three winglets selected for this study are shown in figure 49. Their lengths are normalized by the wing semispan, are 0.0705, 0.141 (baseline), and 0.20. For this parameter study, winglet chordwise location and

leading-edge sweep do not vary, but the taper ratio and area do. The taper ratios are 0.698, 0.338, and 0.048, and the corresponding areas relative to the baseline are 0.619, 1.0, and 1.114. However, in comparing these results with those of the taper ratio and area studies, it will be evident that length is the dominant factor.

The results of winglet length are presented in figures 50a-50e. The difference in the lift curve (fig. 50a) of the 0.0705 $b/2$ winglet compared to the baseline only becomes significant at fairly large lift coefficient. When the winglet length is further increased to 0.20 $b/2$, however, there is an additional increment in lift curve slope. The pitching moment data show that the nosedown moment changes by a fair amount over the range of winglet lengths studied, along with a slight increase in stability. A larger trim drag penalty would be paid as the winglet length increases.

The powerful effect that winglet length has on induced drag is clearly evident in figure 50b. The reductions in C_{D_i} for the three winglets are 6, 11, and 15 drag counts at $C_L = 0.426$. Since winglets reduce induced drag obviously, the performance benefits increase rapidly with increasing cruise C_L . In figure 50c it can be seen that winglet length variation has a larger effect on wing-root bending moment than did the variations in previous parameters. An increasing wing weight penalty might be incurred with winglet length unless the existing wing structure has a more than adequate margin of safety.

The sectional lift coefficients get unreasonably large on the 0.20 $b/2$ winglet (fig. 50d) because the tip chord is very small. In addition, the inboard portion of the winglet, which is common to all three cases, operates at a gradually higher C_L as the length of the winglet increases. This means that as winglet length increases, the winglet section lift coefficient required will increase to the point where flow separation will occur.

Figure 50e shows the increase in optimum winglet loading as the winglet length increases. This condition, combined with the longer moment arm for the winglet and the higher loading on the outboard wing results in a larger wing root bending moment.

A summary plot of the effects of winglet length on induced drag and wing root bending moment at $C_L = 0.426$ is shown in figure 51. The percent changes are based on the wing alone values of C_{D_i} and C_{m_x} from TEA-372. As an example, a winglet with a height of 15% of wing semispan would reduce C_{D_i} by 12.6% and increase wing root bending moment by 3.8%.

III.F WINGLET CANT STUDY-CONSTANT SPAN

The winglet selected for the two cant studies is fairly close to the baseline winglet for the previous parameter studies. It has the same chordwise location, root chord, tip chord, and leading-edge sweep angle. Its length, however, is 0.135 $b/2$ or 106 in. The cant angles studied are shown in figure 52. Note that the span of the wing/winglet combination is always equal to the wing alone span. As the winglet is canted, its root section moves inboard along the wing chord plane so as to maintain constant span, and the wing is clipped off at the wing/winglet intersection.

The effects of winglet cant while maintaining constant span are presented in figures 53a-53e. Lift curve slope (fig. 53a) falls off rapidly at first as the winglet is canted. Wing lift is being lost as the tip is clipped, and the component of the winglet force vector in the lift direction does not compensate for that loss. The 30° cant lift curve is nearly the same as the wing alone lift curve. The rate of lift loss gradually decreases as the winglet cant angle is further increased. Note that when the winglet finally lies in the plane of the wing, the lift curve is considerably below the wing alone lift curve. This result indicates that the outboard region of the wing, for wing alone, is carrying a higher load than should be used for minimum induced drag. Cant angle has a pronounced effect on pitching moment, also. Both the magnitude of the pitching moment and the stability decrease with cant angle. The pitching moment at 40° cant is about the same as that for wing alone.

Figure 53b shows that the minimum induced drag is obtained with a vertical winglet. As the winglet is canted, the drag improvement due to the winglet diminishes. Note, however, that the wing plus winglet polar always remains better than the wing alone polar. When the winglet is canted so that it lies in the plane of the wing ($\phi = 83^\circ$), the loading on the outboard 13.5% of the wing is essentially being allowed to change to minimize drag. This result clearly indicates that the loading on the outboard portion of the wing is not optimum. In Figure 53c the wing-root bending moment is seen to decrease with cant angle in a manner similar to the pitching moment. The bending moment with the winglet at 40° cant is about the same as the wing alone value.

The η values for the wing in figures 53d and 53e are always based on the wing alone semispan even though the wing itself is clipped off. The load carried over the outboard region of the wing drops off steadily as the winglet is canted, while the load over the remainder of the wing steadily increases. At the same time, the winglet is gradually loaded up to match the wing loading at the spanwise station where the wing is being clipped. The point made earlier about the nonoptimum loading on the wing is verified in Figure 53e. When the winglet lies in the plane of the wing, the loading is quite different from that of the wing alone. The outboard loading has decreased, and the inboard loading has increased. This change not only improves the drag but also reduces both the pitching moment and root bending moment.

Figure 54 is a summary plot showing the changes in wing-root bending moment and induced drag with cant angle. The percent changes are referenced to wing alone. Also shown is the percent semispan of the wing that is clipped off as the winglet is canted. The percent changes for $\phi = 0^\circ$ correspond to those on the winglet length summary plot (fig. 51) for $\lambda = 0.135 b/2$. At cant angles greater than 40°, C_{D_i} and C_{m_x} are always less than wing alone.

III.G WINGLET CANT STUDY-VARIABLE SPAN

The final parameter study is one in which the winglet is canted outboard without clipping the wingtip. Thus the span of the configuration is allowed to gradually increase. The specific cant angles studied are shown in figure 55. Note again that the winglet length is $0.135b/2$, the same as for the constant span cant study.

Figures 56a-56e show the large effects of winglet cant with variable span. The lift curve slope (fig. 56a) increases significantly over the entire range of cant angles. This result is anticipated because of the obvious increase in aspect ratio. Increased stability and large increments in nosedown pitching moment also accompany the canting of the winglet. The winglet canted 30° creates a pitching moment increment about twice as large as the uncanted winglet. Thus trim drag could be an increasingly important factor as the net benefit of winglet cant is considered.

The induced drag polar (fig. 56b) improves steadily with cant because of the increasing aspect ratio. However, the rate of improvement decreases as the cant angle increases. Wing root-bending moment (fig. 56c) gets larger as the winglet is canted. Its rate of increase with cant is highest at low cant angles.

Since the lift component of the load carried by the winglet gets larger as the winglet is canted, the wing itself does not have to carry as much load at a given C_L . Figure 56e shows the noticeable drop in loading over the entire wing as the cruise C_L is reached at lower and lower angles of attack. The winglet loading increases gradually from 0° cant to 60° cant. It then shows a rapid increase as the winglet is canted slightly below the plane of the wing. The effect of cant on induced drag and wingroot bending moment with variable span is summarized in figure 57. If the length of the winglet is utilized entirely to increase the wingspan, the induced drag can be reduced almost 24%. This is nearly 10% more than the improvement obtained with a vertical winglet. However, there are concomitant penalties in wing-root bending moment and pitching moment which may be prohibitive.

IV EQUAL AREA TIP EXTENSIONS

Whenever the subject of winglets are discussed as a means of reducing the induced drag of an airplane, the question arises: can the induced drag be reduced more effectively by increasing the wingspan with a tip extension to increase the wing aspect ratio than by using winglets? The term "more effectively" used in relationship with induced drag reducing devices is defined as the device which maximizes the induced drag reduction for a minimum weights and cost increase. A preliminary attempt is made in this section to answer the above question.

The vortex-lattice computer program TEA-372 (see appendix A for program description) was used throughout this portion of this study. The KC-135A airplane was used as the baseline configuration. Various tip extension geometries, but all with equal areas, were optimized for minimum induced drag at a lift coefficient of 0.426 using the vortex-lattice computer program. The tip extension configurations were analyzed and compared to the baseline and to a typical winglet configuration.

IV.A GEOMETRY VARIATIONS

The equal area tip extension geometry variations investigated in this study are shown in figure 58. Four different tip extensions were analyzed. Each tip extension had the same area of 4836.8 in.² per side. A summary of the geometry variations of the extensions is given in table 27. The length of the extensions varied from 45.6 to 106 in.

The only parametric variation made in this tip extension study was the length. Based on the results of Munks analysis, reference 4 only the spanwise vorticity distribution effects the induced drag. Therefore, parameters such as leading-edge sweep and taper ratio which effect the chordwise vorticity distribution only were not investigated.

IV.B AERODYNAMIC PERFORMANCE

The aerodynamic performance predicted by the vortex-lattice computer program (TEA-372) is shown in figures 59a-59e. In general, increasing the length of the tip extension reduced induced drag, increased the lift curve slope, increased the nosedown pitching moments, increased the wing-root bending moment and increased the section lift coefficient required on the tip extension. At a $C_L = 0.426$, the 13.5% semispan tip extension reduced induced drag by 23.3% as compared to the baseline airplane and the 5.8% semispan tip extension reduced the induced drag by 10.4%. However, both the wing-root bending moment and pitching moment increased 9.1% and 65.8% respectively for the 0.135 b/2 extension and 4.1% and 27.9% respectively for the 5.8% extension.

IV.C COMPARISON OF EQUAL AREA TIP EXTENSIONS WITH WINGLETS

An initial attempt was made to determine if winglets are more effective than tip extension in improving airplane performance. The three performance parameters which were used to evaluate these two devices were the induced drag, C_{D_i} the pitching moment, $C_{M,25\bar{c}}$, and the wing-root bending moment, C_{m_x} . A decrease in the induced

drag, of course, indicates an improvement in the aerodynamic efficiency. An increase in the nosedown pitching moment will produce an increase in the trim drag which reduces the aerodynamic efficiency. The final parameter, the change in wing-root bending moment, indicates the change in structural strength required by the wing to enable the attachment of the winglet or tip extension. The airplane weight is related to the wing structural strength and the airplane performance is related to the airplane weight.

A comparison of the the change in induced drag and the change in wing-root bending moment between tip extensions and winglets is shown in figure 60. Figure 61 shows the comparison of the change in pitching moment. The change in the above performance parameters were obtained by the comparison to the baseline airplane which was the KC-135A without wingtip devices.

Using the results presented in figure 60 and 61, two cases were used to evaluate the effectiveness of tip extensions and winglets. The first case considered an equal area tip extension and winglet with the same induced drag improvement, $\Delta C_{Di} = -14\%$. Figure 60 shows for this case that the tip extension produced 31% greater wing root bending moment than the winglet and figure 61 shows the tip extension produced 80% greater nosedown pitching moment. This nosedown pitching moment is equal to about 2 counts of additional trim drag.

Examining the case where the wing-root bending moment change of these wingtip devices were the same, showed the winglet reduced the induced drag by 22.9% more than the tip extension. The tip extension also increased the nosedown pitching moment by 35.7% more than the winglet. Table 28 summaries the results of these two cases. In either case, whether a constant induced drag improvement or a constant wing-root bending moment was selected, the winglet configuration would have lighter wing structures or more aerodynamic performance.

The tip extension and winglet configurations which gave the same induced drag improvement, $\Delta C_{Di} = -14\%$, were analyzed at the 2g, Mach 0.95 structural design condition. The aeroelastic deformations were included in the aerodynamic analysis and at this 2g condition, the tip extension produced 37.2% more wing-root bending moment than the winglet.

The results from this section regarding relative effectiveness of winglets and tip extensions to improve airplane performance is not conclusive. For a complete evaluation, a more detailed analysis of the effects of these wingtip devices must be made. The analysis must include the following items:

1. Loads must be determined for the elastic structure.
2. Structural design of winglets and tip extensions
3. Determine structural modifications required for the wing.
4. Flutter and weights analysis of structures.

5. Aerodynamic drag estimates(ΔC_{D_p} , ΔC_{D_i} , $\Delta C_{D_{TRIM}}$) for both high and low speeds.
6. Airplane performance estimation
7. Cost estimates.

This analysis would then provide for winglets and tip extensions the trade information necessary to determine the cost effectiveness of these devices.

V DESIGN OF A WINGLET FOR THE KC-135

Data from the winglet parameter study provide a good basis for the selection of a final winglet planform and location. However, some additional factors must also be considered. The first one is the profile drag of the winglet itself. The second is wing/winglet interference. Recall that variations in winglet chordwise location, sweep, taper ratio, and area had little influence on induced drag. From an aerodynamic viewpoint, these parameters can therefore be chosen according to their impact on winglet profile drag and interference. On the other hand, selection of winglet length and cant angle will depend primarily on their potential effect on induced drag and secondarily on possible interference problems.

To minimize profile drag the winglet area should be as small as possible within the following constraints: (1) the winglet length must be chosen to obtain the desired reduction in C_{D_i} , and (2) the winglet chord distribution must be large enough so that sectional lift coefficients will not be too high. This latter item also impacts the taper ratio. The winglet sweep should be at least as high as the wing sweep since the winglet lies in the wing flow field. Winglet chordwise location will not affect profile drag but can have a significant influence on wing/winglet interference.

With the above thoughts in mind, a preliminary selection of a winglet planform was made. The trapezoidal planform is that of the upper winglet in figure 62. This is the same planform that was used in the earlier study to obtain a representative number for the potential drag reduction on the KC-135 with winglets. See figure 3. At this point there were still some questions concerning wing/winglet interference. Does the aft location of the winglet result in a satisfactory wing pressure distribution? What effect does cant have on the wing pressure distribution? What role does a lower surface winglet play in conjunction with the upper winglet? To answer these and other questions on interference, several analyses were made with computer program TEA-230 (See appendix A for program description). Both thickness and compressibility effects can be included in this program.

An upper surface winglet having the planform shown in figure 62 was designed in TEA-372 at a cant angle of 0° . The wing and winglet were then paneled up similar to the model shown in figure 63a and 63b, and the complete configuration was analyzed in TEA-230 at $M = .70$. Two other configurations were also analyzed. The upper surface winglet was canted out 20° for the second run. In the third run, the winglet was returned to its 0° cant position, and a lower surface winglet was added at 0° cant. This latter case is shown in figure 62, and the dimensions of the lower winglet are given there. Note that the lower winglet length is $0.03 b/2$.

The effects of upper winglet cant and the addition of a lower winglet are shown in the pressure distributions of figures 64 and 65. Wing pressure distributions at a spanwise location very near to the winglet are presented in figure 64. With the upper winglet at 0° cant and no lower winglet, there is a noticeable valley in the wing pressure distribution at about $x/c = 0.3$. The flow accelerates over the winglet, causing an aft

peak to develop on the wing at about $x/c = 0.6$. This peak will become even more accentuated as the Mach number is increased. This type of pressure distribution is thus undesirable because of a potential strong shock development and separation problems.

When the winglet is canted out 20° , there is some improvement in the pressure distribution. The valley is filled in slightly, and the aft peak drops and moves forward. Lower surface pressures show some increase. The addition of the lower winglet has similar beneficial effects. The valley is filled in considerably more than with cant, but the aft peak does not drop quite as much. The noticeable increase in pressure on the lower surface brings to light an important use of the lower winglet. Suppose that the outboard wing section cannot carry the desired increase in loading through reduction of upper surface pressures. A lower winglet could be added so that part of this load is carried by increasing the lower surface pressures. (A redesign of the upper winglet would be required). This might improve the upper surface flow enough so that the section would work properly. The analysis of the addition of a lower winglet estimated a 2% reduction in induced drag. The lower winglet also reduced the upper winglet leading-edge pressure peaks to provide pressure gradients which are more favorable to the boundary layer. This configuration would therefore be suitable for the low speed, high lift conditions that produce locally high crossflow components at the wing tip.

Figure 65 shows corresponding pressure data on the upper winglet at a section close to the wing. The primary effect of both cant and the lower winglet is the change in the leading-edge peak. When the winglet is canted outboard, the peak gets much higher (lower pressure). This result indicates that a winglet designed for a specific cant may not work well at another arbitrary cant angle. When the winglet is placed in a different crossflow field (by canting), the leading-edge droop must be changed to properly align it with the flow. The lower surface winglet has an opposite effect. It acts as a local flow straightener and results in a significant drop in the upper winglet peak (higher pressure). It has a negligible effect on the pressures over the remainder of the upper winglet. A lower winglet should not be required, though, to control the leading-edge pressure on the upper winglet. It should be possible to obtain a reasonable peak pressure by proper drooping.

V.A FINAL DESIGN

The final winglet planform selected for the KC-135 is shown in figure 66. A cant of 20° was chosen to obtain additional induced drag benefit and to reduce wing/winglet interference. The obvious difference of this planform from any previously considered is the presence of a strake. The strake was added because it significantly reduces the amount of twist required at the winglet root. This in turn facilitates the blending of the winglet into the wing via a smooth transition region.

The spanwise variation of twist and camber for the winglet were obtained from a TEA-372 design run in which the desired chordwise loading was specified. A thickness distribution used during previous winglet design work was then combined with the TEA-372 camber lines. The same thickness distribution was used across the entire span. Maximum streamwise thickness ratio was 0.066. Three streamwise sections through the final winglet are shown in figure 67. Note that over half of the winglet has a constant

section. Figure 68 shows the twist distribution of the final winglet. Winglet twist defined in an analogous manner to wing twist. For a winglet with 0° cant viewed from above, the twist angle is referenced to the streamwise direction with positive being leading edge inboard.

V.B ANALYSIS OF DESIGN

The TEA-230 modeling of the straked winglet is shown in figures 63a and 63b. Pressure data on the final wing/winglet configuration are shown in figures 69a-69e for the wing and figures 70a-70f for the winglet. Data are presented at configuration lift coefficients of 0.426 and 0.735. Corresponding winglet lift coefficients (based on its trapezoidal area) are 0.624 and 0.908. The first condition is the design cruise C_L . The second condition is one at which the winglet is roughly estimated to carry its highest possible load. It is provided for the purpose of determining winglet and outboard wing structural requirements.

Note that the shape of the wing pressure distribution at $\eta = 0.983$ (figure 69e) is much improved over those shown in figure 64. The winglet strake is the major factor in this improvement. Also, the leading-edge peaks across the winglet have been lowered to more acceptable levels than those in figure 65.

Span loadings from the TEA-230 wing alone and wing plus winglet solutions were analyzed in another computer program to obtain the induced drag reduction due to winglets. The calculated ΔC_{Di} was -15.5 drag counts. This compares with -13.4 counts which would be obtained using the TEA-372 data in figure 54. Winglet profile drag for the full-scale cruise condition was calculated by first adjusting the 3-D pressure data to $M = 0.77$ and then analyzing it in strips across the winglet in a 2-D boundary-layer program. A drag integration over the strips was finally made to obtain the value of 2.1 counts for both winglets. The profile drag change of the wing due to the lower cruise angle of attack was estimated from KC-135 wind tunnel data. This value is -3.4 counts. Note that it does not include the increase in profile drag that would occur on the outboard part of the wing due to its higher local angle of attack. The final estimate of full-scale drag improvement on the KC-135 is shown below.

ΔC_{Di}	=	-0.00155	<u>Flight Condition</u>
$\Delta C_{Dp\text{winglets}}$	=	0.00021	M = 0.77
$\Delta C_{Dp\text{wing}}$	=	-0.00034	$C_L = 0.426$
<hr/>			
net ΔC_D	=	-0.00168	

Airplane C_D without winglets = 0.0240 (ref. Boeing Document D3- 5599)

$$\text{Percent Improvement} = \frac{0.00168}{0.0240} \times 100 = 7.0\%$$

VI CONCLUSIONS

Due to the dihedral effect, the potential induced drag reduction of winglets on a KC-135 is greater than on a C-141. At their respective cruise conditions, 13.5% semispan winglets produced a 14% reduction in induced drag on the KC-135 and a 11% reduction on the C-141.

A stress analysis of the KC-135A wing subjected to the additional loads produced by winglets concluded the stress levels in the existing wing structure in the region of the 91% span station exceed the allowables as given by the KC-135 wing stress analysis document, reference 2. Therefore, for the KC-135A, only the outboard section of the wing would require structural modification for the addition of a winglet at the wingtip. An additional 204 lb. of wing weight would be required for a production installation of winglets and 364 lb for a prototype installation. The production winglet and attachment was estimated to weigh 388 lb. for a total installation weight of 592 lb. The total prototype installation weight was estimated to be 827 lb.

The advanced composite and advanced metallic winglet designs were estimated to weigh 24 and 27% less respectively than the conventional winglet structure. The prototype winglet fabrication costs were estimated to be 60 and 40% less respectively than the conventional design. For a production run of a hundred winglet sets, the fabrication costs were 18 and 27% less.

The drag polars for the KC-135A with winglets were estimated. The estimates include the profile drag of the winglets and the change in the wing drag. With these drag polars and the engine characteristics, the KC-135 with winglets was reoptimized for the cruise condition at a gross weight of 210 000 lb. The winglet configuration optimized to a higher altitude, Mach number and lift coefficient than the basic KC-135. Comparing the cruise conditions, the winglet configuration altitude is 3.4% higher, Mach number is 0.52% higher, C_L is 4.88% greater, L/D is 7.8% greater, M(L/D) 8.4% greater, TSFC is 0.3% greater, range factor is 8.1% greater and the range, for the ferry mission is 7.5% improvement. The preliminary flutter analysis indicated that the KC-135A with winglets would be flutter free up to and including 1.15 V_D condition. A more detailed flutter analyses, considering a variety of fuel loadings, will be required in future studies.

The winglet described in section V.A was designed for the KC-135 and this design was used to build a set of 0.035 scale winglet wind tunnel models and a 0.070 scale wind tunnel model. The 0.035 scale winglets will be tested on a full model of the KC-135. This model will include nacelles, vertical stabilizer and horizontal stabilizers and is a sting mounted, internal strain gage balance model. The incidence angle of the winglet will be variable to allow the optimization of this parameter.

The 0.070 scale winglet was constructed for a half-model of KC-135 which is owned by the NASA-Langley Research Center. This particular winglet did not have the variable incidence capability. This winglet configuration has been tested in the NASA 8 ft

Transonic Wind Tunnel. Preliminary unpublished test data have substantiated the analytical procedures used by the Boeing Company to determine the aerodynamic characteristics and performance benefits from winglets on the KC-135 aircraft.

Equal area wingtip extensions were analyzed and compared with winglets. A general conclusion made from this study was that winglet can reduce the induced drag with smaller increase in wing-root bending moment and pitching moment than a wingtip extension.

This study has shown the winglets produce a significant reduction in fuel consumption on the KC-135A. The preliminary analyses and designs completed in aerodynamic, flutter, stress, loads, weights, and manufacturing disciplines indicate no major problems. However, as final proof of the winglet performance, a flight demonstration program is recommended. This program should include the detailed design, fabrication, installation, ground tests and flight tests of winglets on a KC-135A, see reference 5.

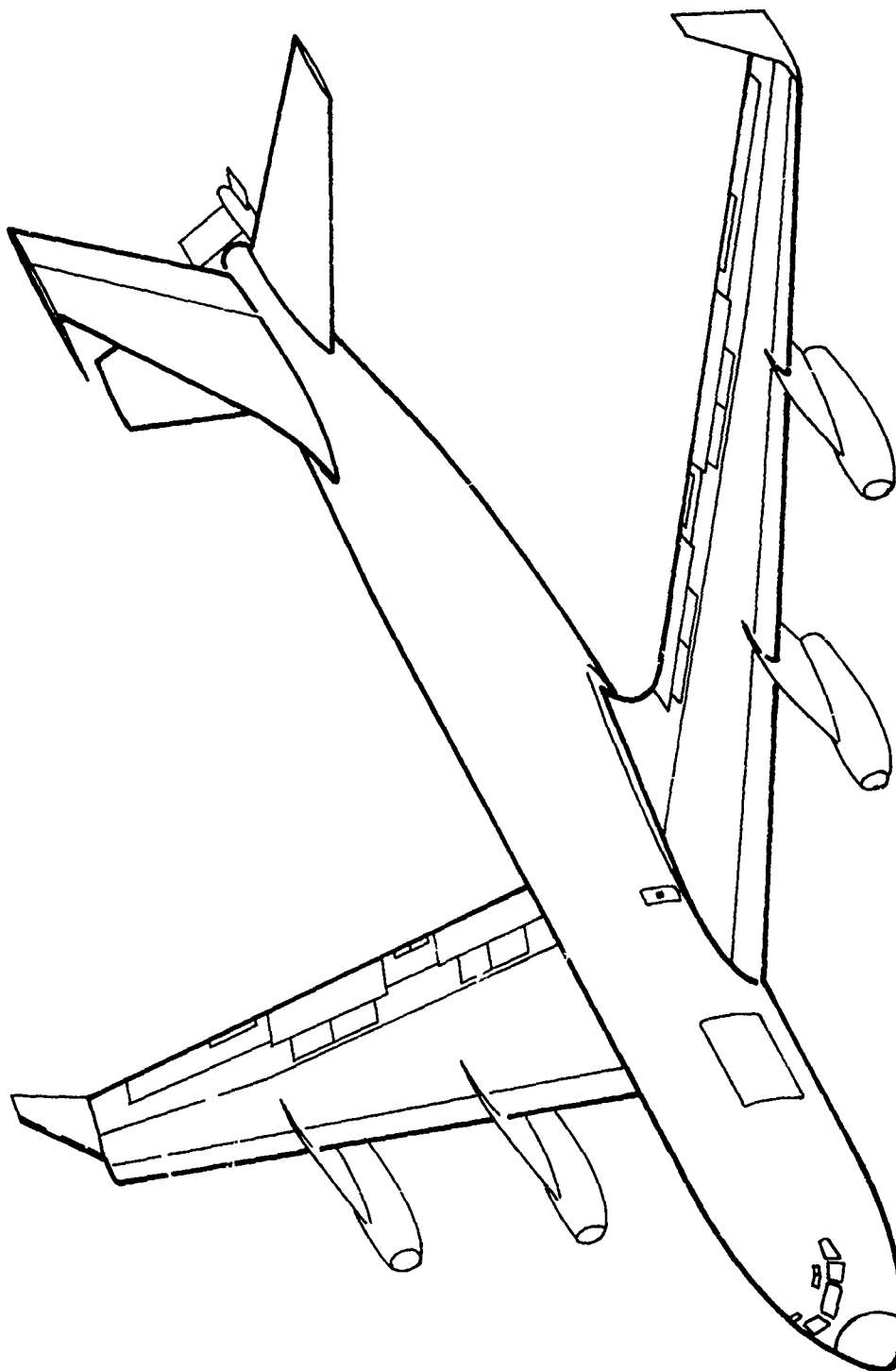


Figure 1.—Typical Winglet Application

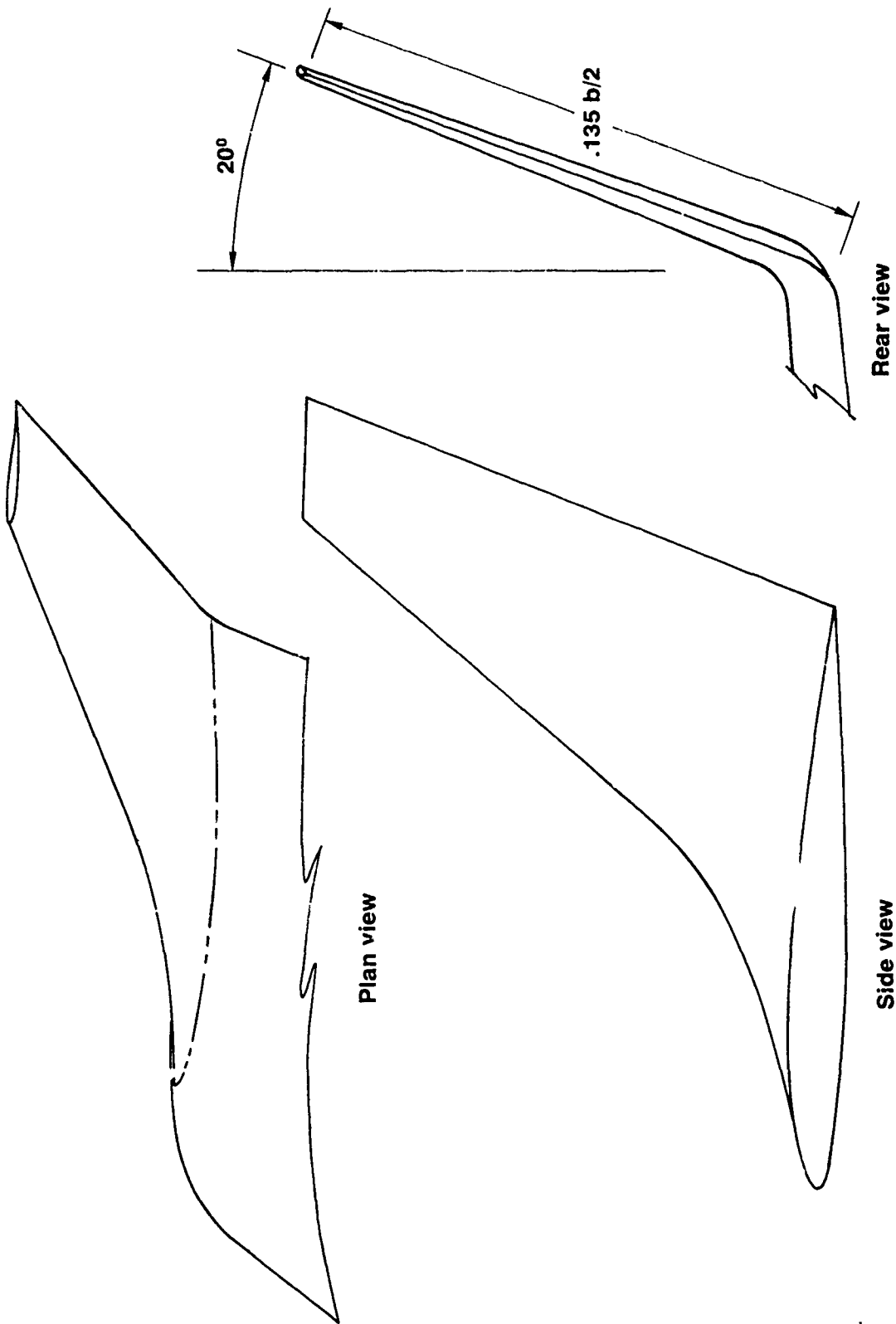


Figure 2.—Wind Tunnel Model Winglet Design

Taper ratio = .338
AR = 2.33

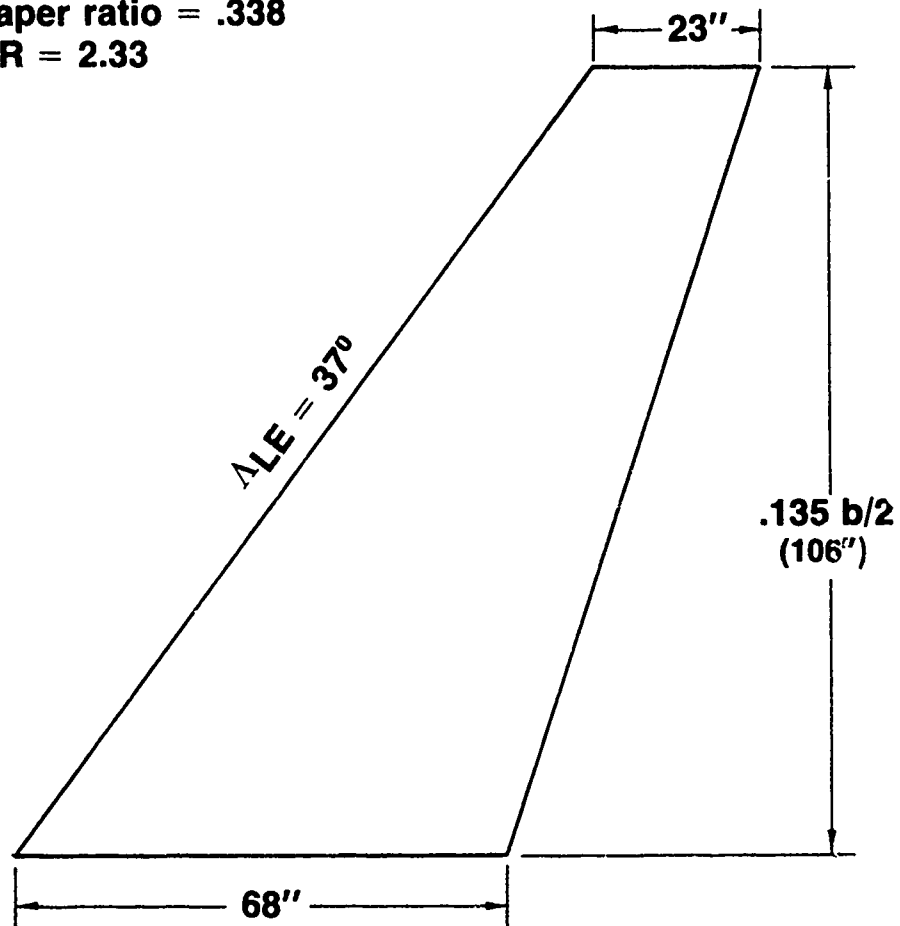
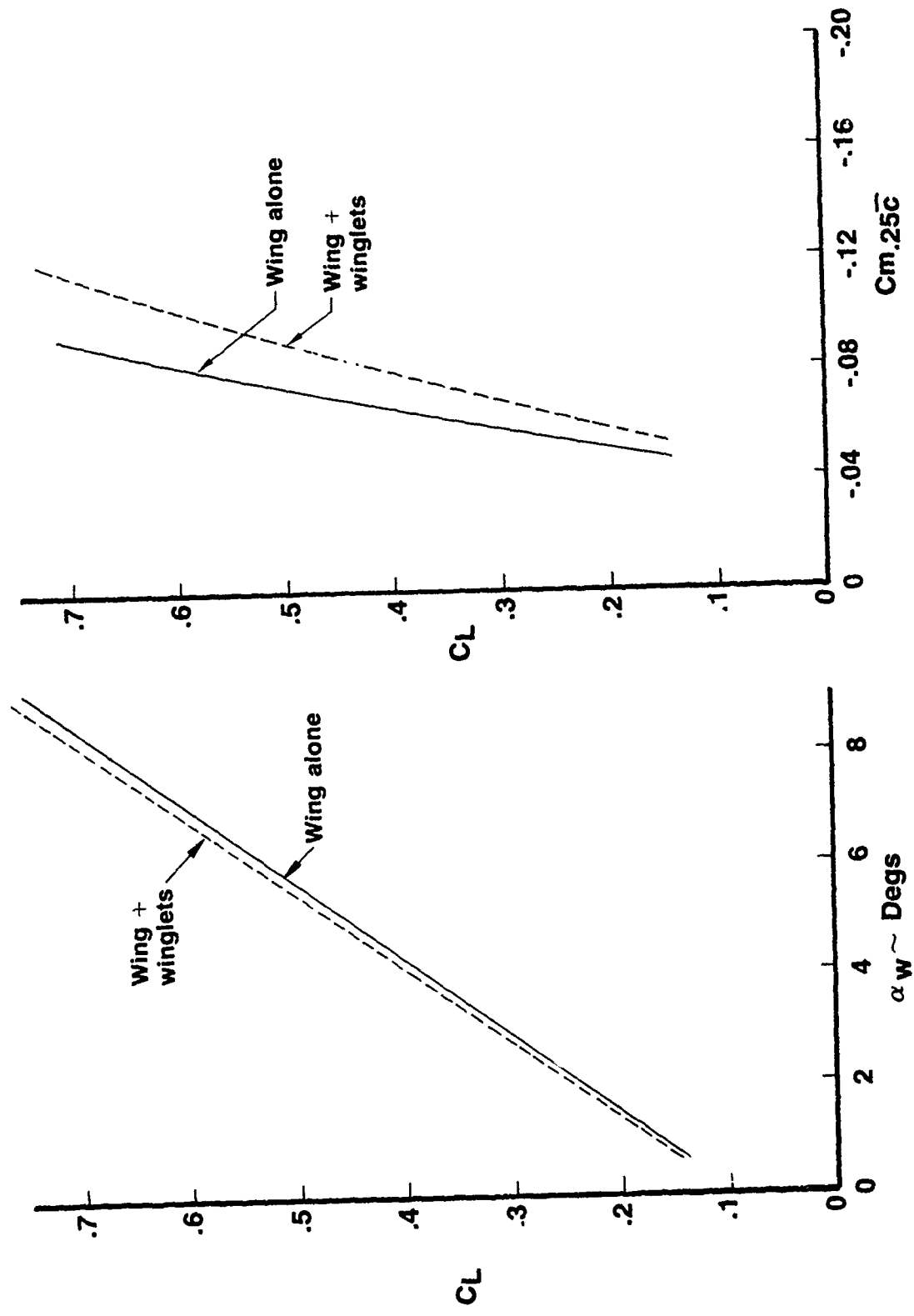
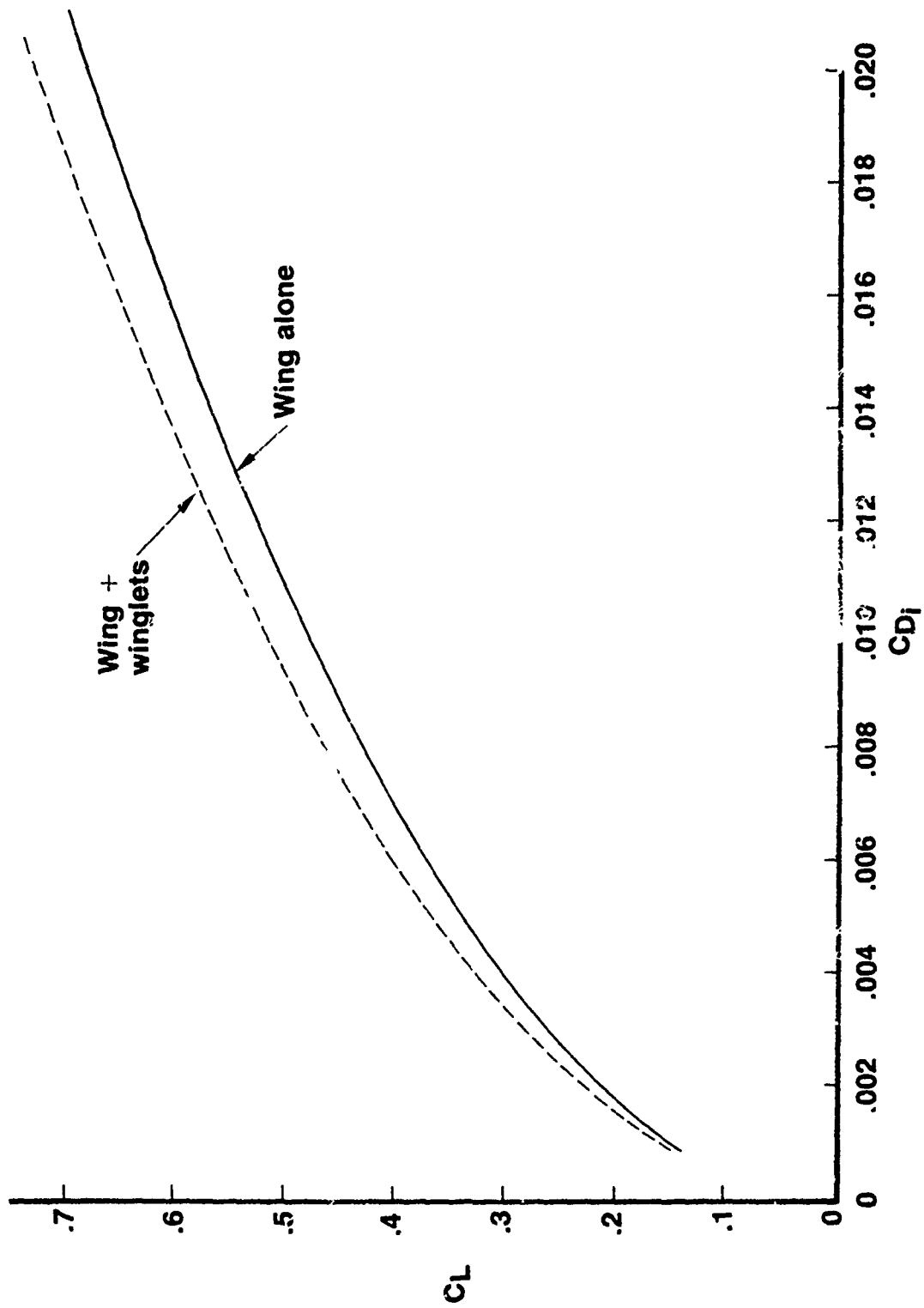


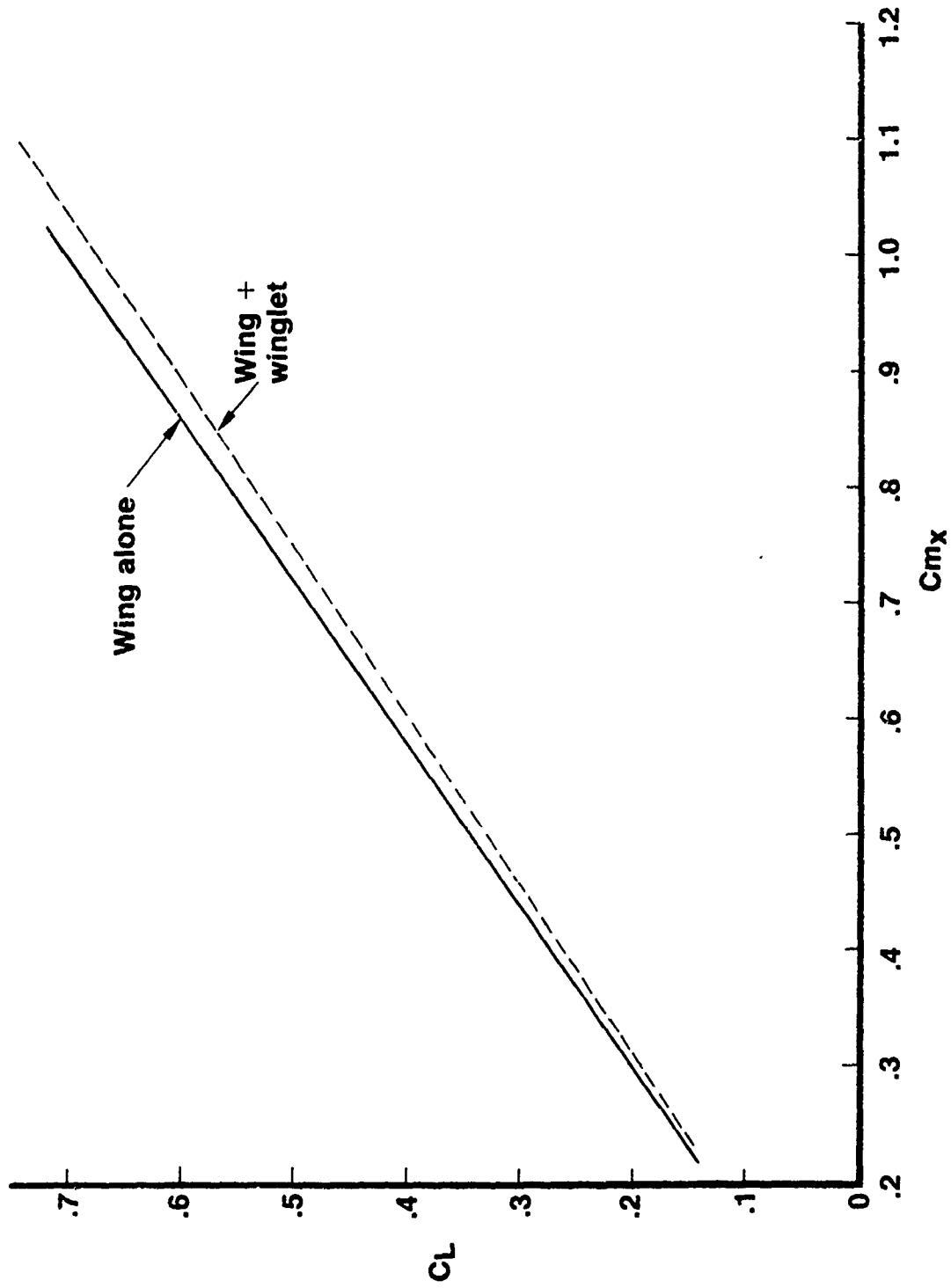
Figure 3.—KC-135 Winglet Planform



a (Lift and Pitching Moment)
 Figure 4.--Effect of 0.135 b/2 Winglets on KC-135



b (Induced Drag)
 Figure 4.—(Continued)



c (Wing-Root Bending Moment)
 Figure 4. - (Concluded)

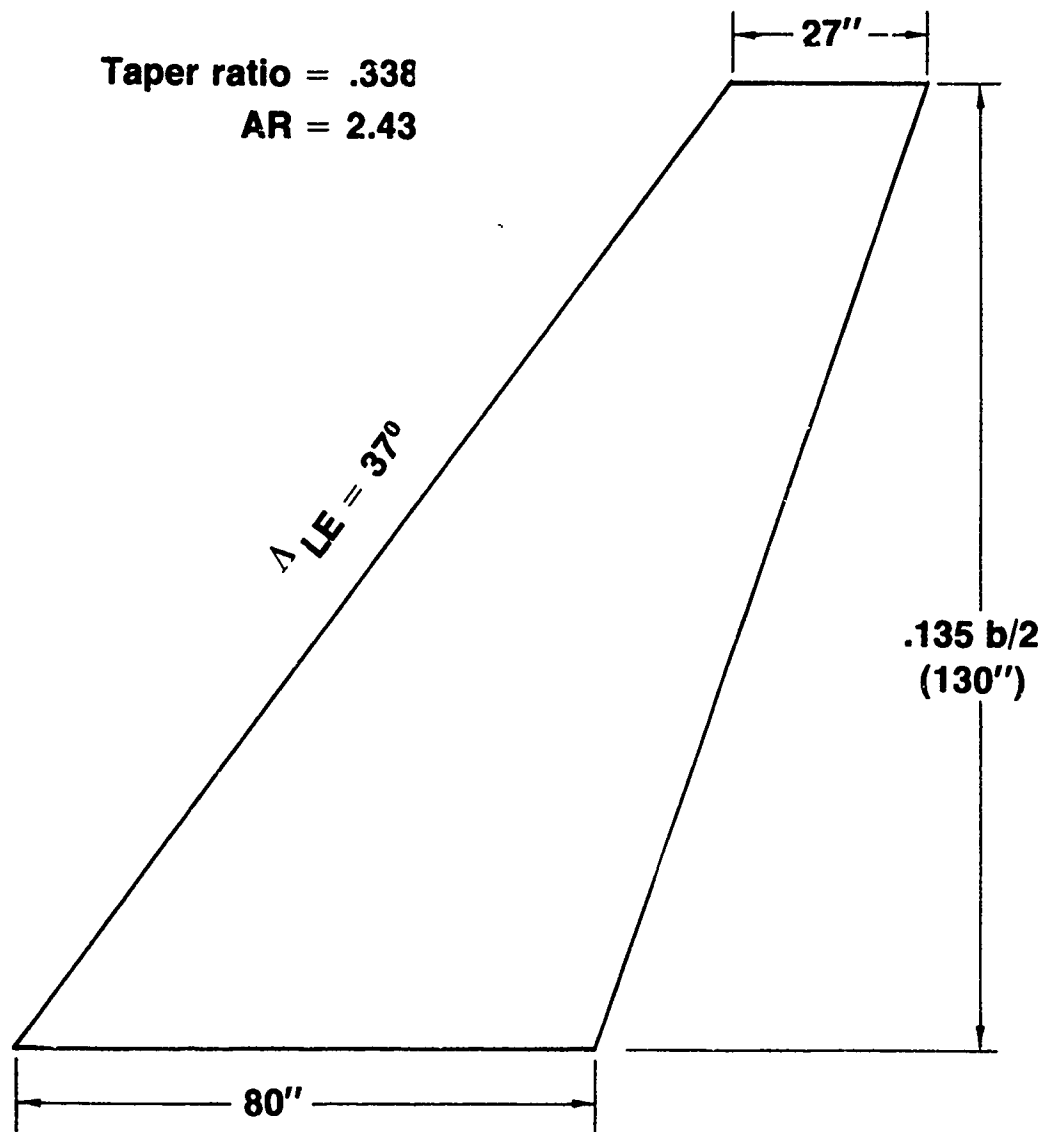
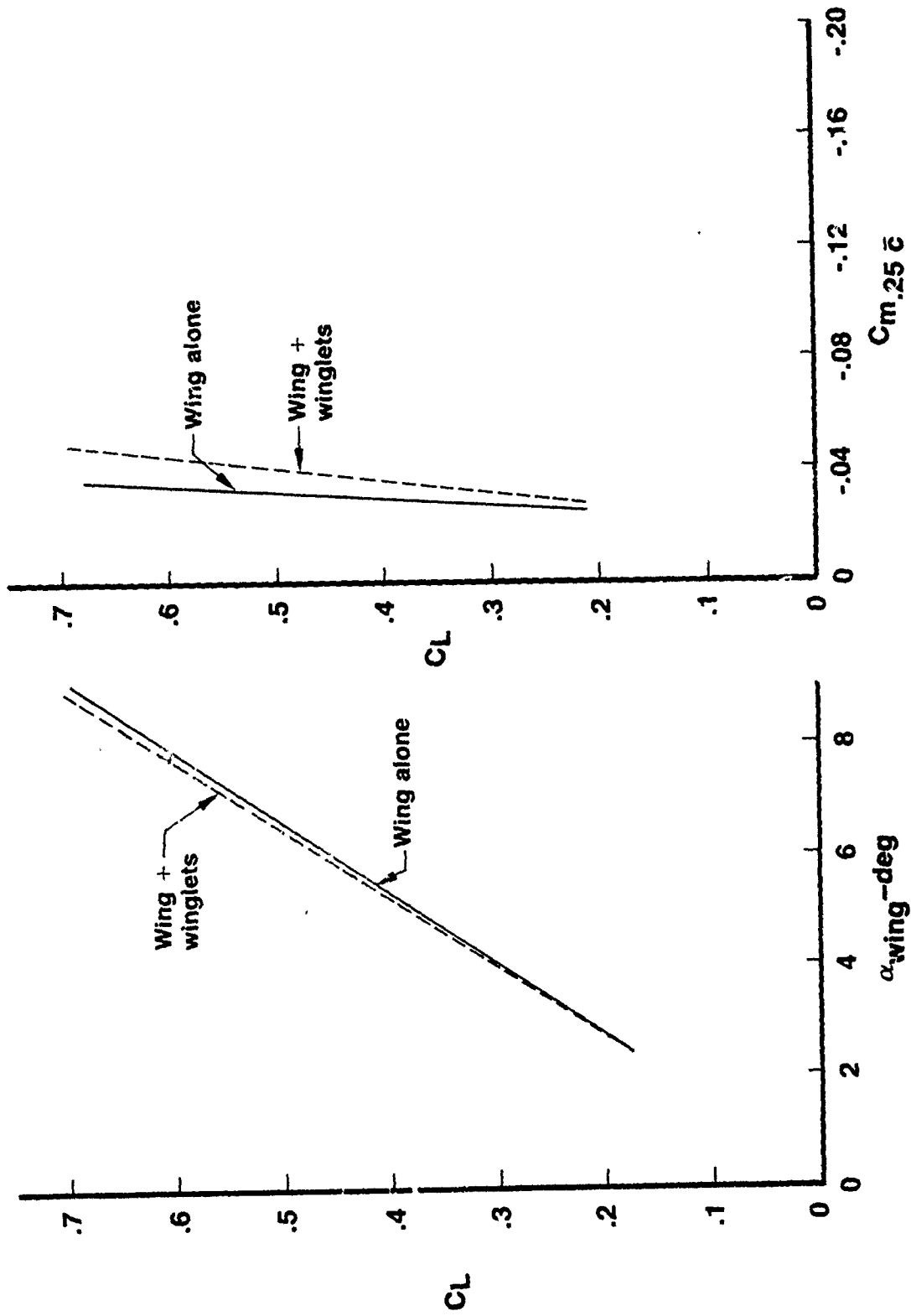
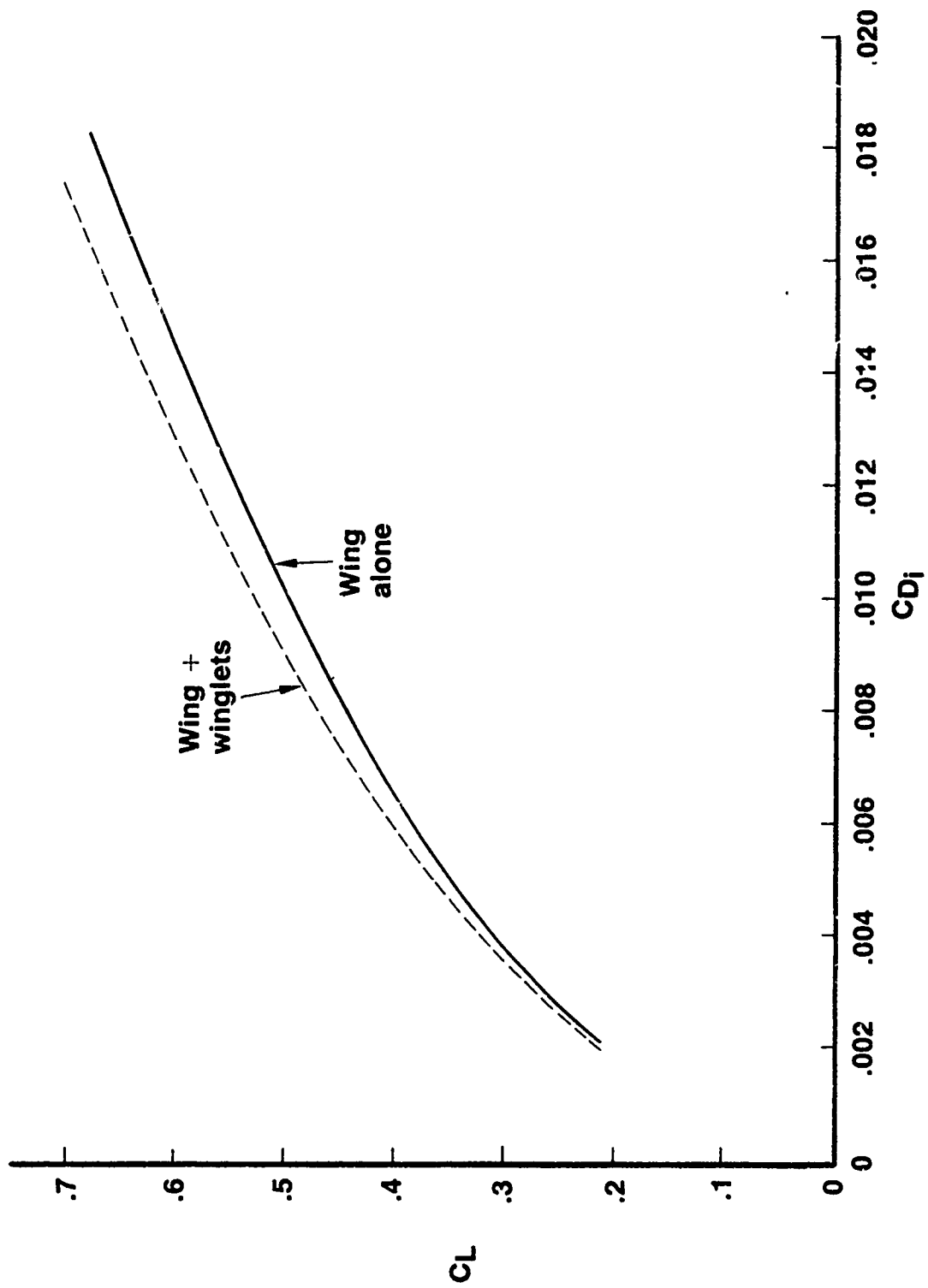


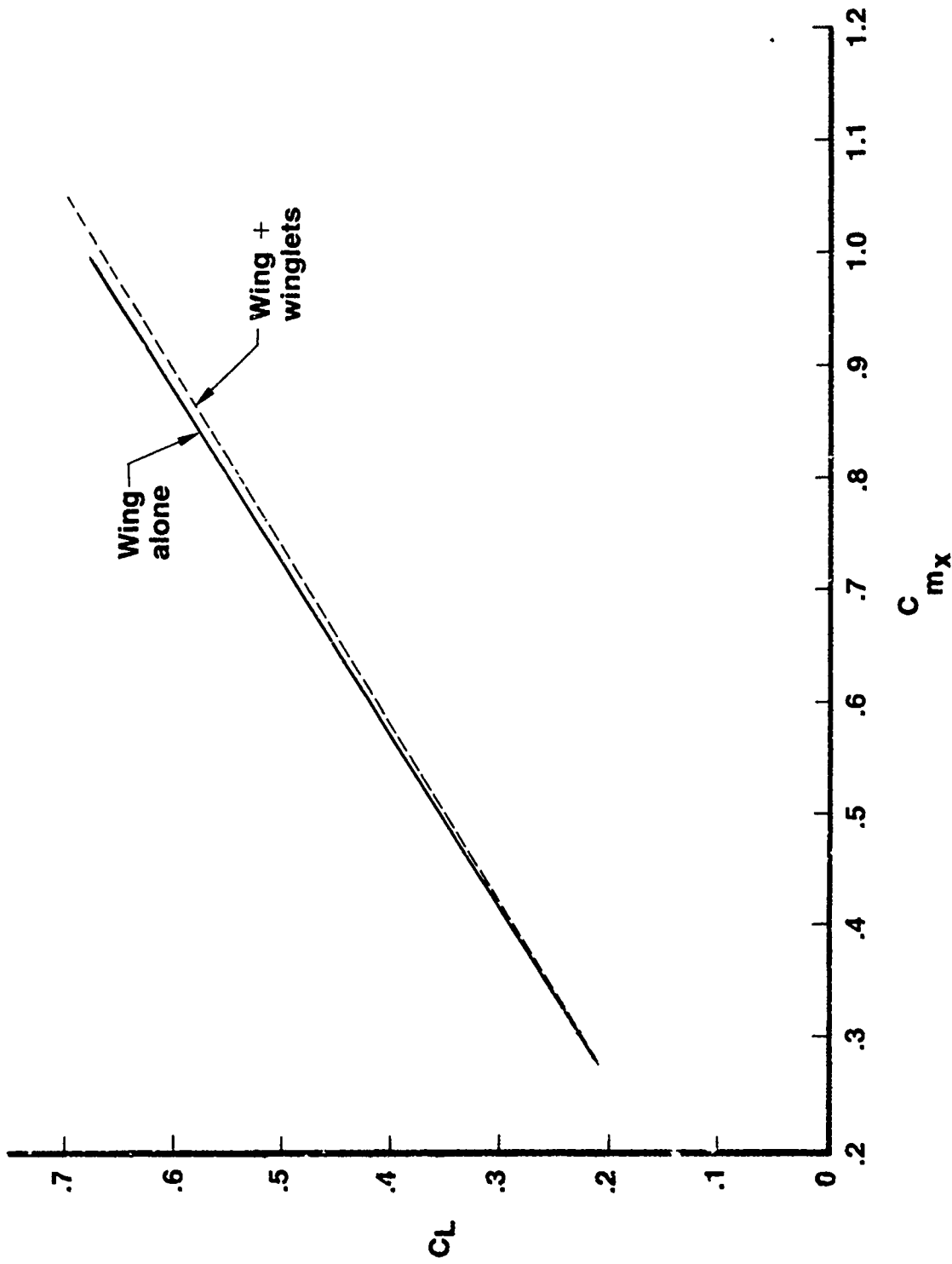
Figure 5. - C-141 Winglet Planform



a (Lift and Pitching Moment)
 Figure 6.—Effect of 0.135 b/2 Winglets on C-141

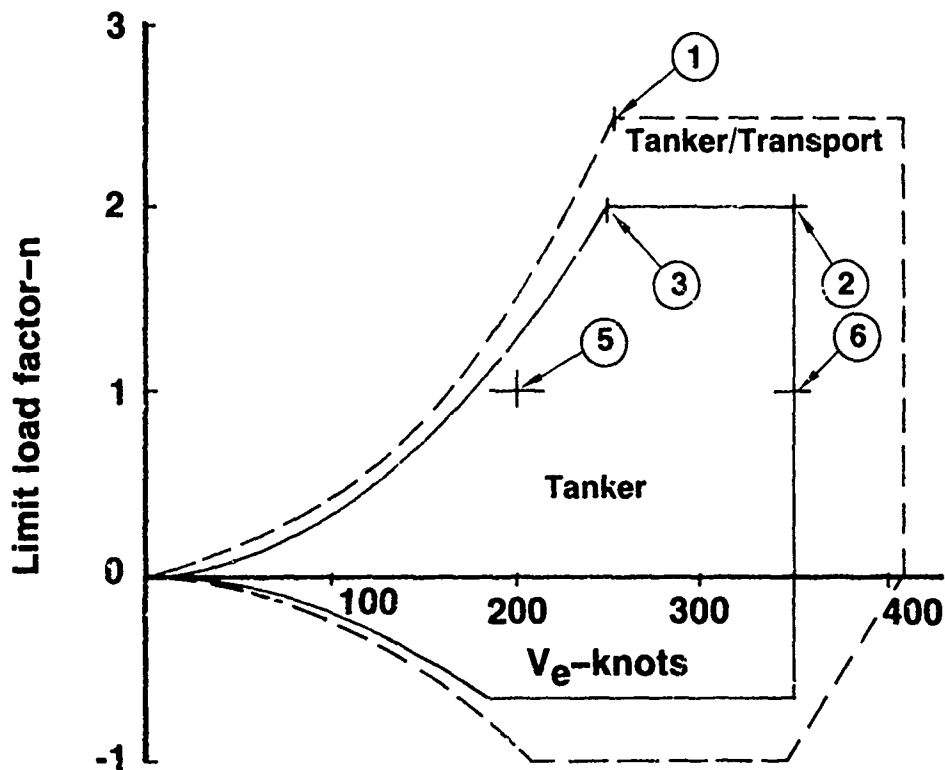


b (Induced Drag)
 Figure 6.--(Continued)



c (Wing-Root Bending Moment)
 Figure 6. - (Concluded)

- Flight V-n envelope**
- Gross weight = 297,000 lbs
 - Altitude = sea level
 - Flaps up



Note:

- Wing design condition-1, 2, and 3
- Winglet design condition-1, 2, 5, and 6
- Condition 2 is the same on the V-n diagram but at 29,000 ft
- Condition 5 side gust velocity-65 ft/sec
- Condition 6 side gust velocity-50 ft/sec and at 24,000 ft (vertical fin gust cond.)

Figure 7.—Symmetric Manuever Conditions

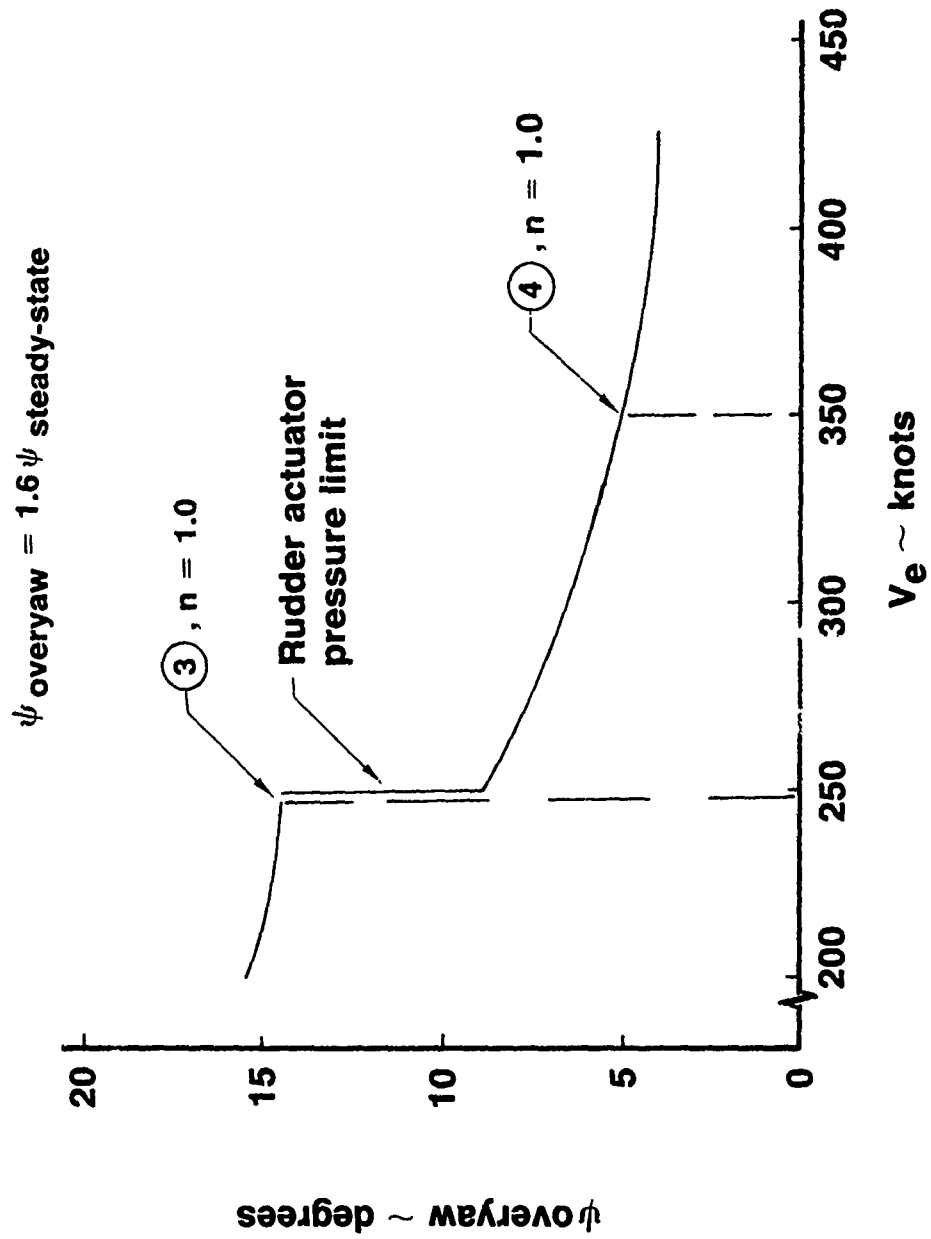


Figure 8.—Overyaw Conditions

$$\eta = \frac{y}{106}$$

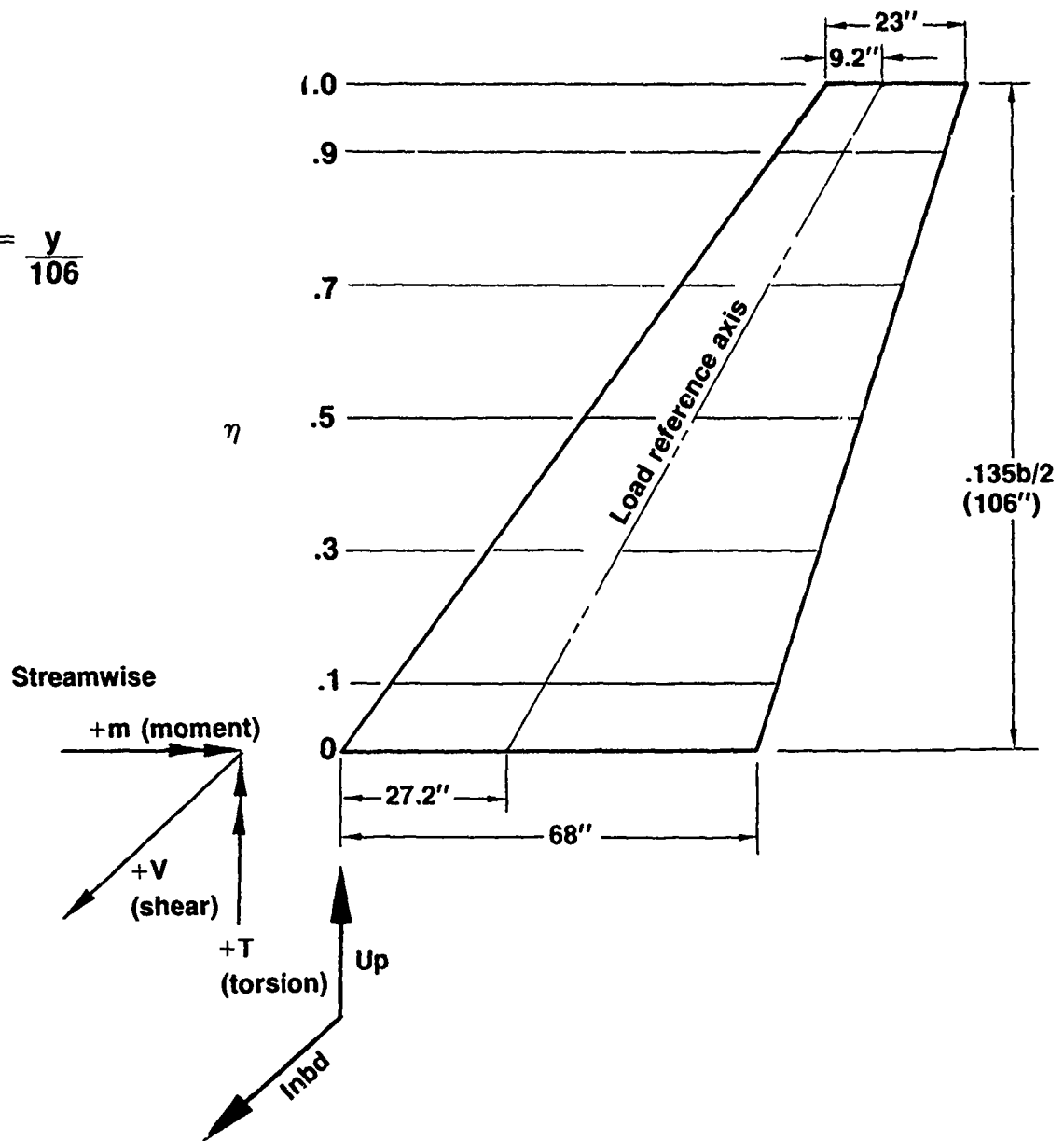


Figure 9.— KC-135A Winglet Load Reference Axis

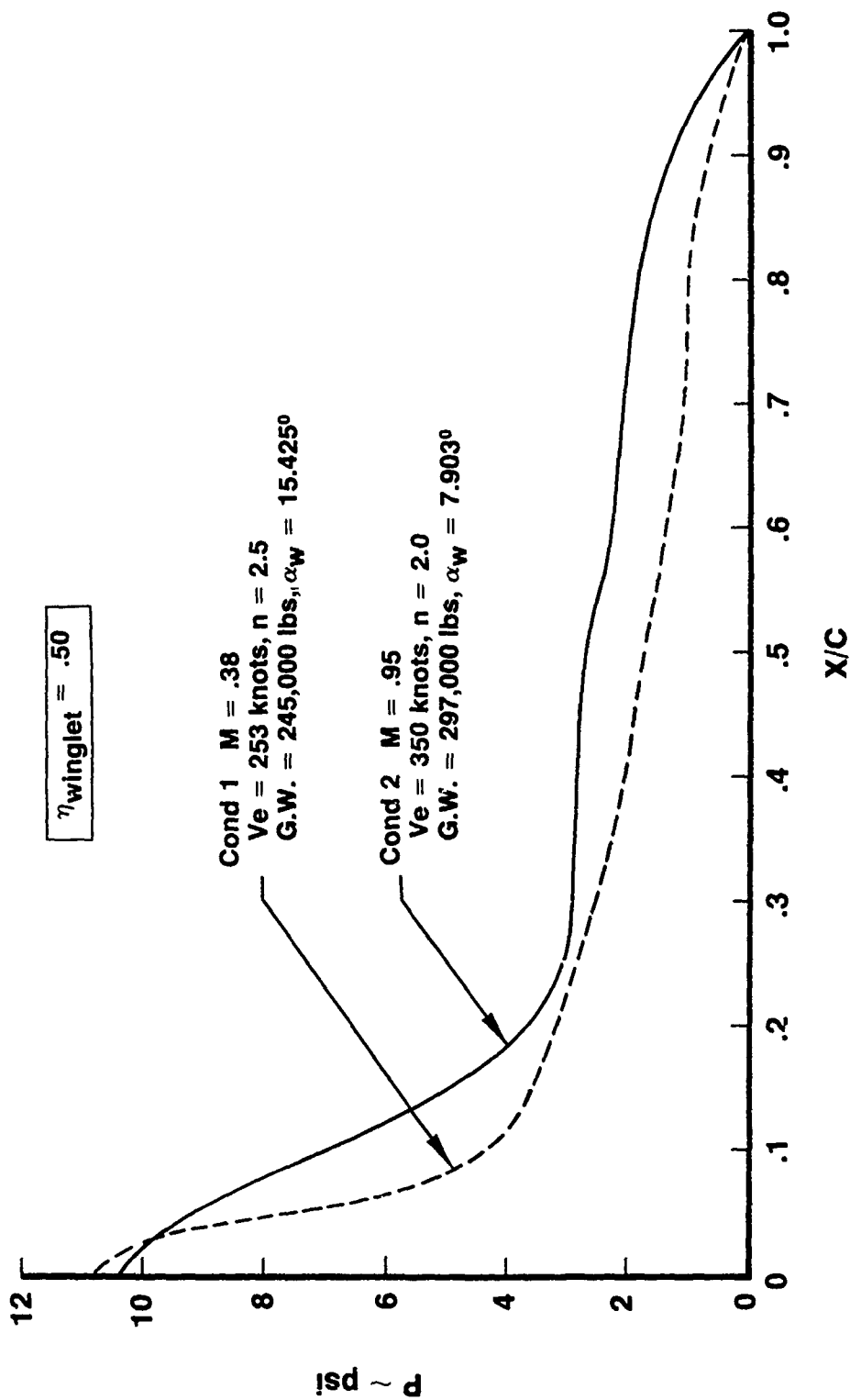


Figure 10.— Ultimate Chordwise Pressure Distribution for Symmetric Flight Conditions

$\eta_{\text{winglet}} = .50$

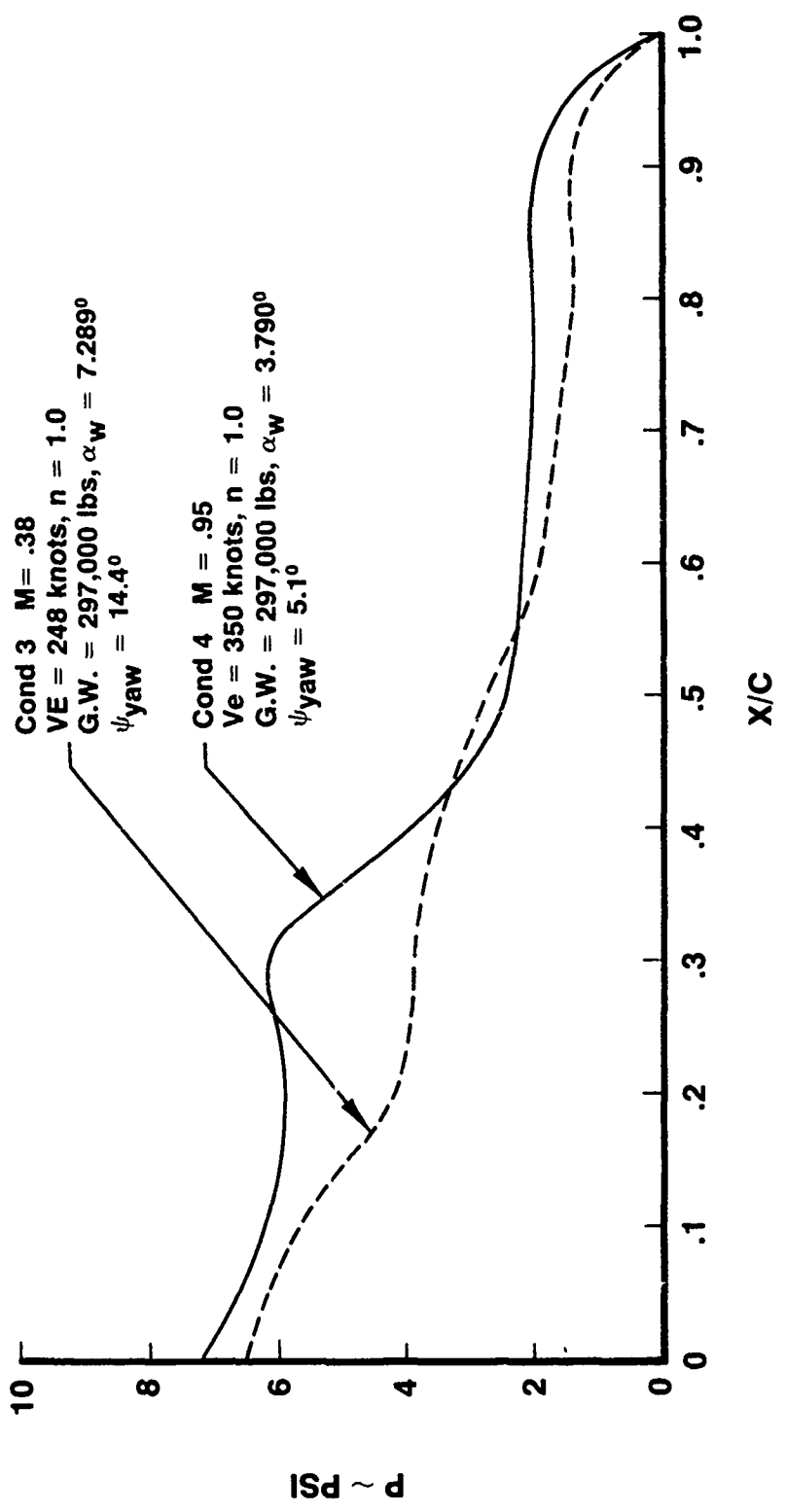


Figure 11.—Ultimate Chordwise Pressure Distribution for Unsymmetric Flight Conditions

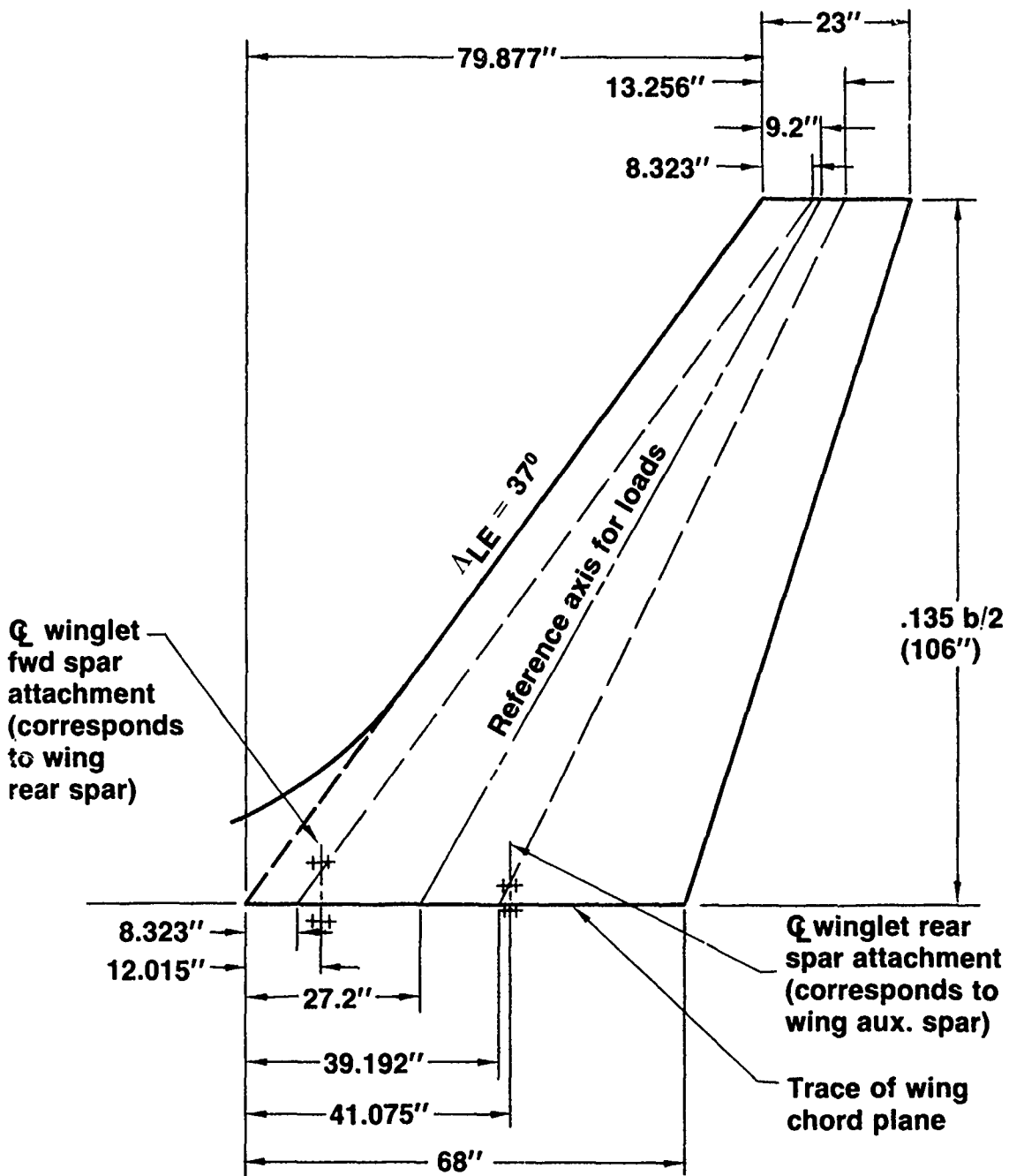


Figure 12.—Winglet Geometry

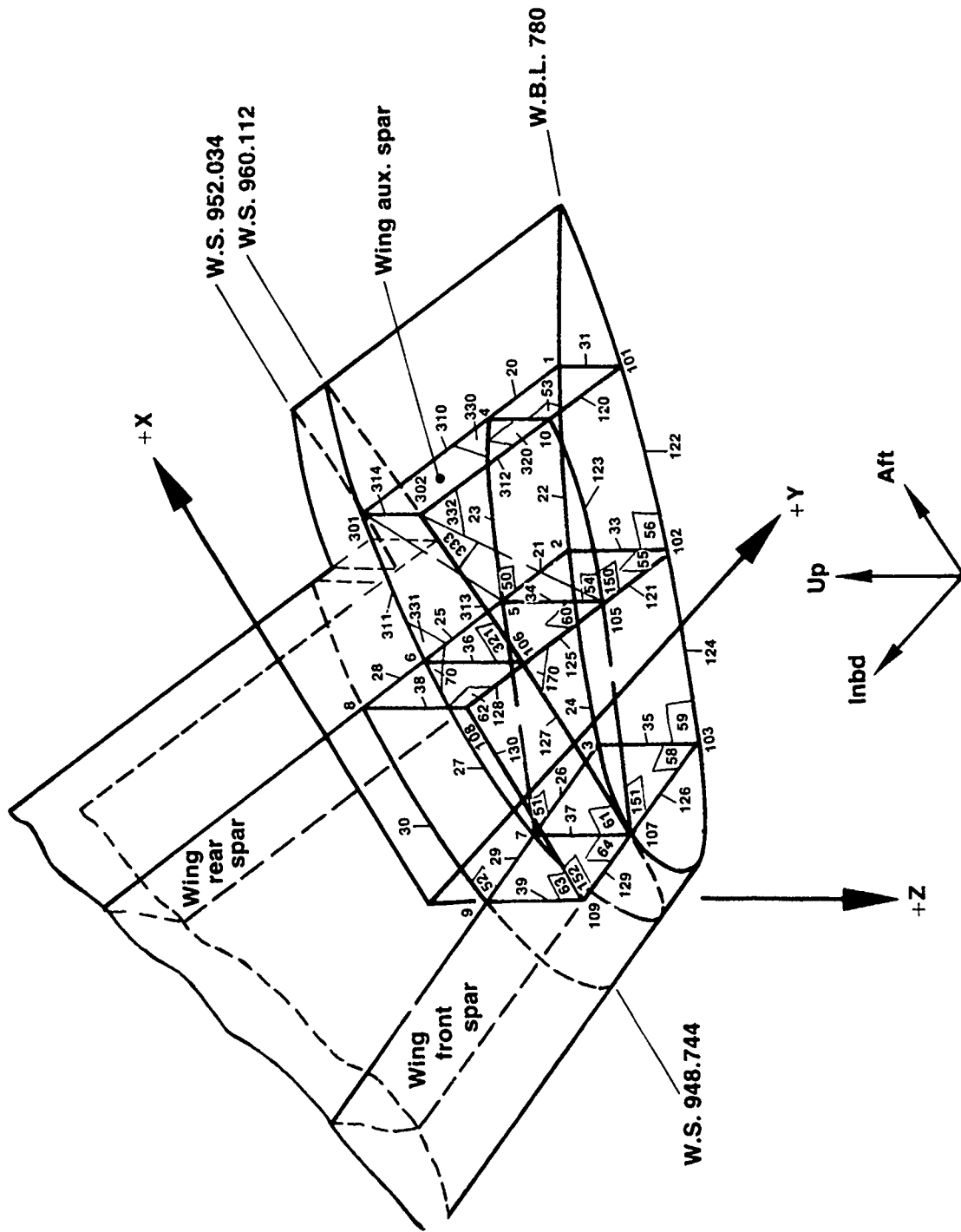


Figure 13.— Nastran Model, Winglet to Wingtip Detail

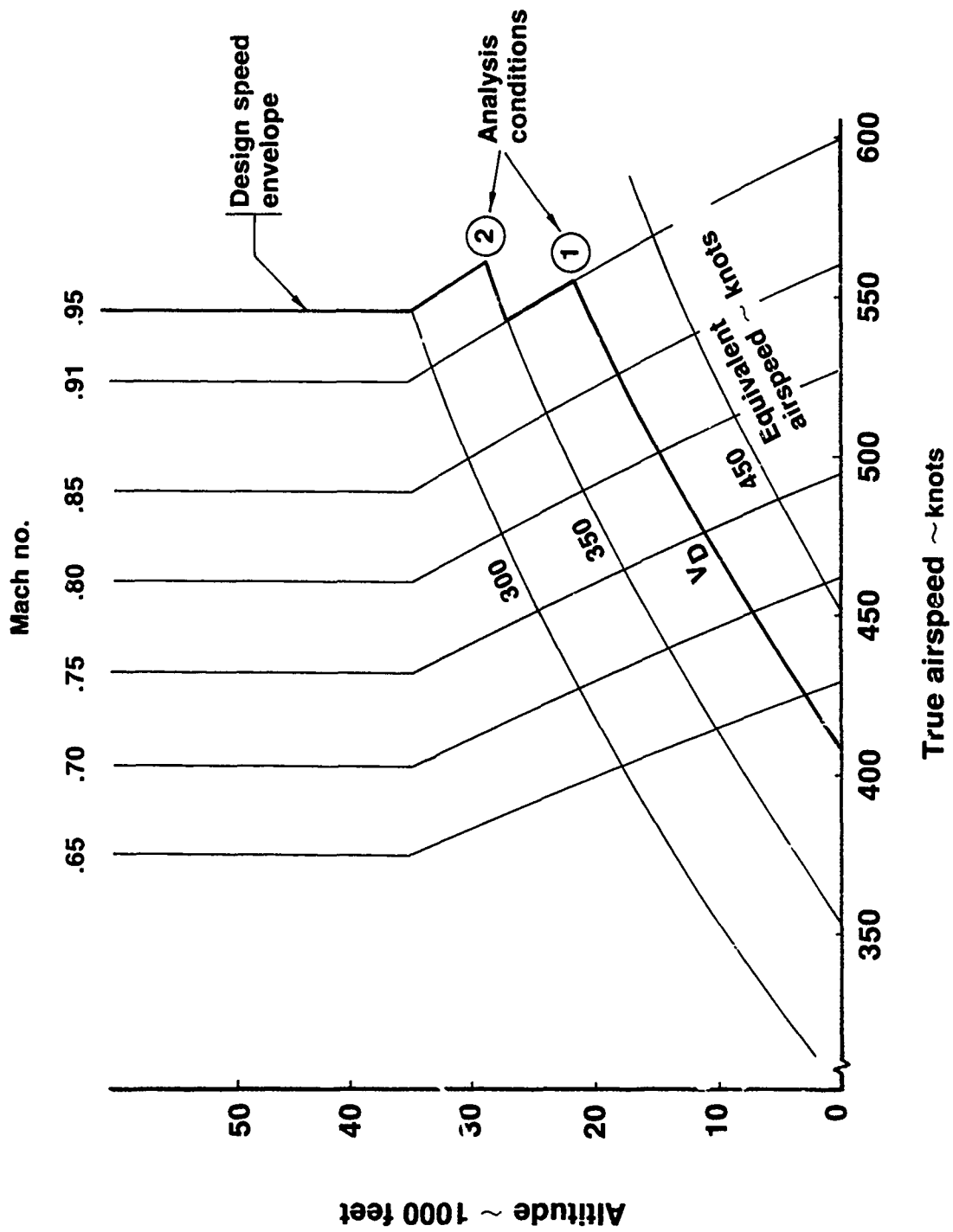


Figure 14. - Flutter Analysis Conditions

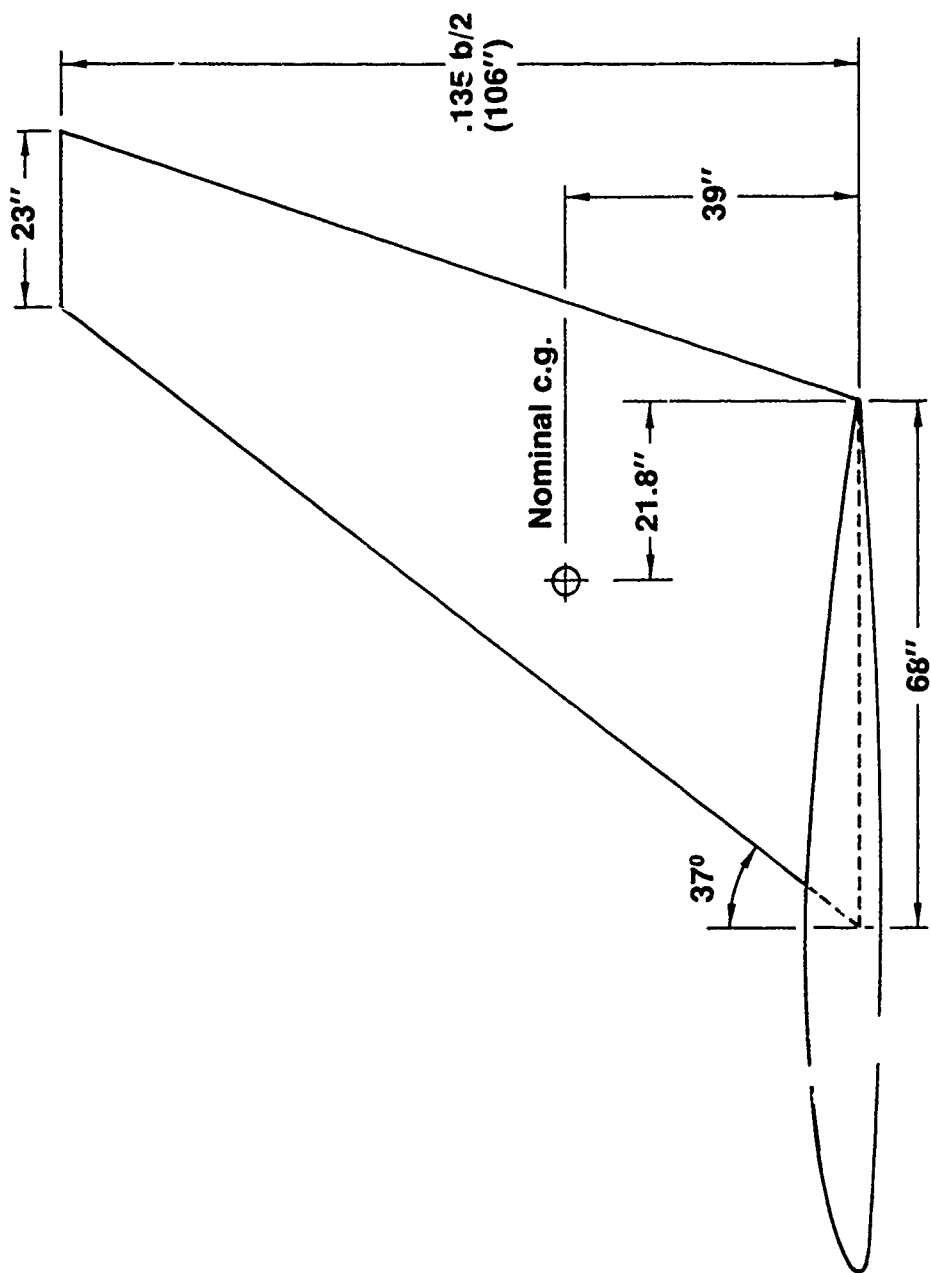


Figure 15.—Nominal KC-135A Winglet

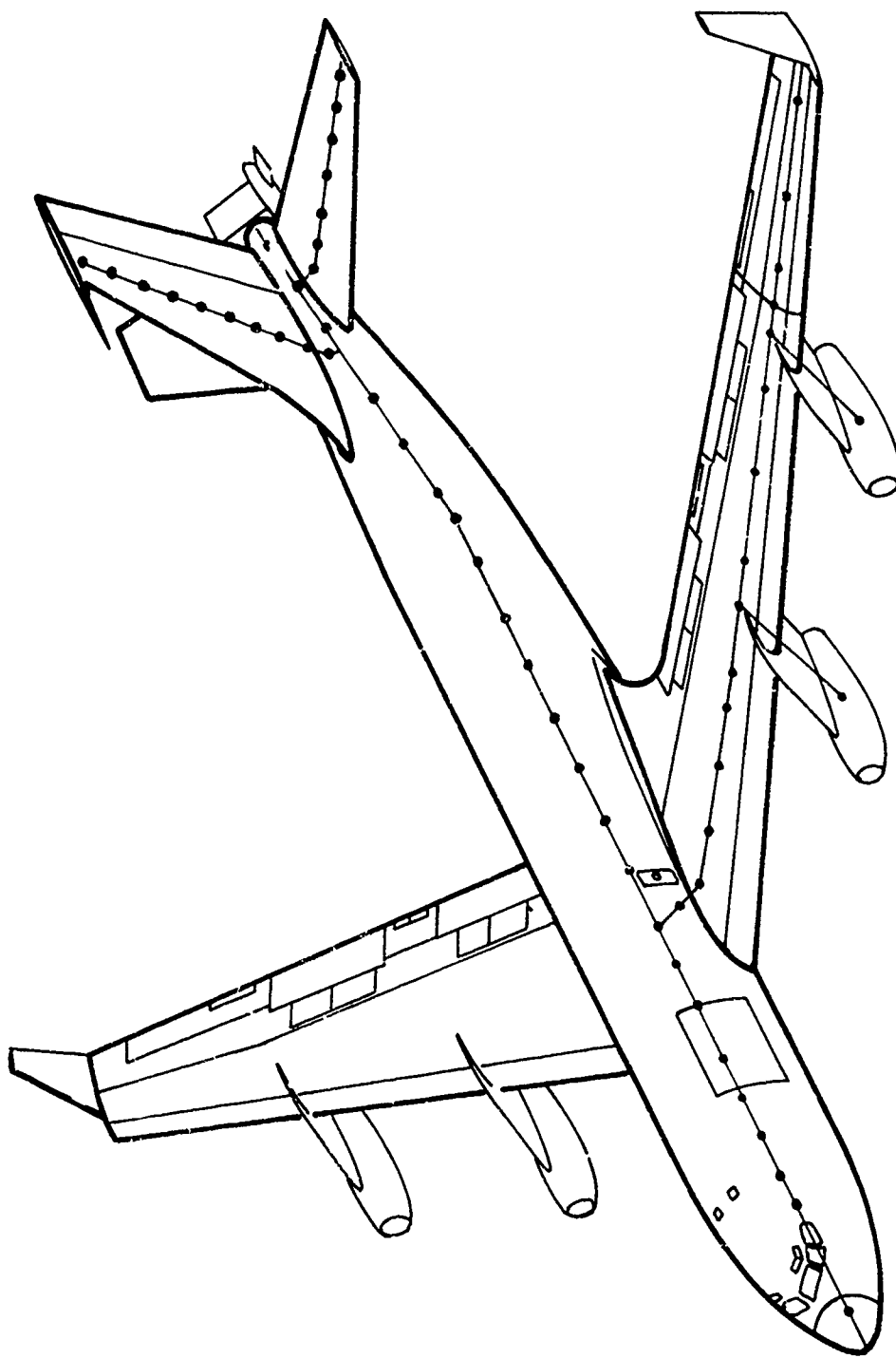


Figure 16.— Vibration Model

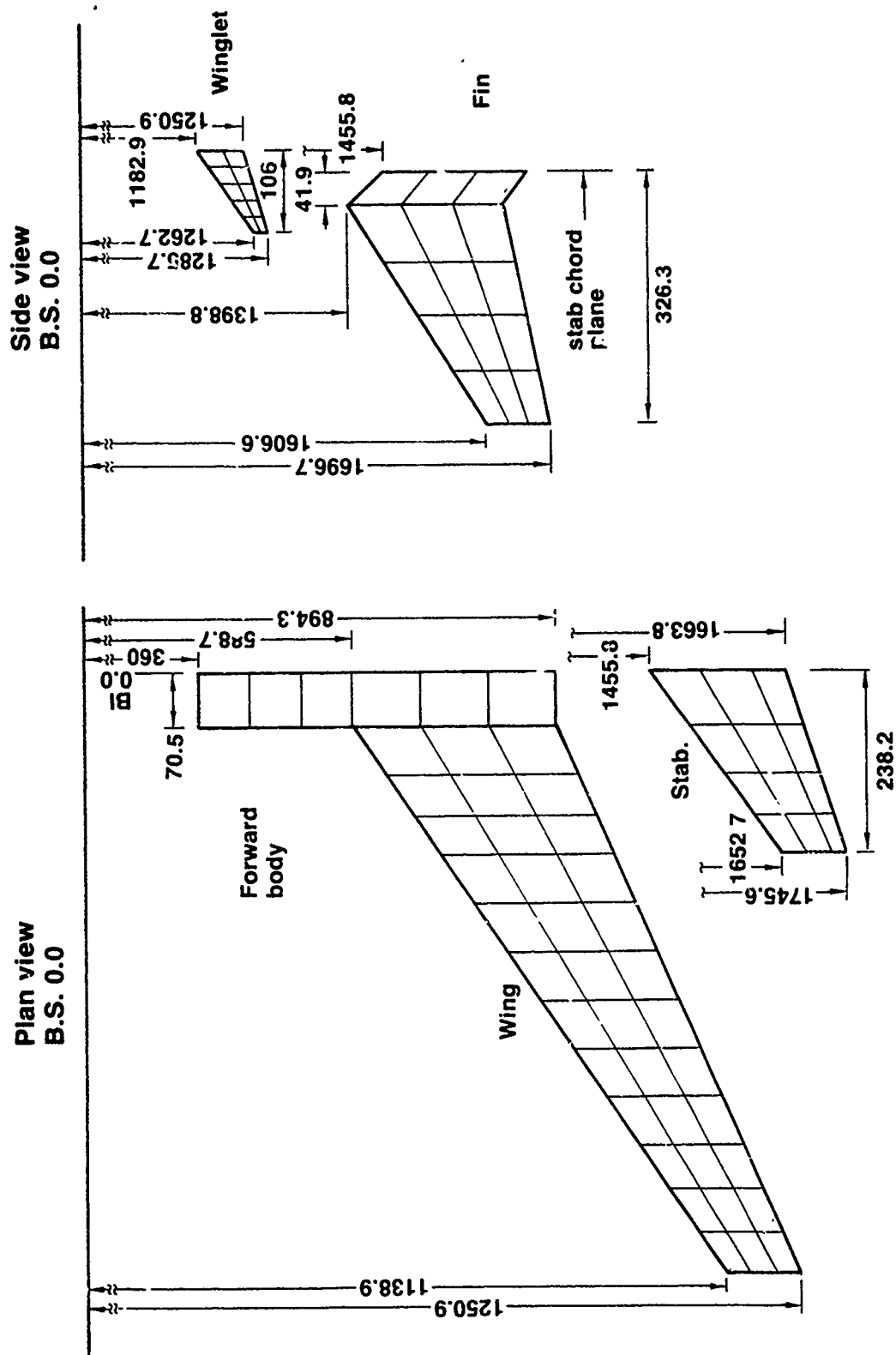


Figure 17. — Aerodynamic Panels in the X-Y and Y-Z Planes

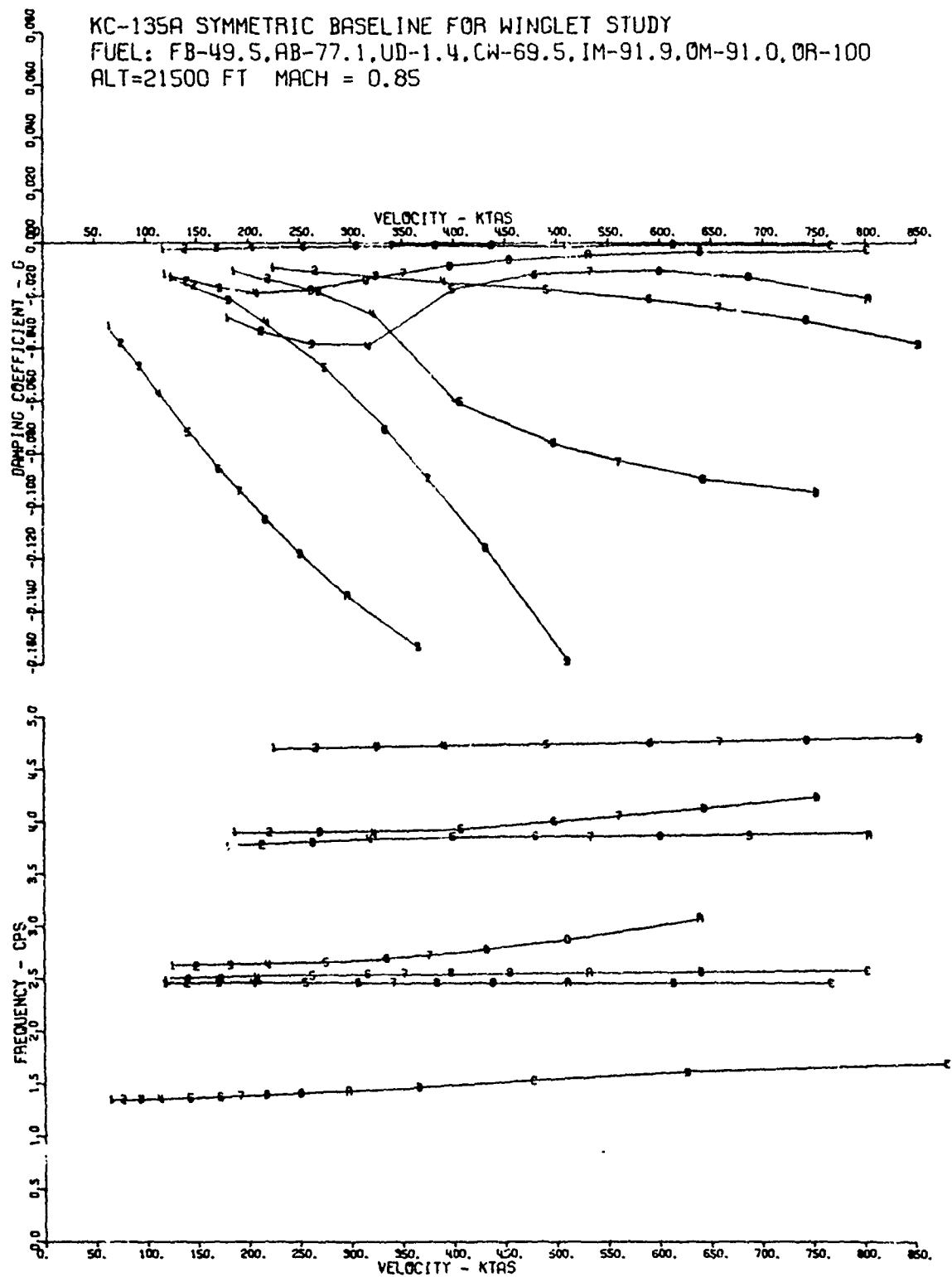


Figure 18.-- Symmetric Baseline

KC-135A SYMMETRIC WITH NOMINAL WINGLET AT WBL 780
 FUEL: FB-49.5, AB-77.1, UD-1.4, CW-69.5, IM-91.9, OM-91.0, OR-100
 ALT=21500 FT WINGLET WT=141.3 LB MACH=0.85

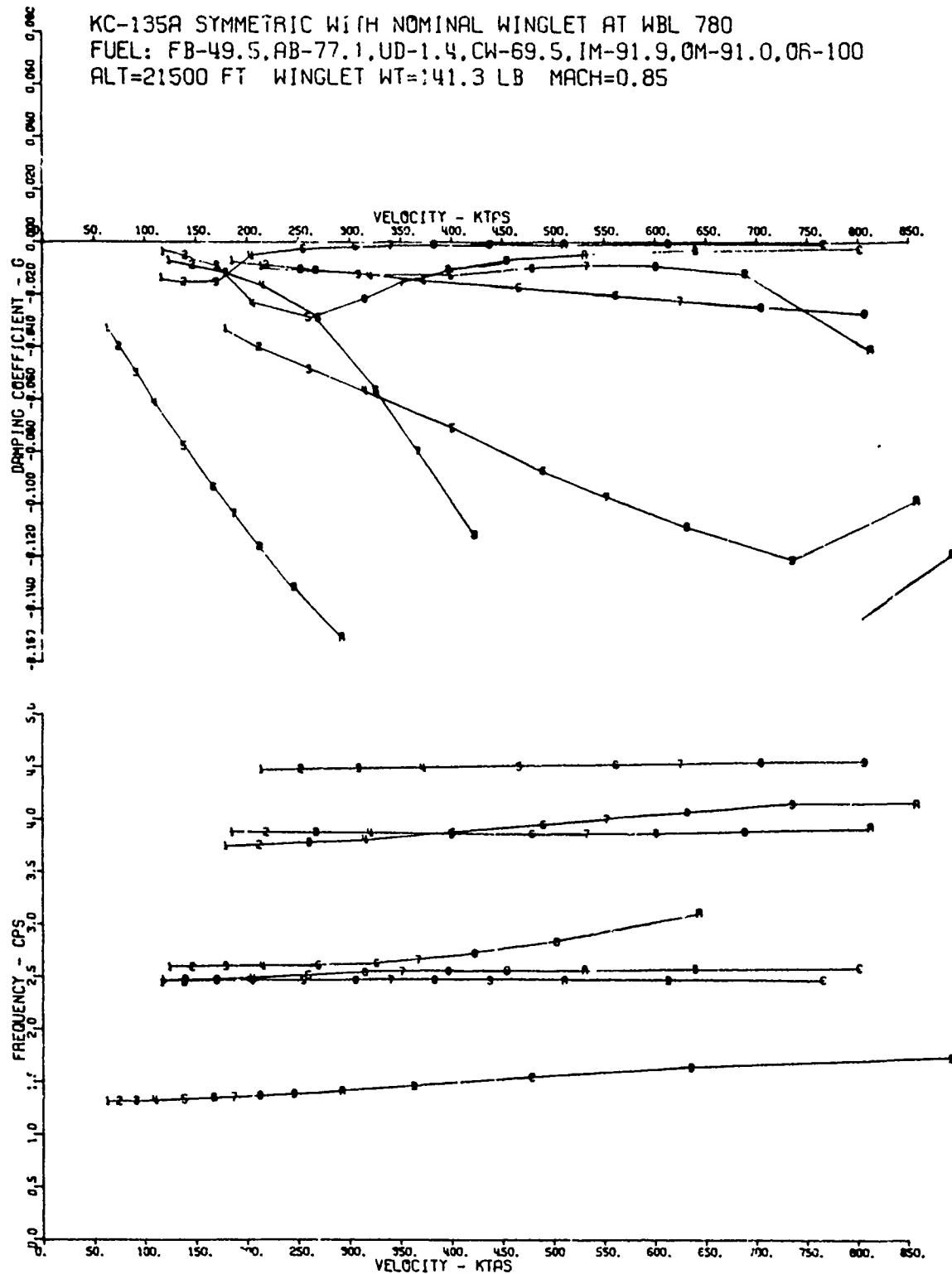


Figure 19.--Symmetric with Nominal Winglet

KC-135A ANTISYMMETRIC BASELINE FOR WINGLET STUDY
 FUEL: FR-49.5, AB-77.1, UD-1.4, CW-69.5, IM-91.9, OM-91.0, OR-100
 ALT=21500 FT MACH=0.85

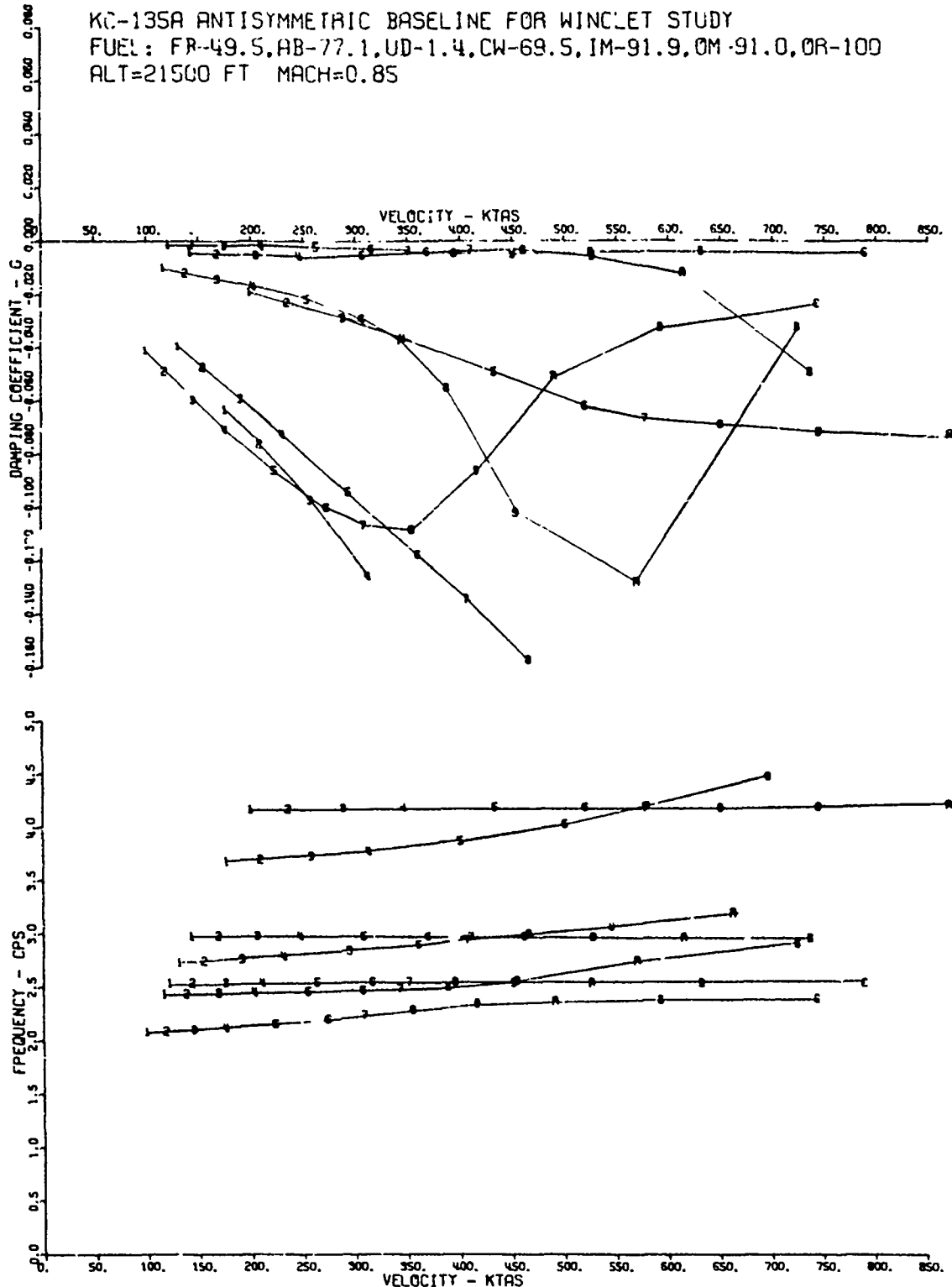


Figure 20.— Antisymmetric Baseline

KC-135A ANTISYMMETRIC WITH NOMINAL WINGLET AT WBL 780
 FUEL: FB-49.5, AB-77.1, UD-1.4, CW-69.5, IM-91.9, OM-91.0, OR-100
 ALT=21500 FT WINGLET WT=141.3 LB MACH=0.85

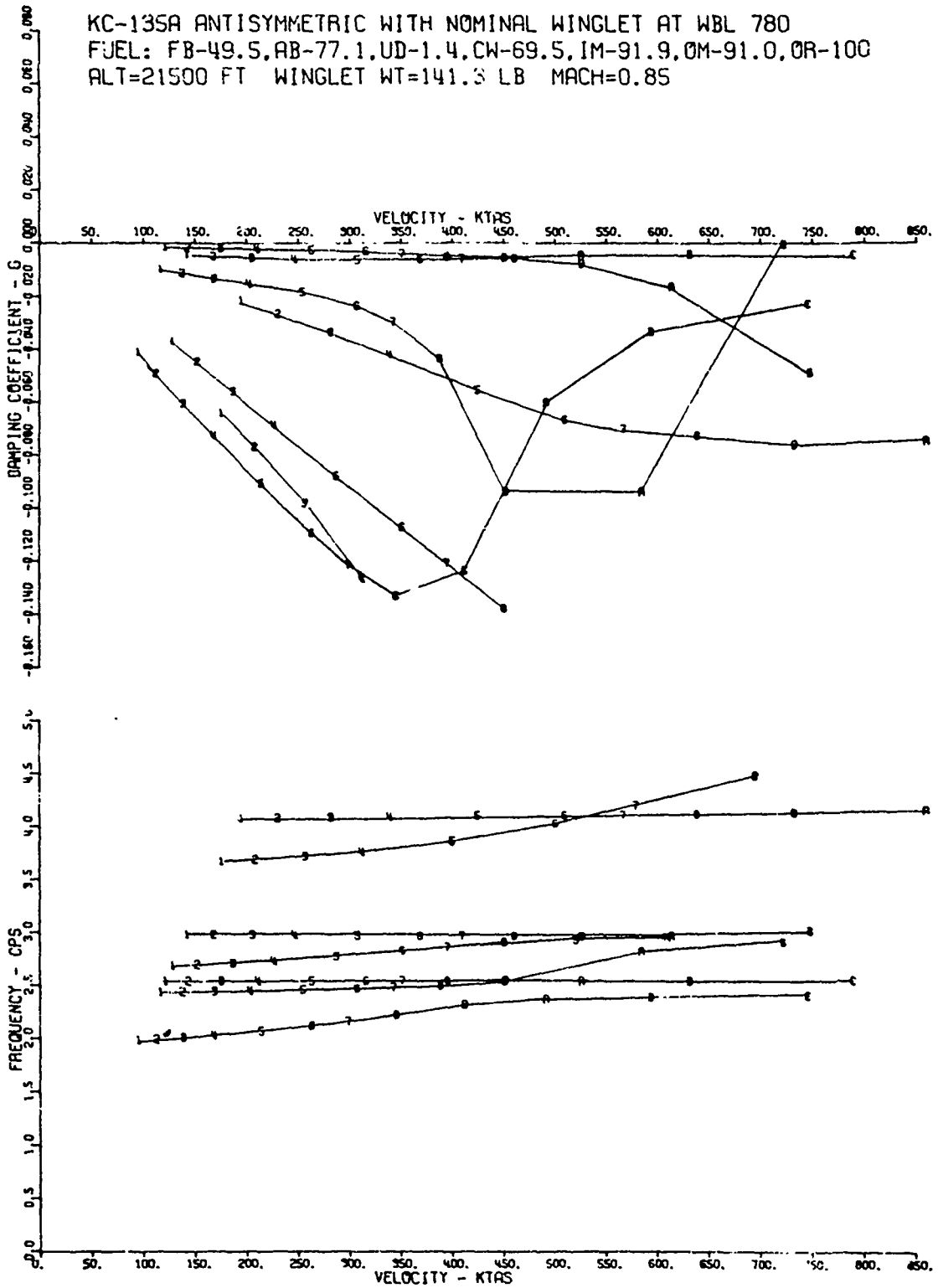


Figure 21.— Antisymmetric with Nominal Winglet

KC-135A ANTISYMMETRIC WITH WINGLET AT WBL 780
 FUEL: FB-49.5, AB-77.1, UD-1.4, CW-69.5, IM-91.9, OM-91.0, OR-100
 ALT=21500 FT WINGLET WT=300.0 LB MACH=0.85

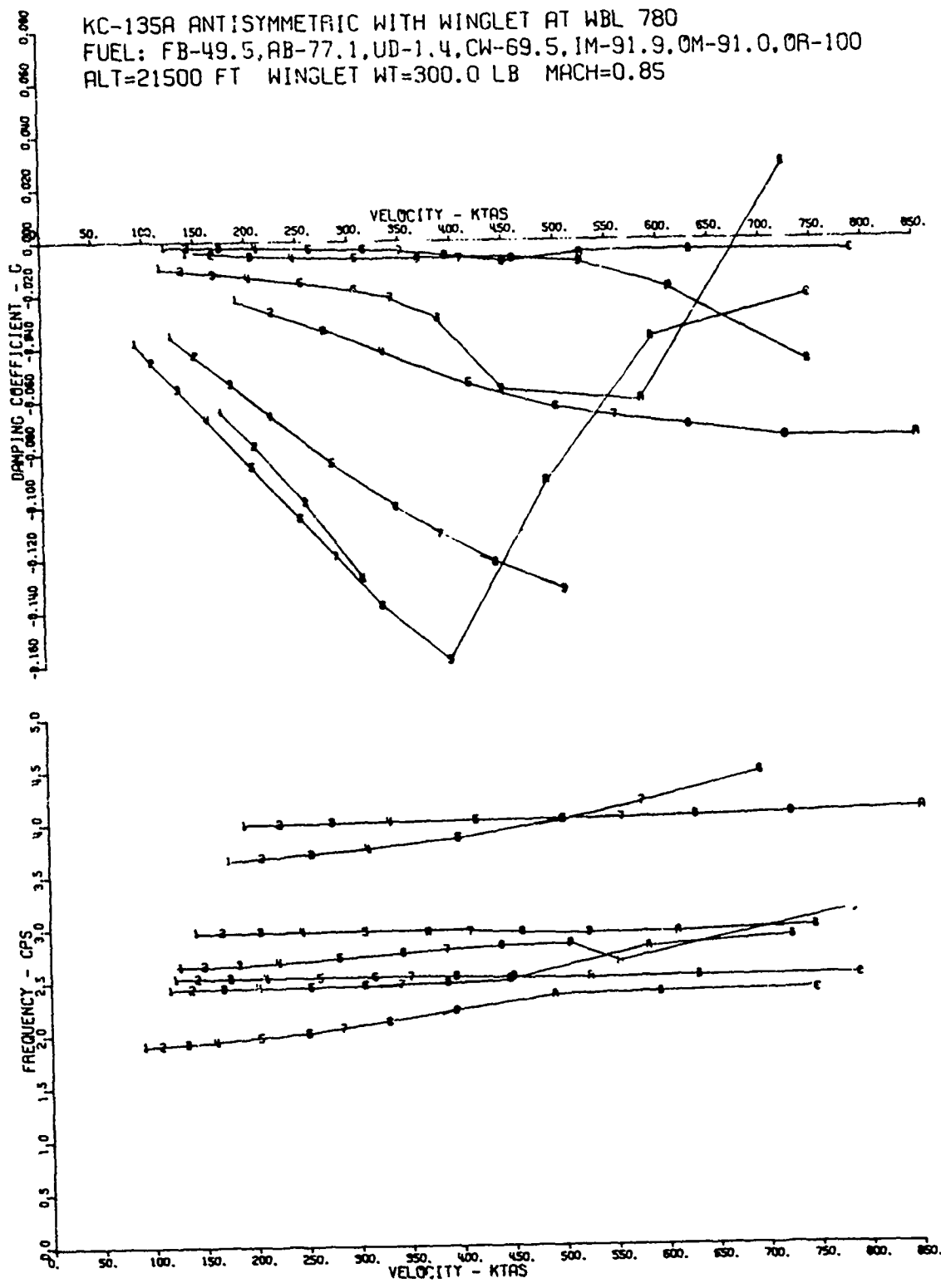


Figure 22.— Antisymmetric with 300 Lb. Winglet

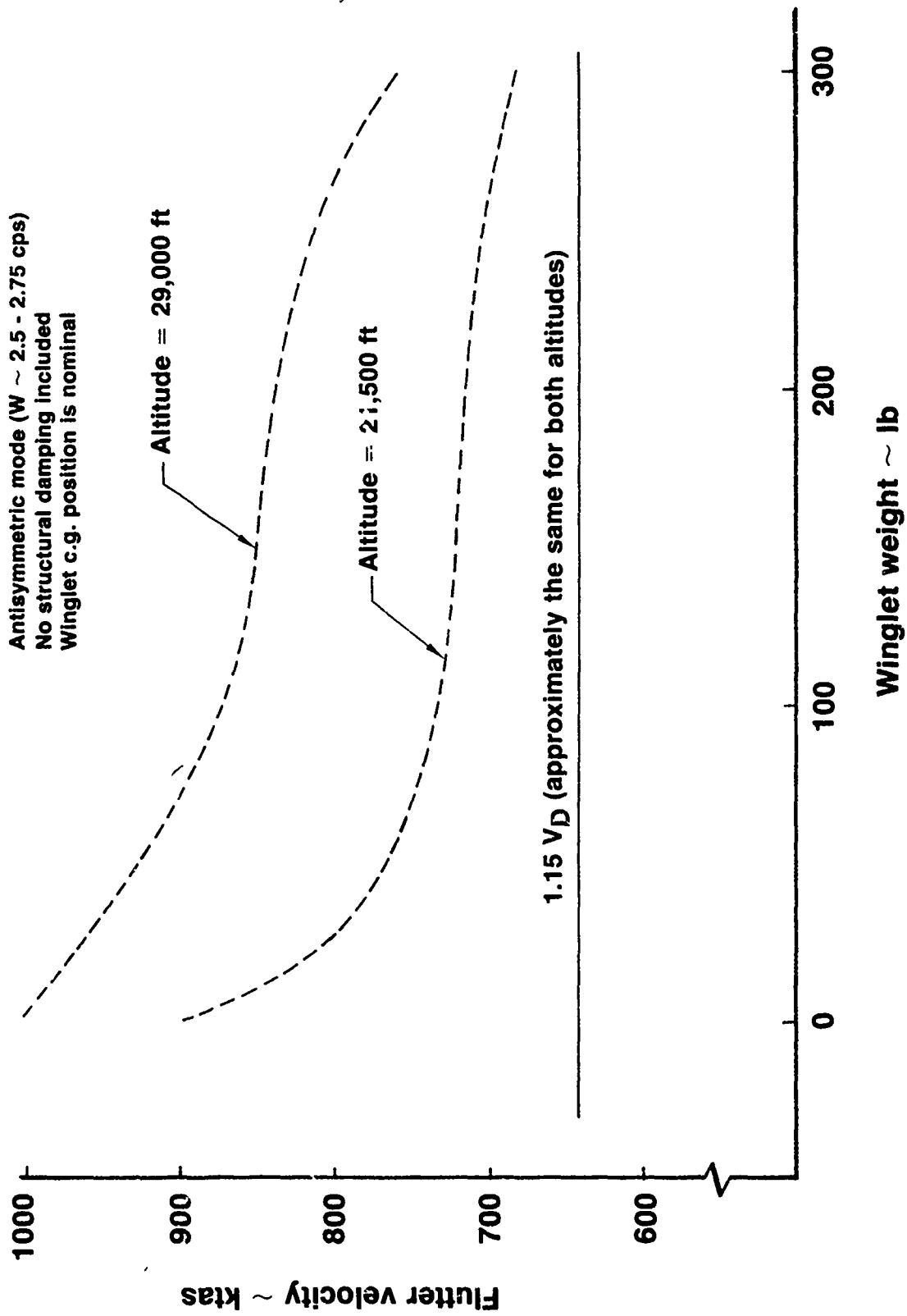


Figure 23. — Antisymmetric Flutter Boundary Vs Winglet Weight

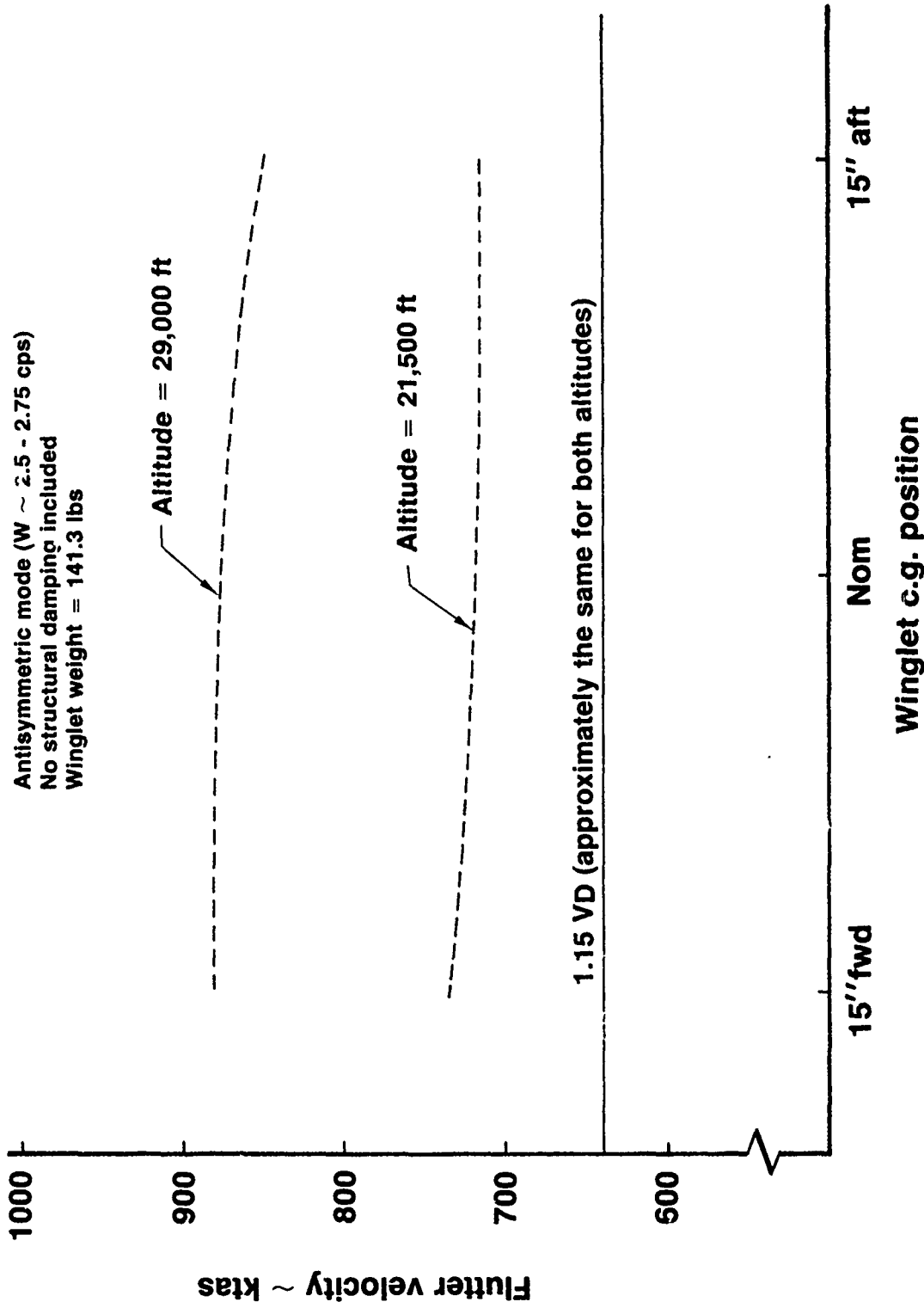
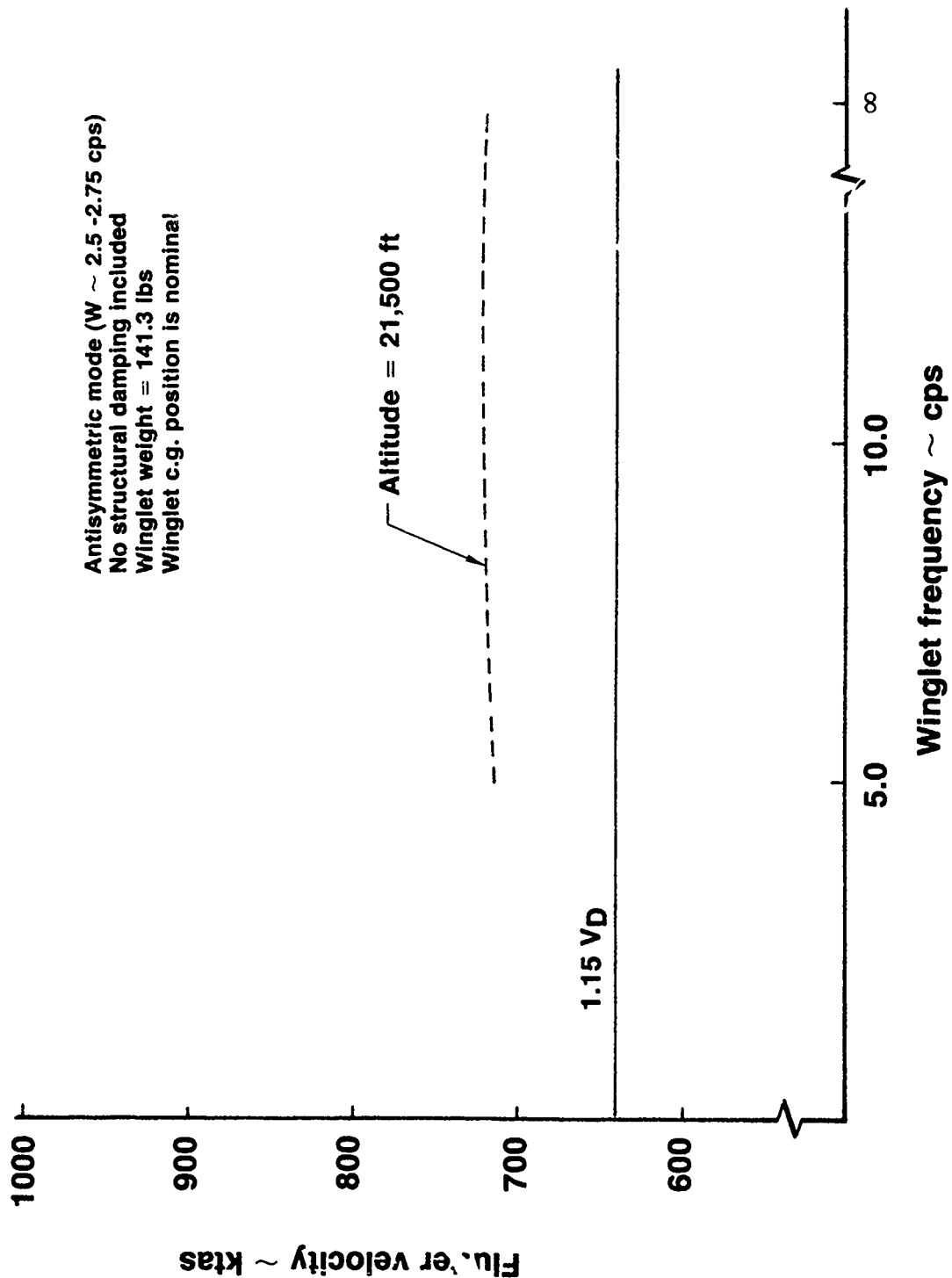


Figure 24. — Antisymmetric Flutter Boundary Versus Winglet C.G. Position

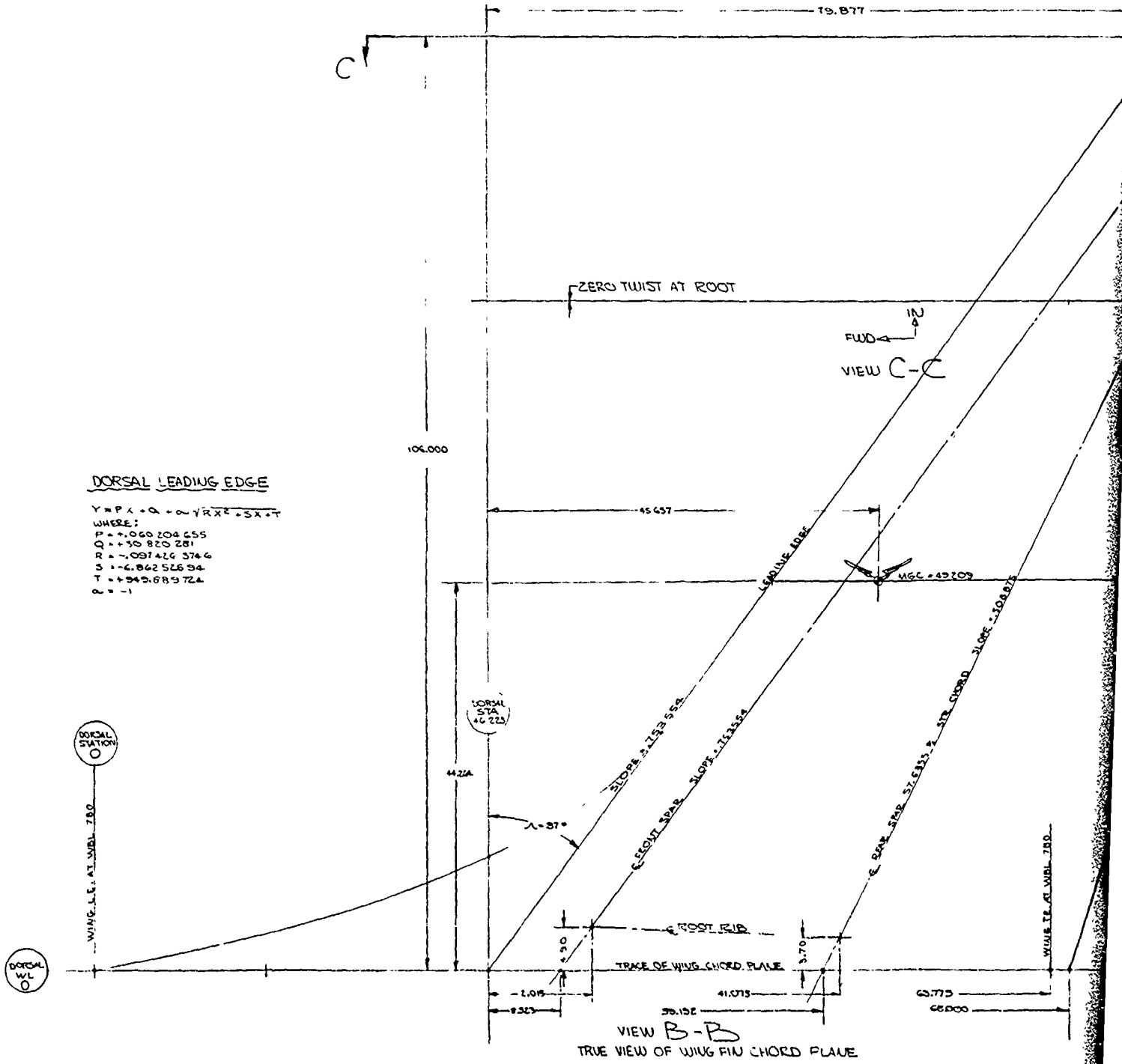


Antisymmetric mode (W ~ 2.5 -2.75 cps)
 No structural damping included
 Winglet weight = 141.3 lbs
 Winglet c.g. position is nominal

Figure 25. — Antisymmetric Flutter Boundary Vs Winglet Frequency

DORSAL LEADING EDGE

$Y = P X^2 + Q X + R X^3 + S X^4 + T$
 WHERE:
 P = +0.060 204 655
 Q = +30 820 281
 R = -.097 426 374
 S = +6.862 526 34
 T = +345.689 724
 P = -1



PRECEDING PAGE BLANK-NOT FILMED

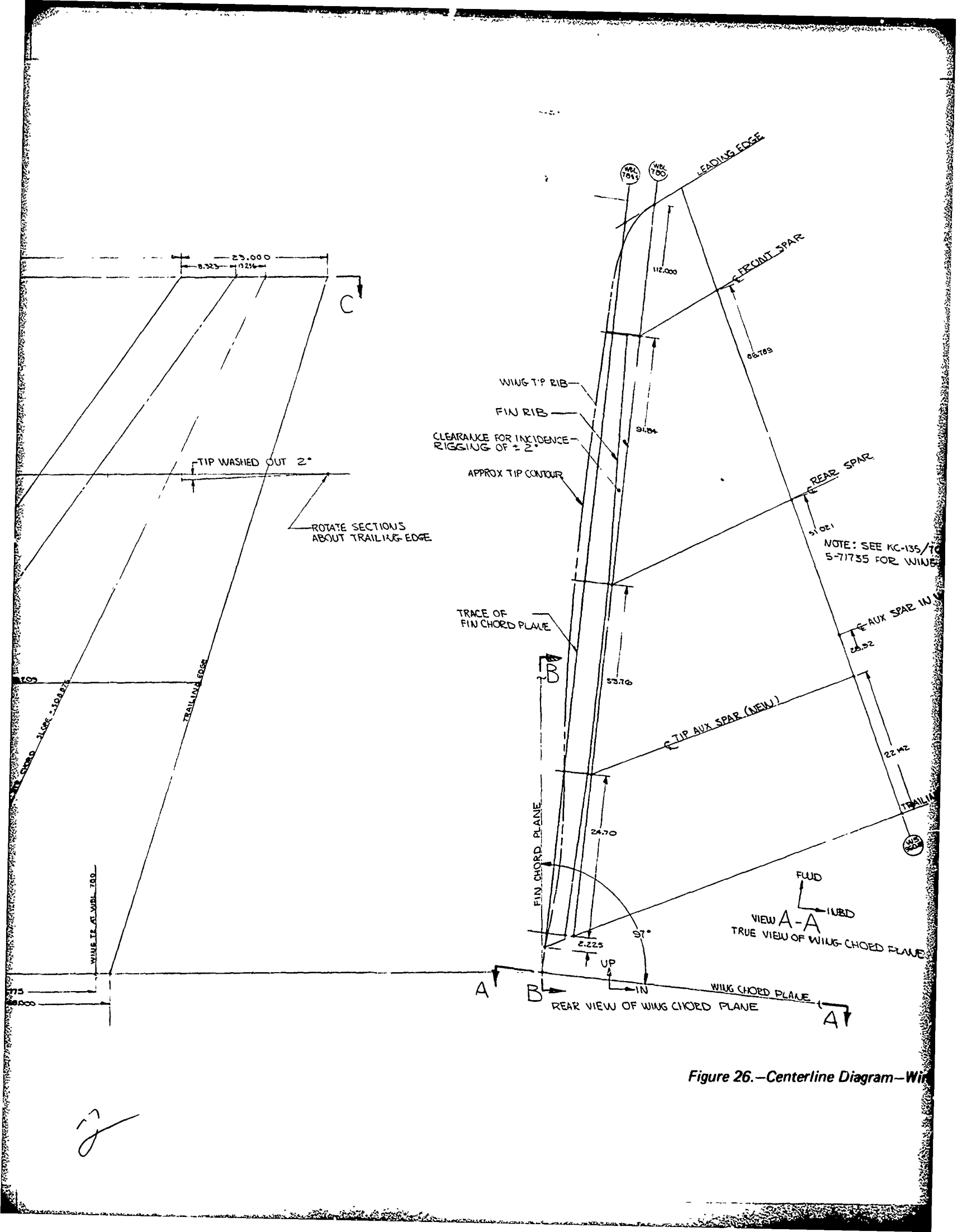
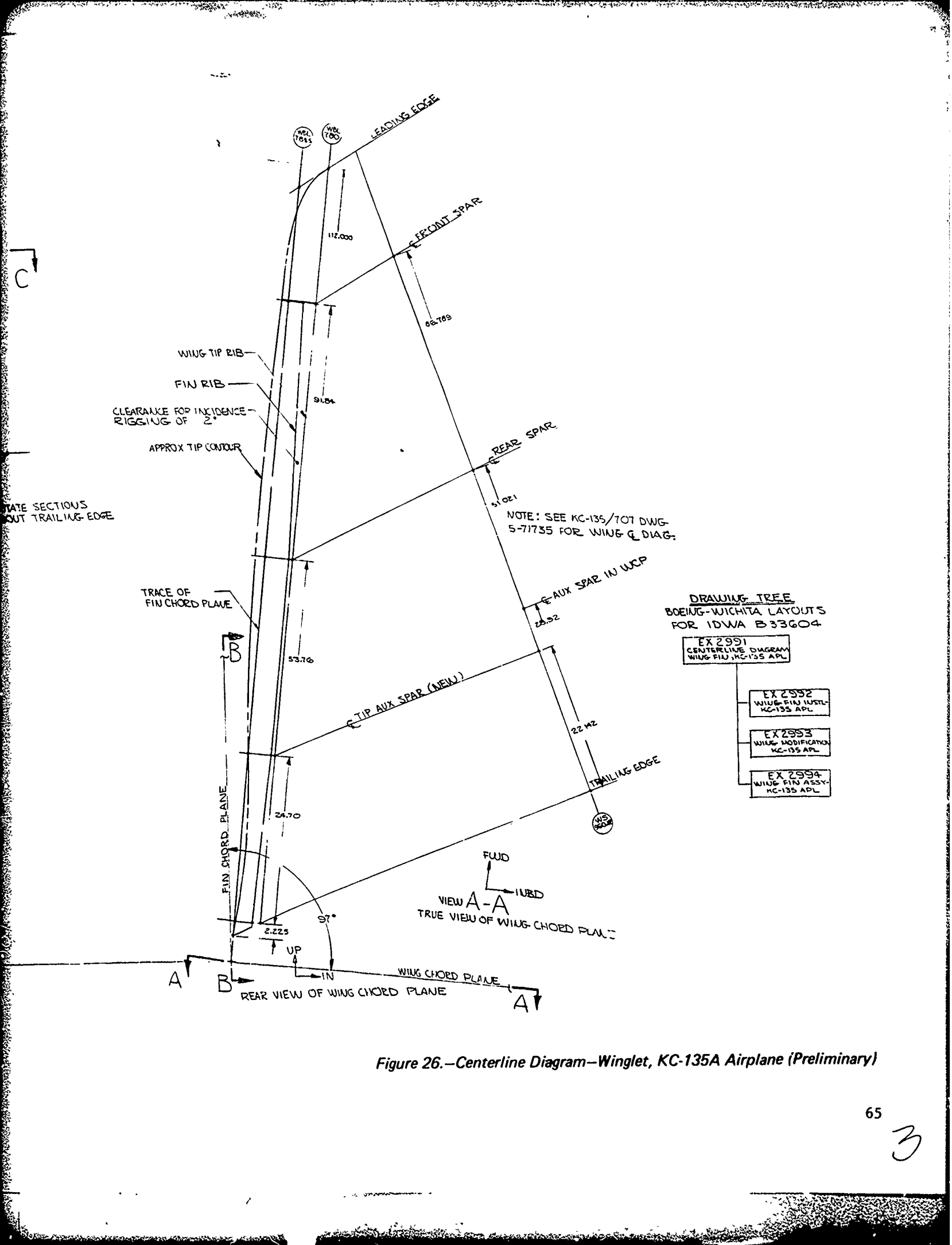


Figure 26.—Centerline Diagram—Wing



C

STATE SECTIONS
OUT TRAILING-EDGE

WING TIP RIB
FIN RIB
CLEARANCE FOR INCIDENCE -
RIGGING OF 2°
APPROX TIP CONTOUR

TRACE OF
FIN CHORD PLANE

B

FIN CHORD PLANE

A

B

REAR VIEW OF WING CHORD PLANE

WING CHORD PLANE

A

FWD
UP
IN

VIEW A-A
TRUE VIEW OF WING CHORD PLANE

LEADING EDGE

FRONT SPAR

REAR SPAR

AUX SPAR IN WCP

TIP AUX SPAR (NEW)

TRAILING EDGE

NOTE: SEE KC-135/707 DWG-
5-71735 FOR WING Q DIAG.

DRAWING TREE
BOEING-WICHITA LAYOUTS
FOR IDWA B33604

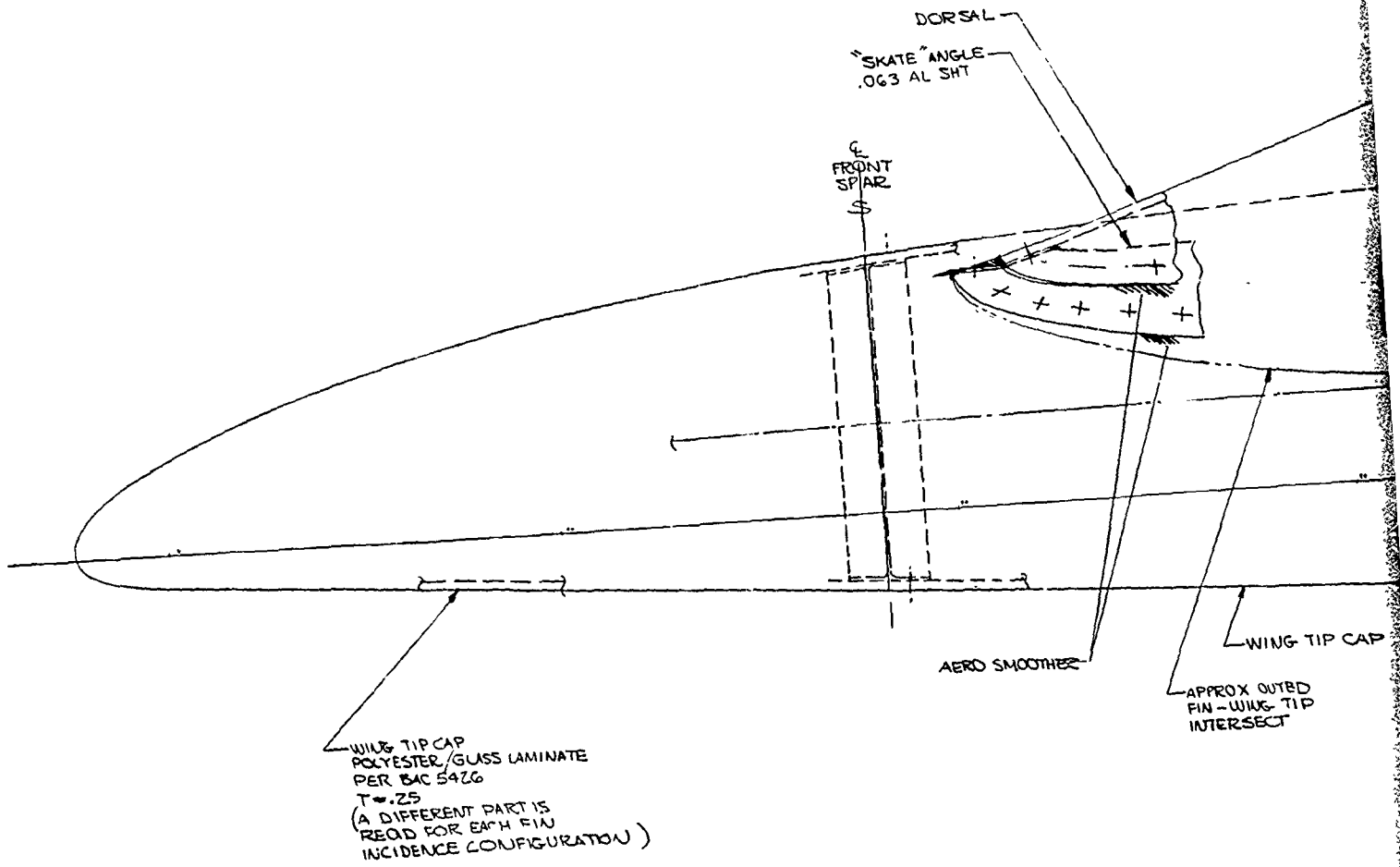
EX 2991
CENTERLINE DIAGRAM
WING-FIN, KC-135 APL

EX 2992
WING-FIN INSTL
KC-135 APL

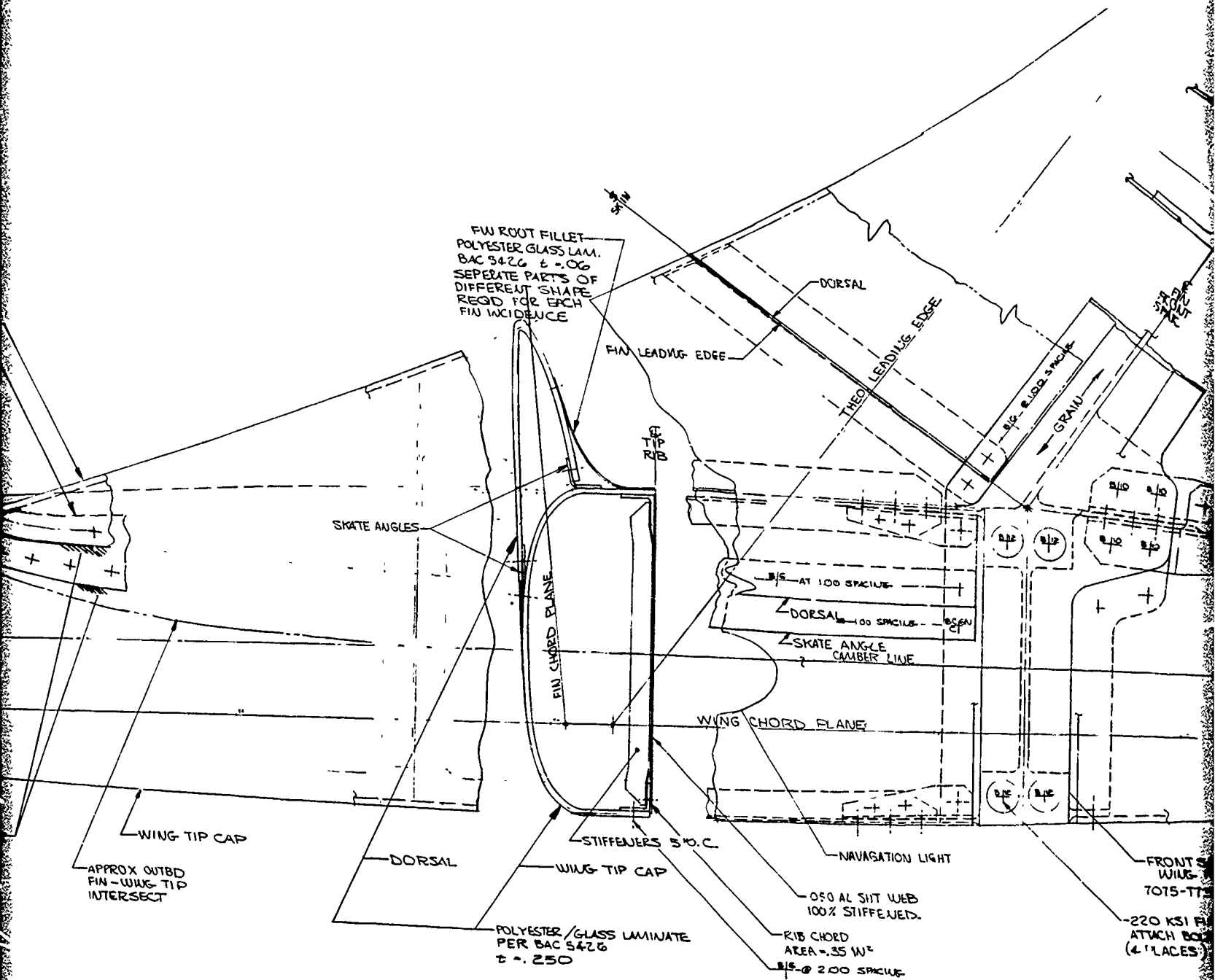
EX 2993
WING MODIFICATION
KC-135 APL

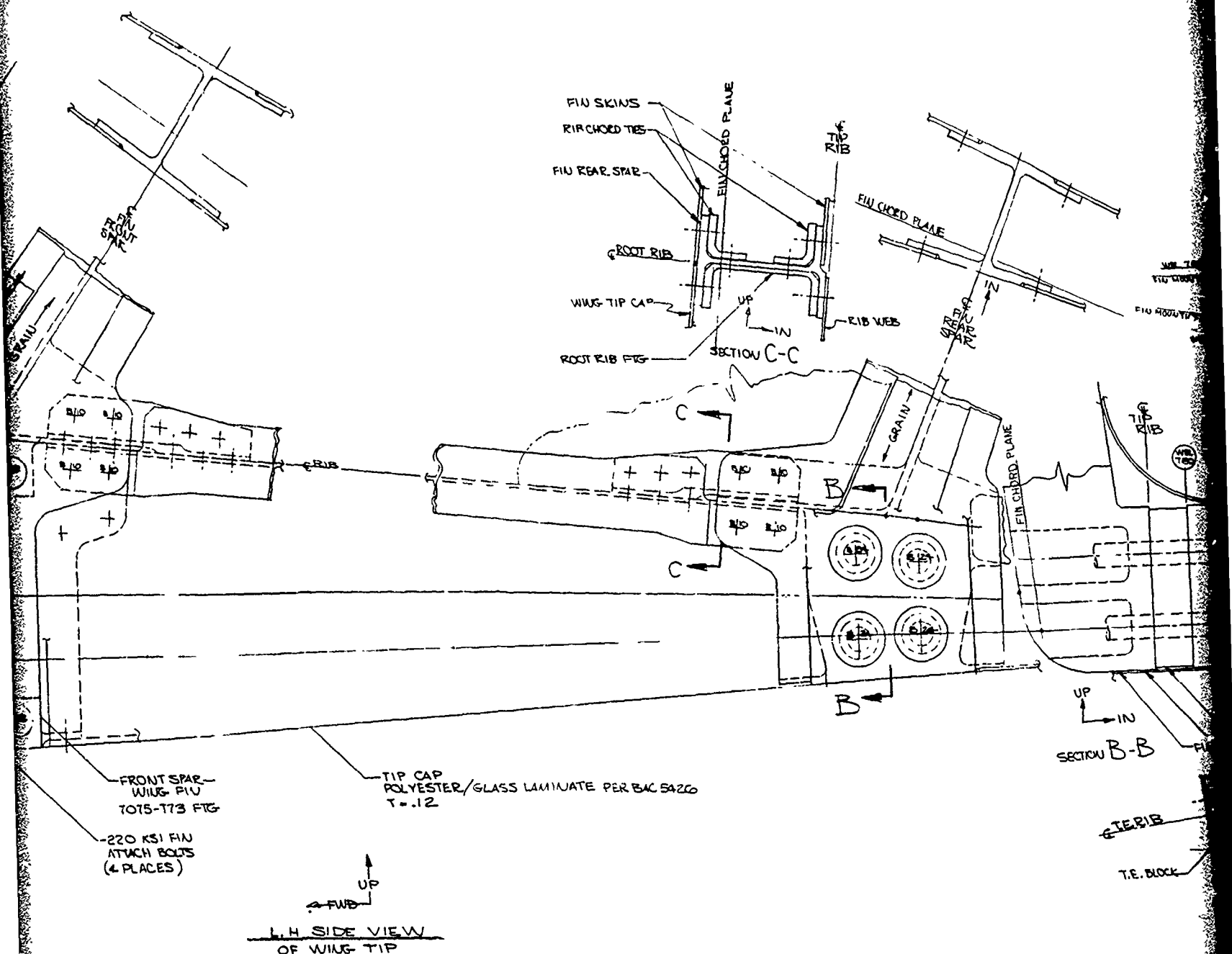
EX 2994
WING-FIN ASSY
KC-135 APL

Figure 26.—Centerline Diagram—Winglet, KC-135A Airplane (Preliminary)



PRECEDING PAGE BLANK - NOT FILMED





3

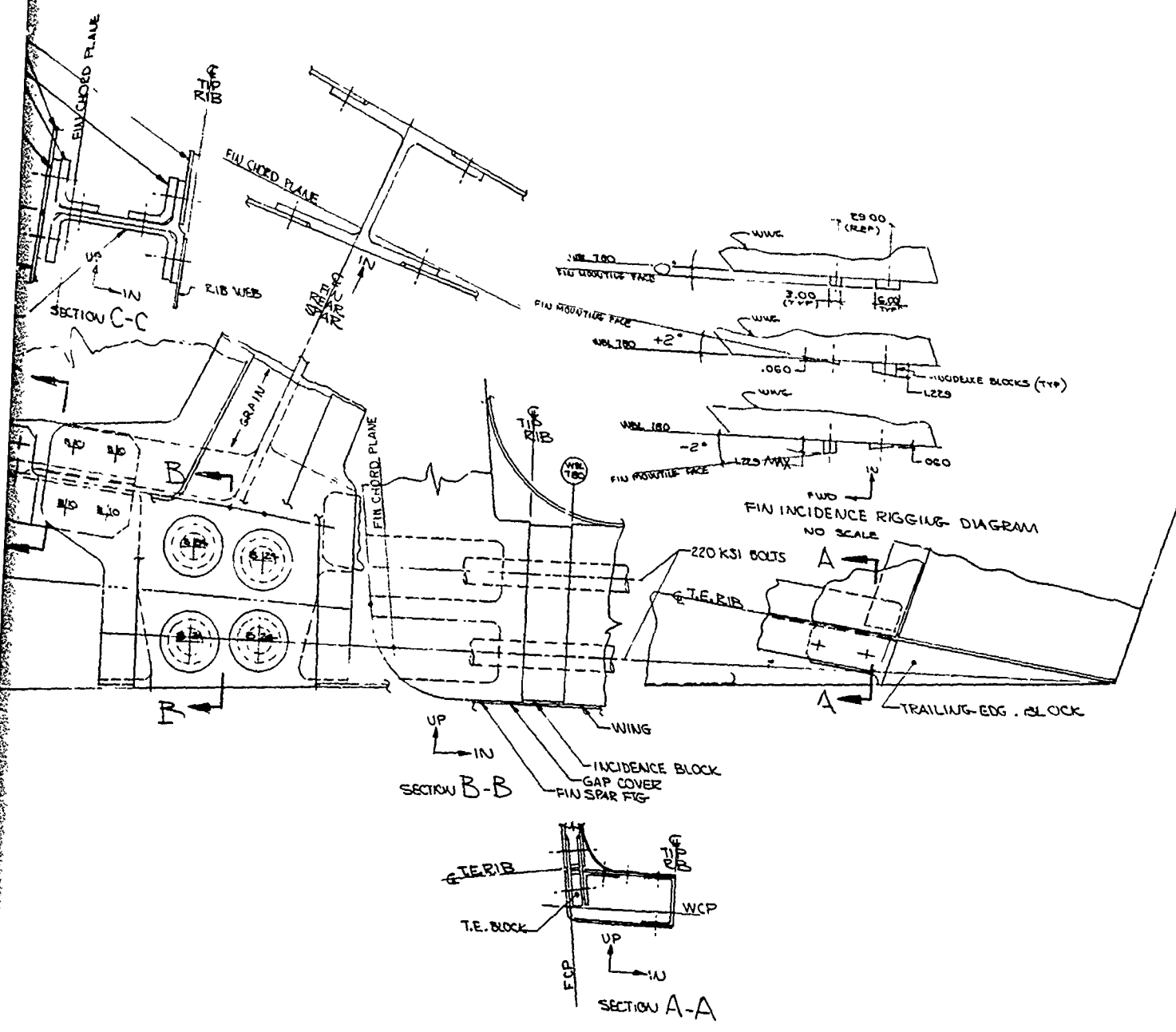


Figure 27.—Winglet Installation KC-135A Airplane (Preliminary)

4

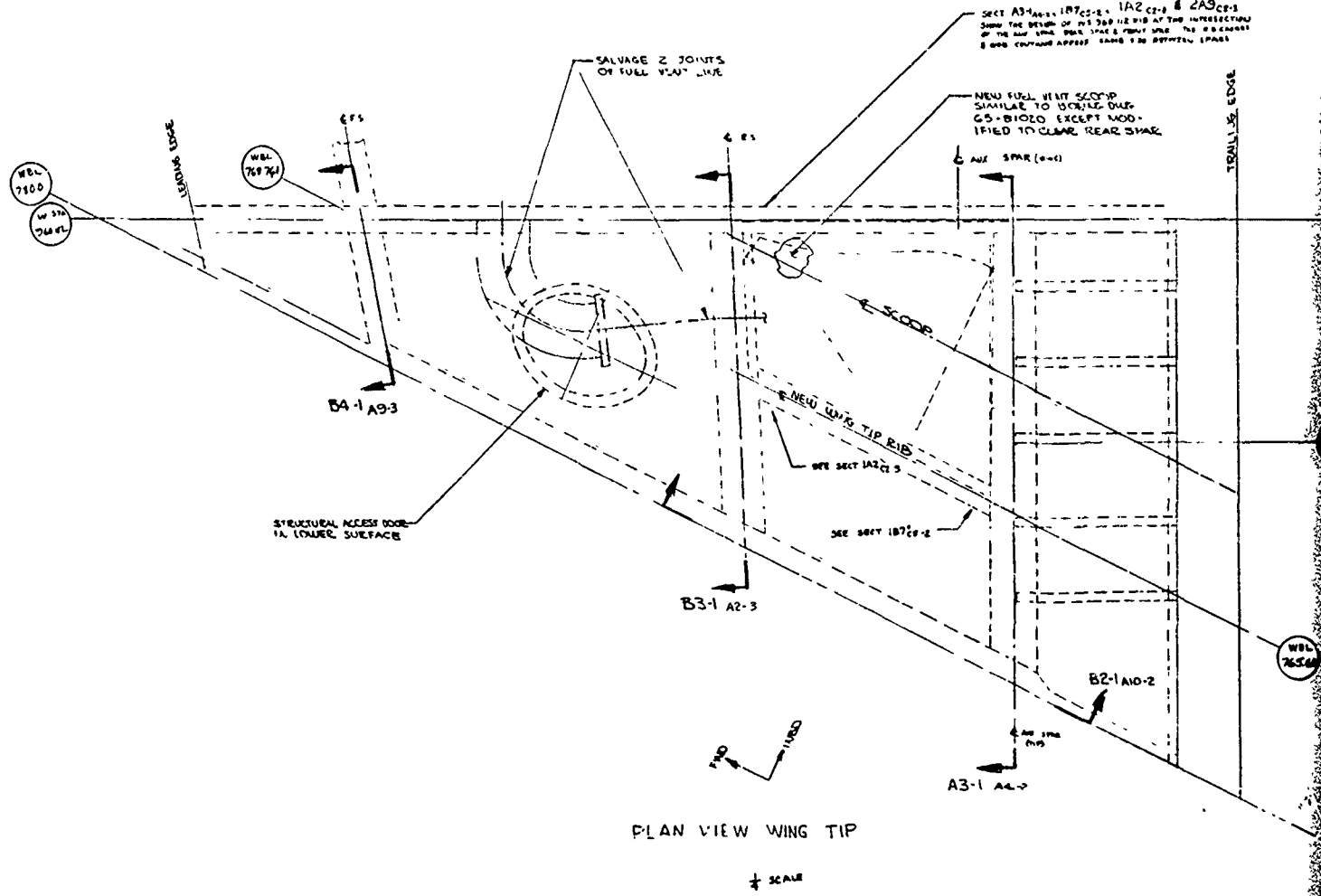


Figure 28.—Wing Modification

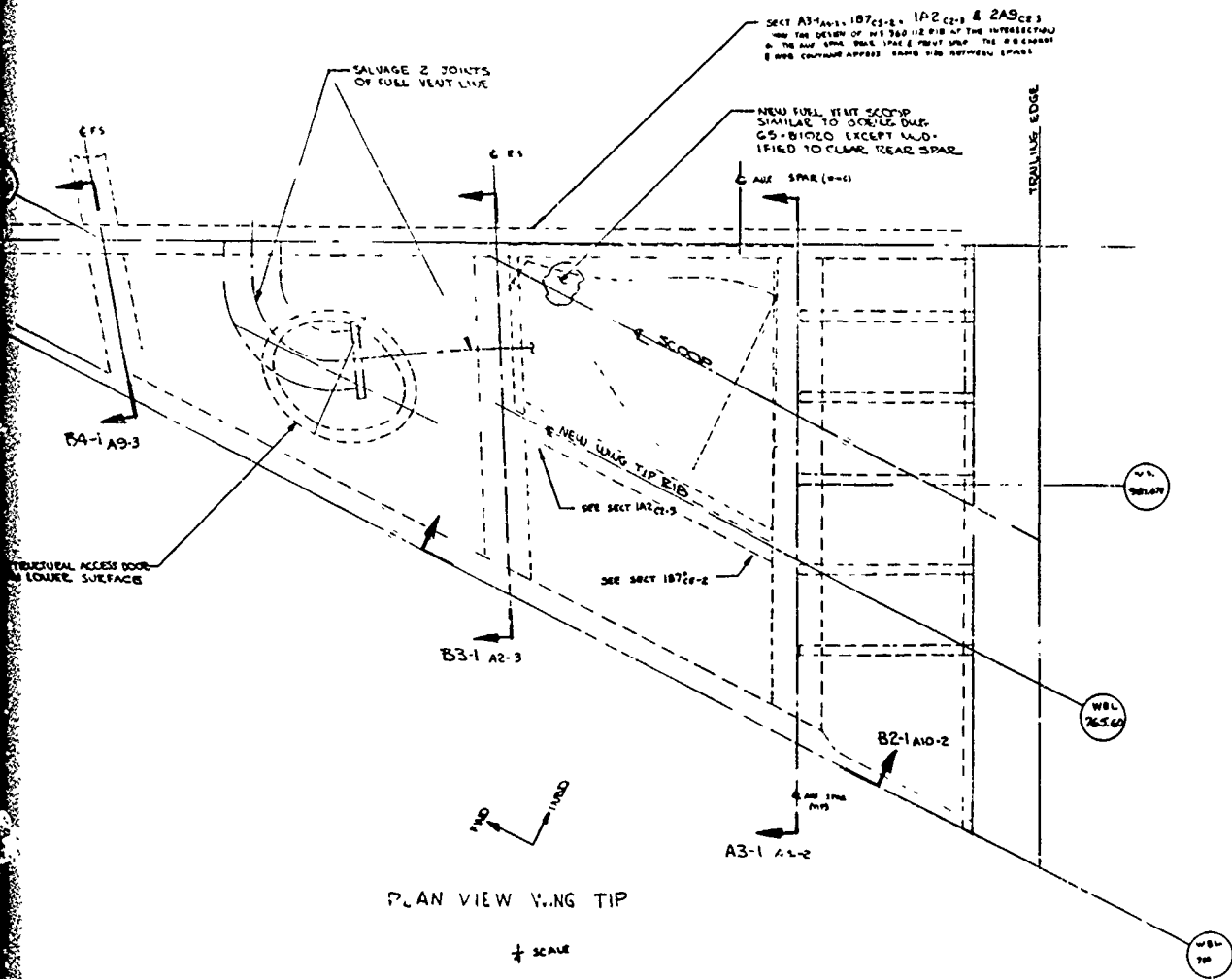
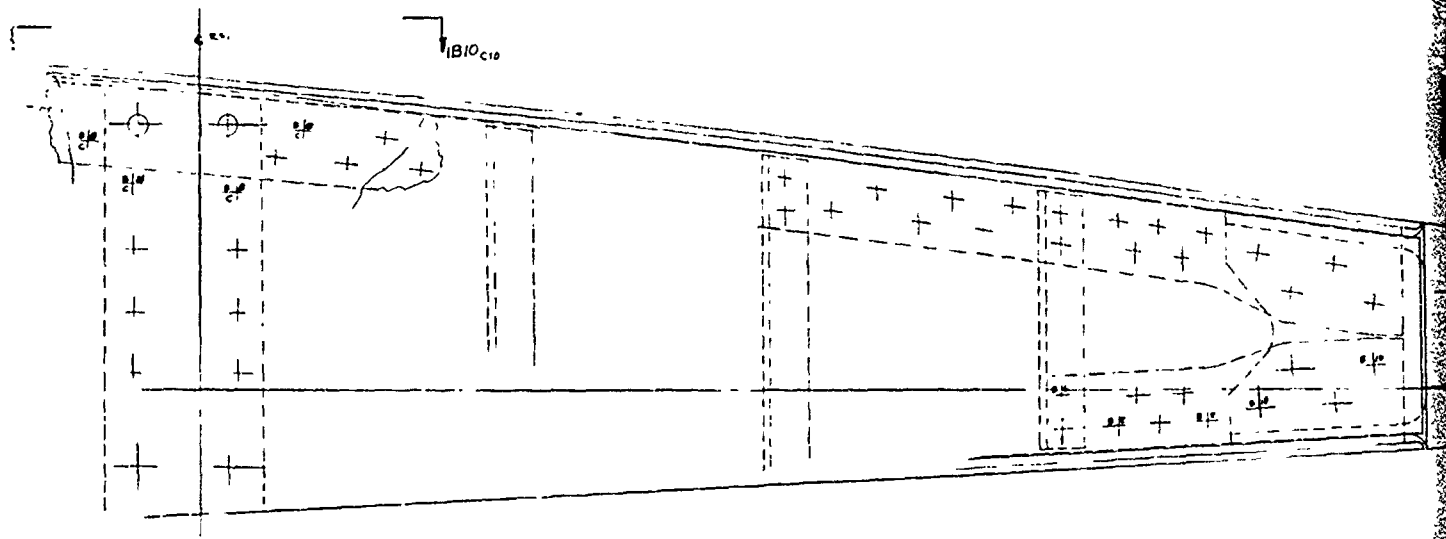
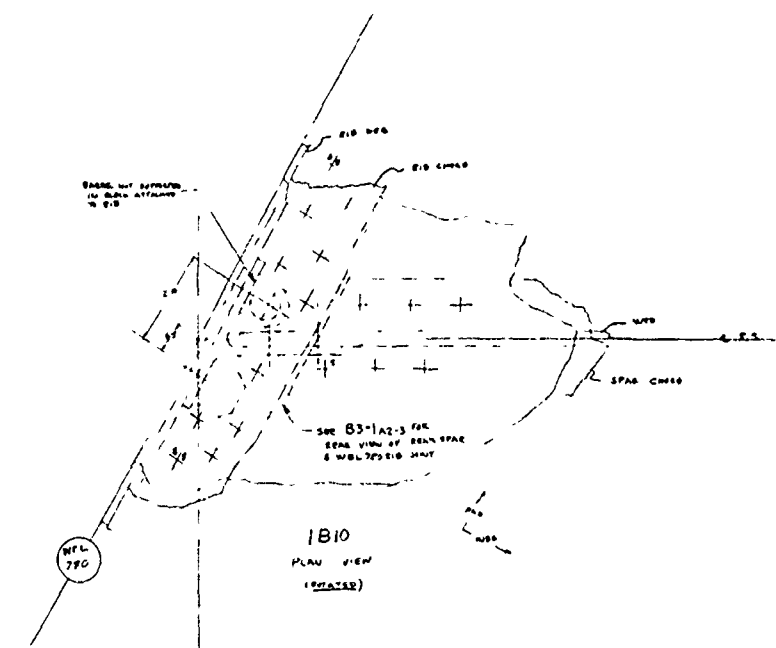
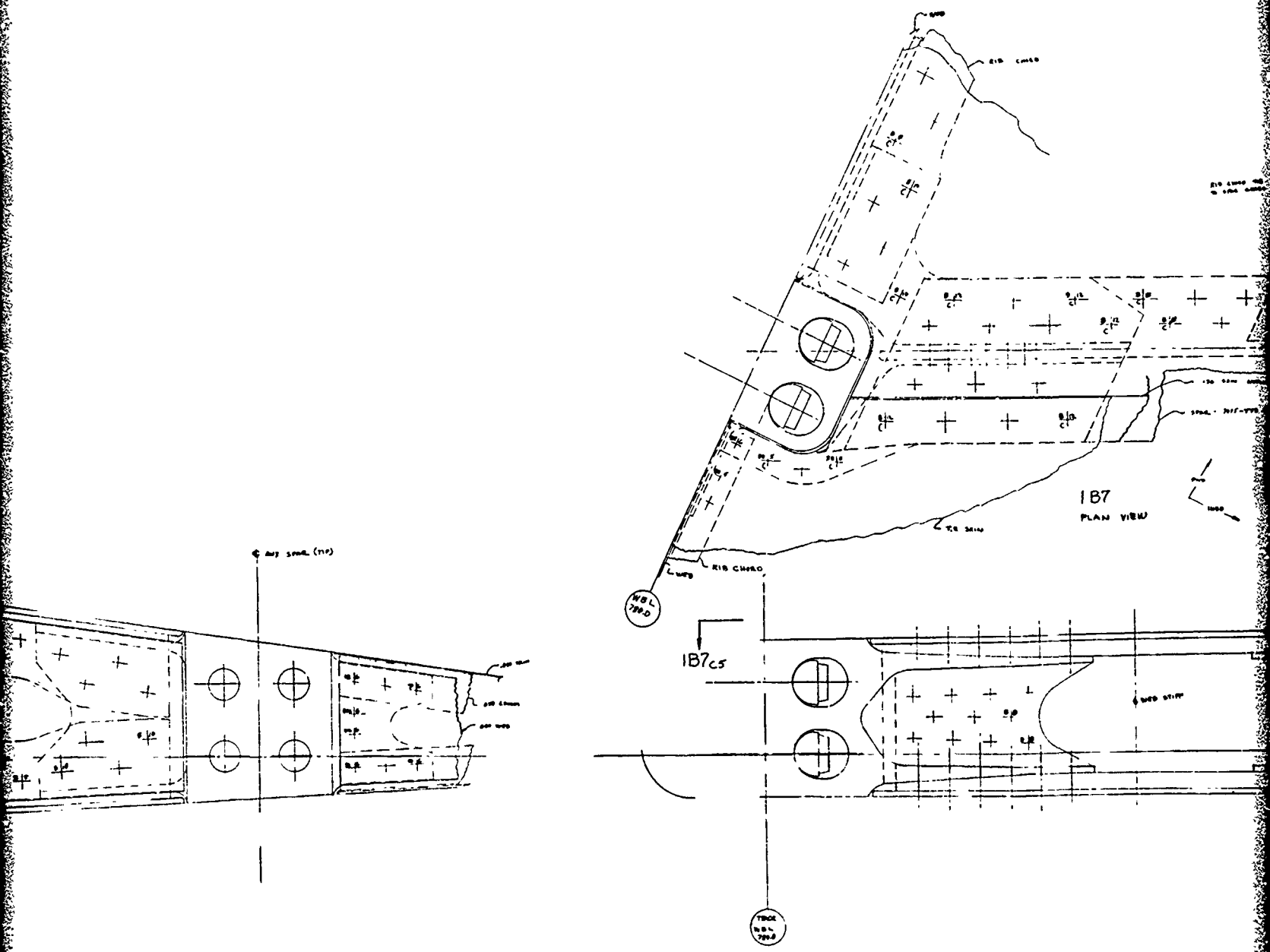
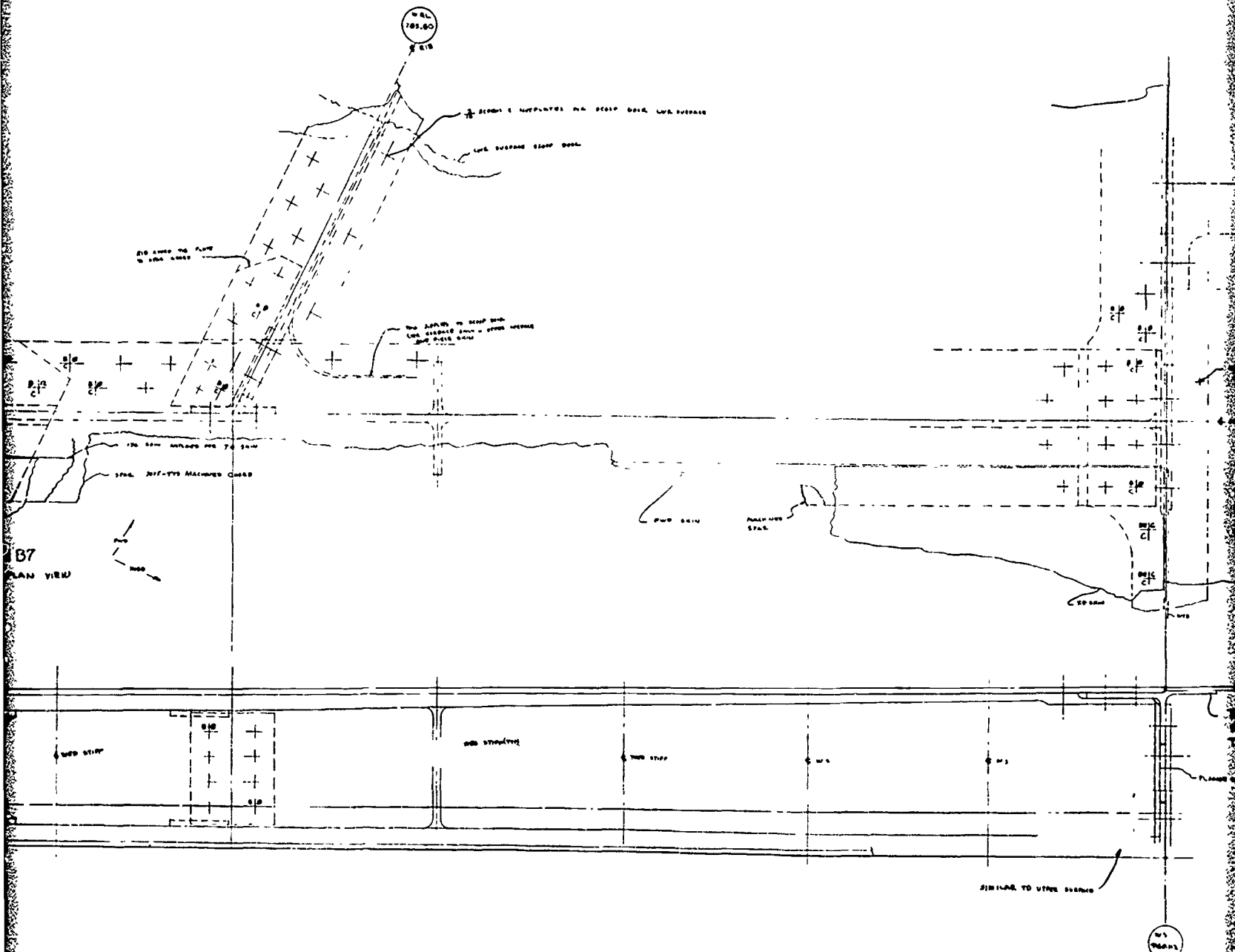


Figure 28.—Wing Modification—Winglet Provisions (Preliminary)



SECTION B2-1
L.H. SIDE VIEW
WEL 780 E10





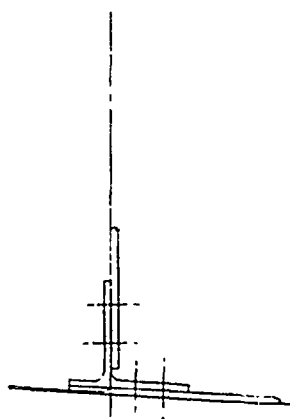
SECTION A3-1

REAR VIEW AND SPAL (D.P.)



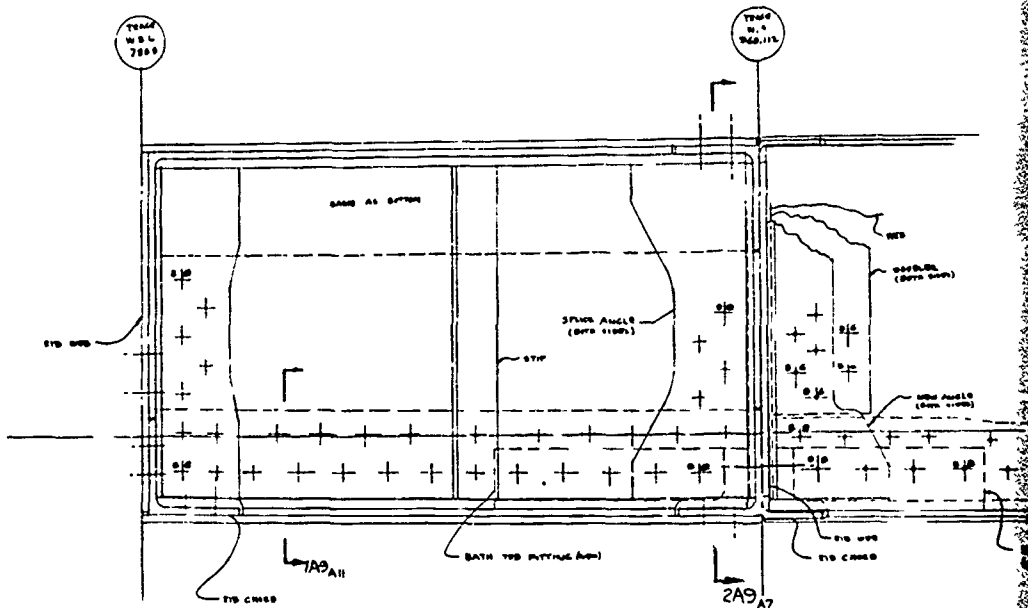
Figure 29.—Wing Modification

3



1A9

TYP. FOR 1A9B C1000



B4-1

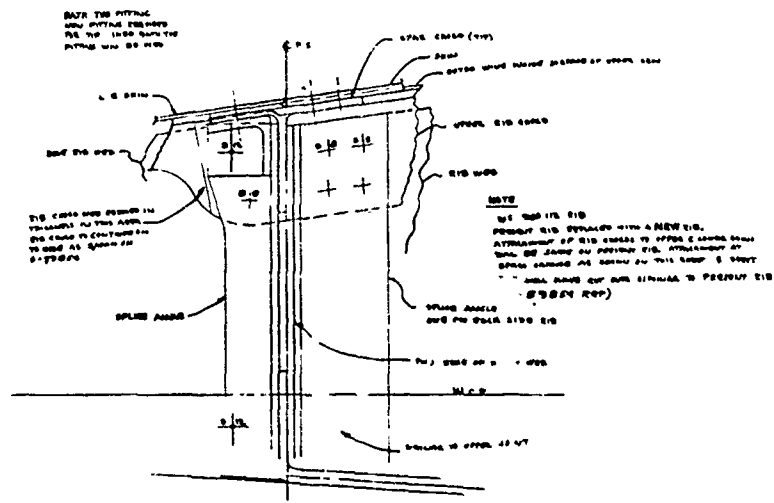
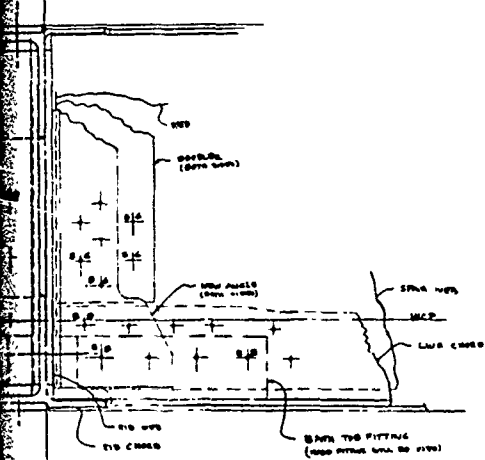
REAR VIEW
FRONT SPAR



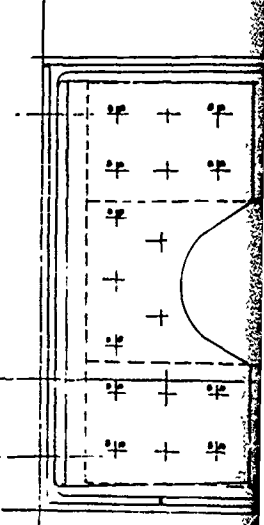
PRECEDING PAGE BLANK-NOT FILMED

SEE 1810 CD-3
FOR PLAN VIEW
OF R.S. & WDL 780

229
A7



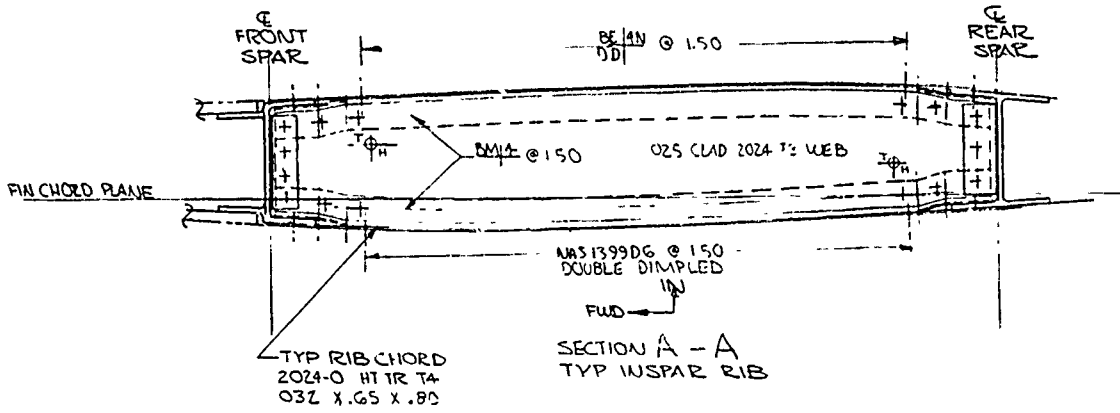
229
A7



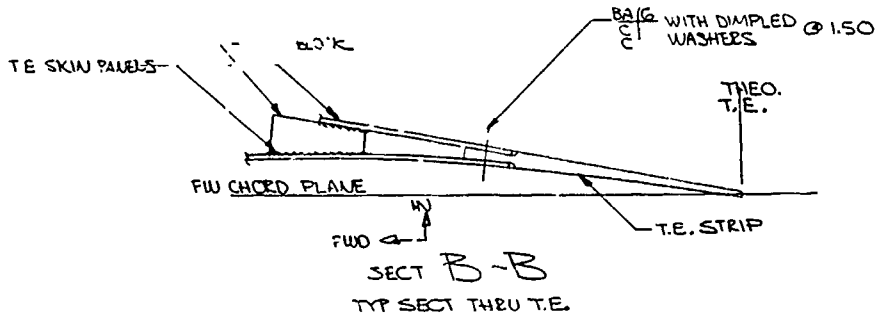
229
A7

2

4 0 0 0 0 X 1 3



NOTE: SEE EX 2992 FOR ADDITIONAL DETAILS IN FIN ROOT AREA



OUTBD FLAT

INBD FLAT

MACHINED FIN SPARS - 7075-F HAND FORGED BLOCKS. SAW & FLUGH MACHINE. HT-T2 TO T-73 & FINISH MACHINE. SEE DWG EX 2992 FOR DETAILS NOT SHOWN.

PROVIDE 2 #12 AWG. BONDING JUMPERS

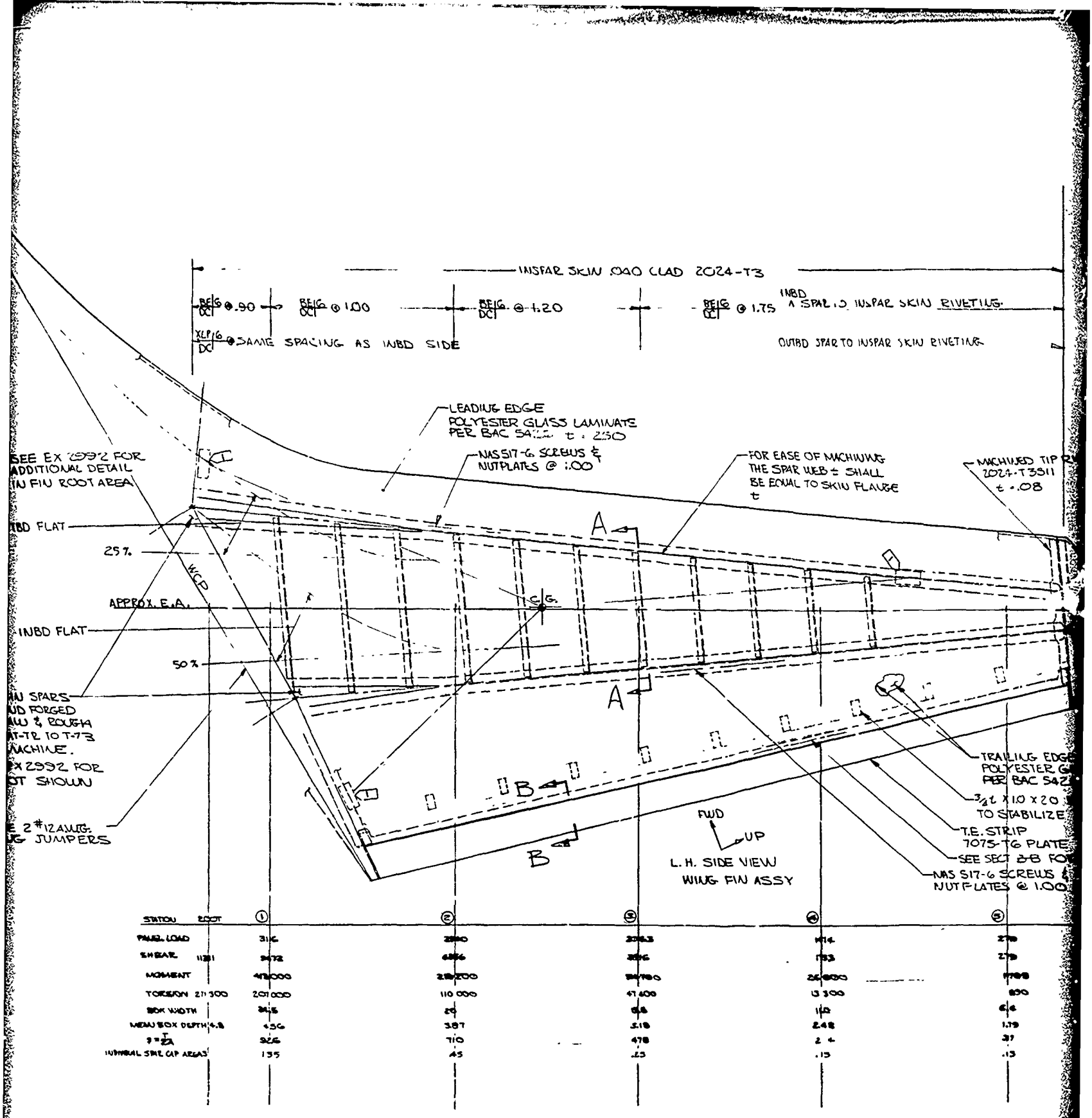


Figure 31.-Winglet A

2

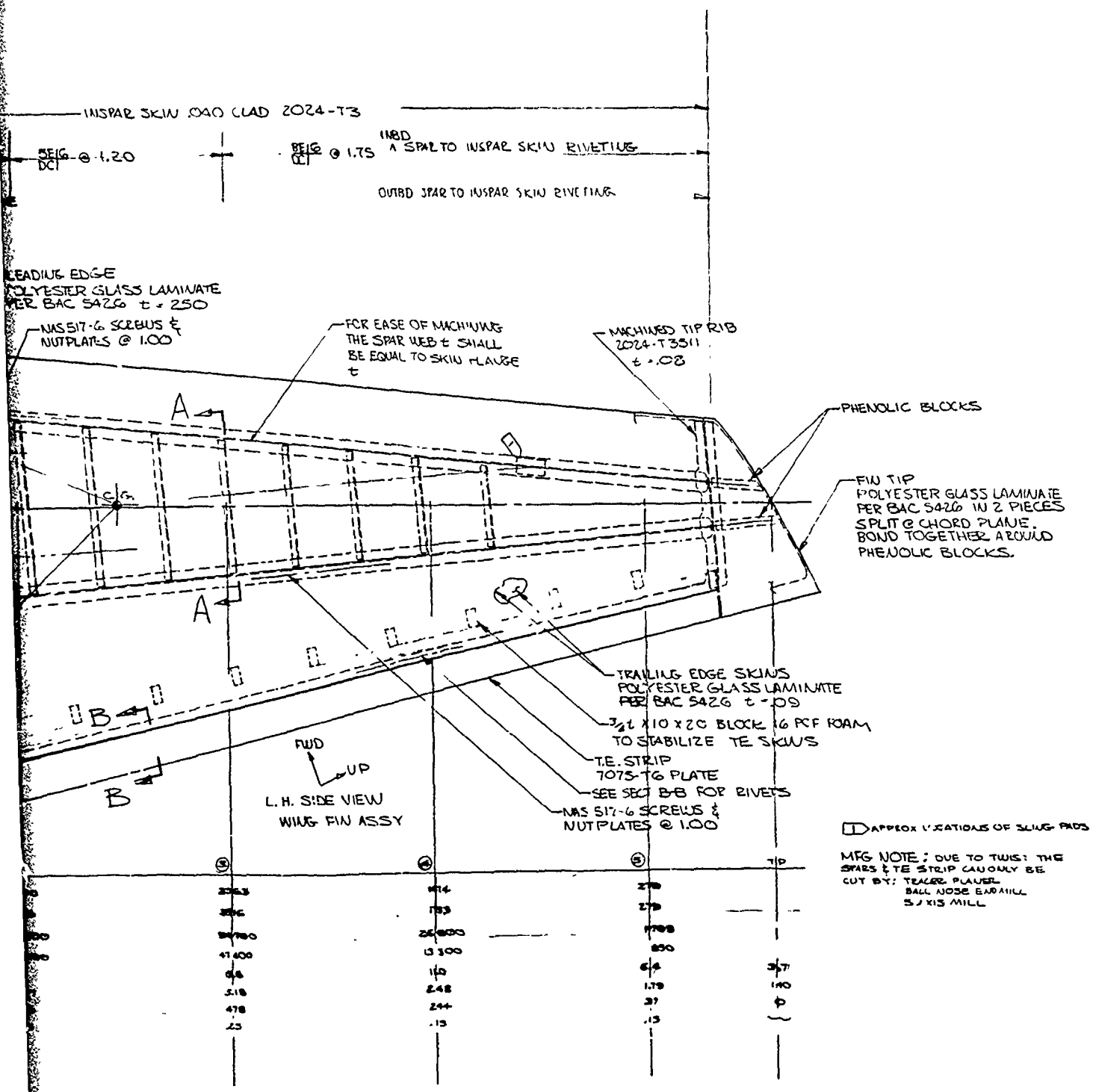
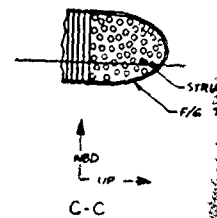


Figure 31.—Winglet Assembly Drawing—KC-135A Airplane (Preliminary)



SPAR CAP
 SAME AS RS EXCEPT
 51 PLYS AT ROOT STEP
 TAPERED TO 6 PLYS AT
 TIP. (2 PLACES)

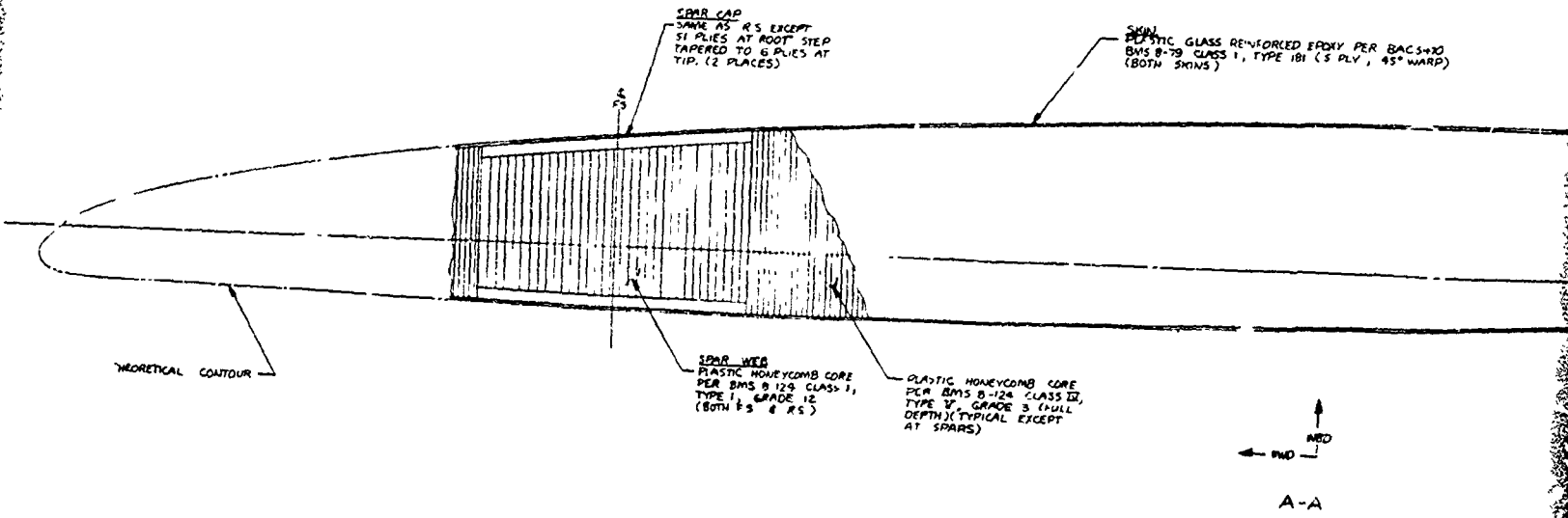
SKIN
 PLASTIC GLASS REINFORCED EPOXY PER BACS-40
 BMS 8-79 CLASS 1, TYPE 1B1 (5 PLY, 45° WARP)
 (BOTH SKINS)

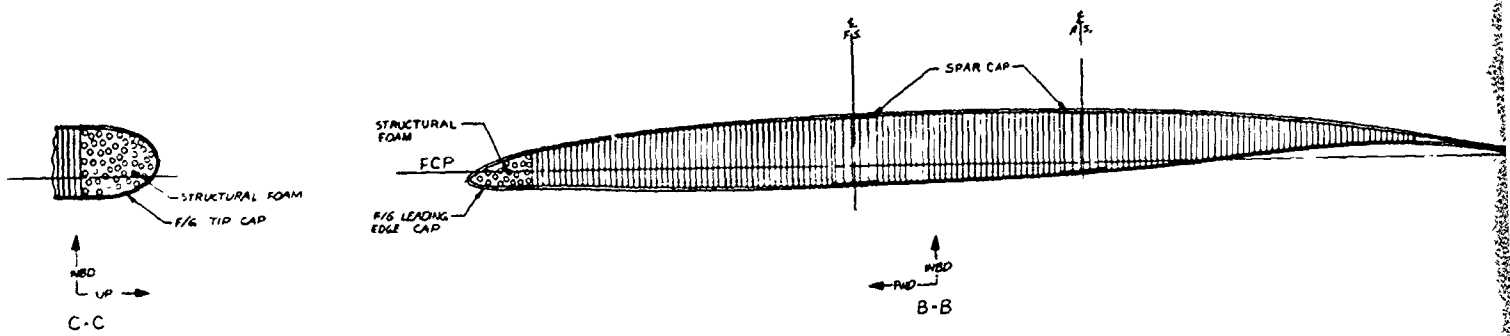
SPAR WEB
 PLASTIC HONEYCOMB CORE
 PER BMS 8-124 CLASS 1,
 TYPE 1, GRADE 12
 (BOTH FS & RS)

PLASTIC HONEYCOMB CORE
 PER BMS 8-124 CLASS II,
 TYPE 1, GRADE 3 (FULL
 DEPTH) (TYPICAL EXCEPT
 AT SPARS)



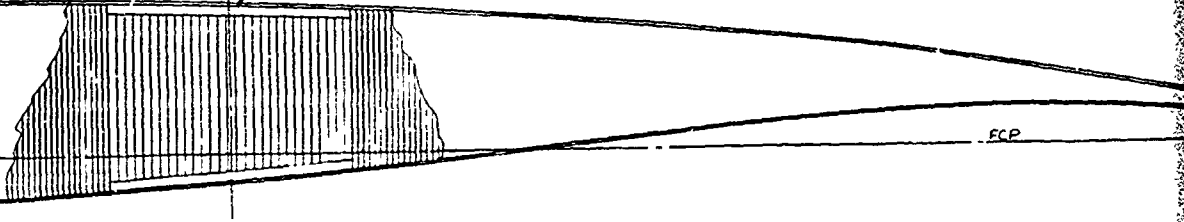
THEORETICAL CONTOUR





REINFORCED EPOXY PER BAC 5470
TYPE 181 (5 PLY, 45° WARP)

SPAR CAP
OF GRAPHITE EPOXY TYPE A3/3002
45 PLYS AT ROOT STEADY TAPERED
TO 4 PLYS AT TIP (2 PLACES)
PLASTIC GLASS REINFORCED EPOXY
PER BAC 5470 BMS 8-73 CLASS 1, TYPE
181, ONE PLY, FULL SPAN, OF WARP
BETWEEN G/R/E/P AND F/G SKIN



A-A

21

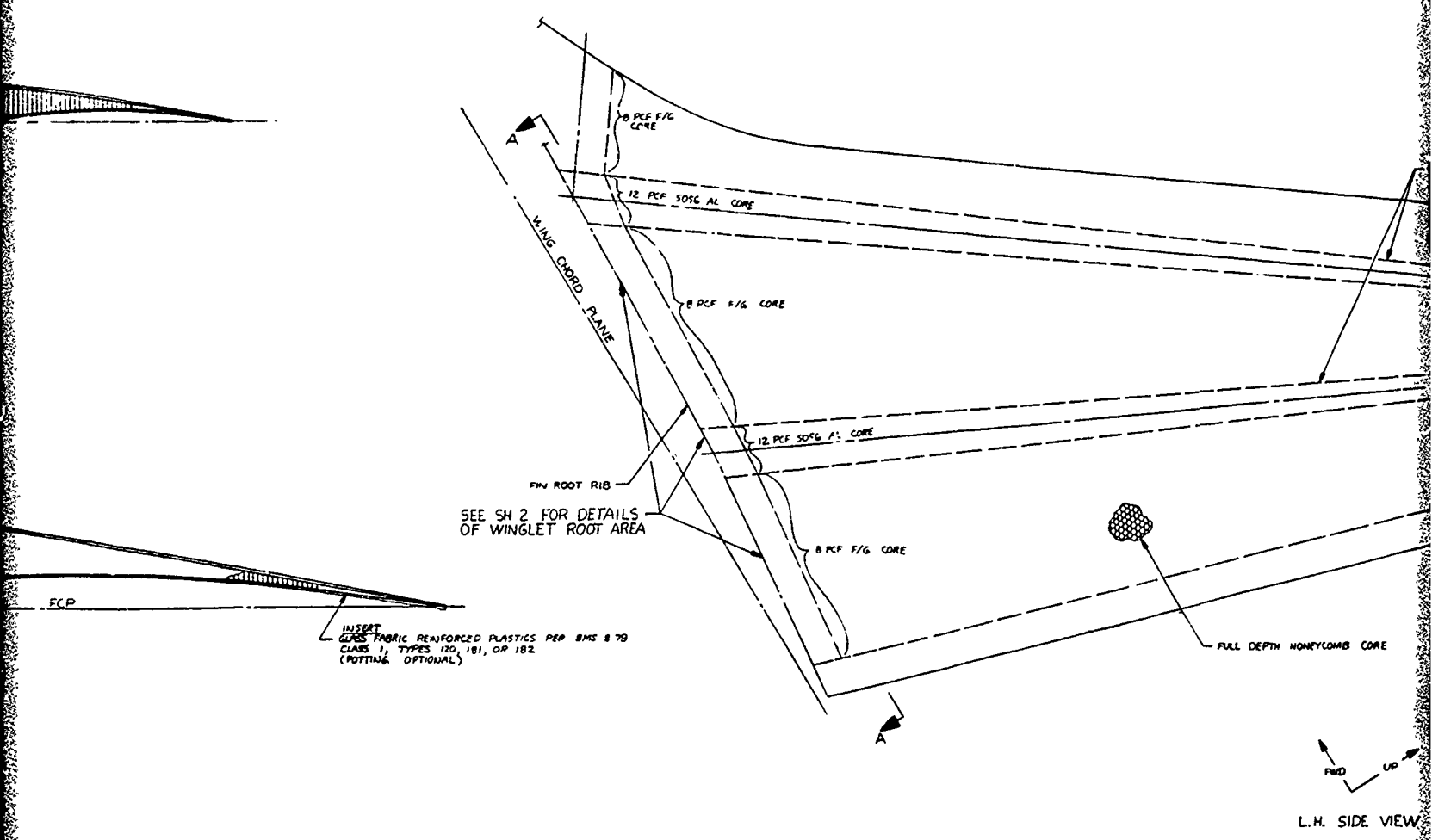


Figure 32.—Winglet Assembly—KC

32

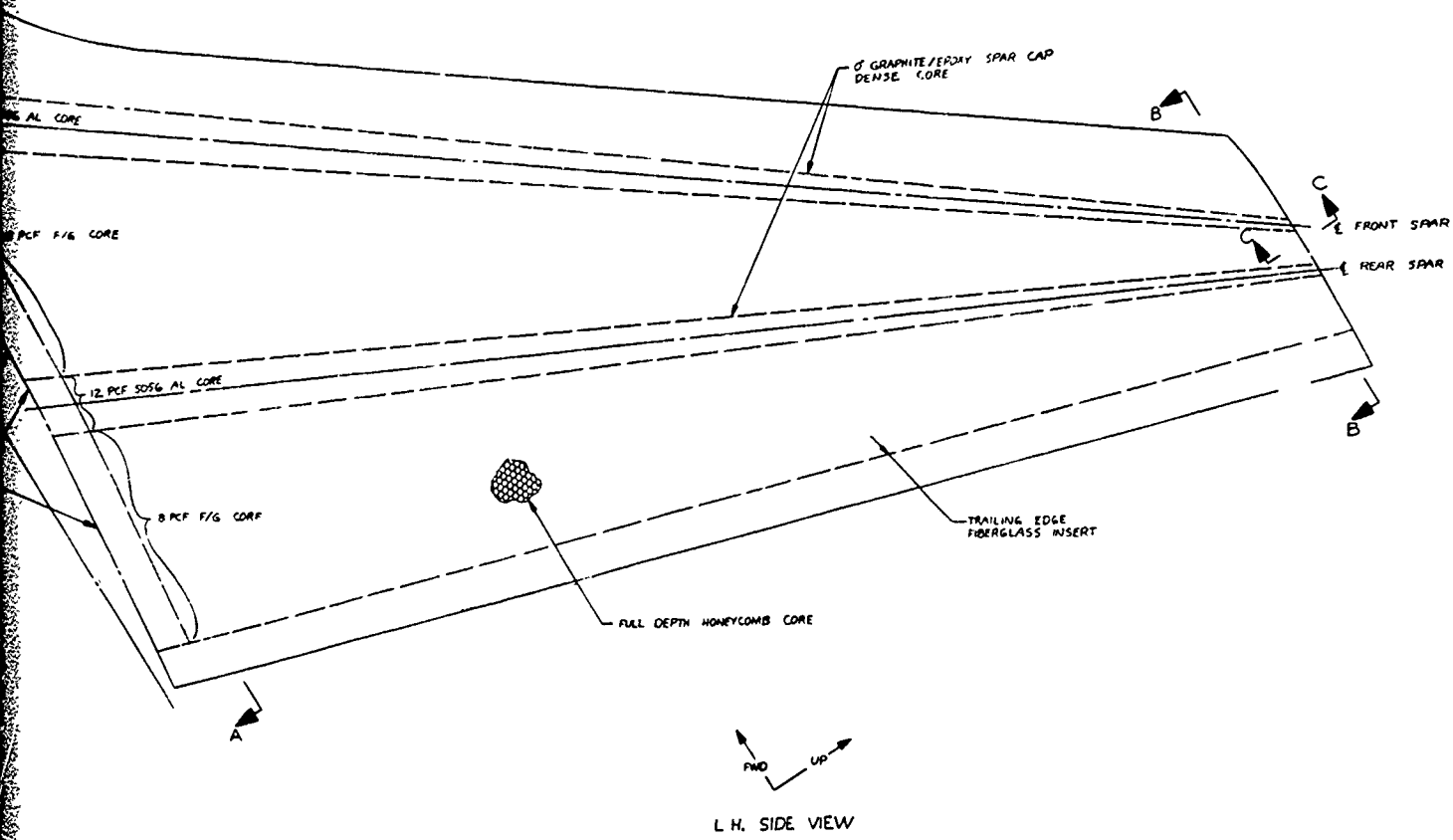
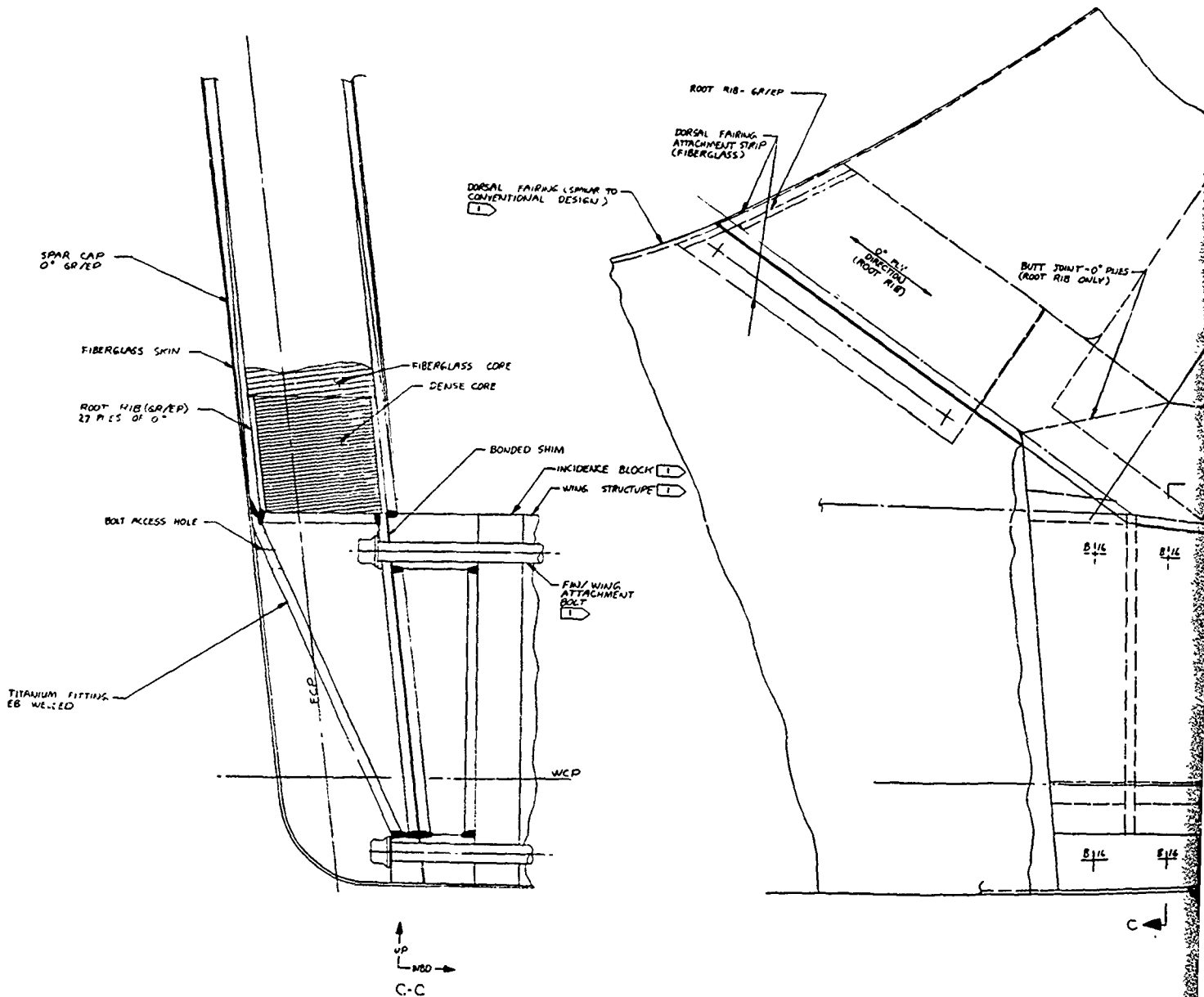
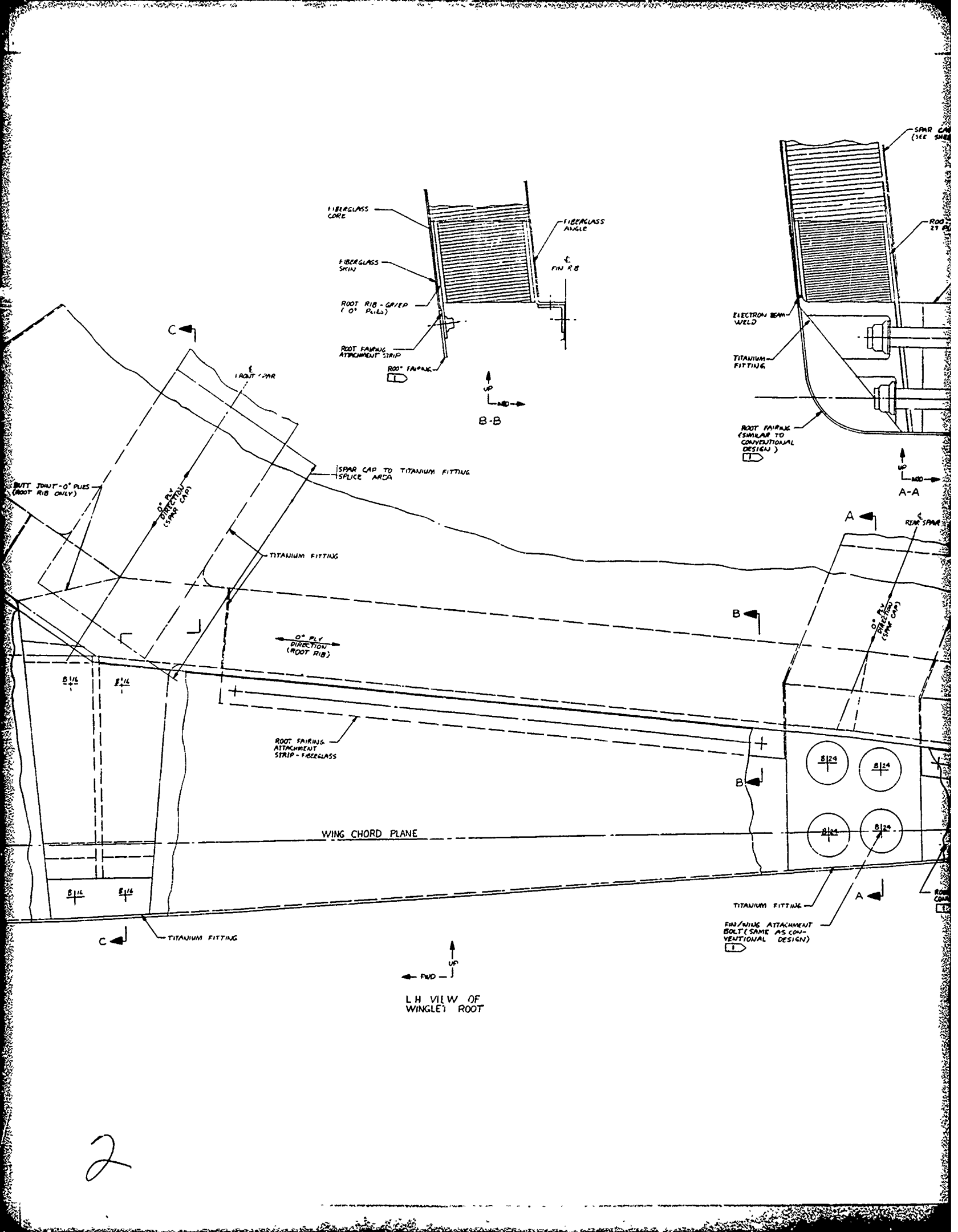
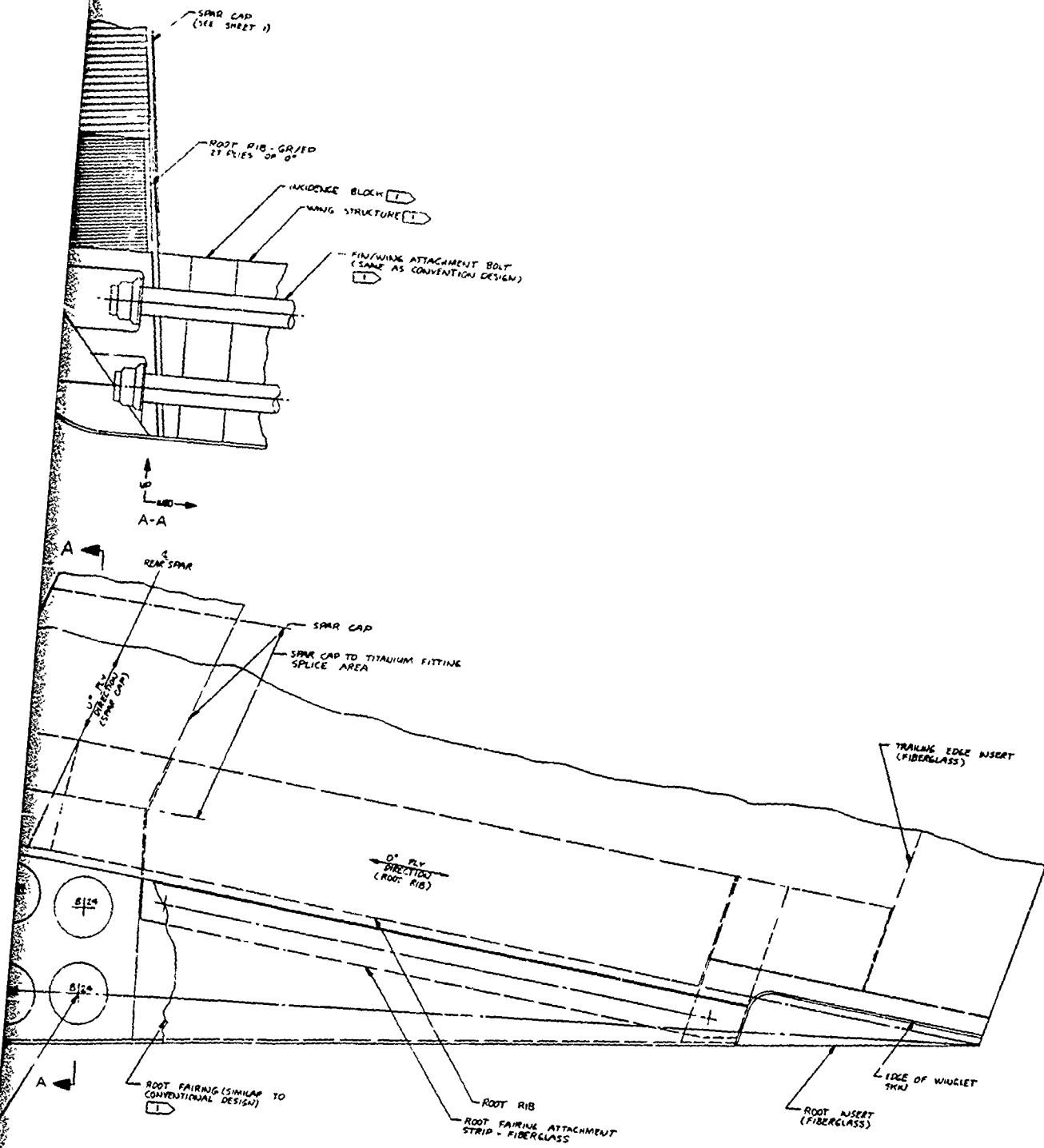


Figure 32.—Winglet Assembly—KC-135A Airplane (Advanced Composite Structural Concept)





2



NOT PART OF WINGLET ASSY. SEE EX 2992 (WINGLET W/STL - CONVENTIONAL DESIGN)

Figure 33.—Winglet Attachment—KC-135A Airplane (Advanced Composite Structural Concept)

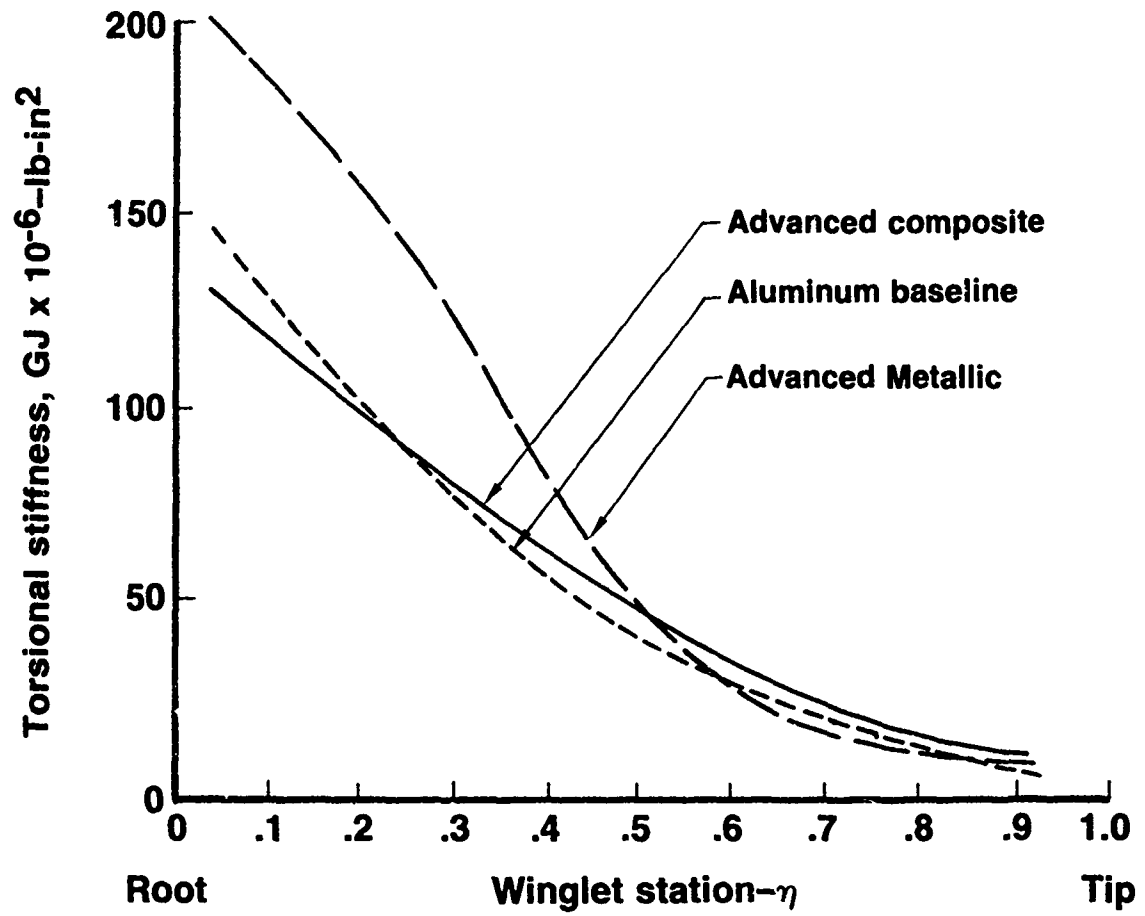


Figure 34.— Preliminary Torsional Stiffness Distribution of Winglet Designs

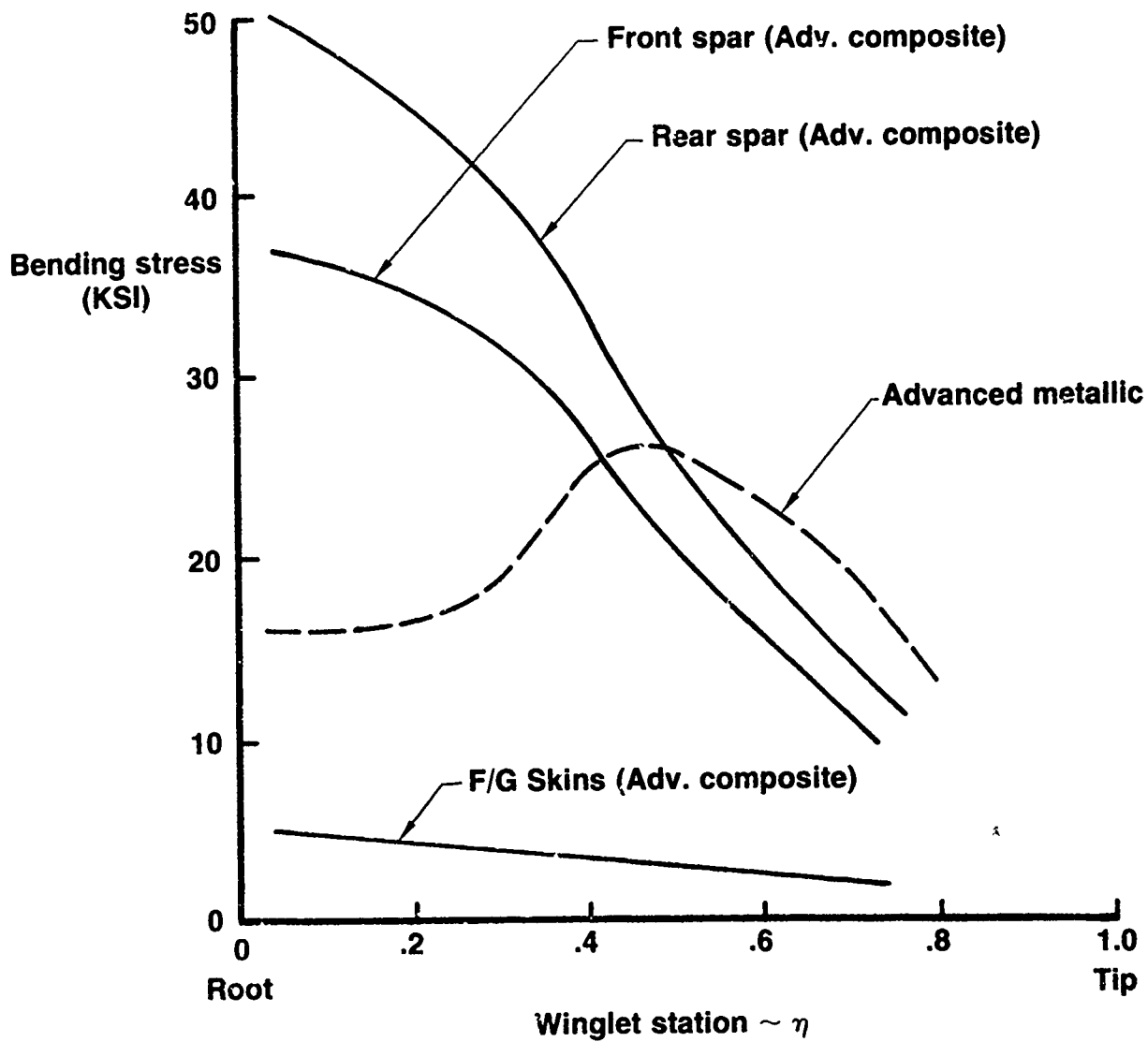
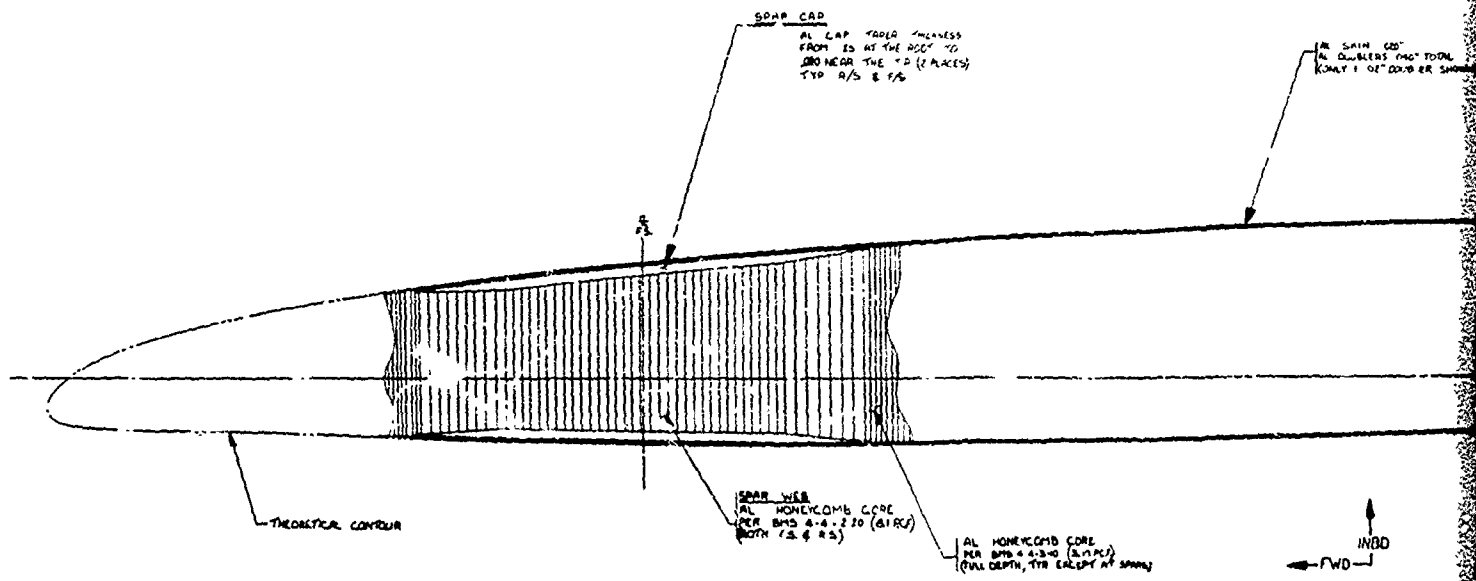
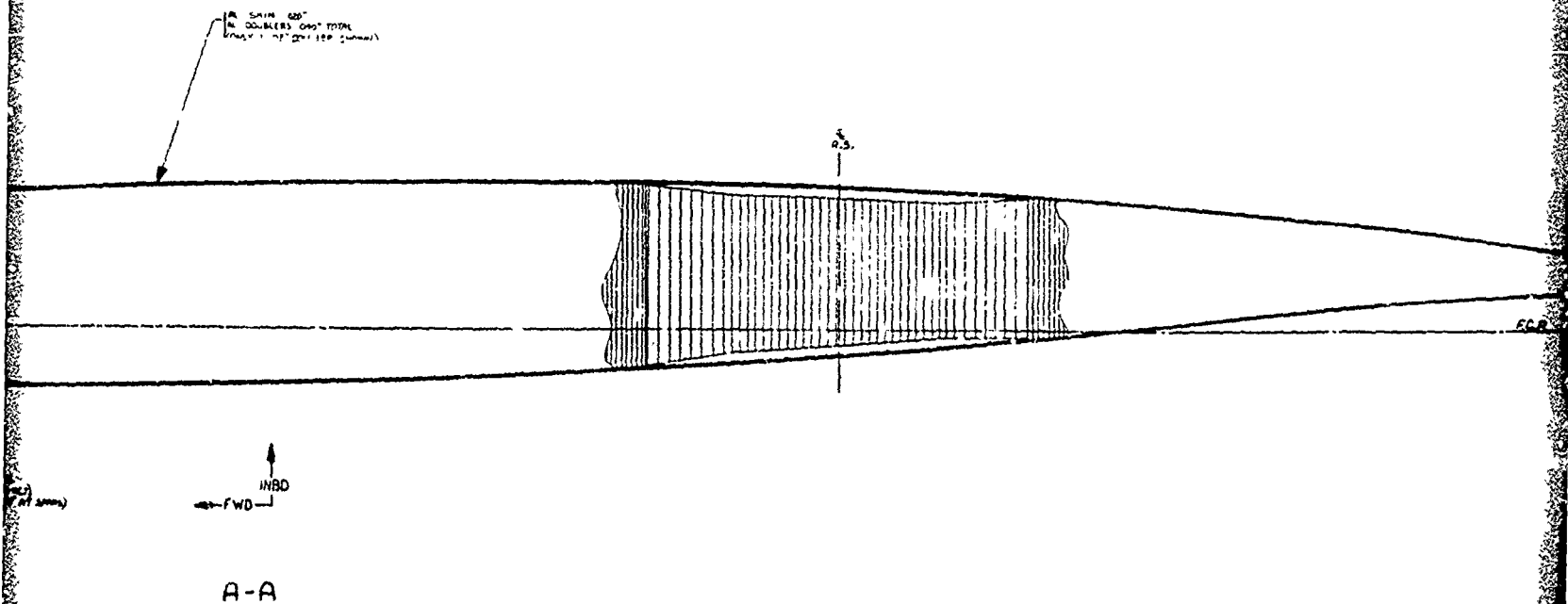
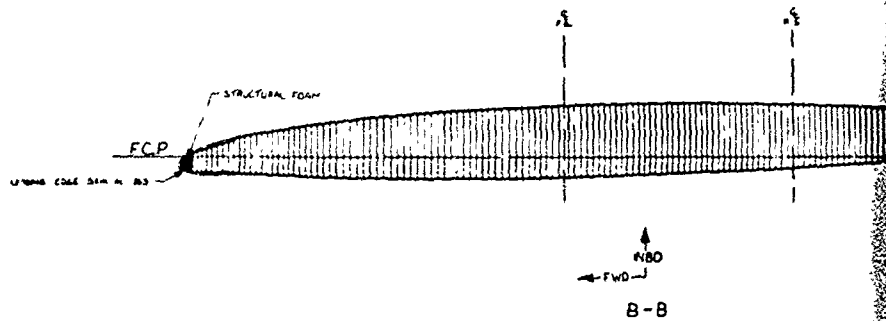


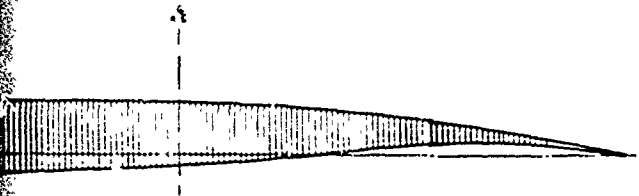
Figure 35.—Preliminary Maximum Bending Stress of Winglet Concepts



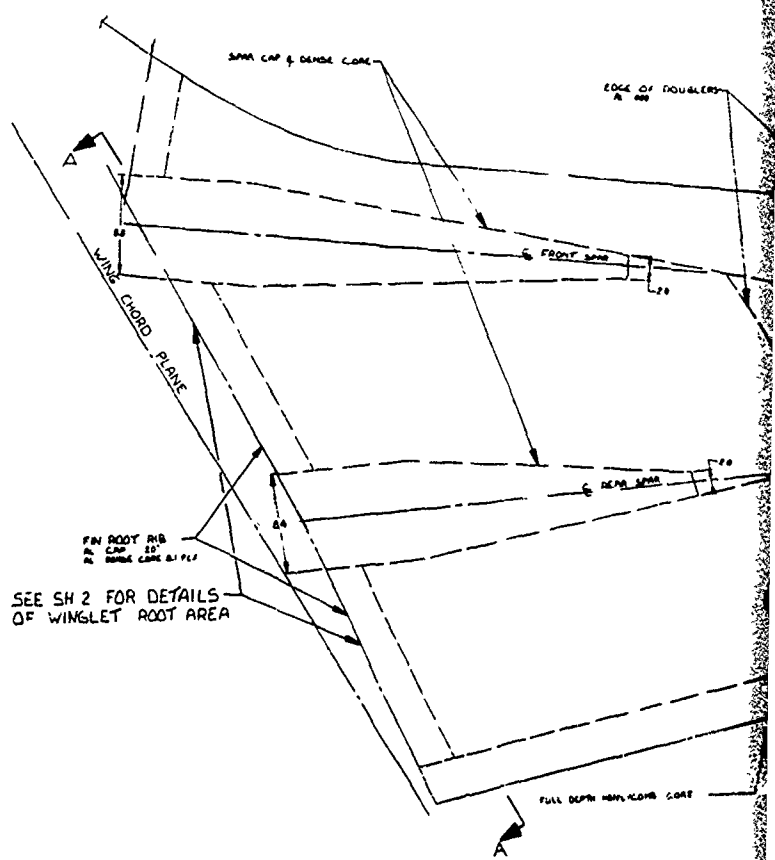
A-A



2



NBD
B-B



INSERT
GLASS FIBRE REINFORCED PLASTICS
PER SH 2 TO CLASS 1 TYPE 120,
181 OR 182

3

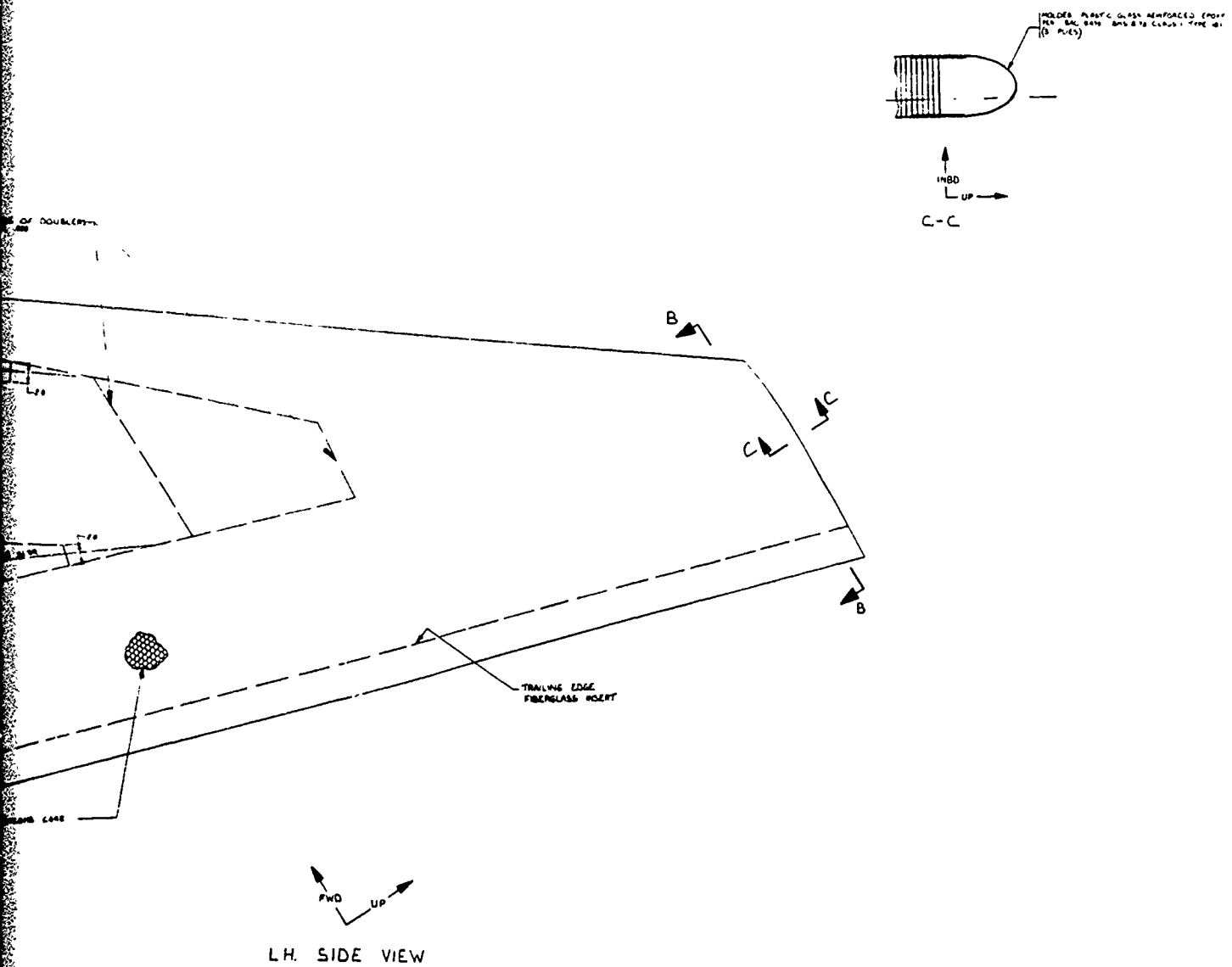
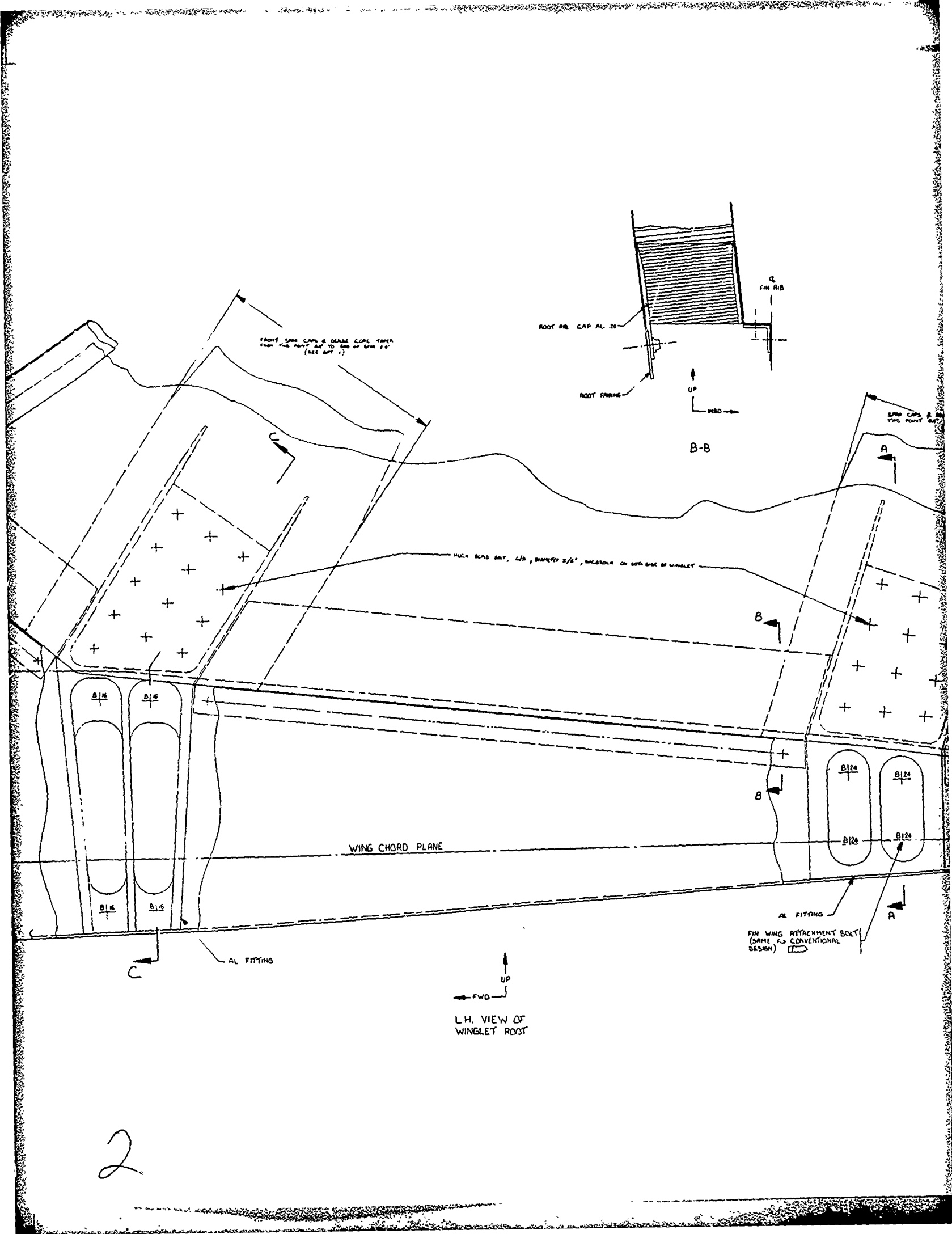


Figure 36.—Winglet Assembly KC-135A Airplane (Advanced Metallic Structural Concept)



FRONT SIDE CAPS & DEAD CORN TAKEN FROM THE POINT UP TO END OF RIB 20 (SEE RIB 1)

ROOT RIB CAP AL 20

FIN RIB

ROOT FRINGE

B-B

FRONT SIDE CAPS & DEAD CORN TAKEN FROM THE POINT UP TO END OF RIB 20 (SEE RIB 1)

MUCH BLAD MAT, 1/8" DIAMETER 2/8", MESSOR ON BOTH SIDE OF WINGLET

WING CHORD PLANE

AL FITTING
PIN WING ATTACHMENT BOLT (SAME AS CONVENTIONAL DESIGN)



L.H. VIEW OF WINGLET ROOT

2

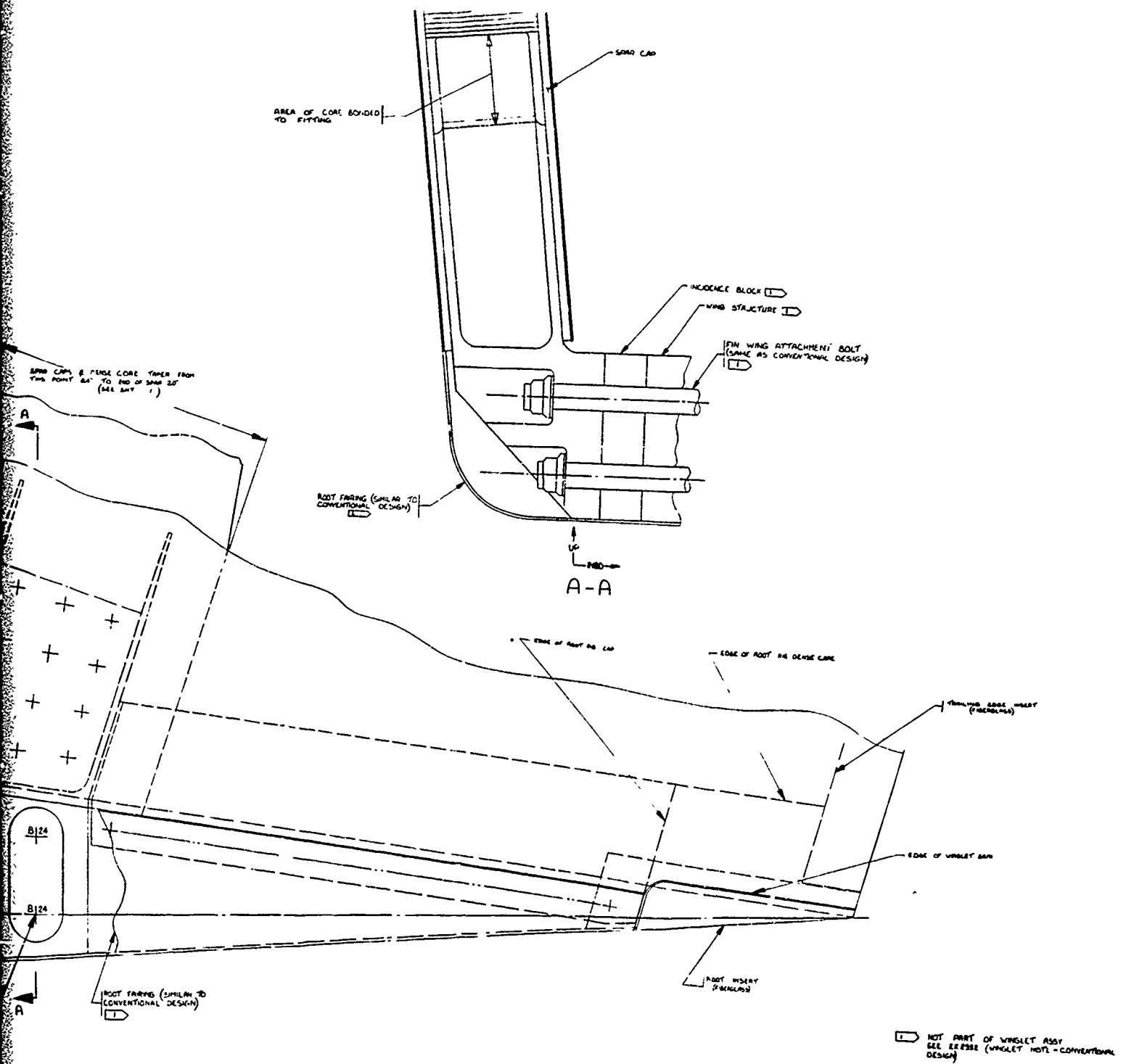


Figure 37.—Winglet Attachment KC-135A Airplane (Advanced Metallic Structural Concept)

Range factor improvement	+ 8.1%
O.E.W. increase (592 lbs.)	- .6%
Change in ferry mission range	+ 7.5%

Weight ~ lbs	KC-135A	KC-135A with winglets
Max weight	297,000	294,000
O.E.W.	104,450	105,042

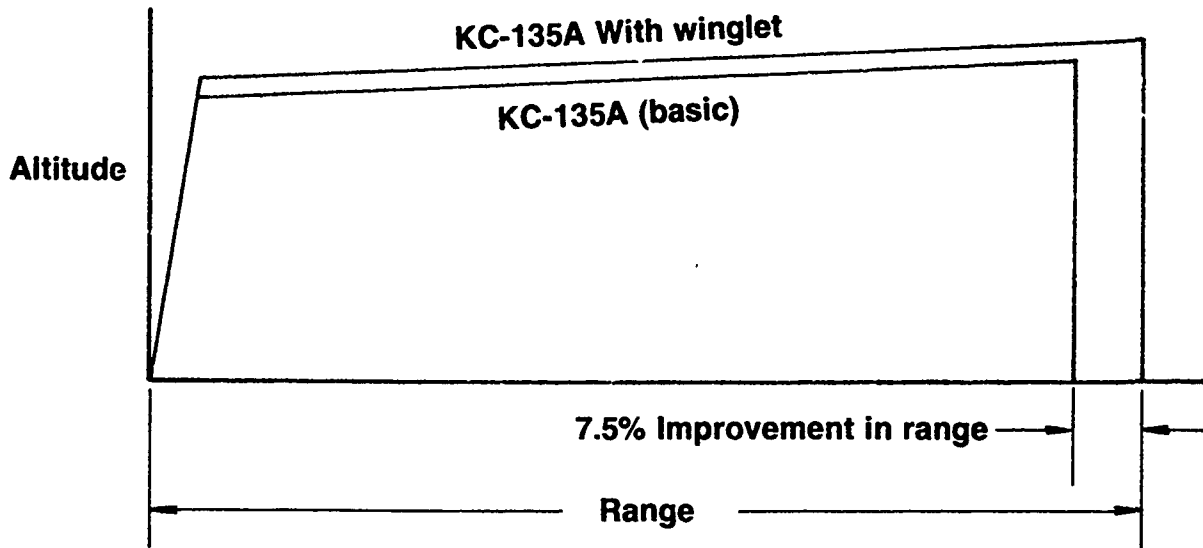
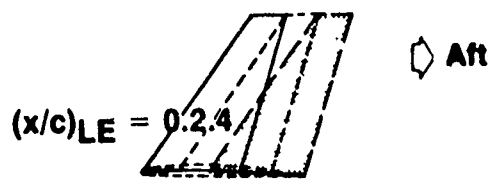
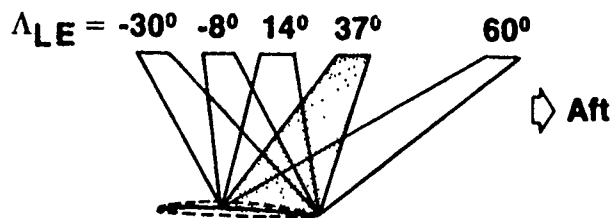


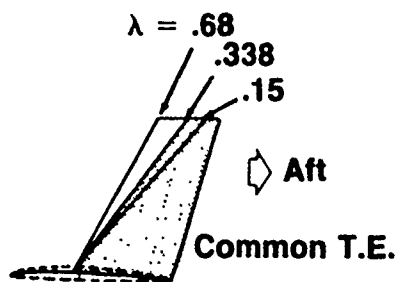
Figure 38.— Effect of Winglets on Range Performance (Ferry Mission)



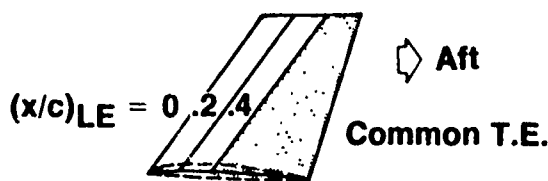
Chordwise location study



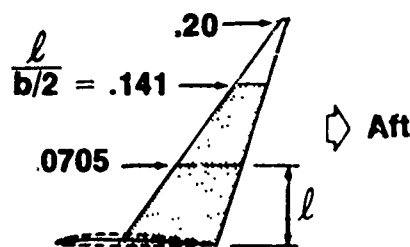
Sweep study



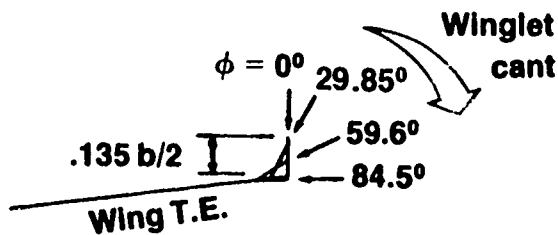
Taper ratio study



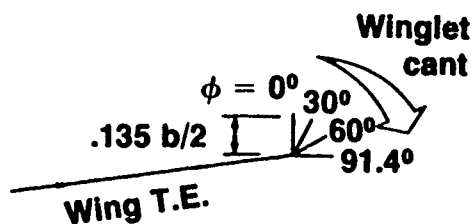
Area study



Length study



Cant study-constant span



Cant study-variable span

Figure 39.—Winglet Parameters Analyzed on KC-135 Wing

Taper ratio = .338
AR = 2.43

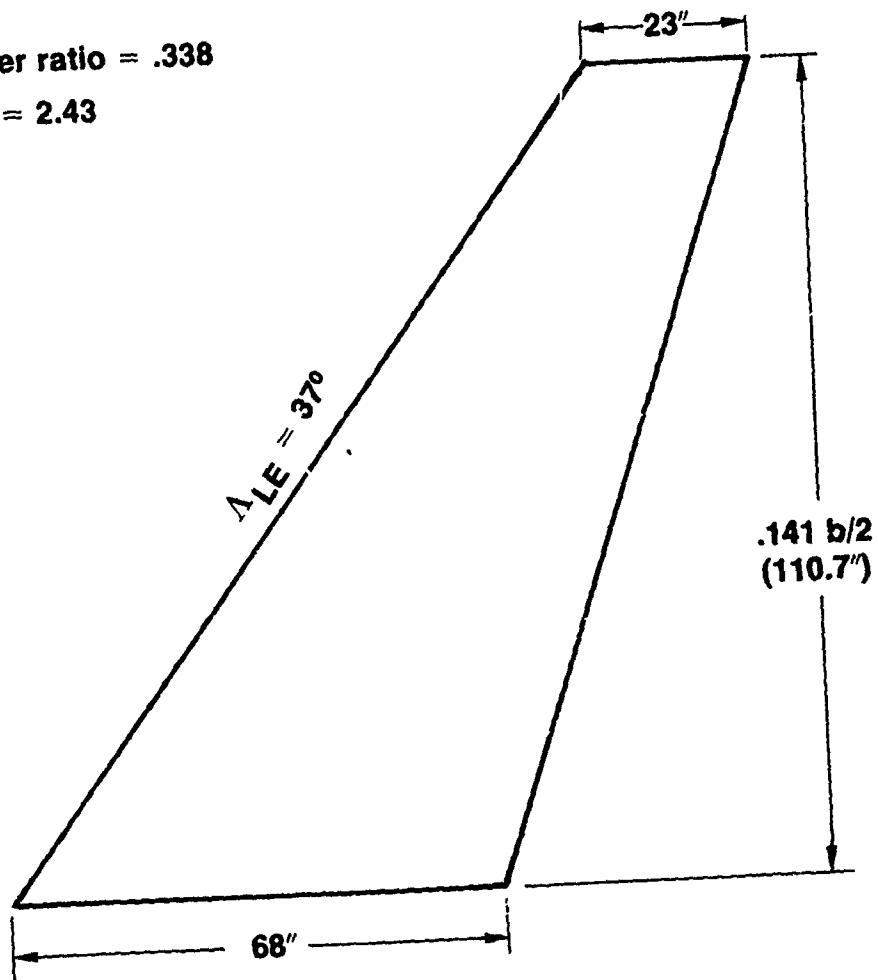


Figure 40.— Baseline Winglet Planform for the First 5 Parameter Studies

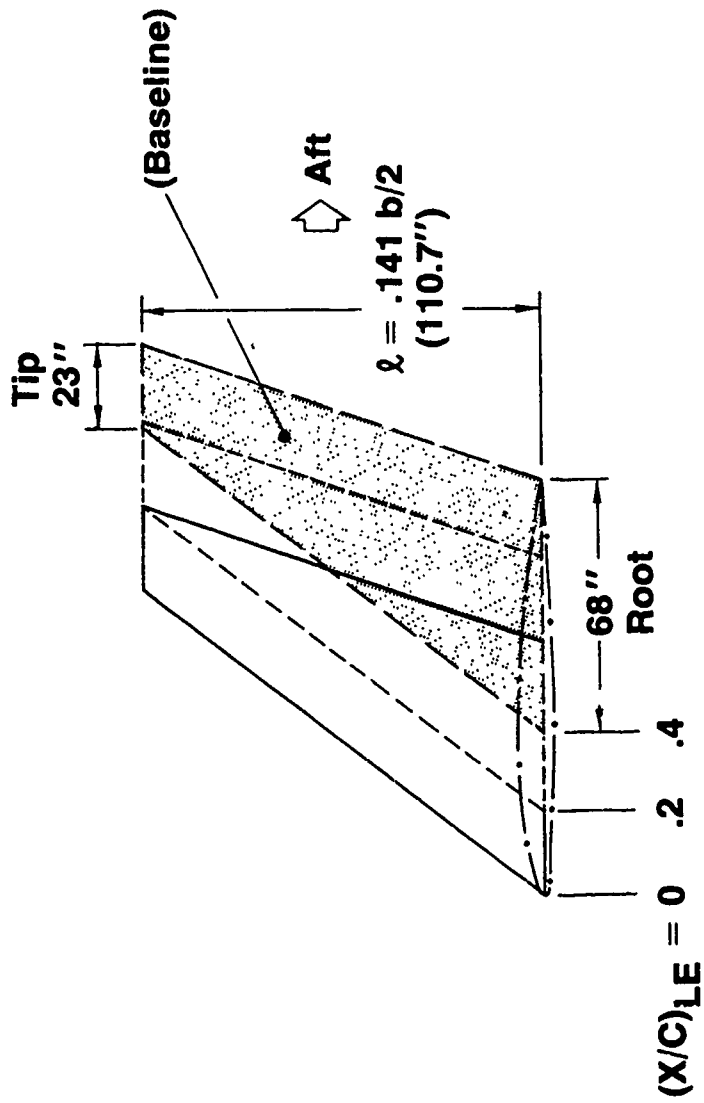
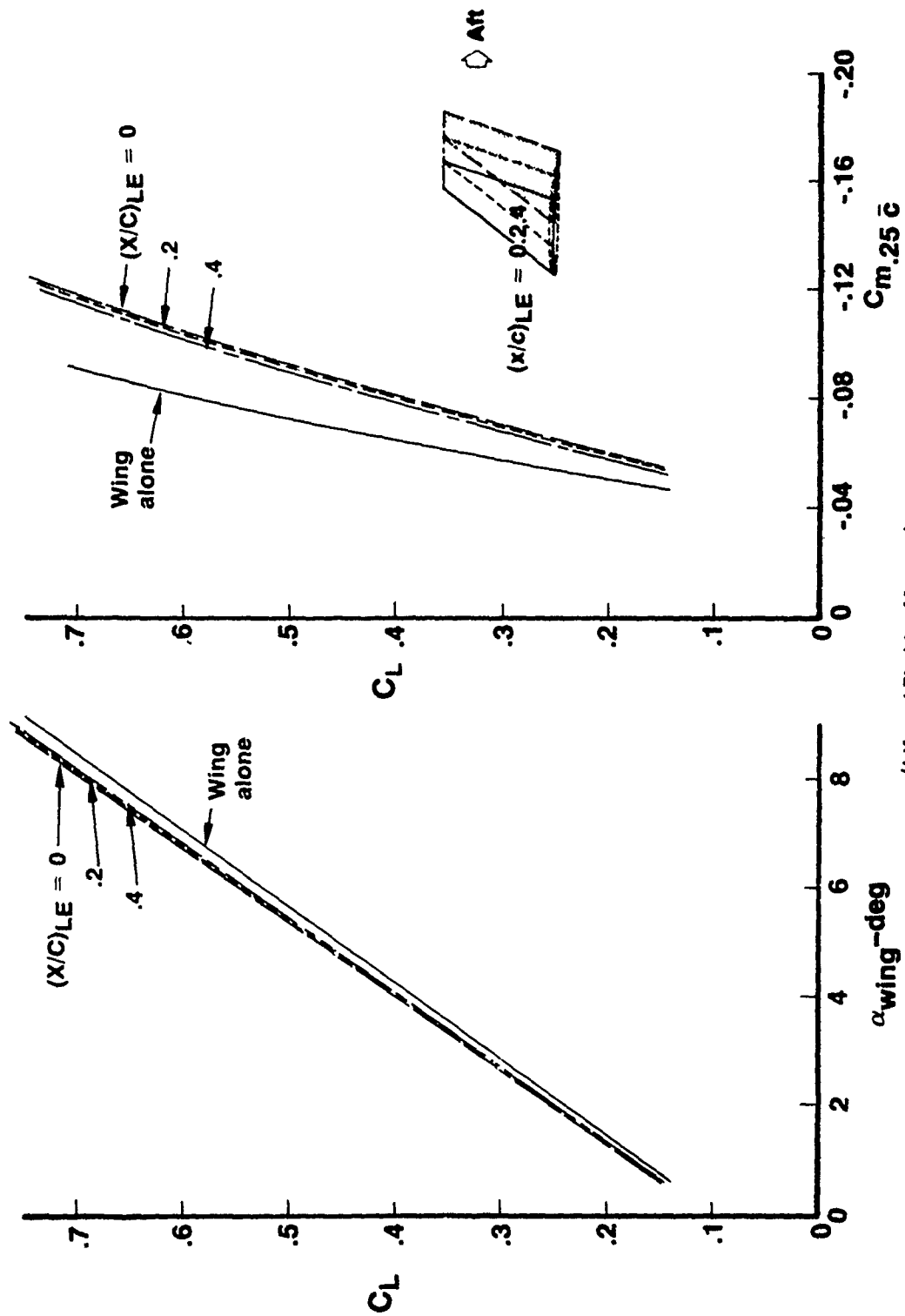
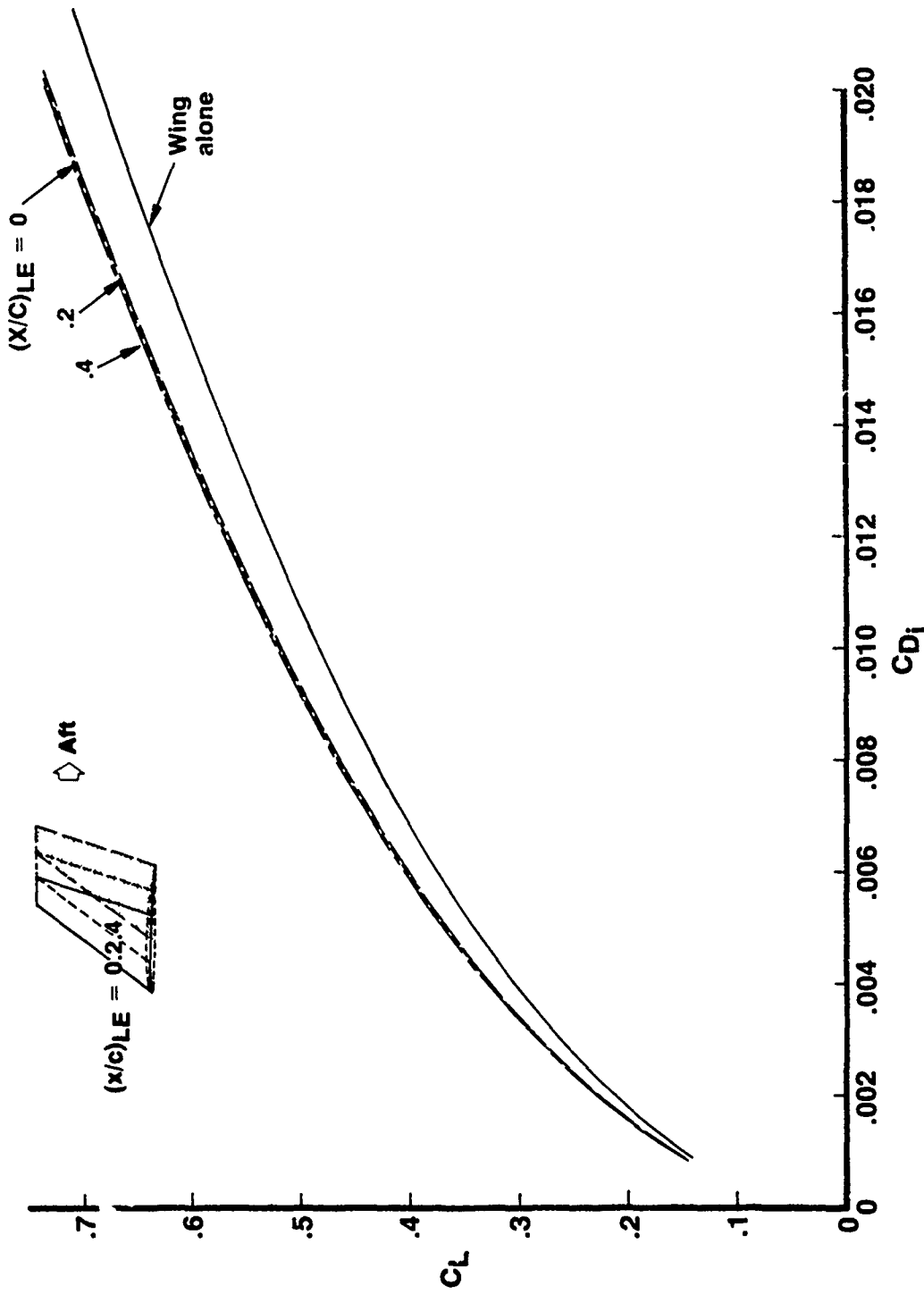


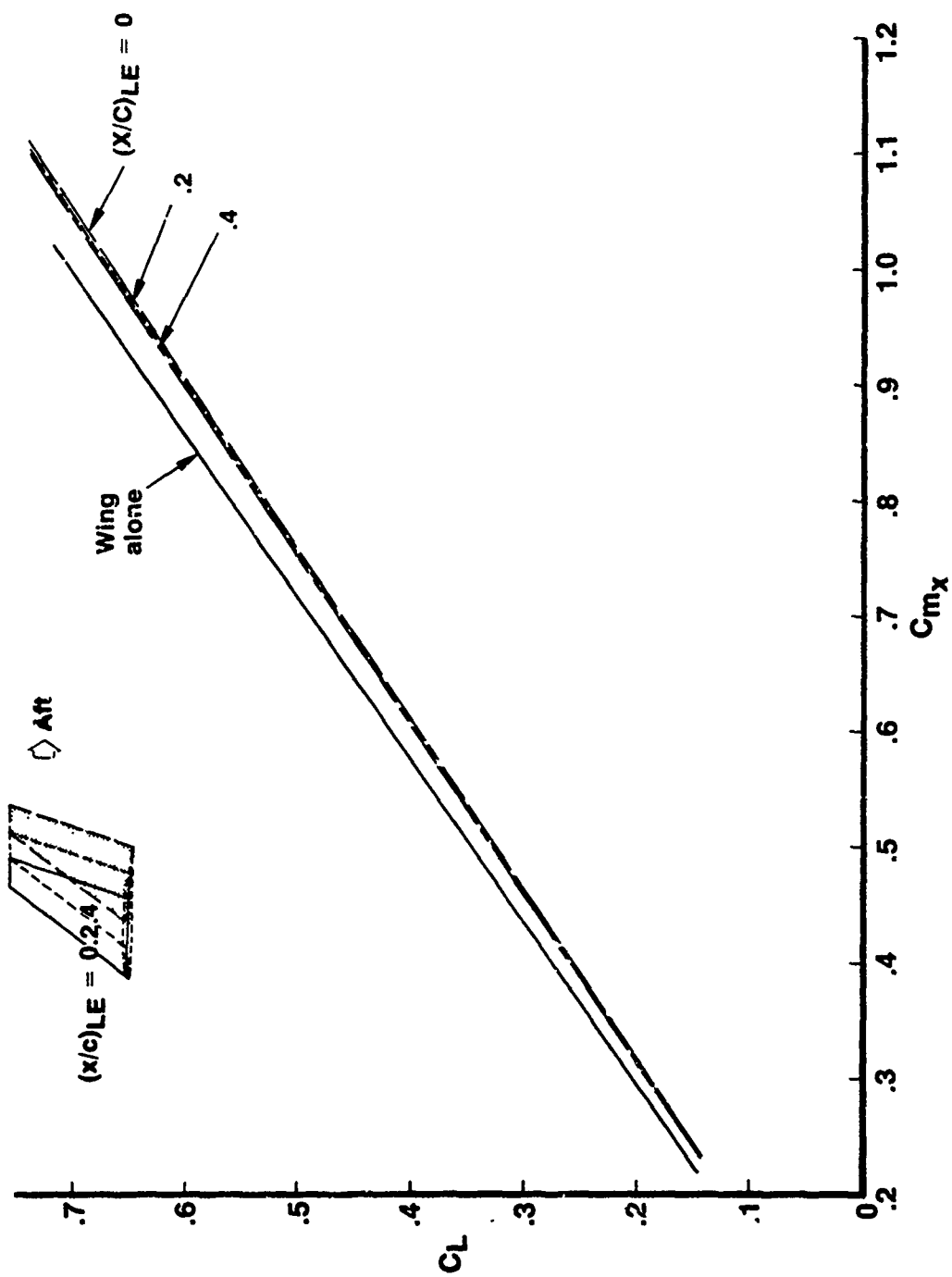
Figure 41.—Winglets Chordwise Location Study



a (Lift and Pitching Moment)
 Figure 42.— Effect of Winglet Chordwise Location

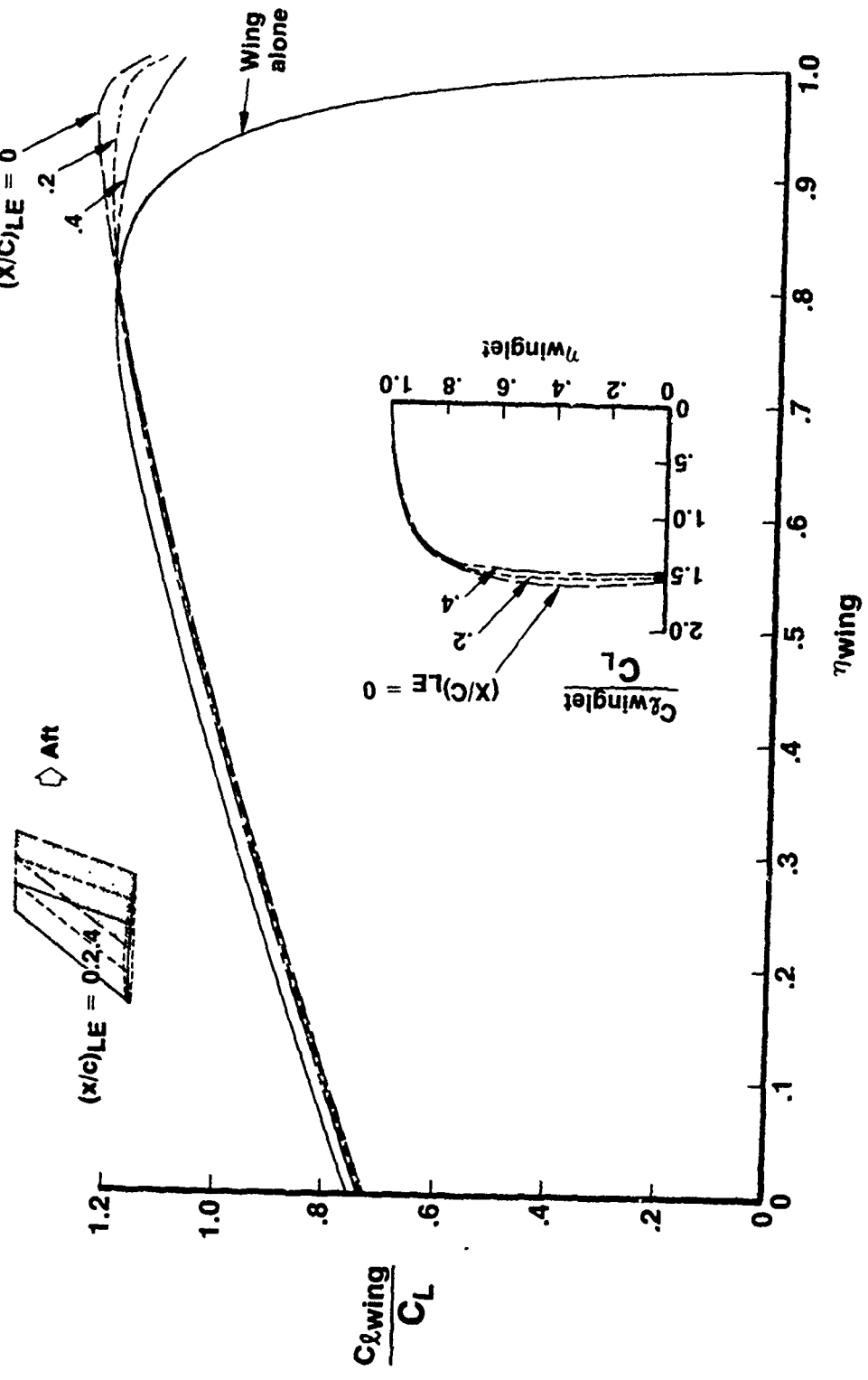


b (Induced Drag)
Figure 42. - (Continued)

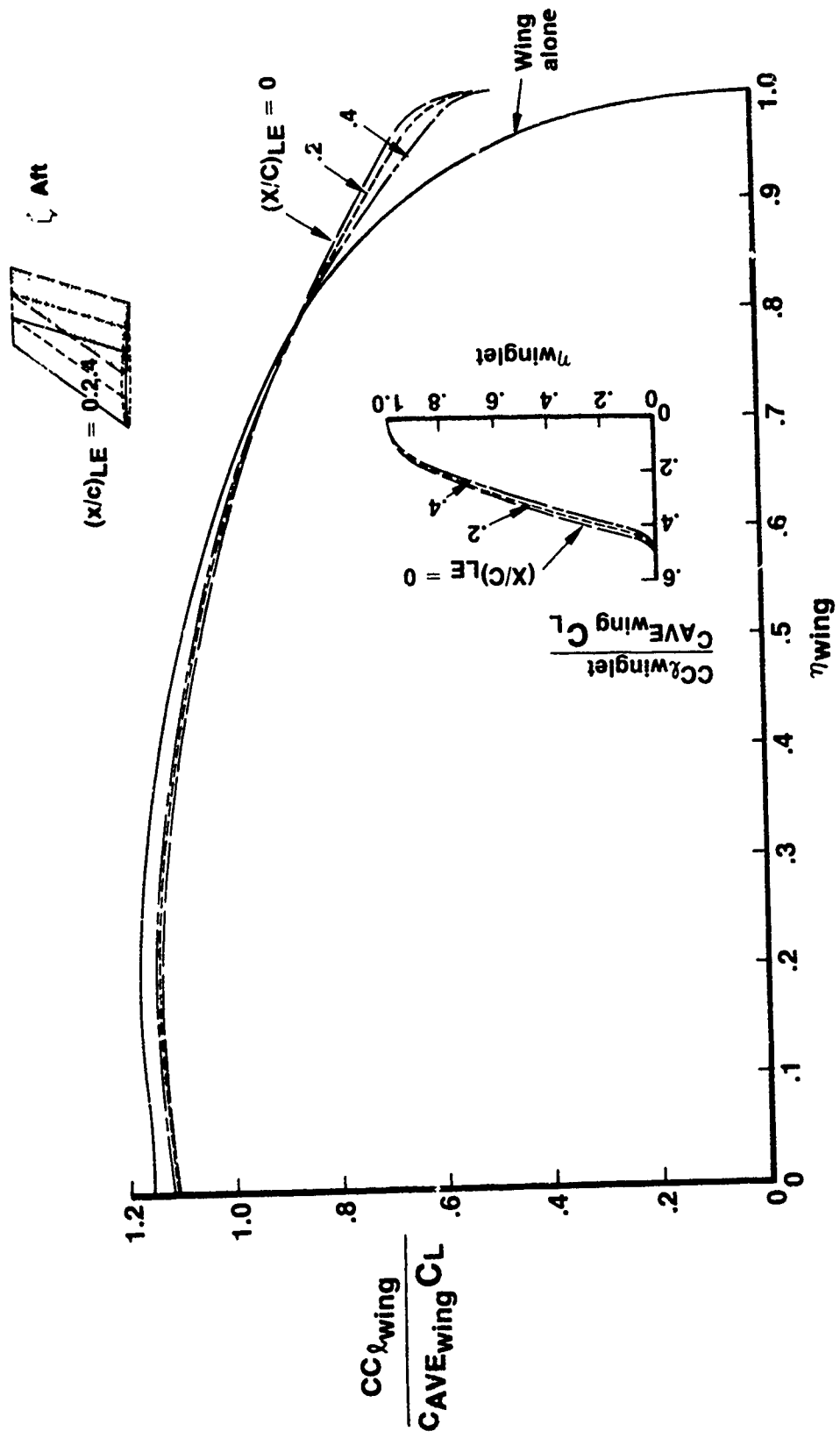


c (Wing-Root Bending Moment)
Figure 42. — (Continued)

$C_L = .426$



d (Sectional Lift)
Figure 42.— (Continued)



e (Span Loading)
Figure 42.-- (Concluded)

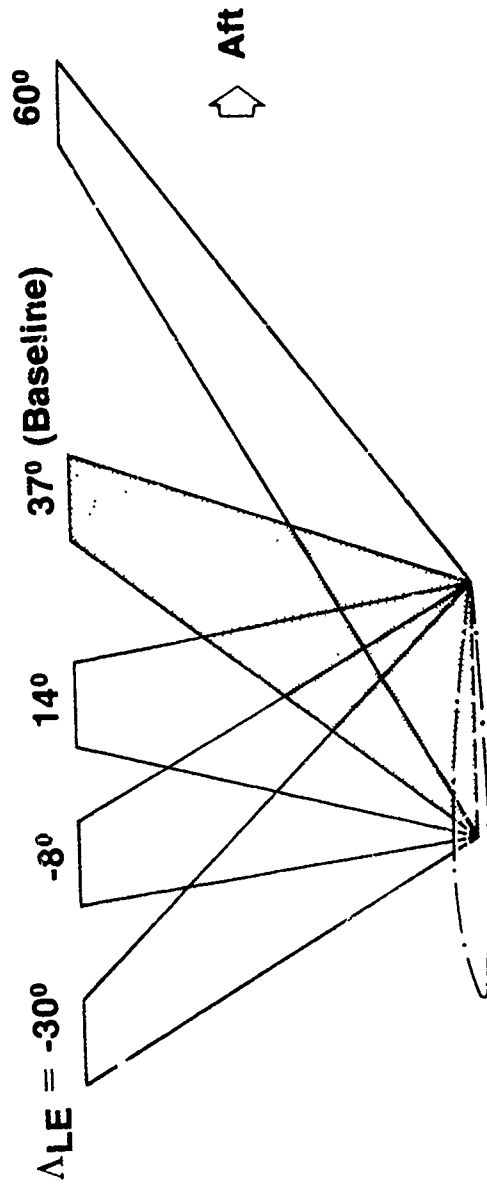
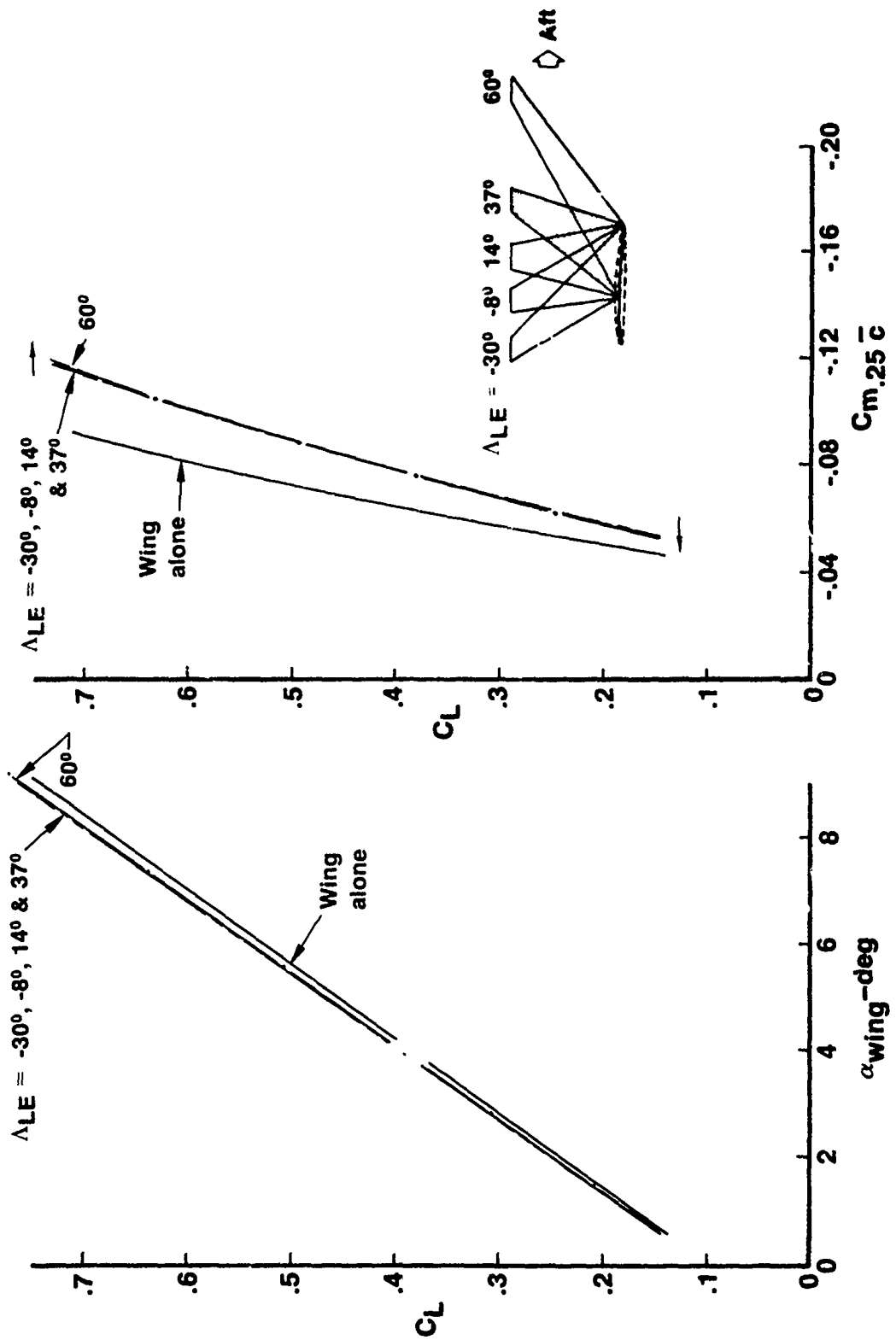
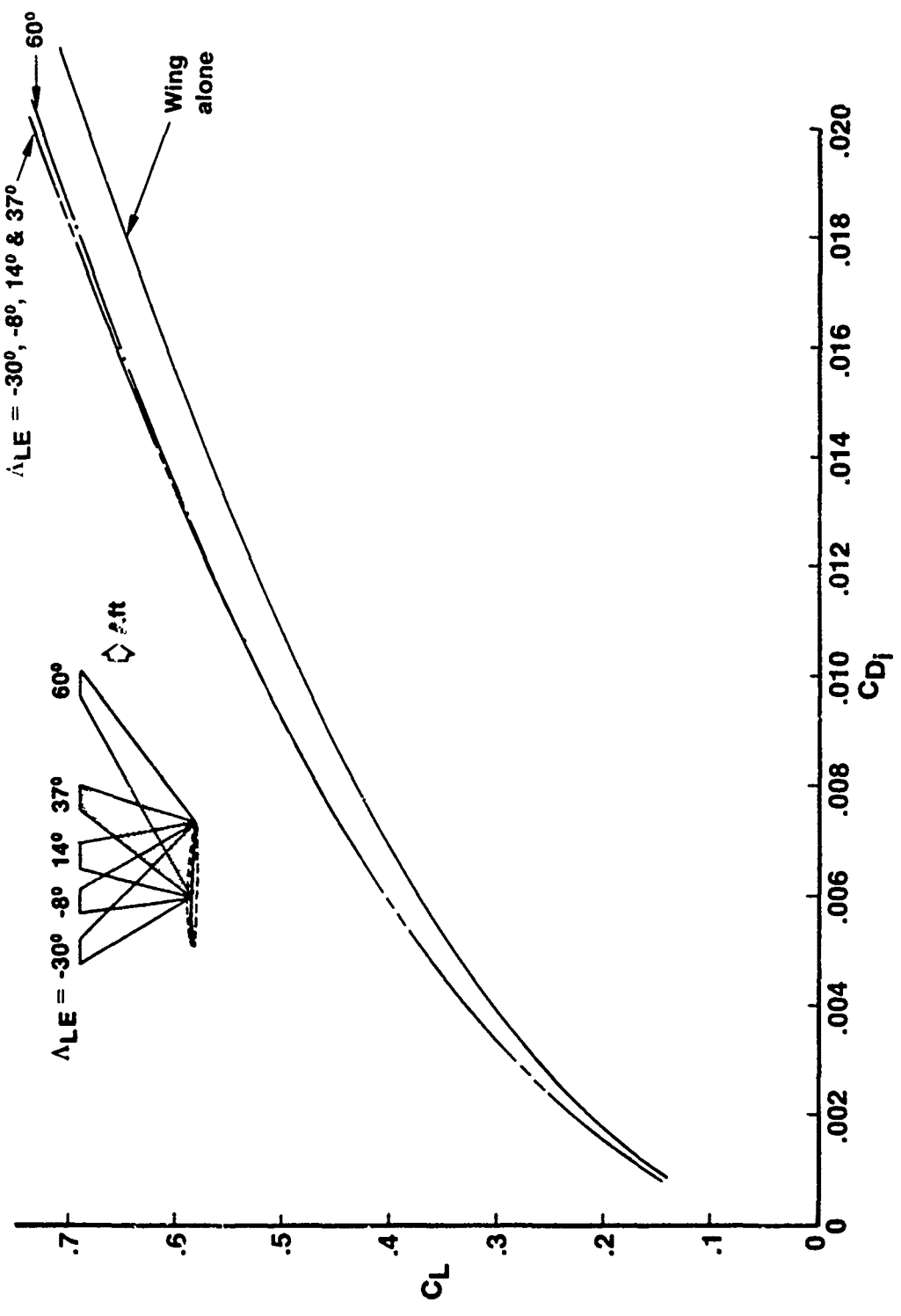


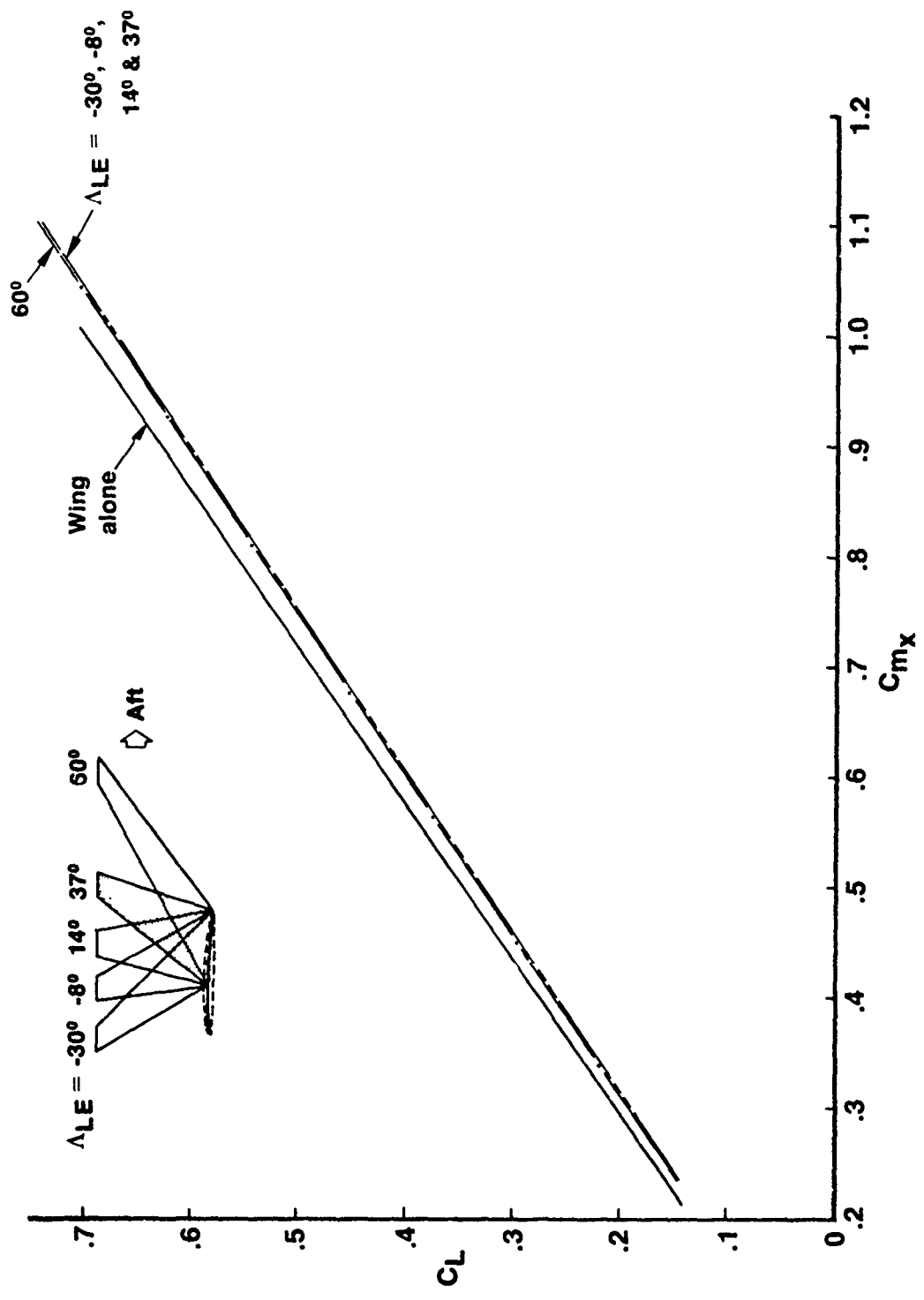
Figure 43. —Winglets for Sweep Study



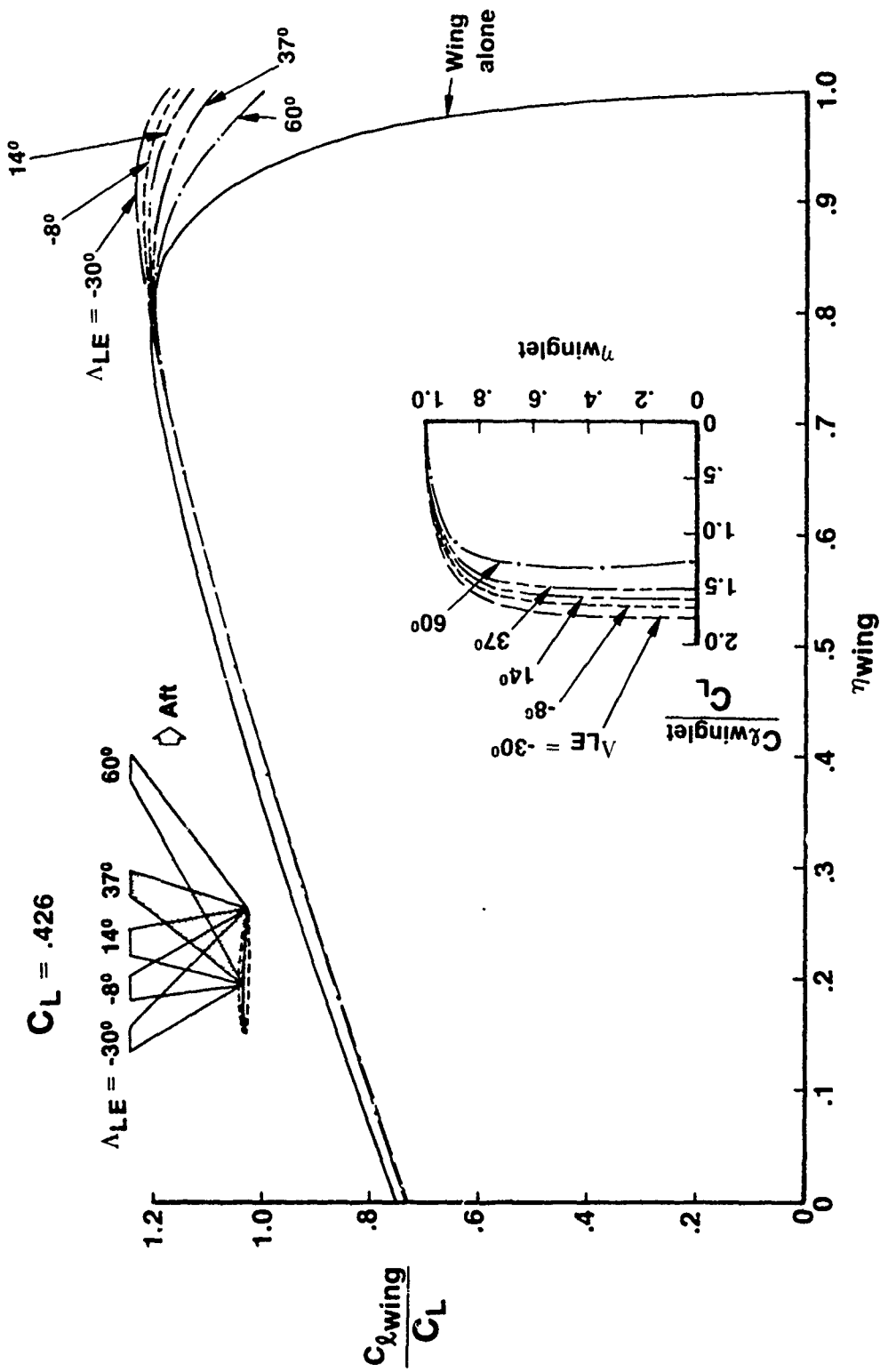
a (Lift and Pitching Moment)
 Figure 44.—Effect of Winglet Sweep



b (Induced Drag)
 Figure 44. - (Continued)

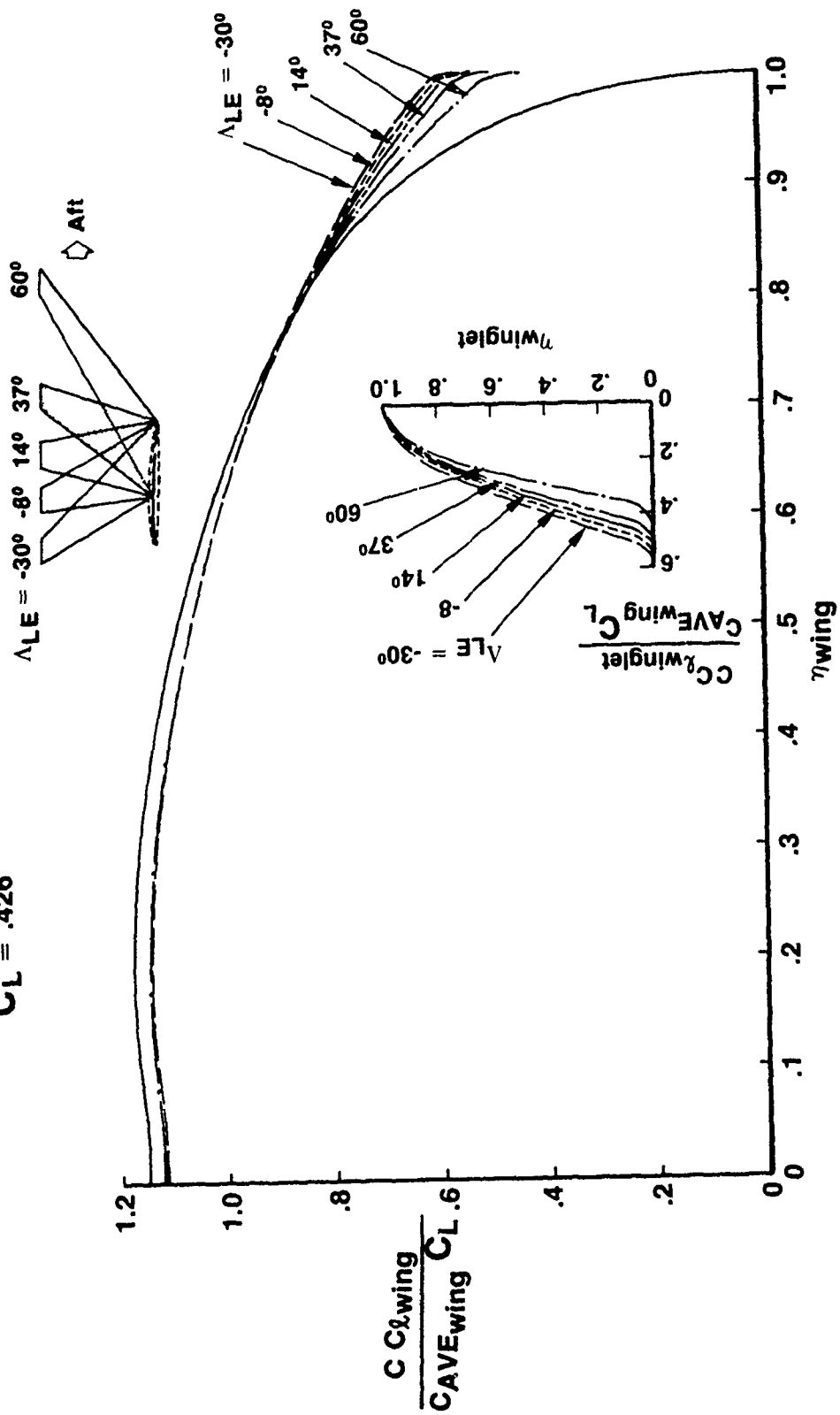


c (Wing-Root Bending Moment)
 Figure 44.—(Continued)



d (Sectional Lift)
 Figure 44. — (Continued)

$C_L = .426$



e (Span Loading)
Figure 44. - (Concluded)

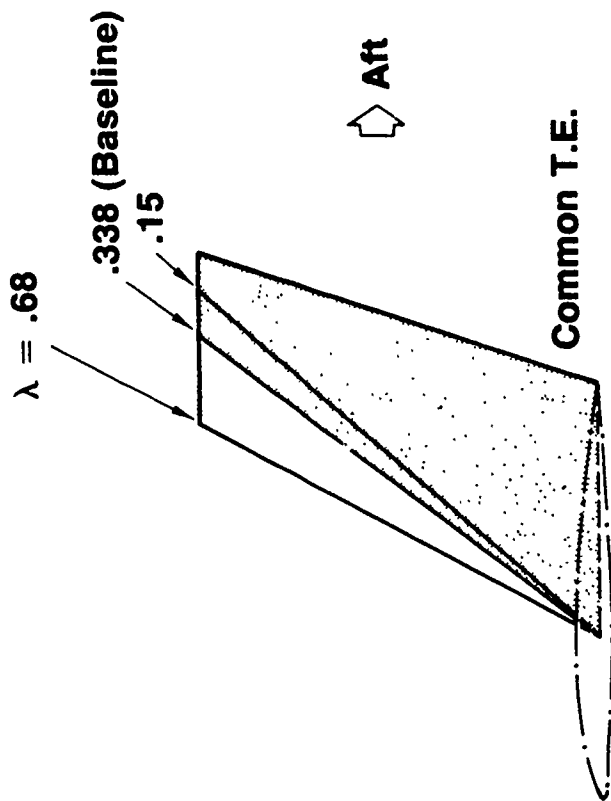
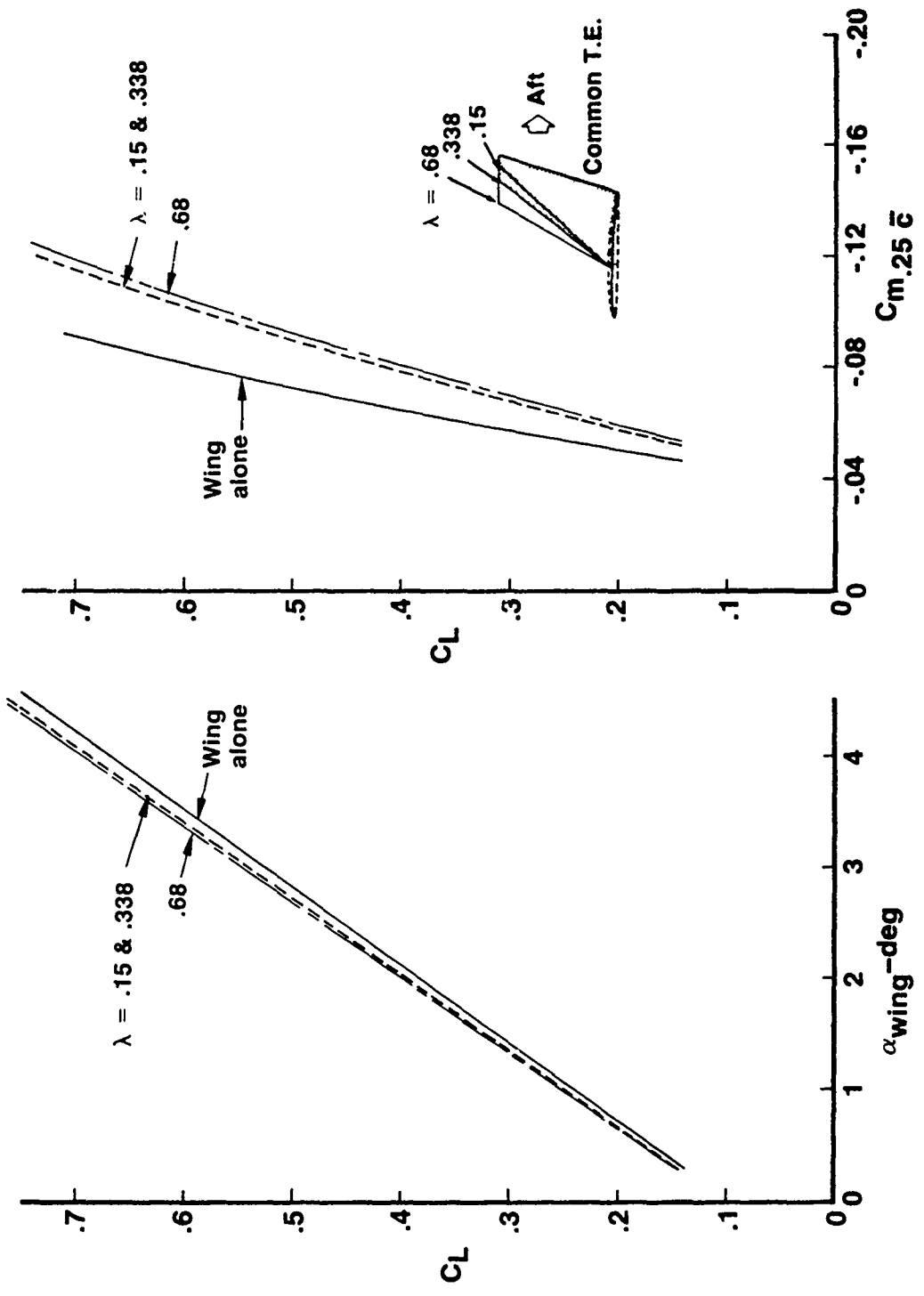
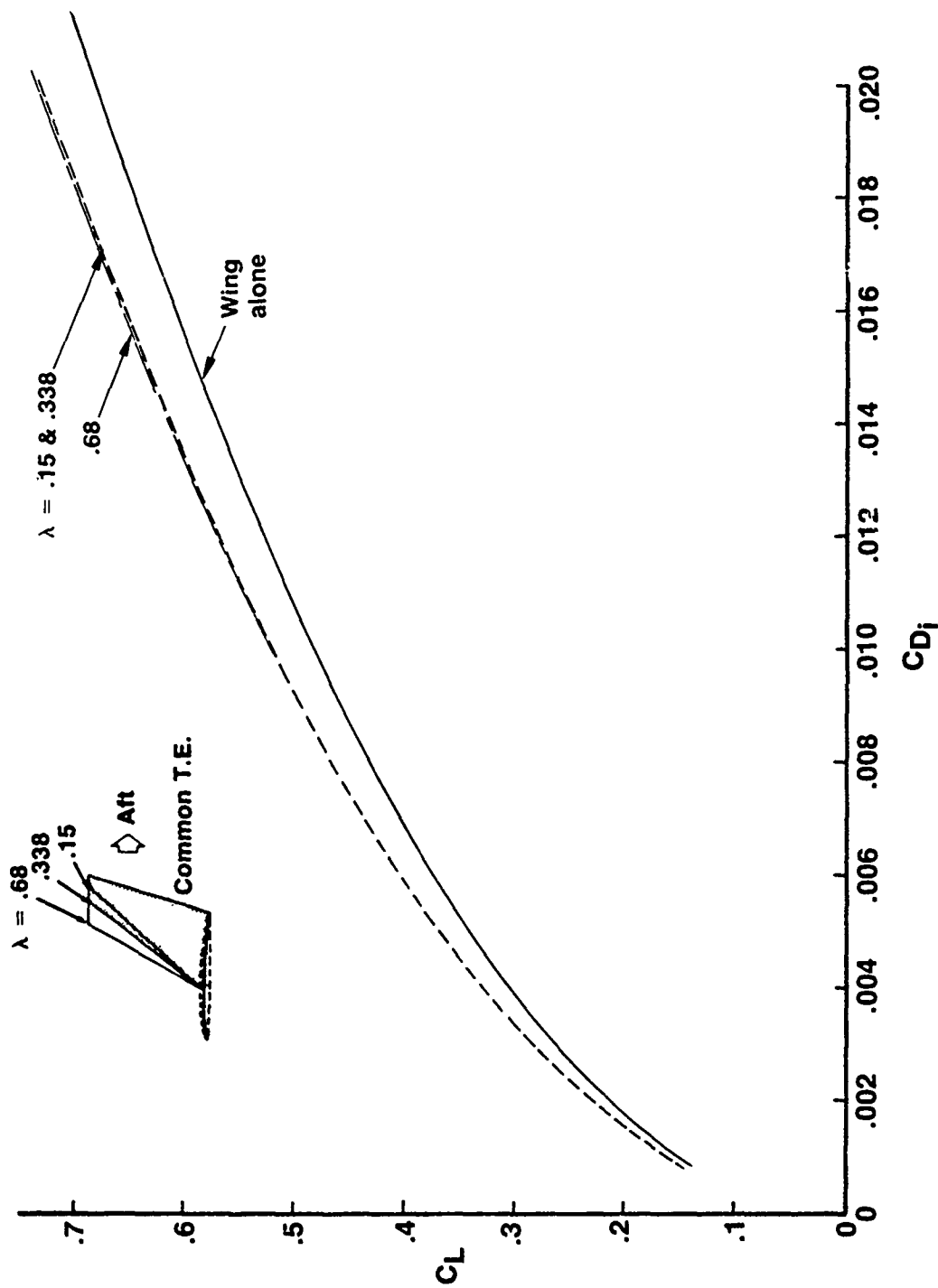


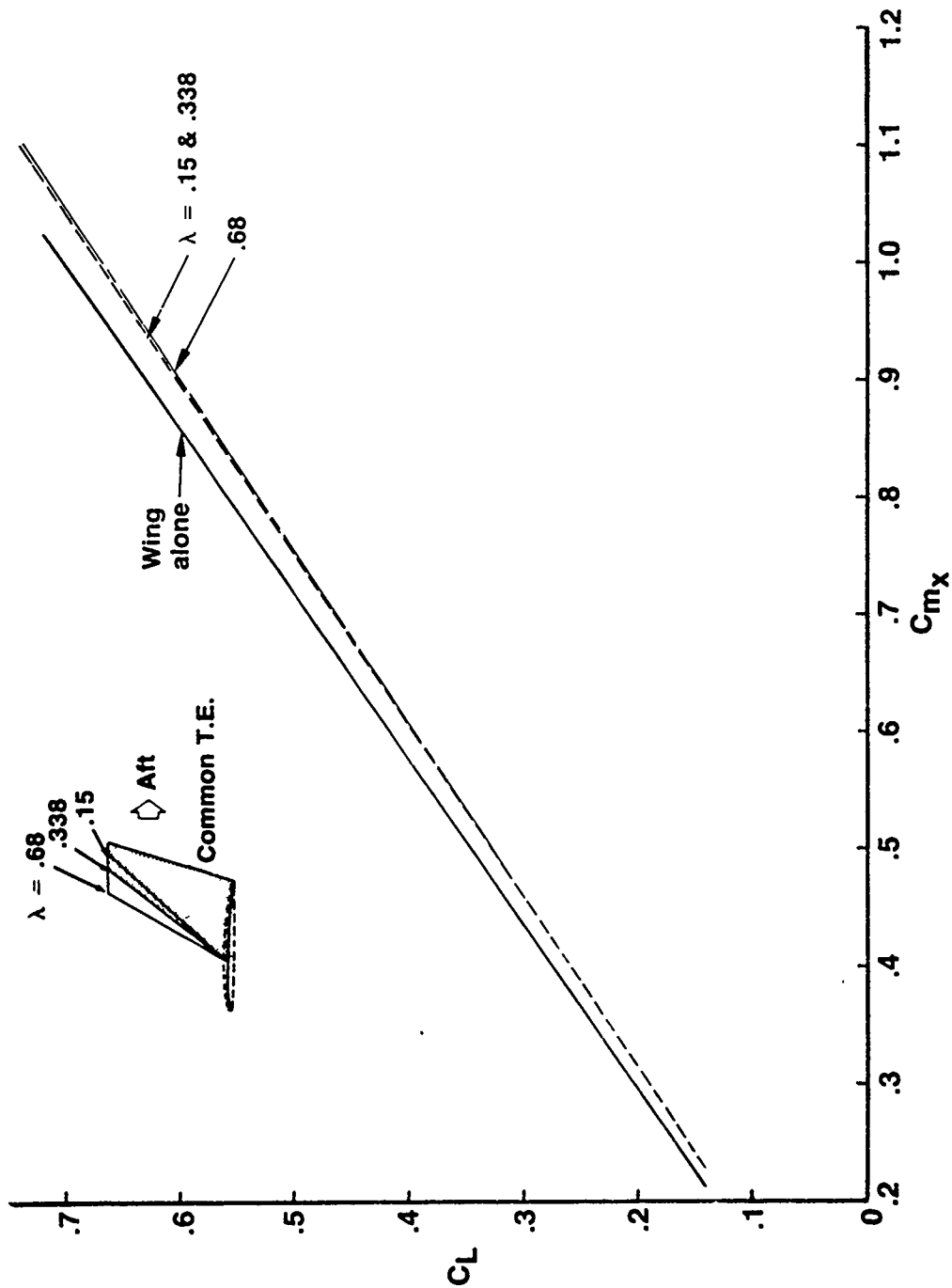
Figure 45. - Winglets for Taper Ratio Study



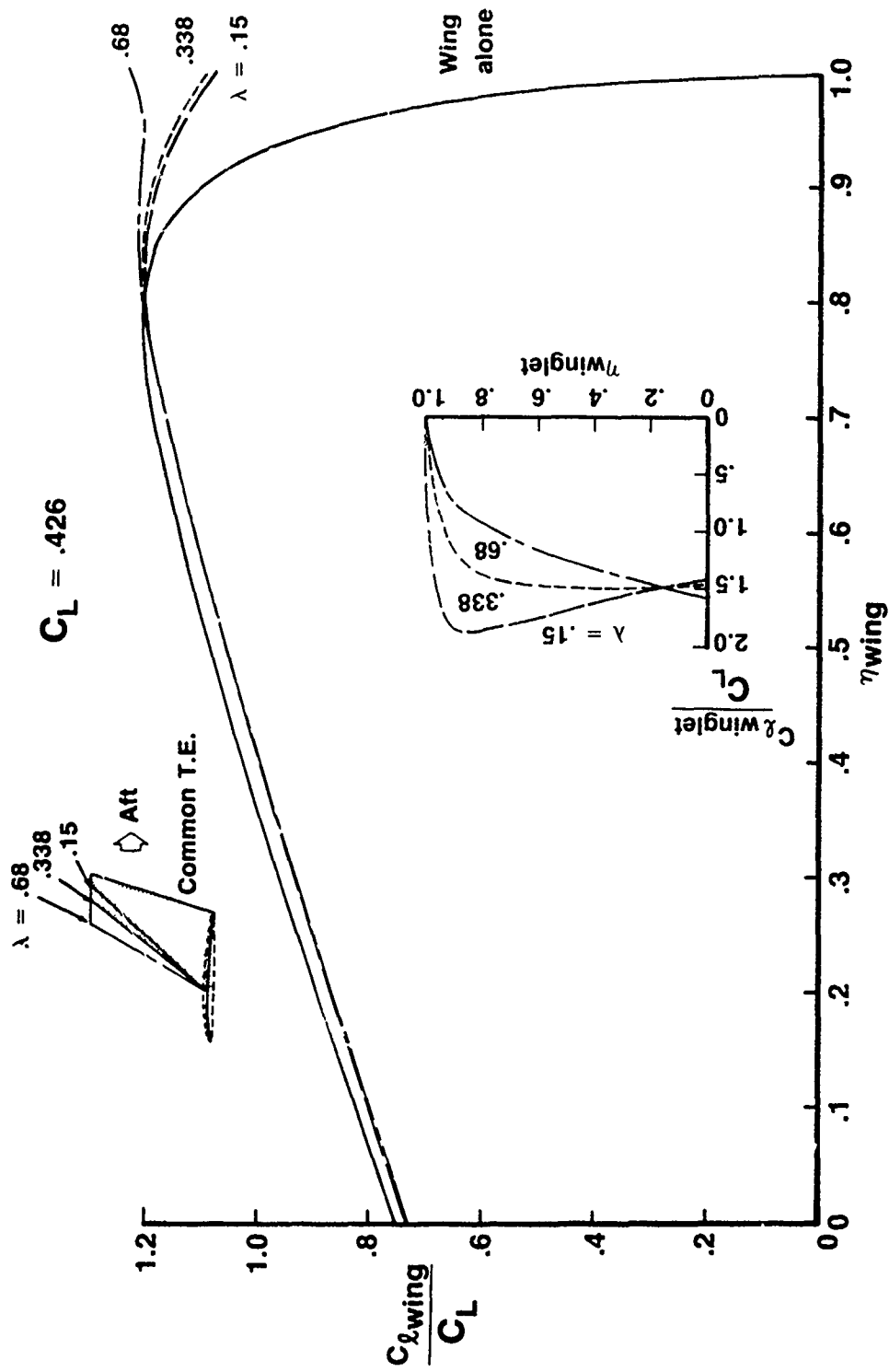
a (Lift and Pitching Moment)
 Figure 46.—Effect of Winglet Taper Ratio



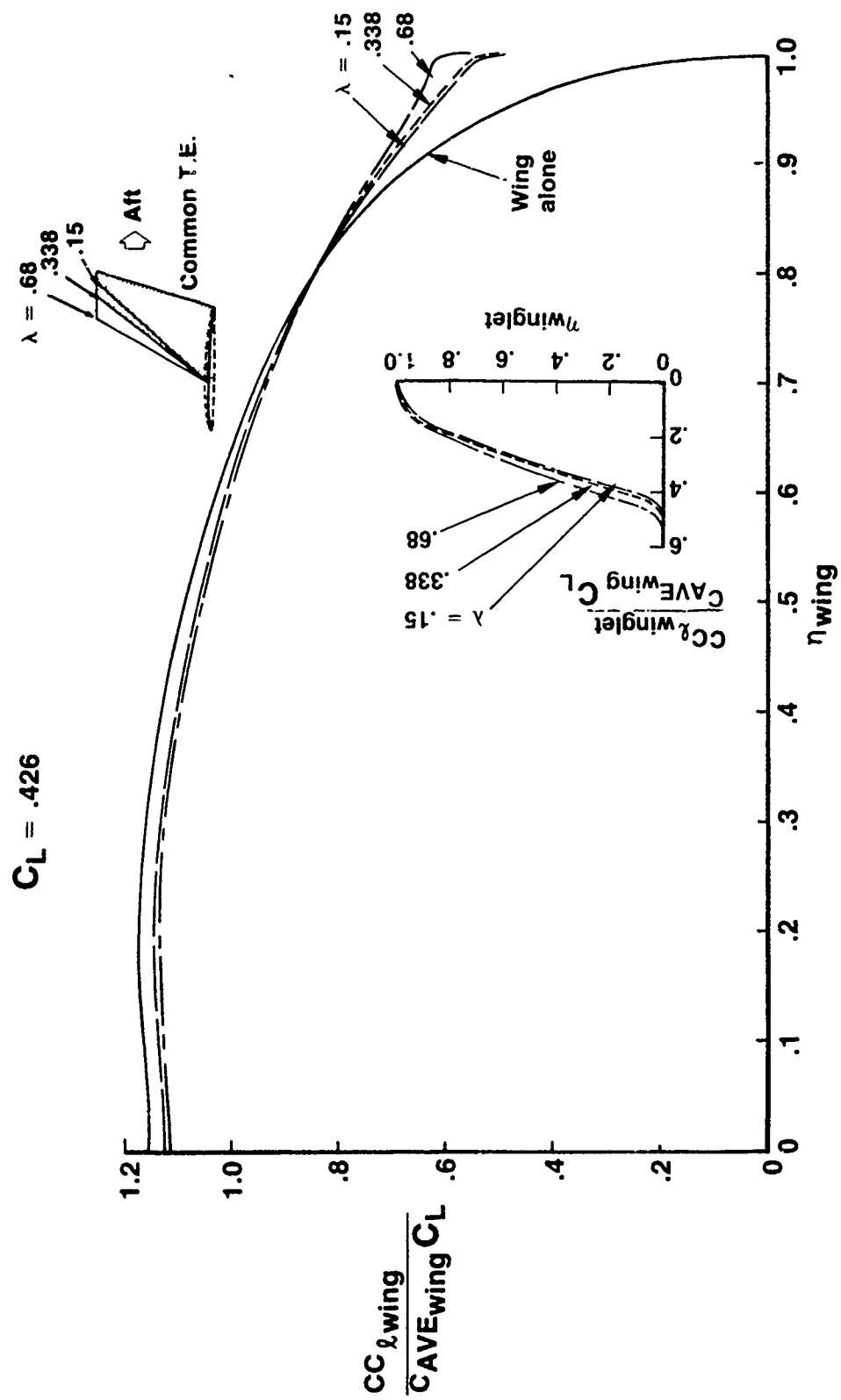
b (Induced Drag)
Figure 46. - (Continued)



c (Wing-Root Bending Moment)
Figure 46.—(Continued)



d (Sectional Lift)
Figure 46. — (Continued)



e (Span Loading)
Figure 46. — (Concluded)

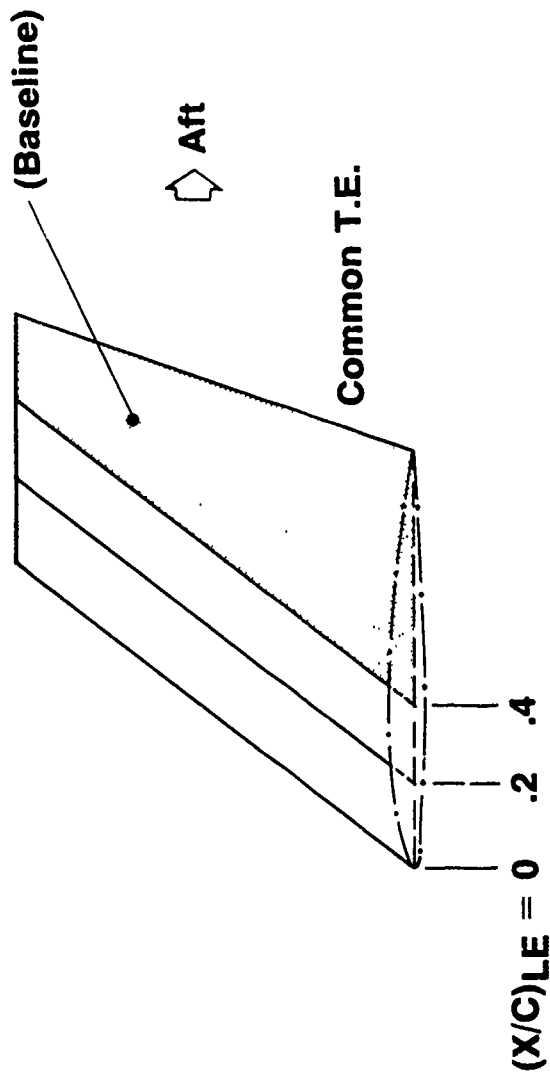
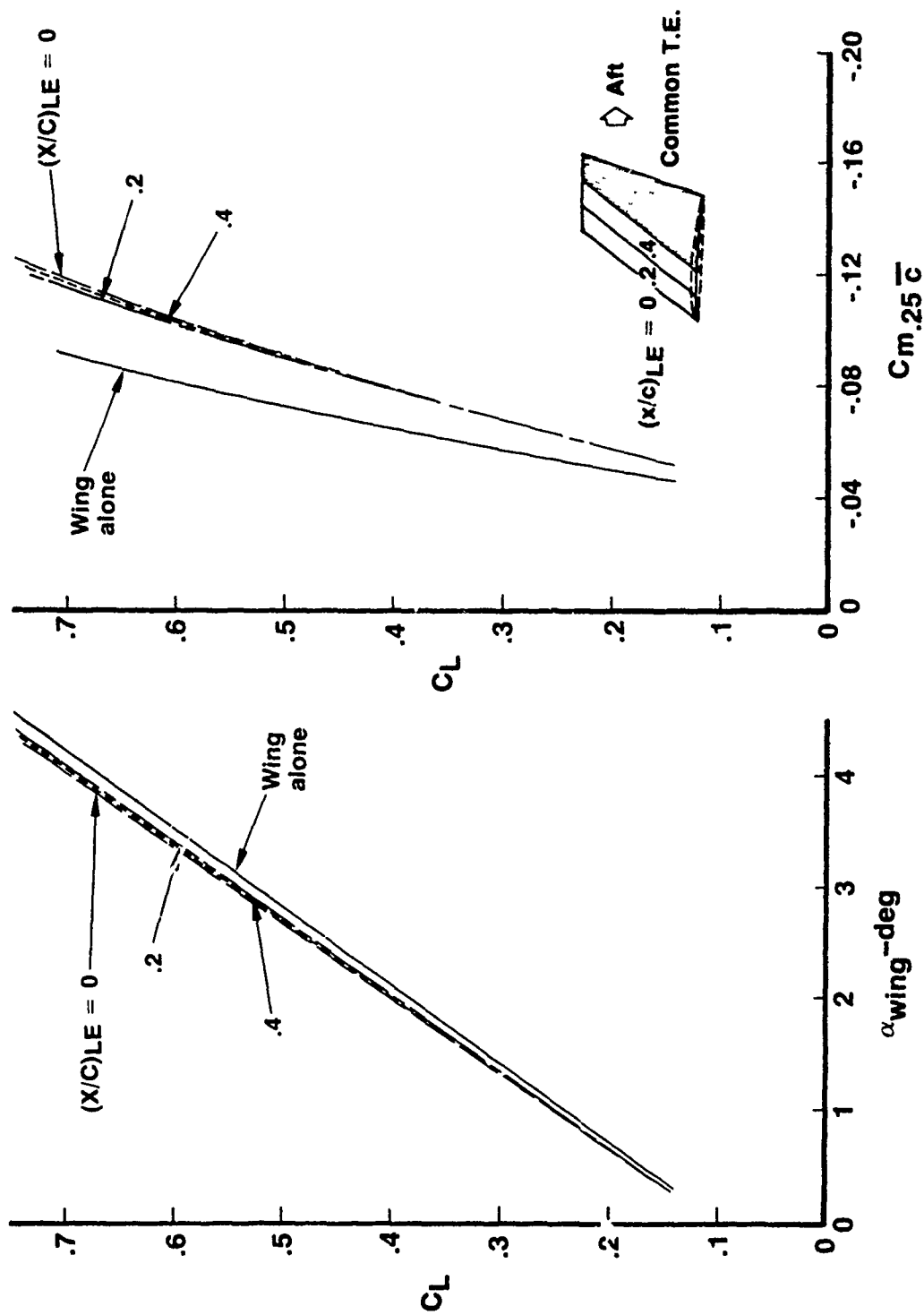
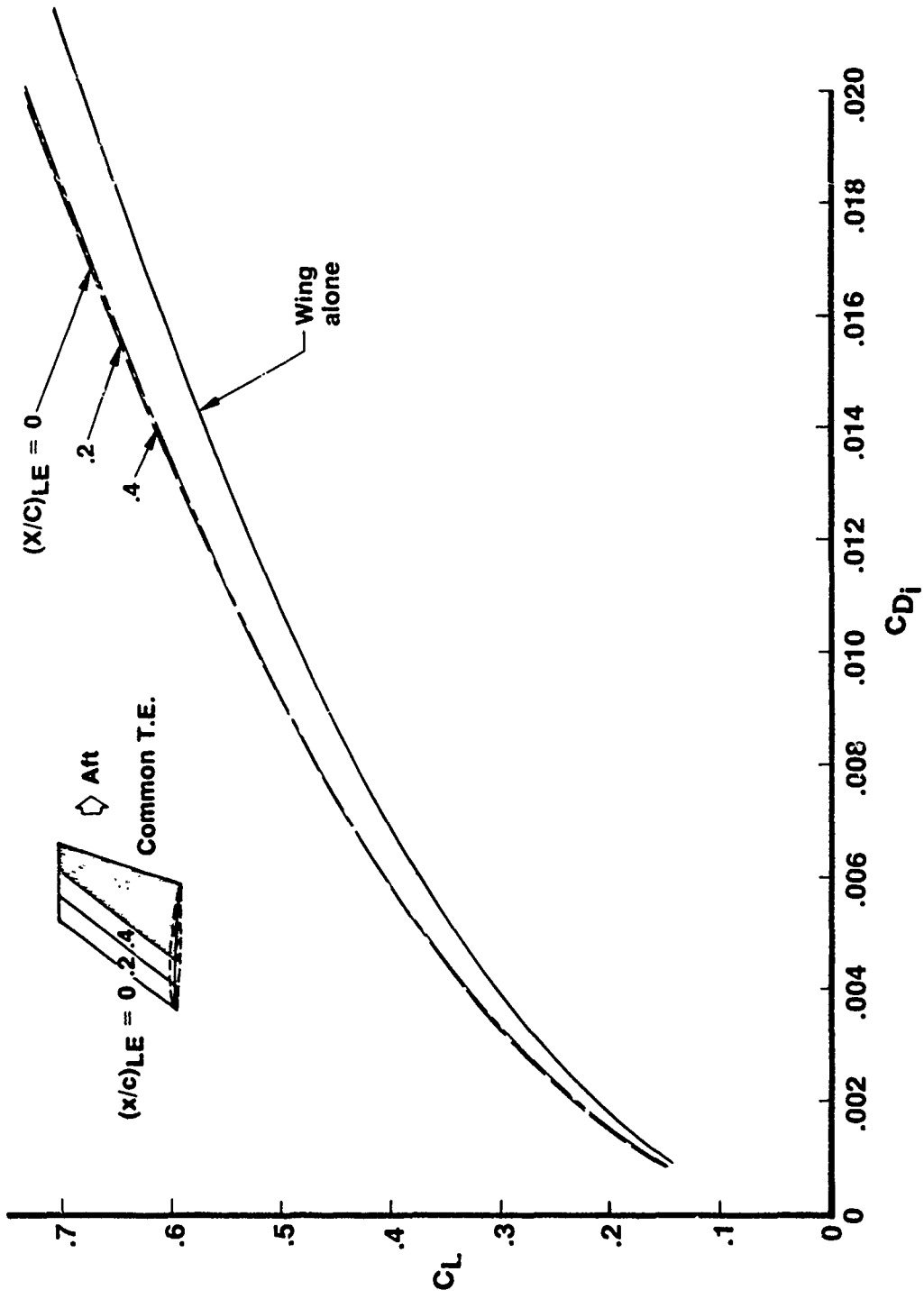


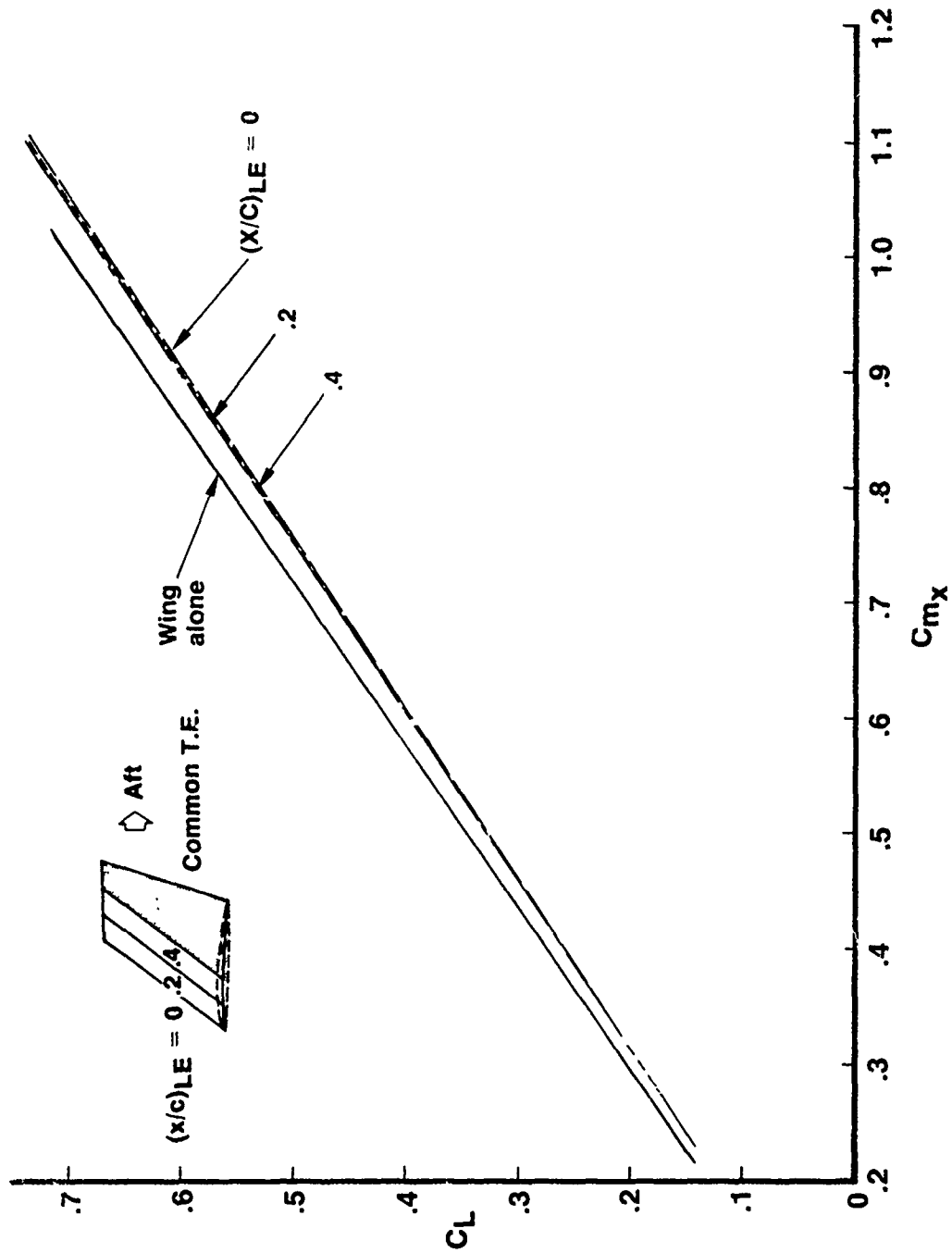
Figure 47.— Winglets for Area Study



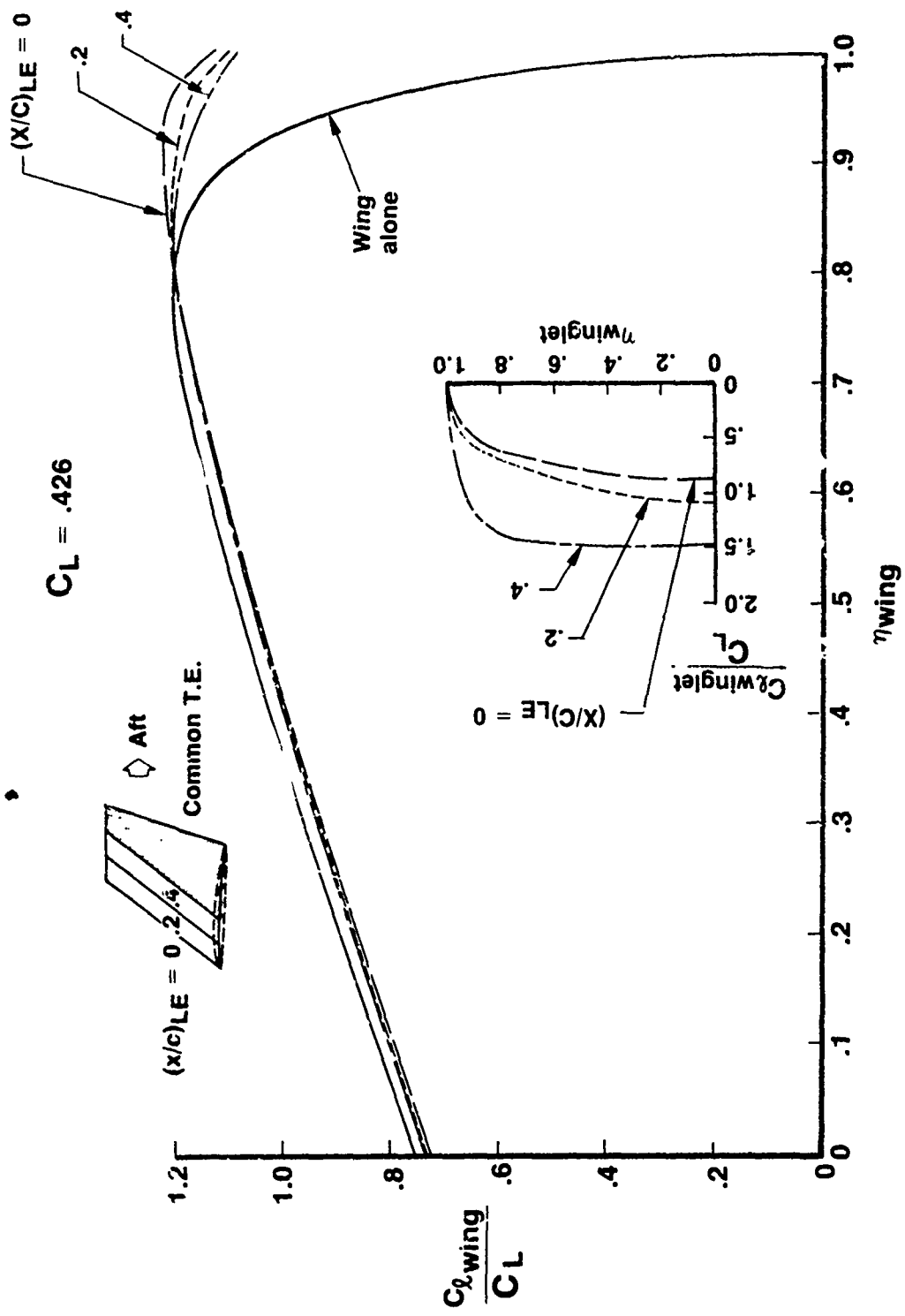
a (Lift and Pitching Moment)
 Figure 48.—Effect of Winglet Area



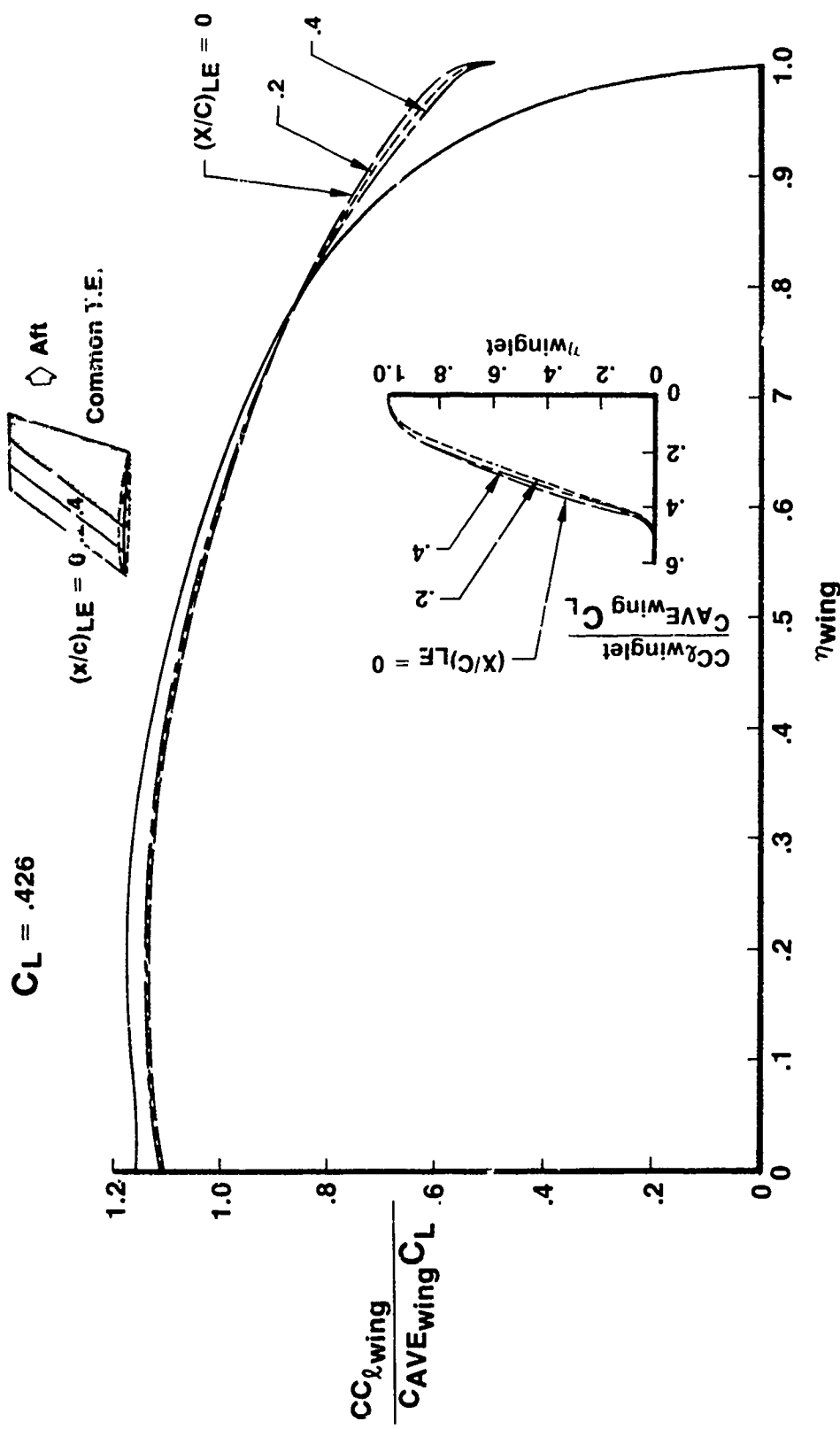
b (Induced Drag)
 Figure 48. — (Continued)



c (Wing-Root Bending Moment)
Figure 48. — (Continued)



d (Sectional Lift)
Figure 48.—(Continued)



e (Span Loading)
Figure 48. — (Concluded)

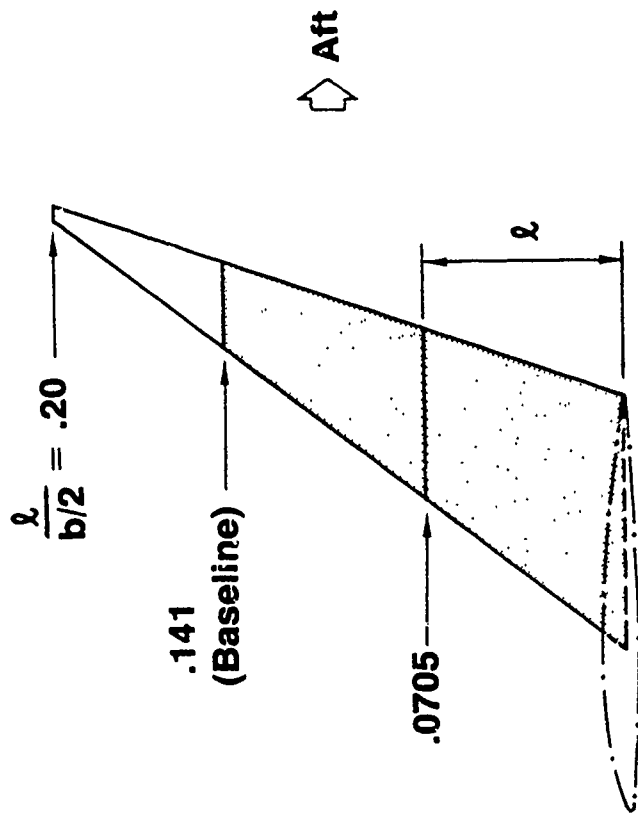
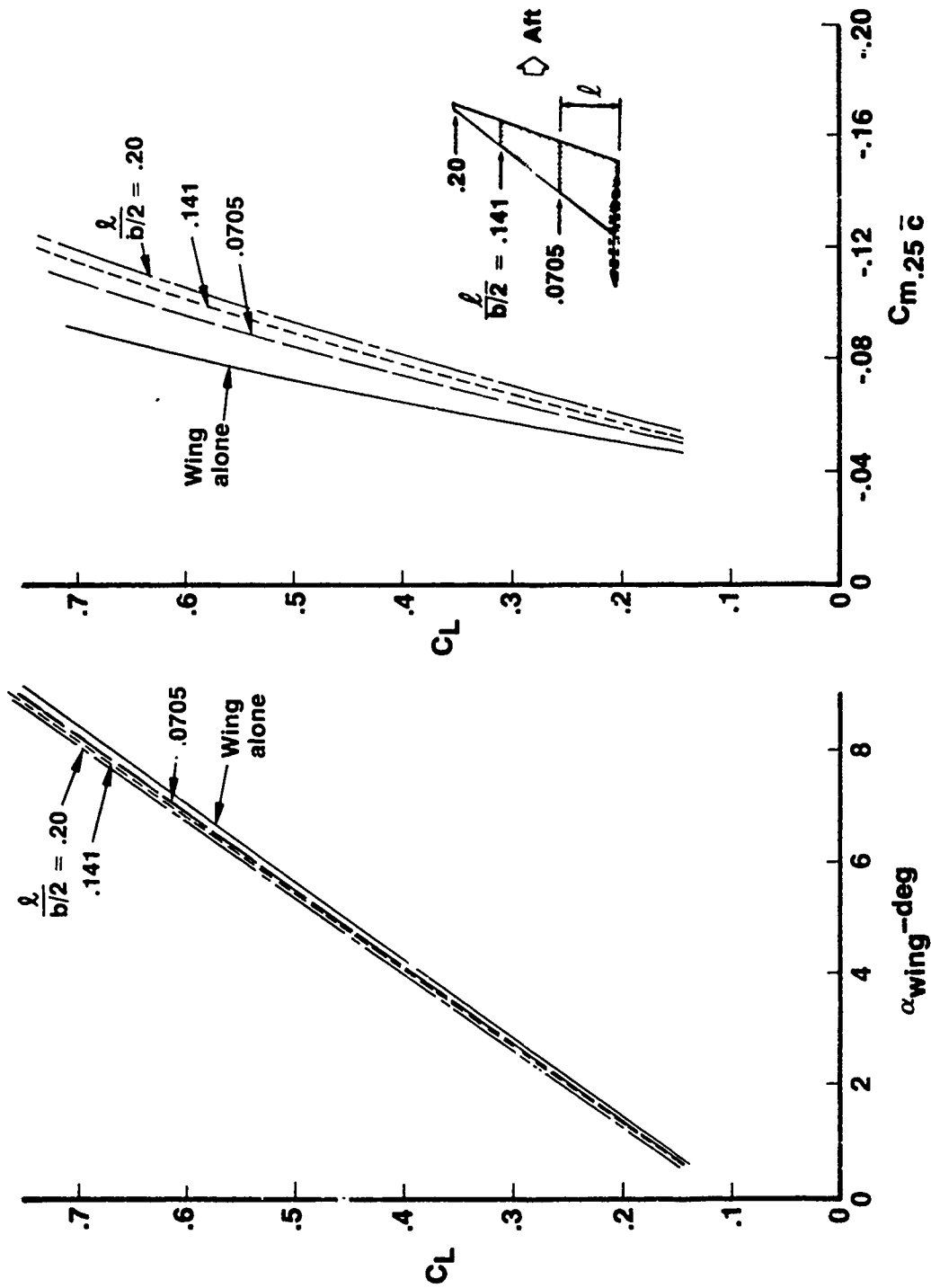
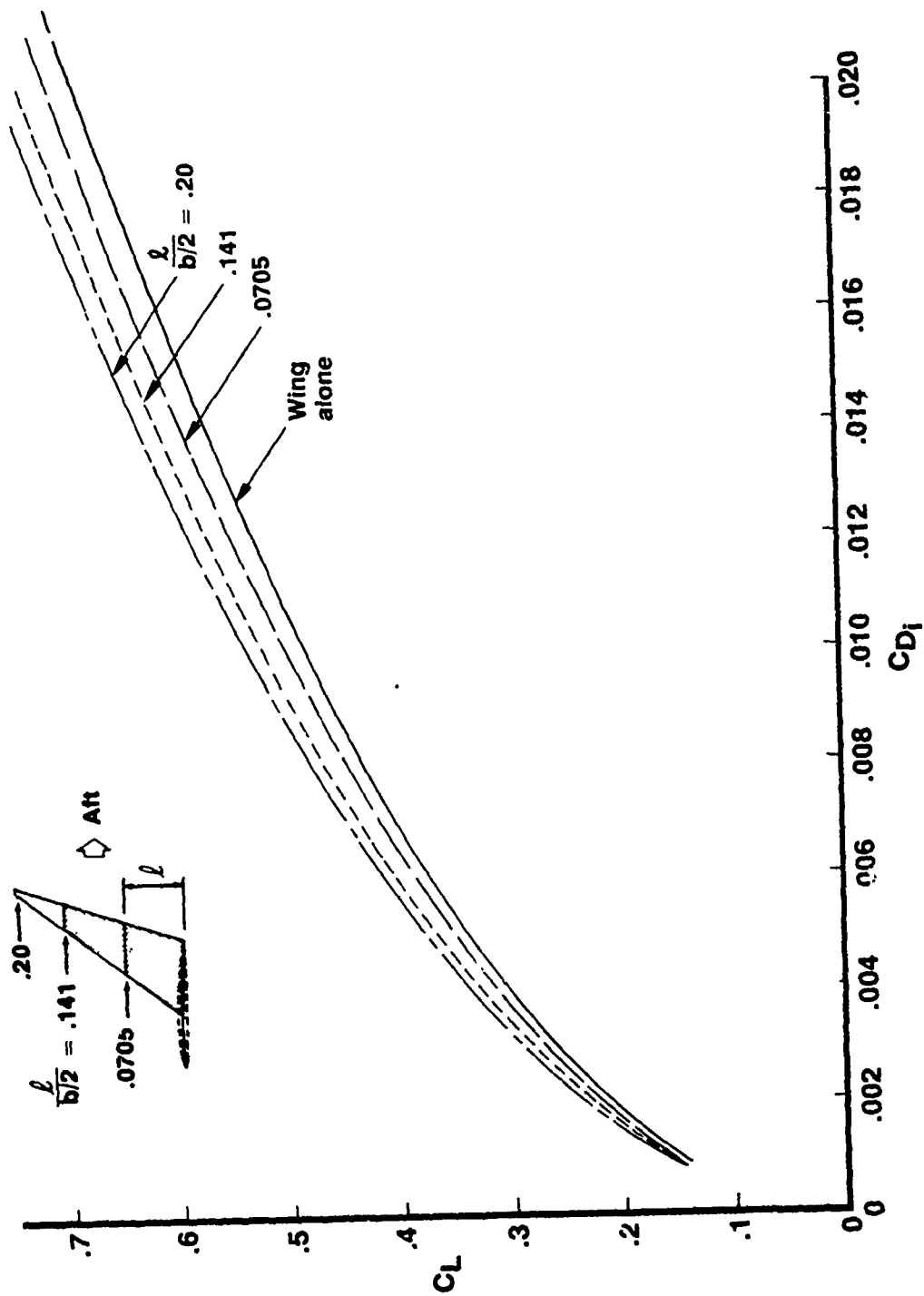


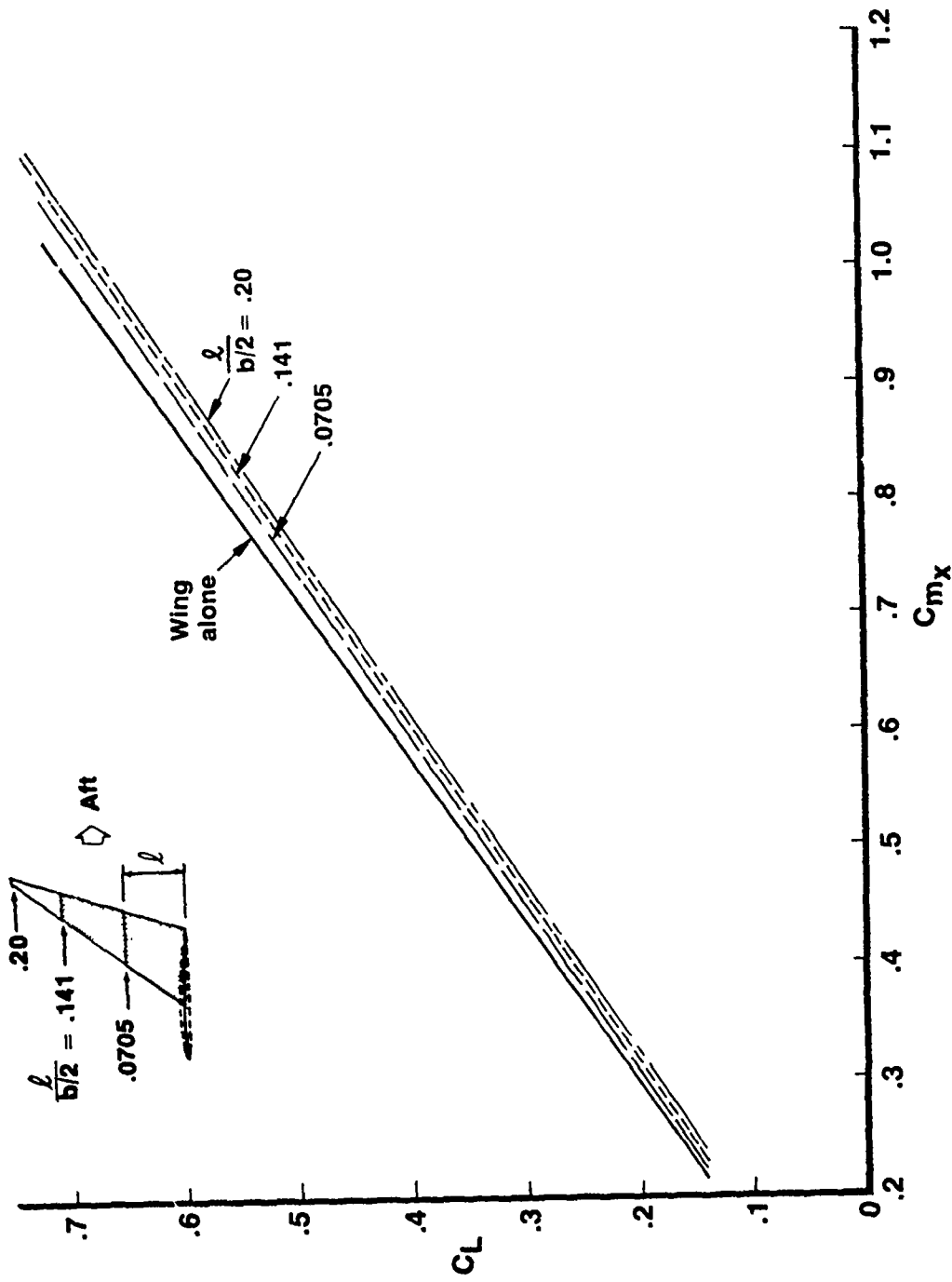
Figure 49.— Winglets for Length Study



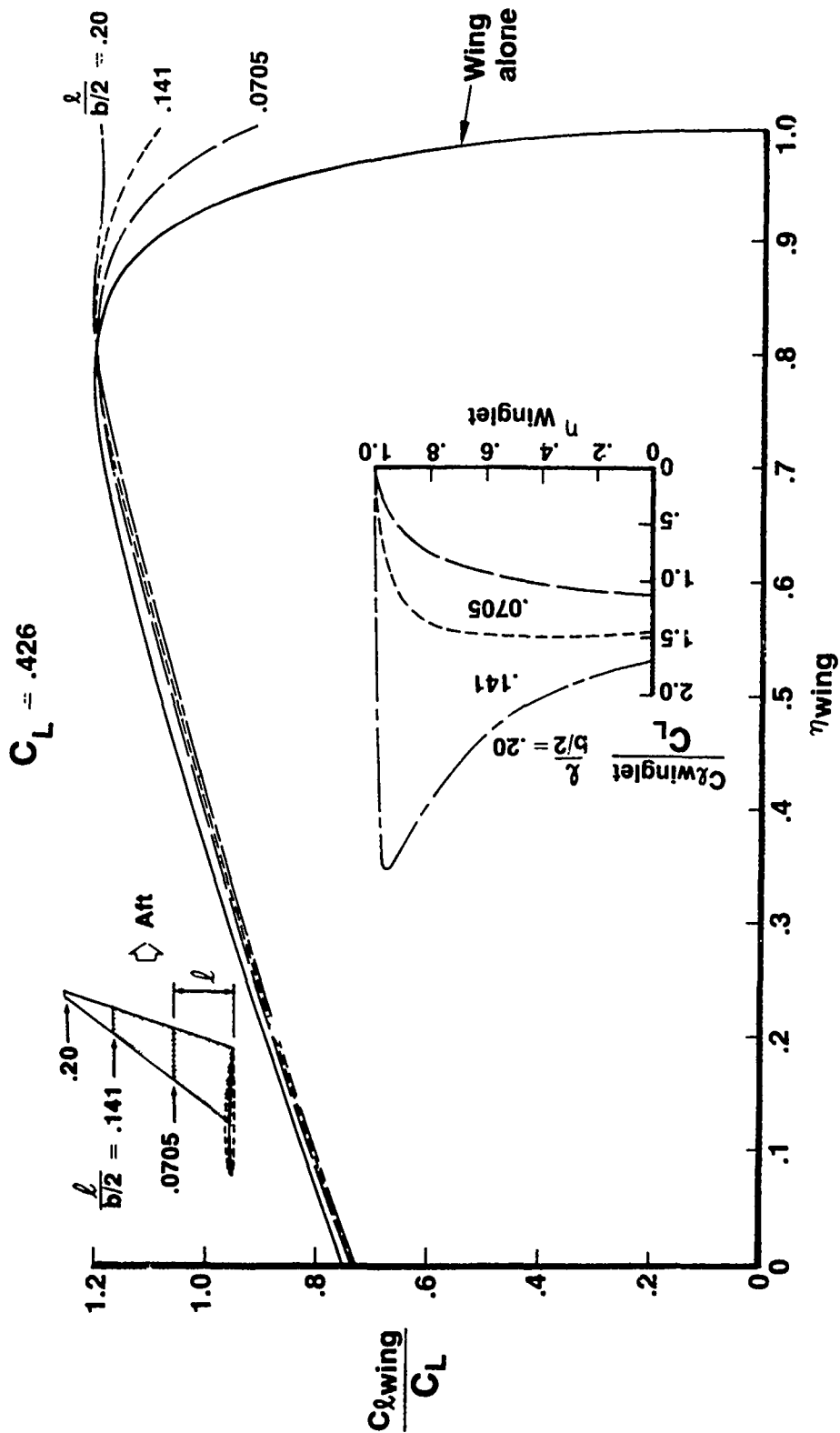
a (Lift and Pitching Moment)
 Figure 50. — Effect of Winglet Length



b (Induced Drag)
Figure 50. — (Continued)

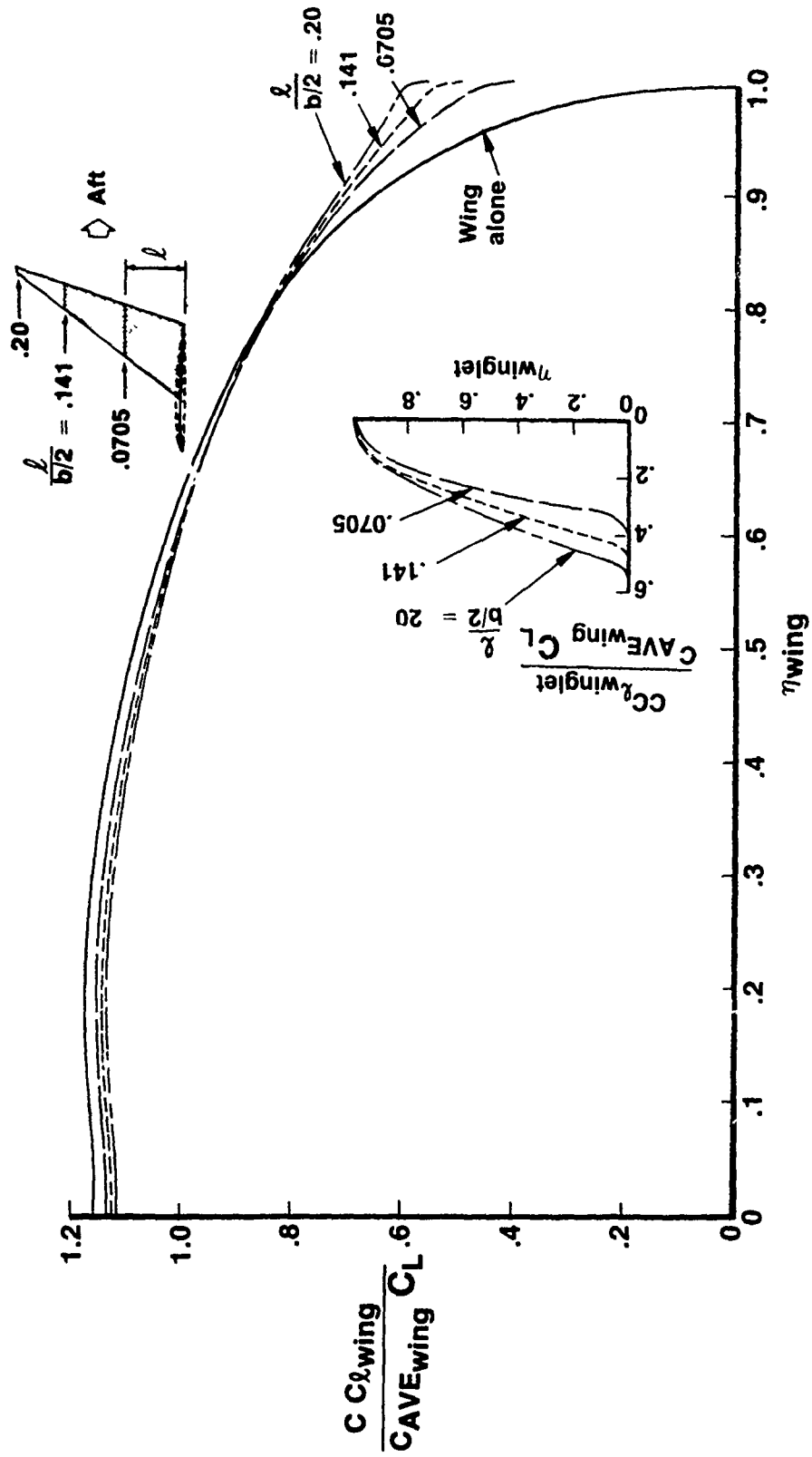


c (Wing-Root Bending Moment)
Figure 50.— (Continued)



d (Sectional Lift)
Figure 50. — (Continued)

$C_L = .426$



e (Span Loading)
Figure 50.— (Concluded)

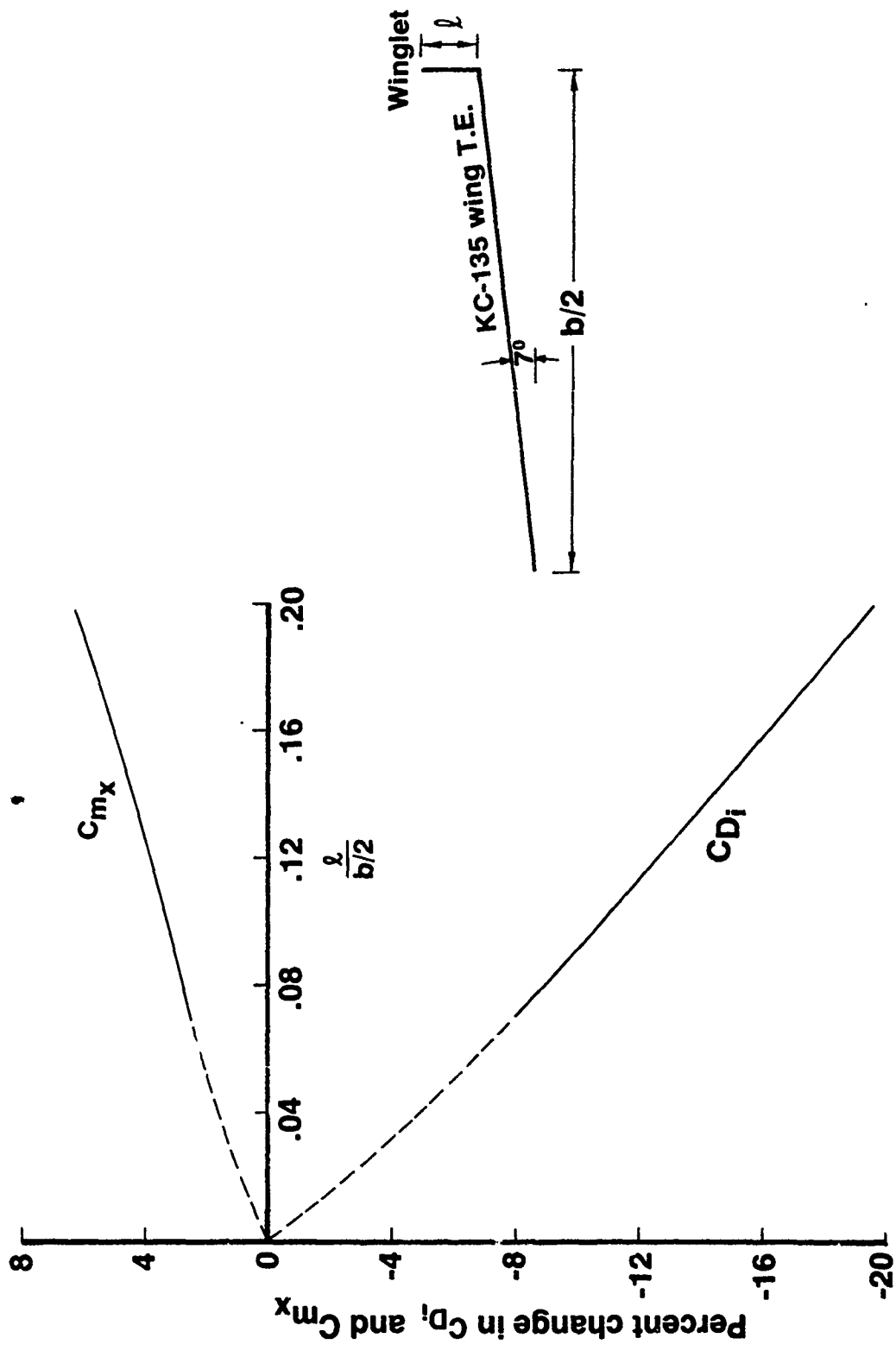


Figure 51.— Winglet Length Study at α^0 Cant, $C_{L_{config}} = 0.426$

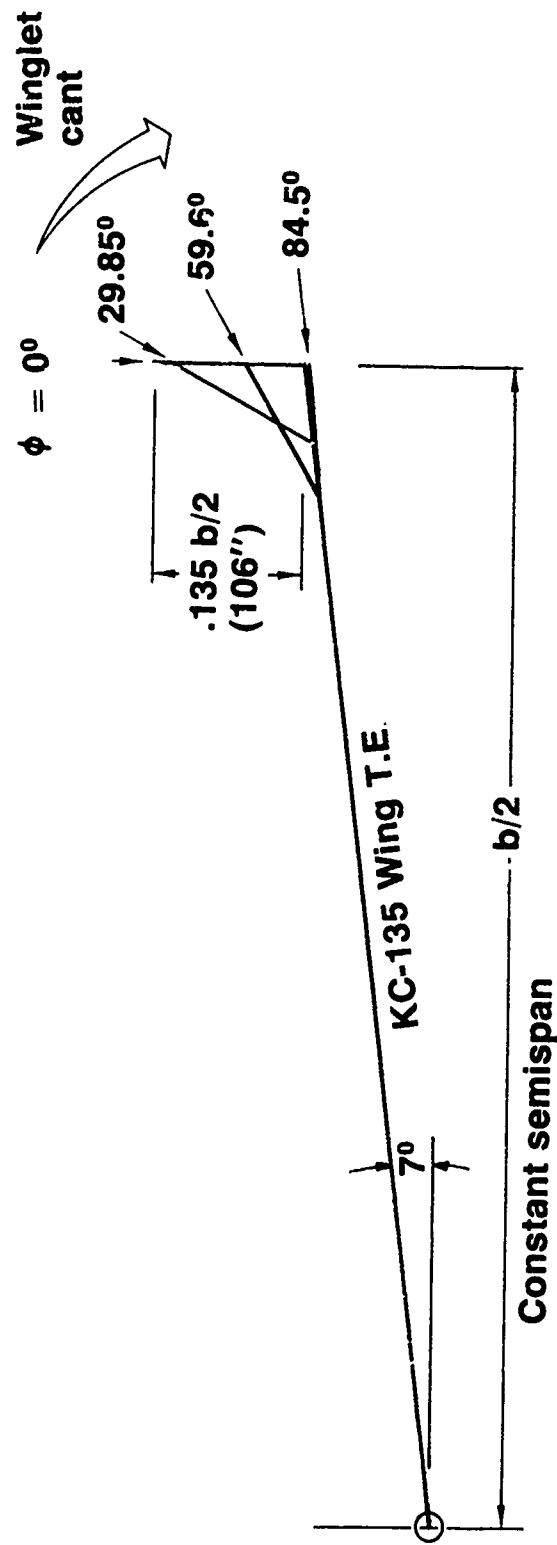
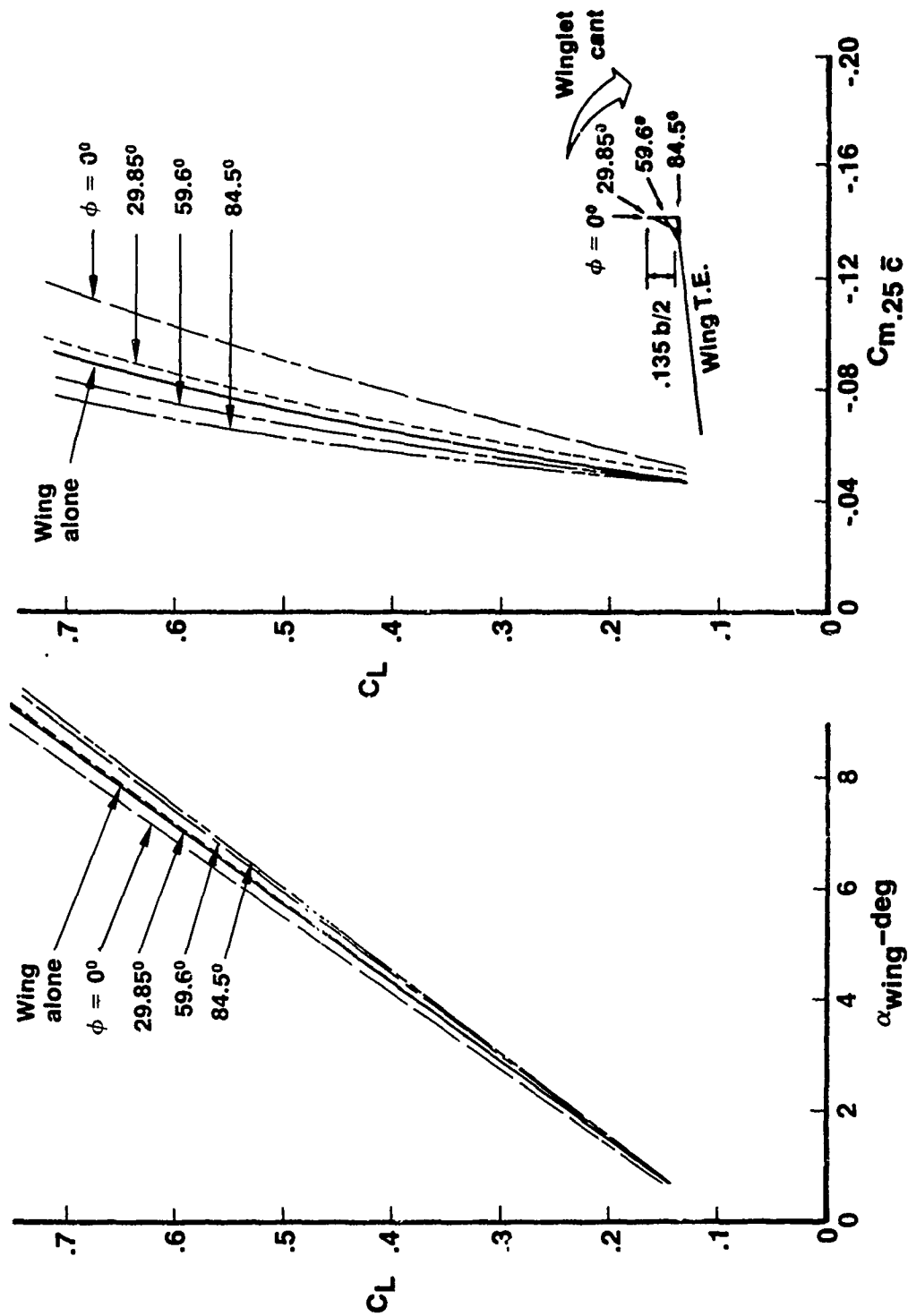
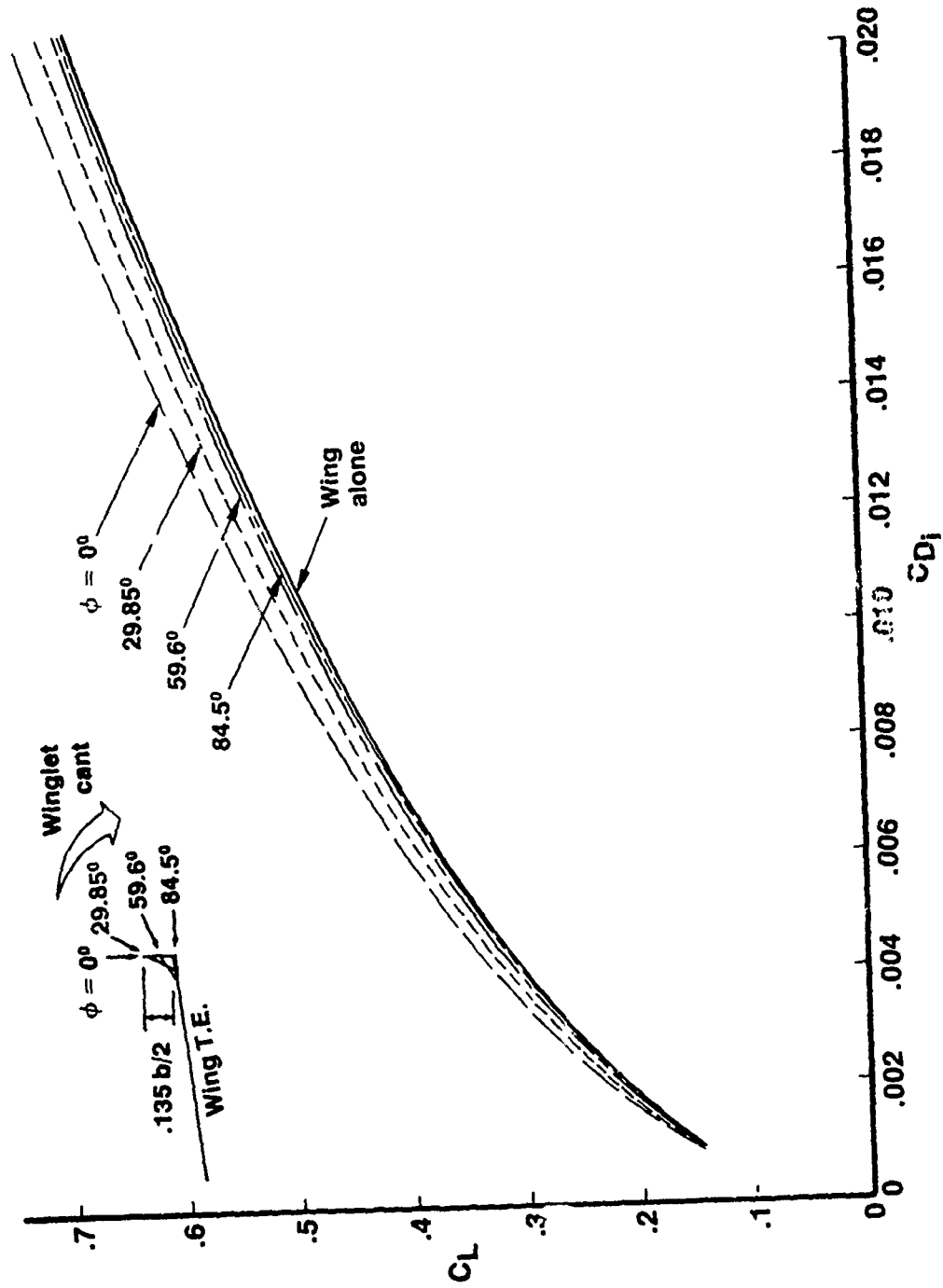


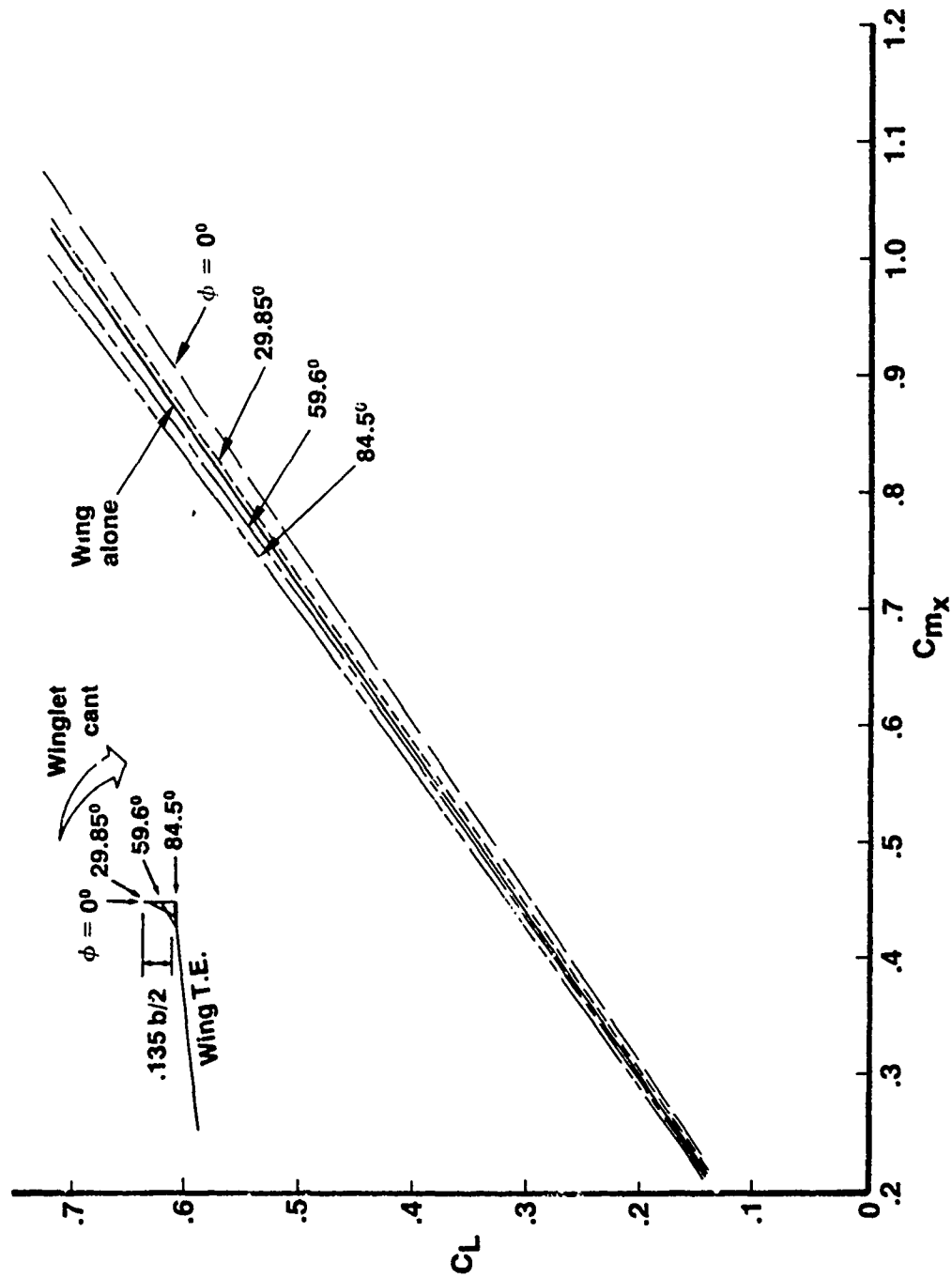
Figure 52.—Winglets for Constant Span Cant Study



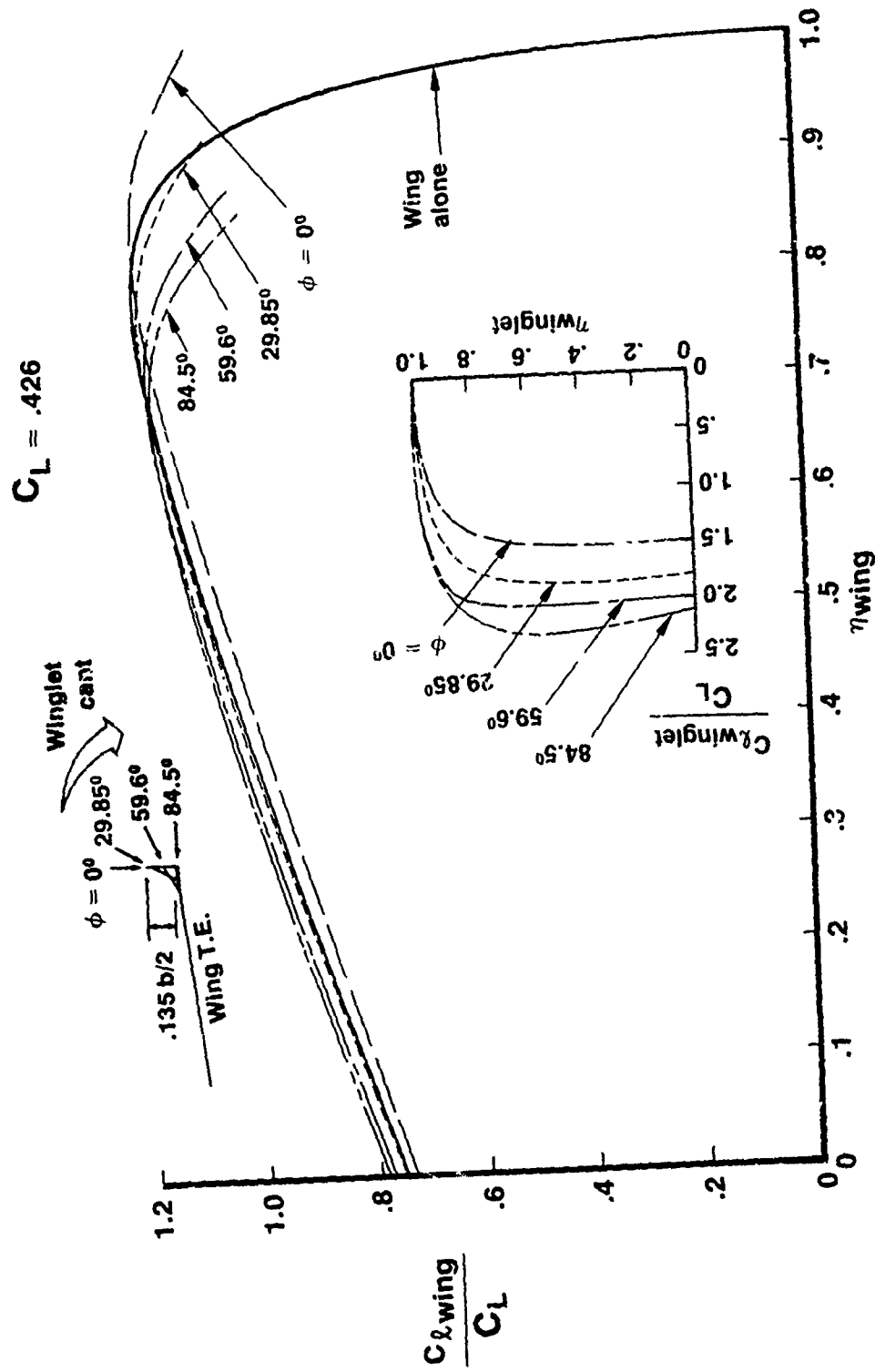
a (Lift and Pitching Moment--Constant Span)
 Figure 53. — Effect of Winglet Cant



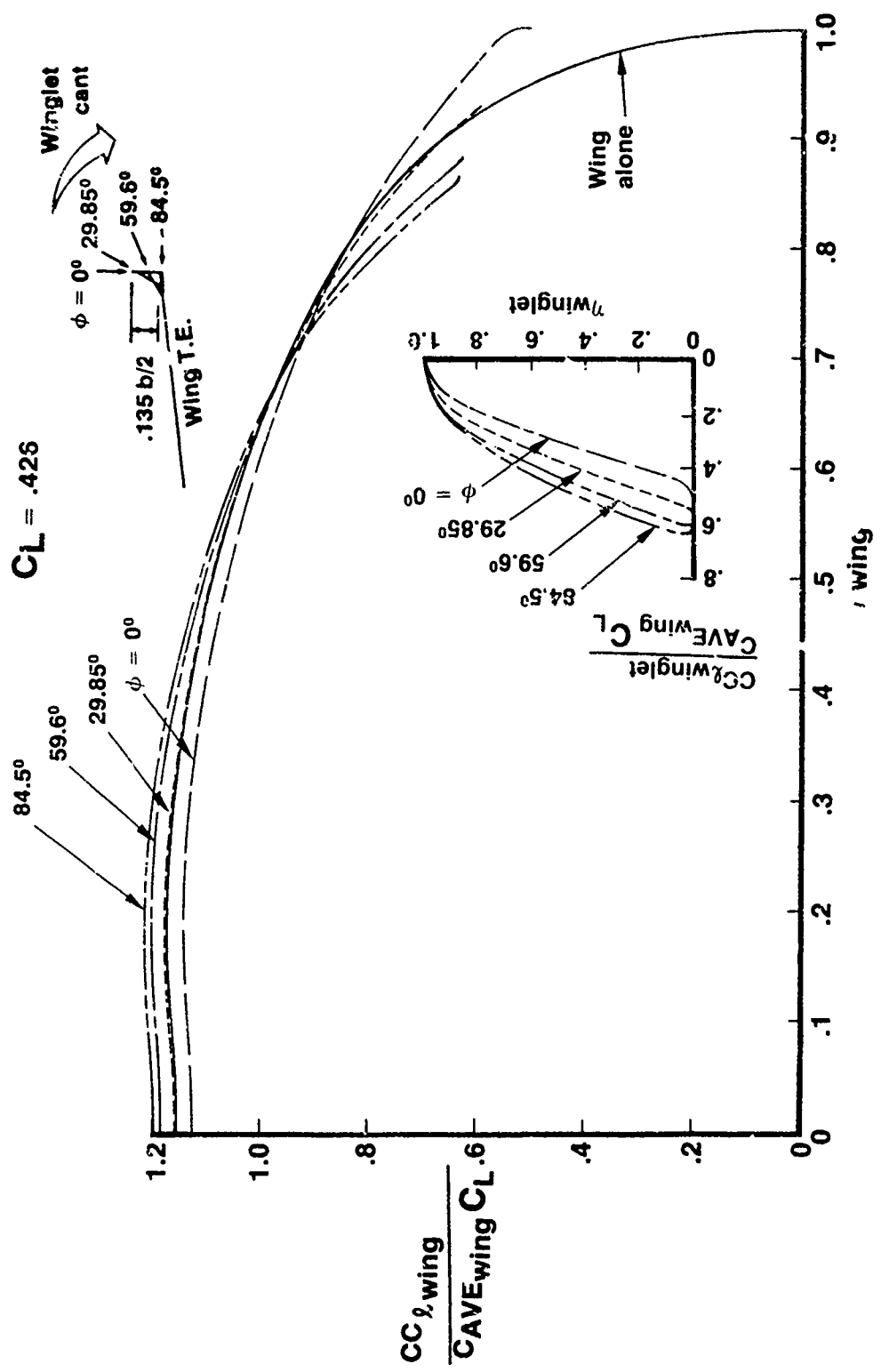
b (Induced Drag—Constant Span)
Figure 53. — (Continued)



c (Wing-Root Blending Moment—Constant Span)
Figure 53.—(Continued)



d (Sectional Lift—Constant Span)
Figure 53. — (Continued)



e (Span Loading—Constant Span)
Figure 53.—(Concluded)

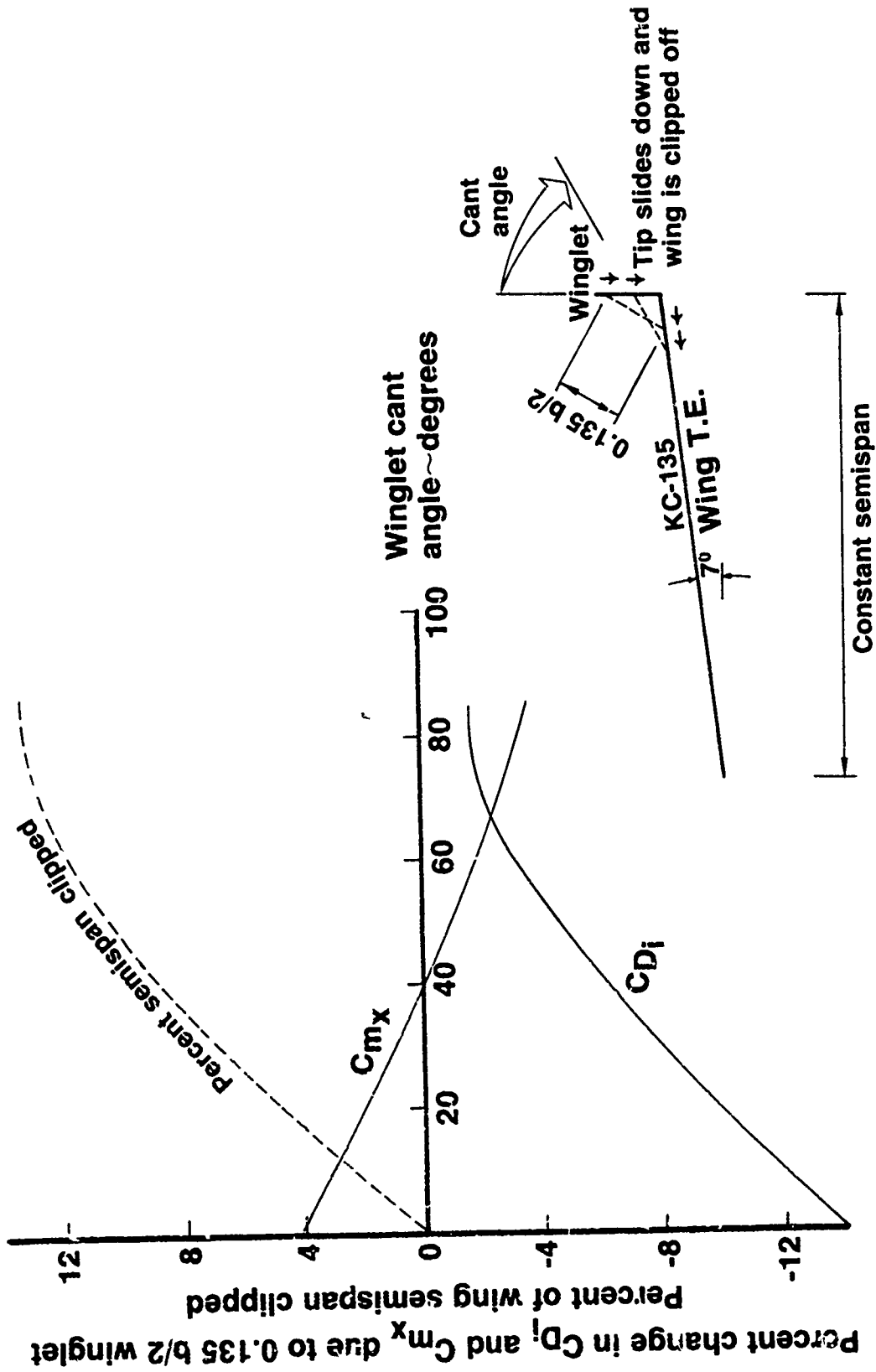


Figure 54 — Winglet Cant Study With Constant Span, $C_{L_{config}} = 0.426$

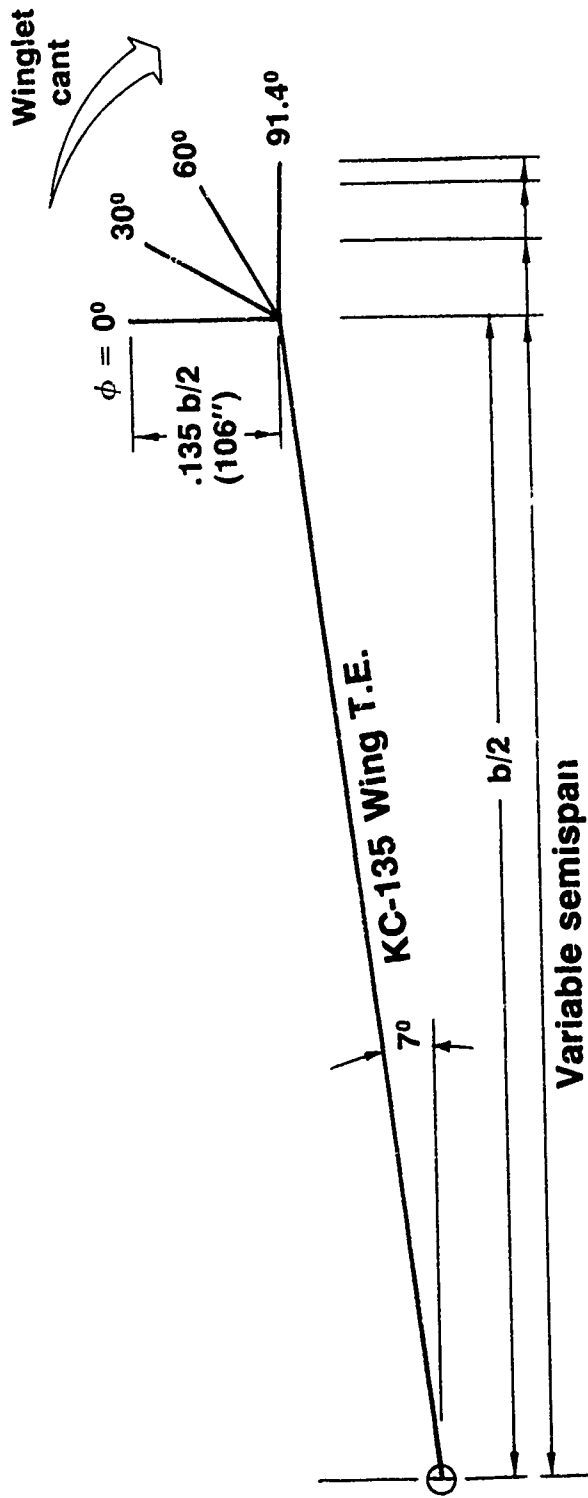
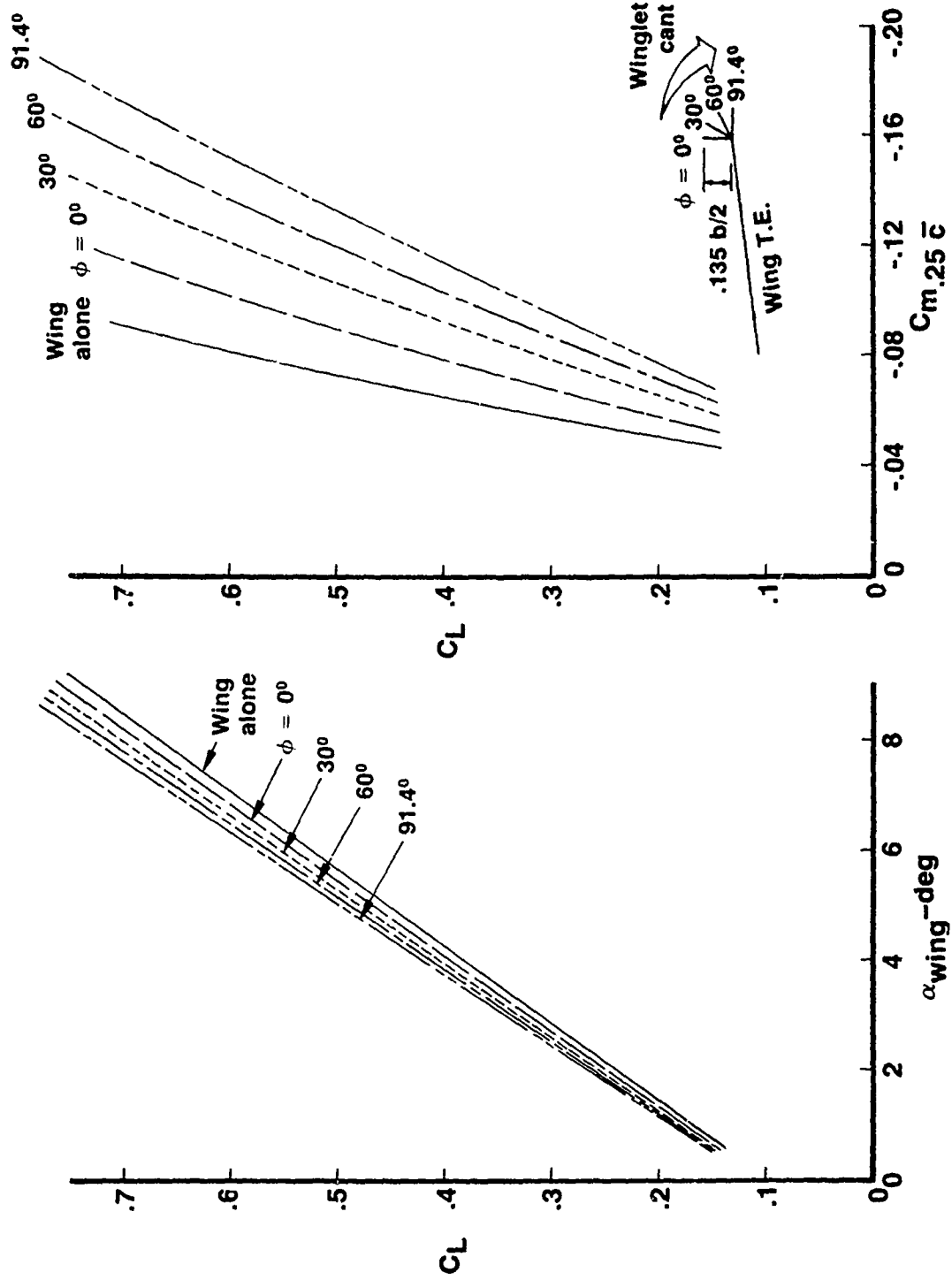
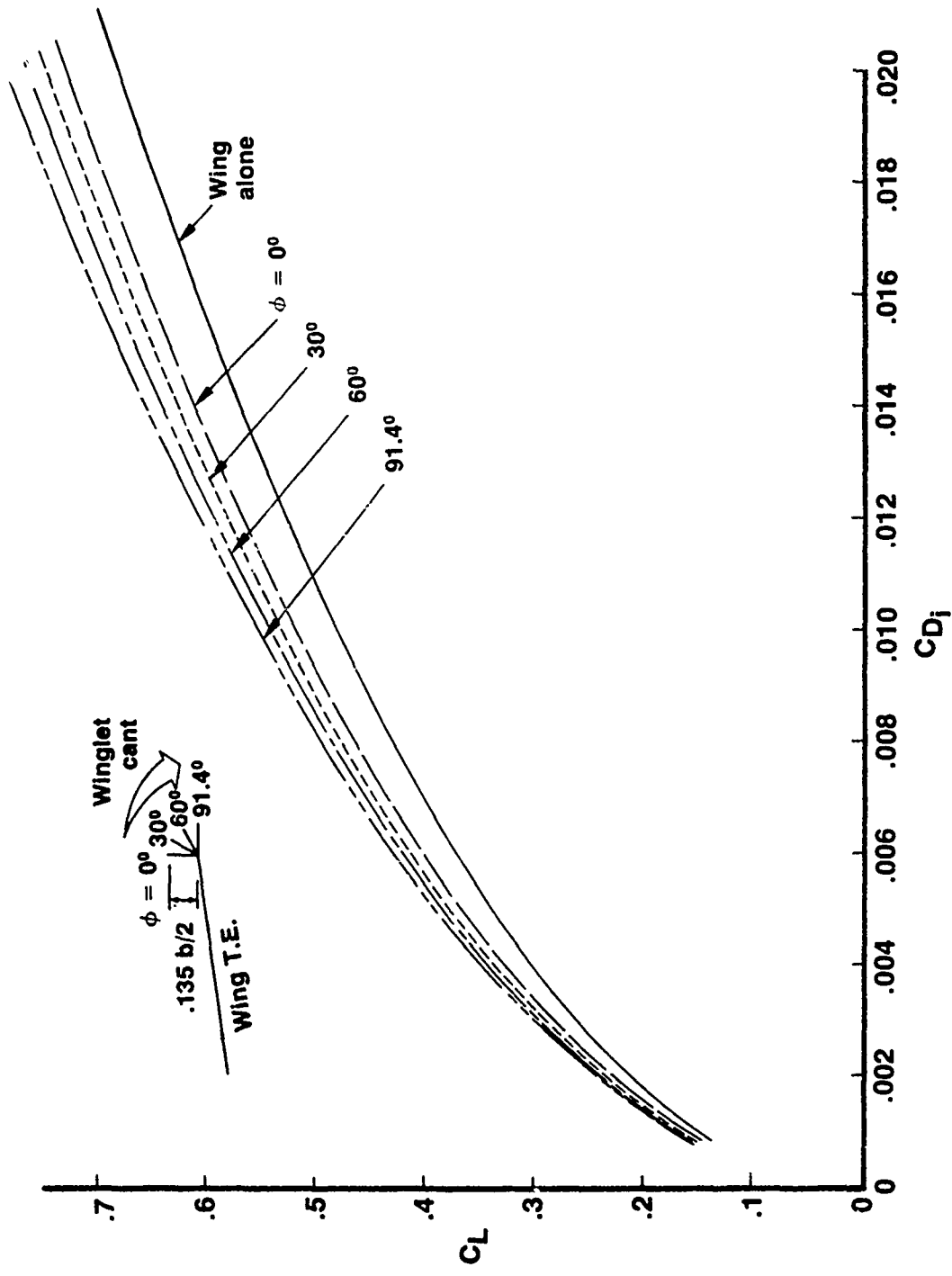


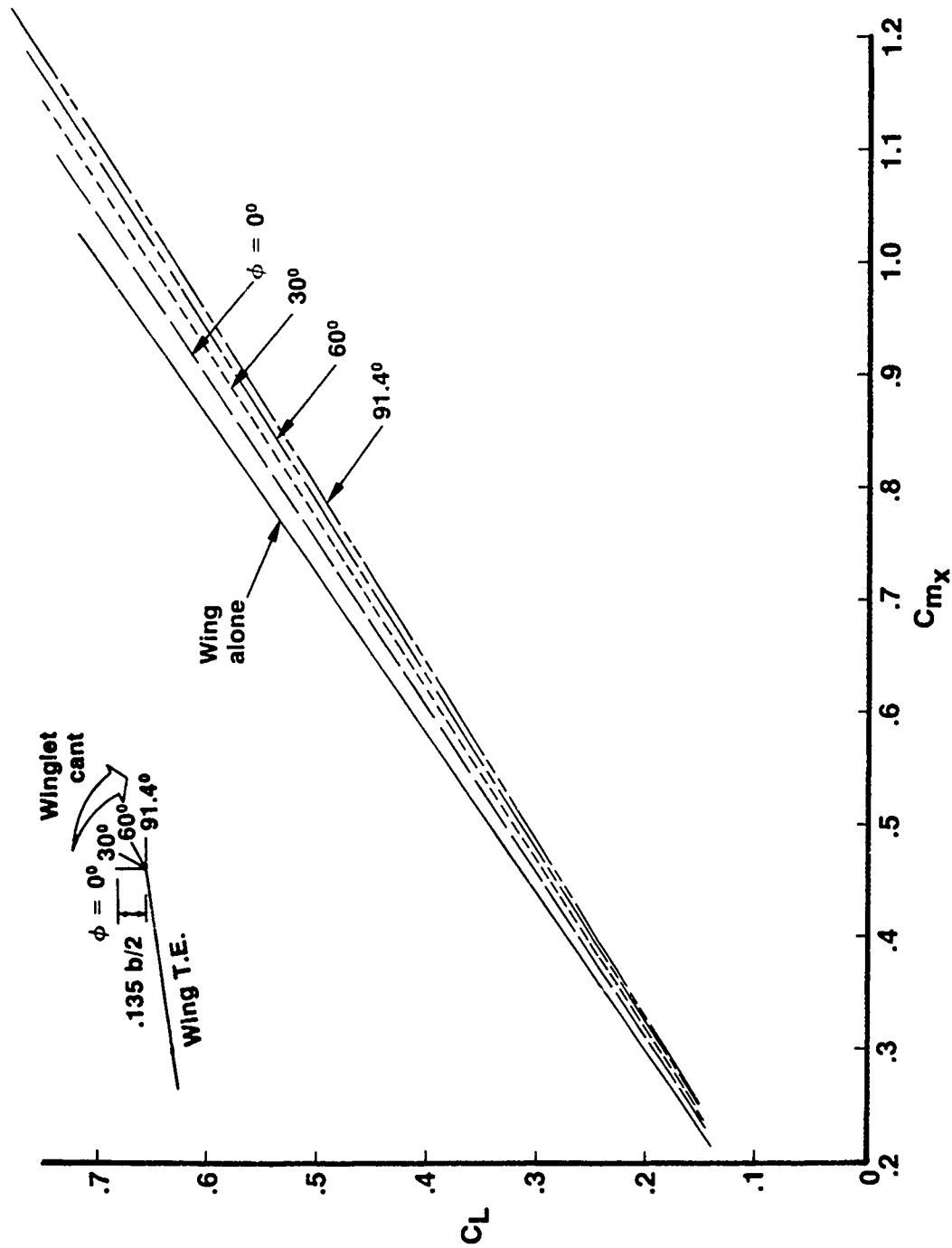
Figure 55.—Winglets for Variable Span Cant Study



a (Lift and Pitching Moment—Variable Span)
 Figure 56.—Effect of Winglet Cant

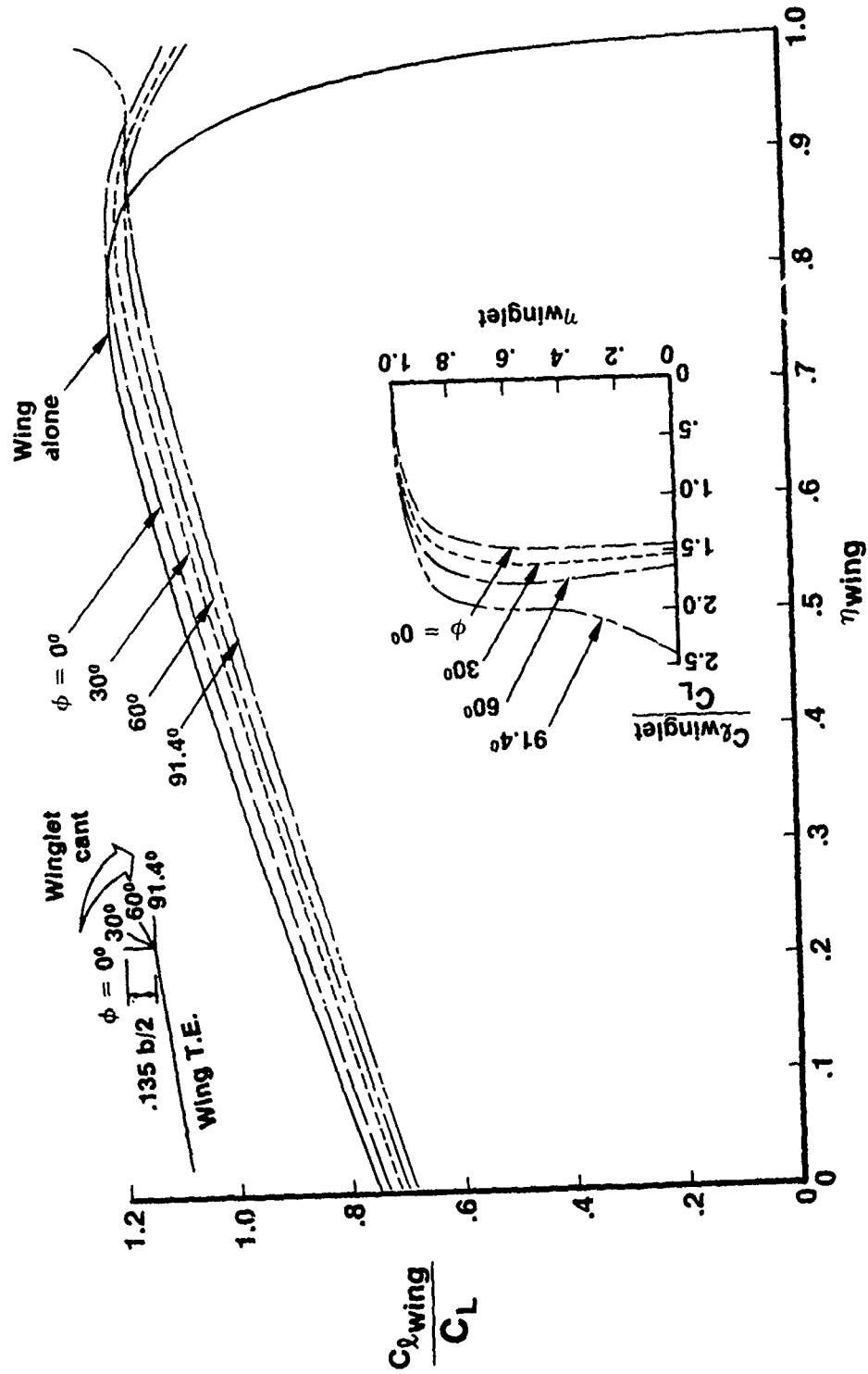


b (Induced Drag—Variable Span)
Figure 56.— (Continued)

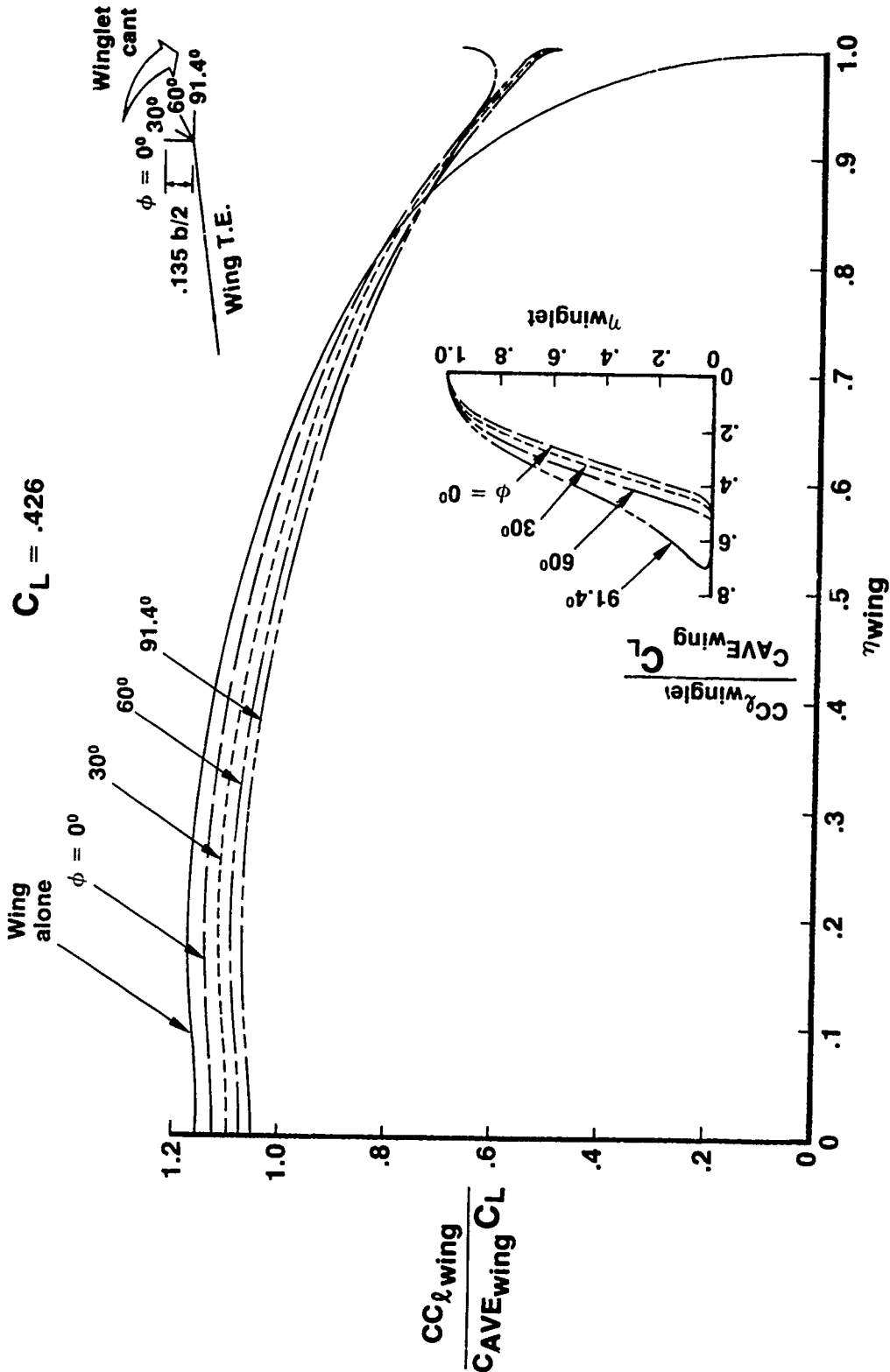


c (Wing-Root Bending Moment—Variable Span)
Figure 56. — (Continued)

$C_L = .426$



d (Sectional Lift—Variable Span)
Figure 56.— (Continued)



e (Span Loading—Variable Span)
Figure 56.—(Concluded)

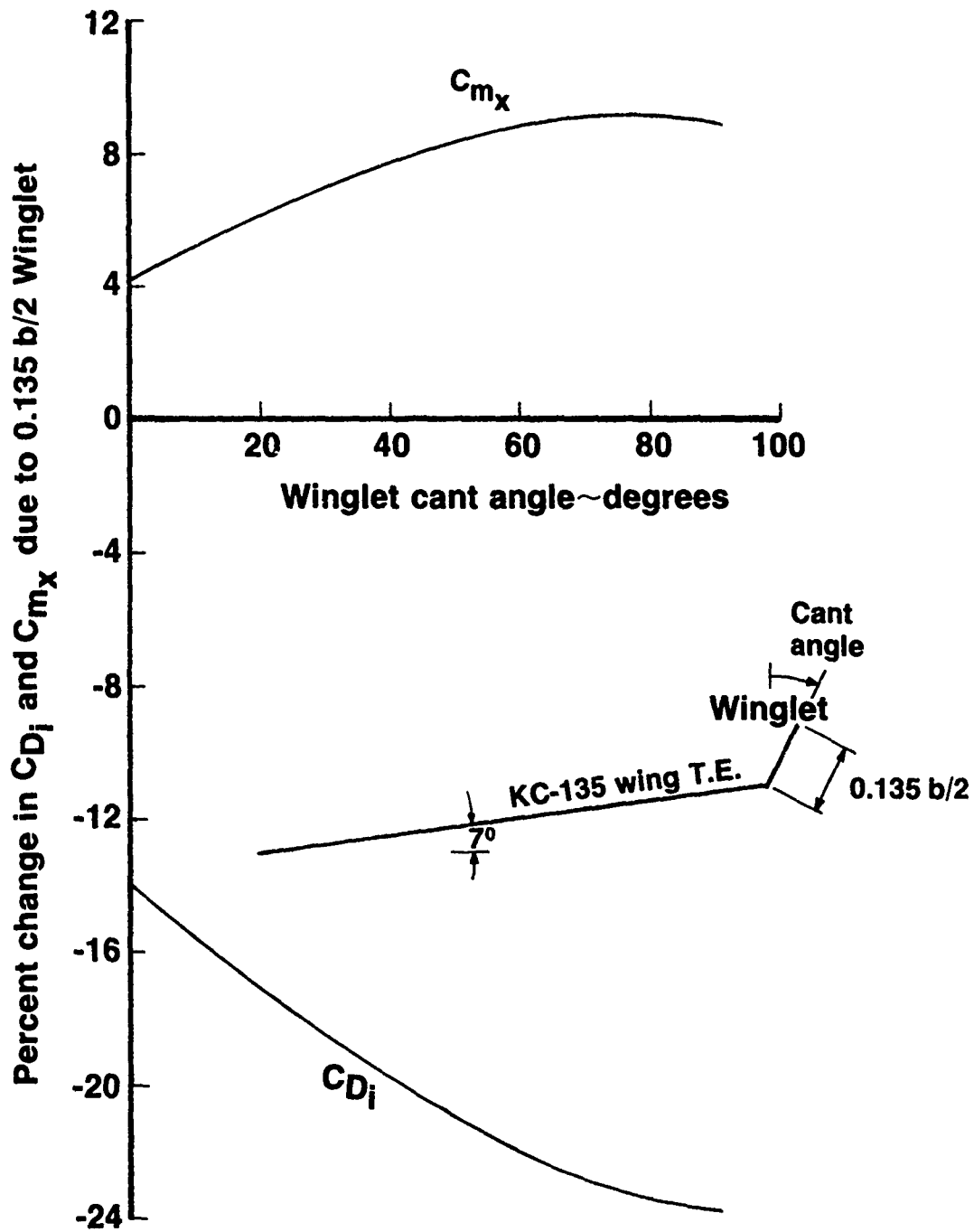


Figure 57.— Winglet Cant Study With Variable Span, $C_{L_{config}} = 0.426$

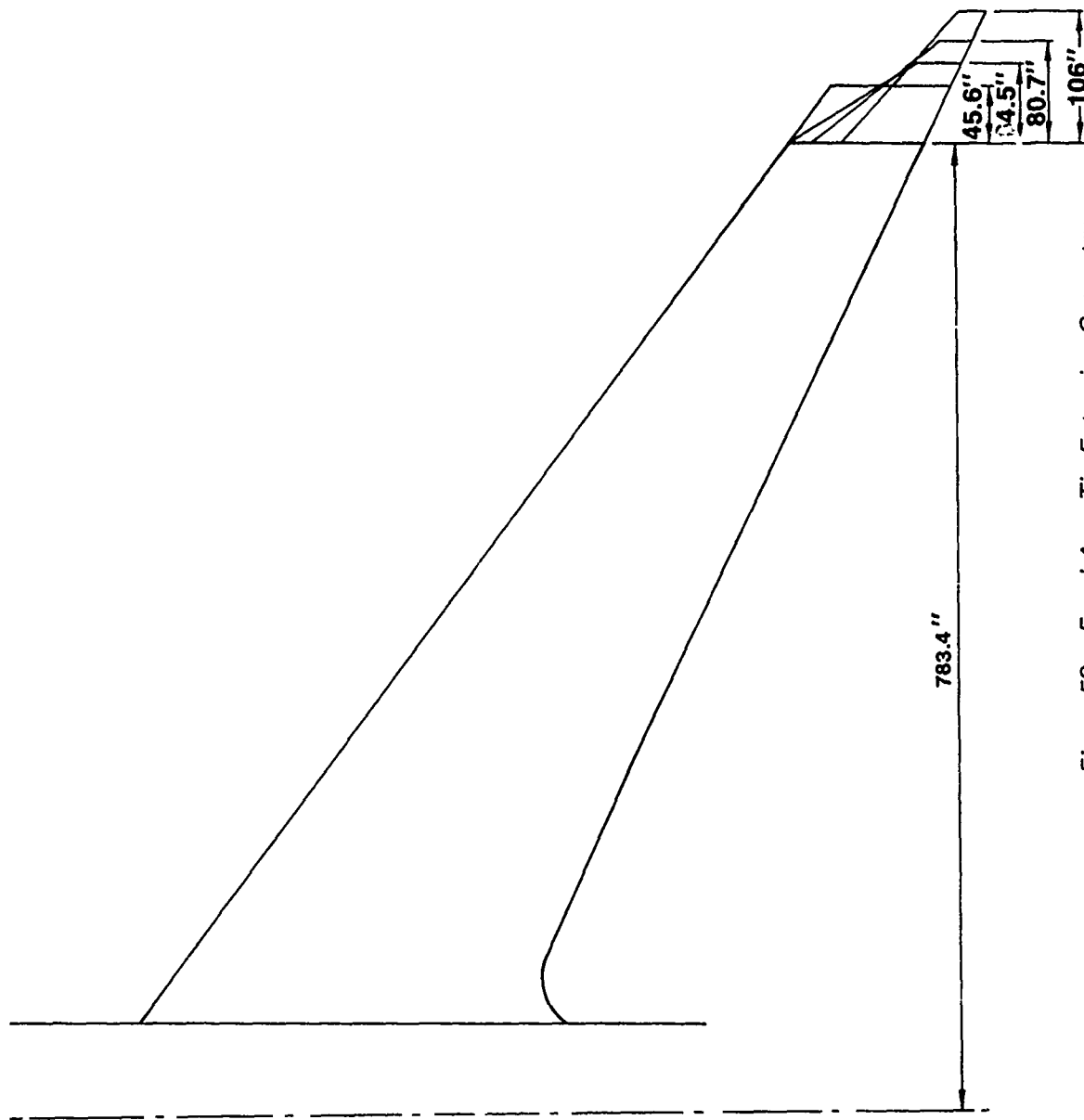
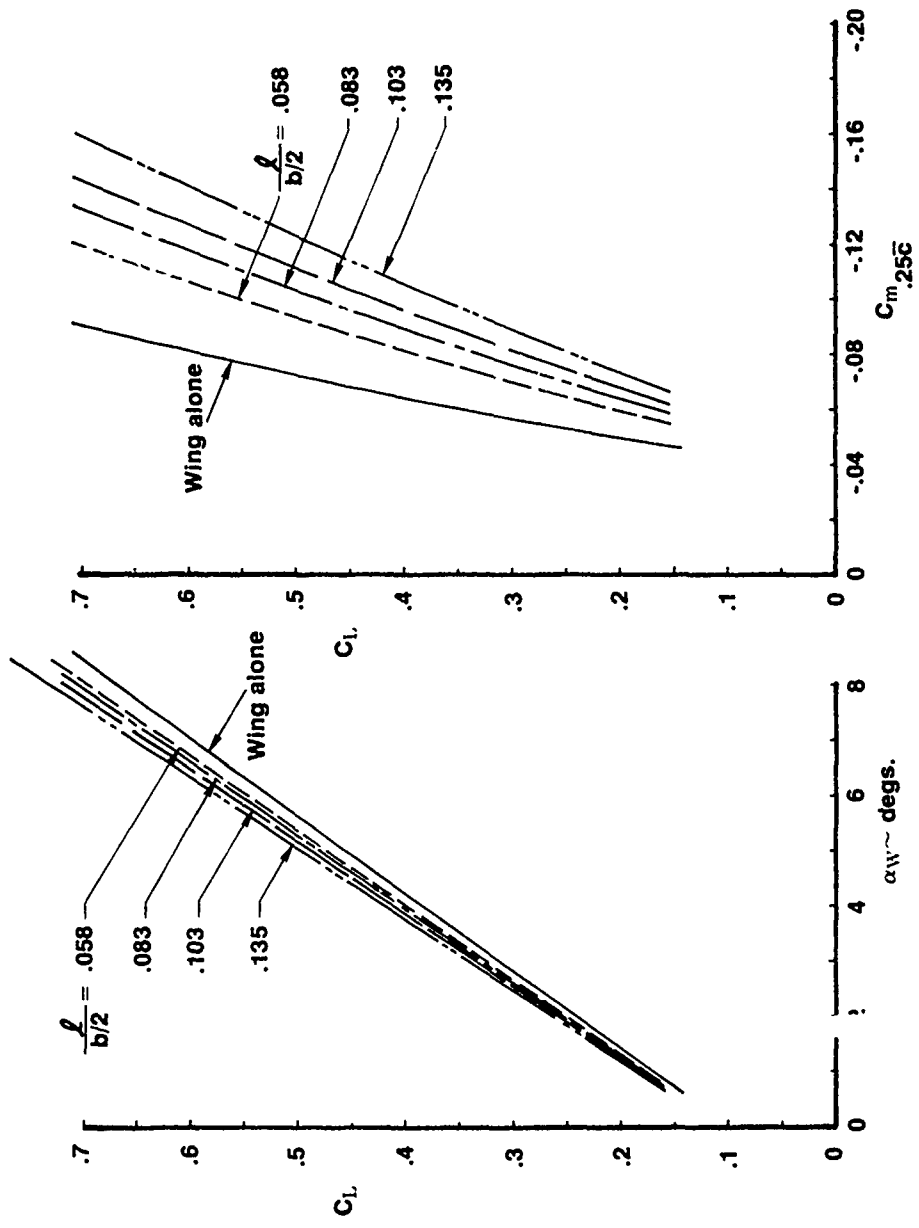
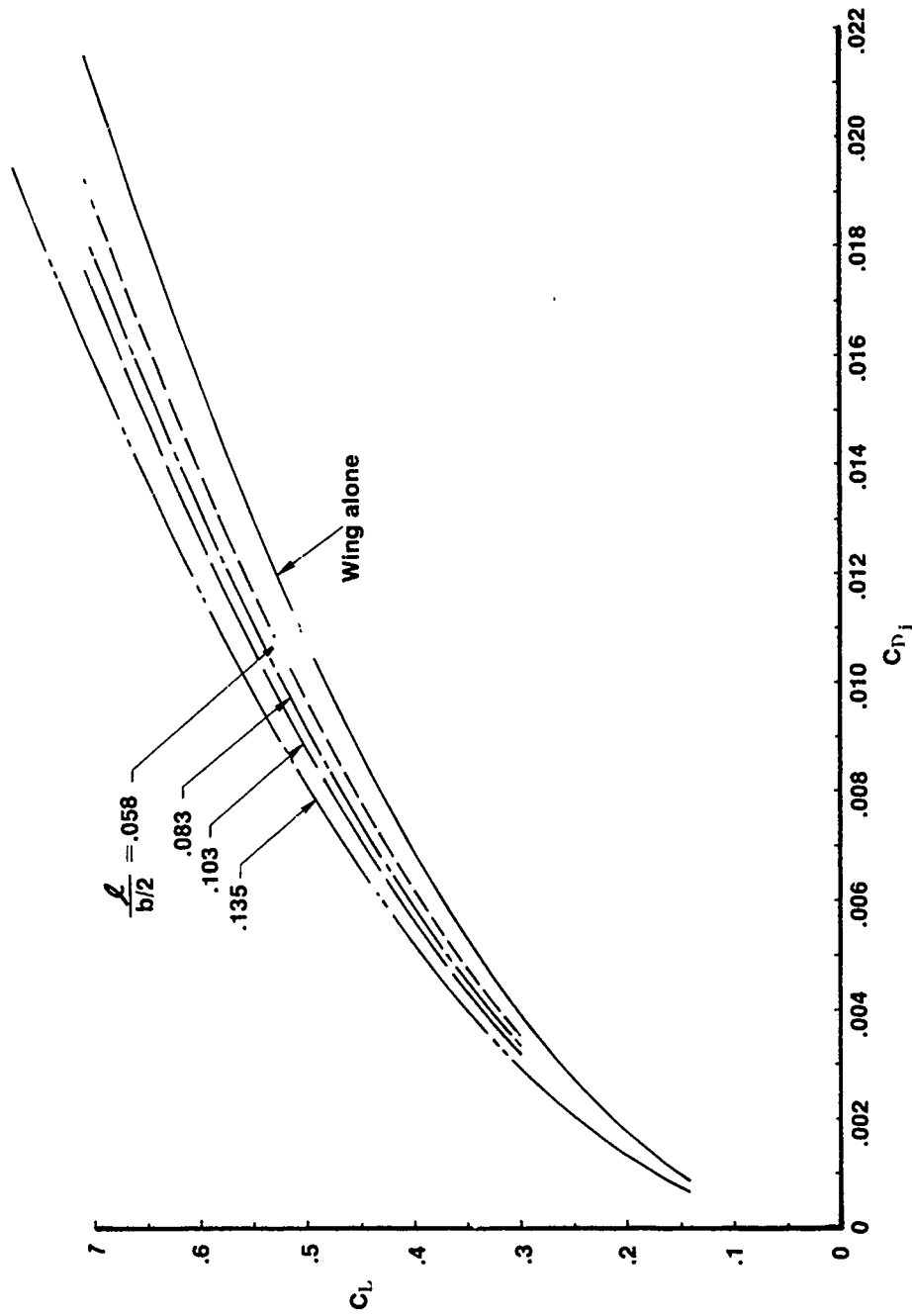


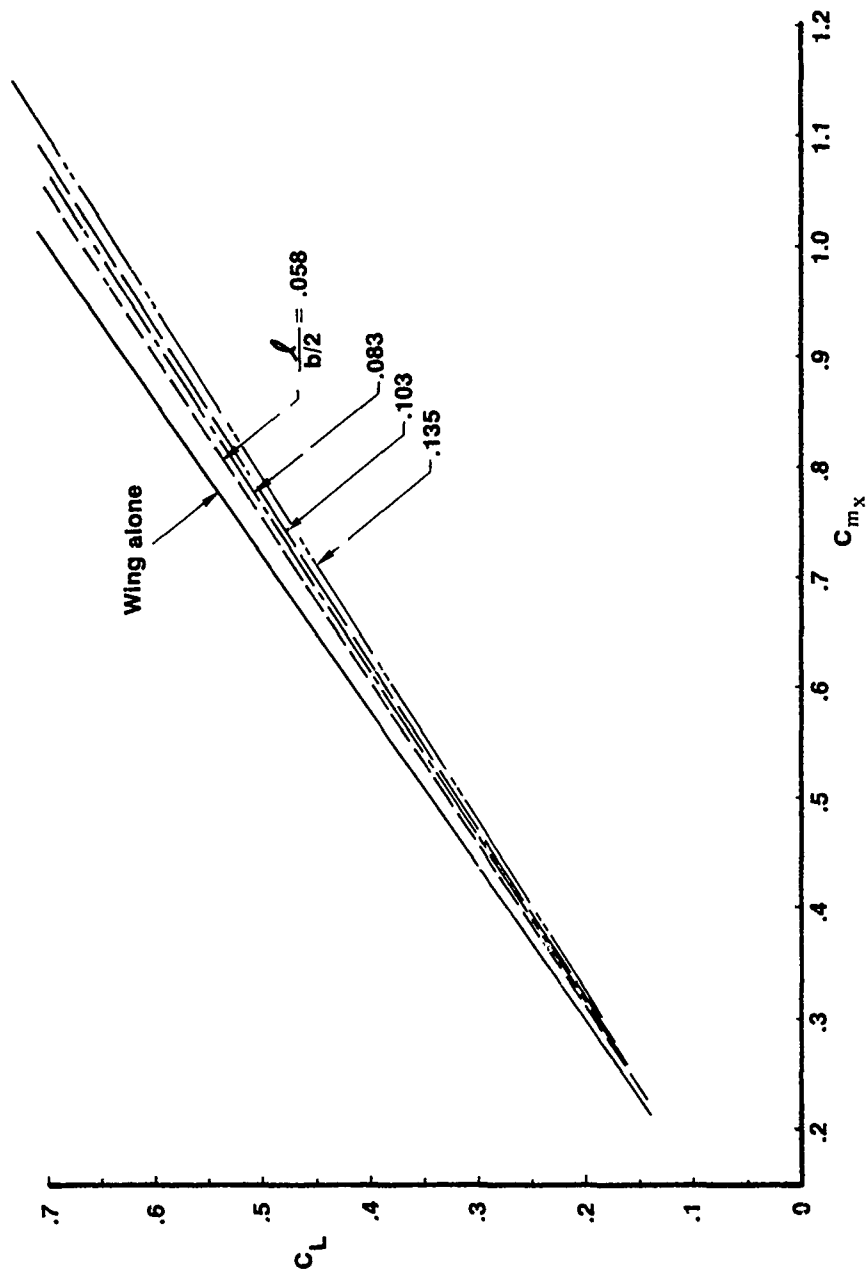
Figure 58. -- Equal Area Tip Extension Geometry



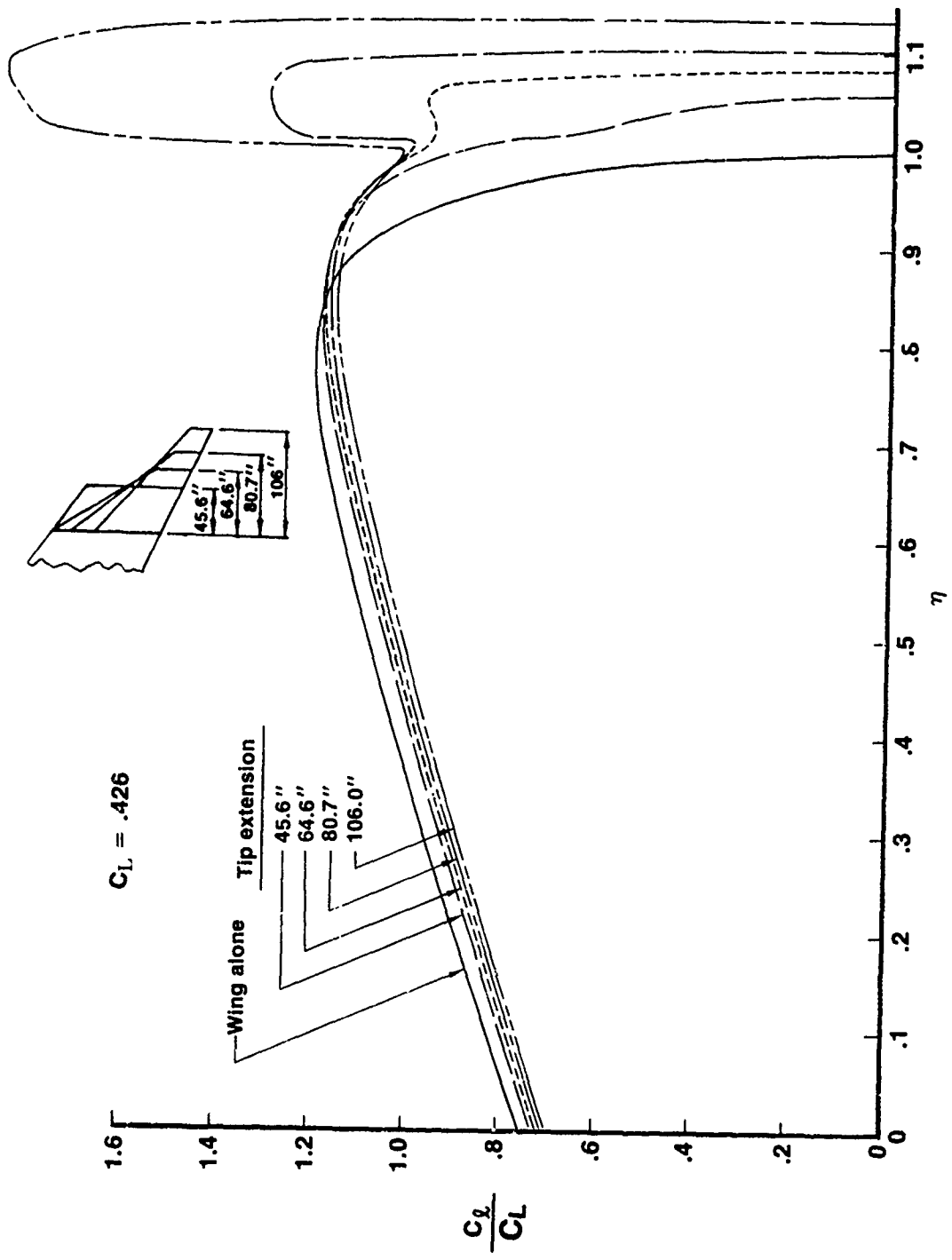
a (Lift and Pitching Moment)
 Figure 59. — Effect of Tip Extension



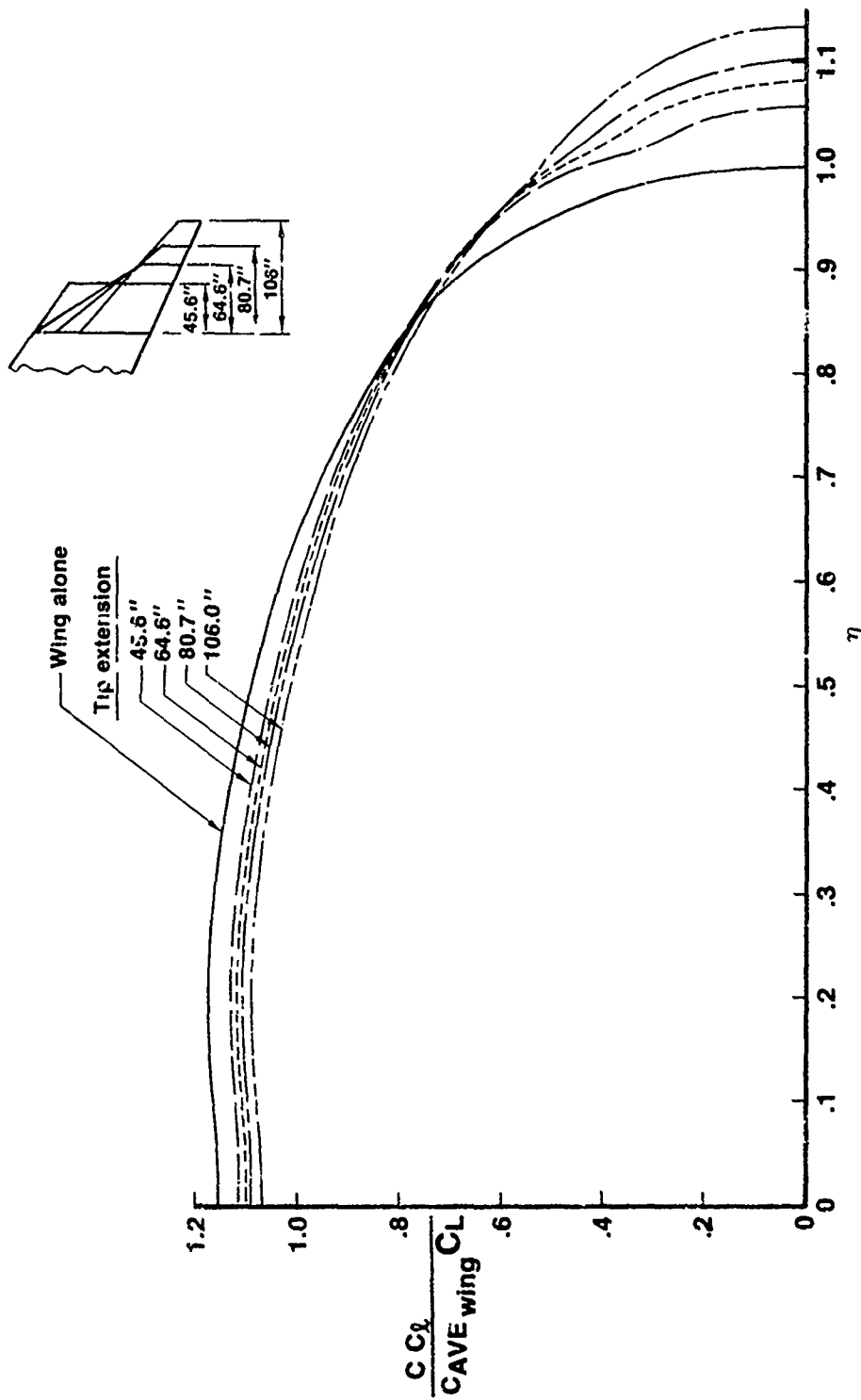
b (Induced Drag)
 Figure 59. — (Continued)



c (Wing-Root Bending Moment)
 Figure 59.— (Continued)



d (Sectional Lift)
 Figure 59. — (Continued)



e (Span Loading)
Figure 59.--(Concluded)

$$C_L = .426$$

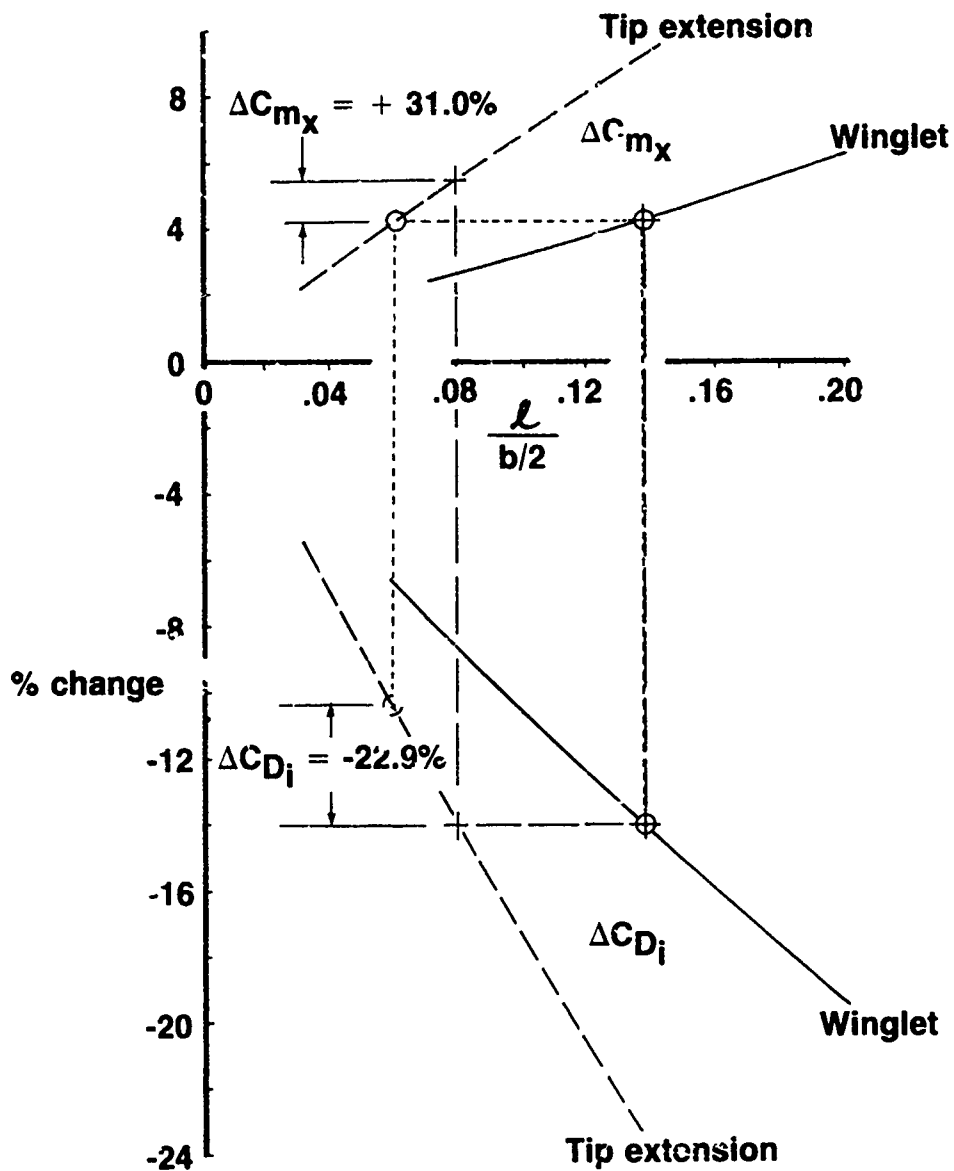


Figure 60.—Comparison of Induced Drag and Wing—Root Bending Moment Increments Between Winglets and Tip Extensions

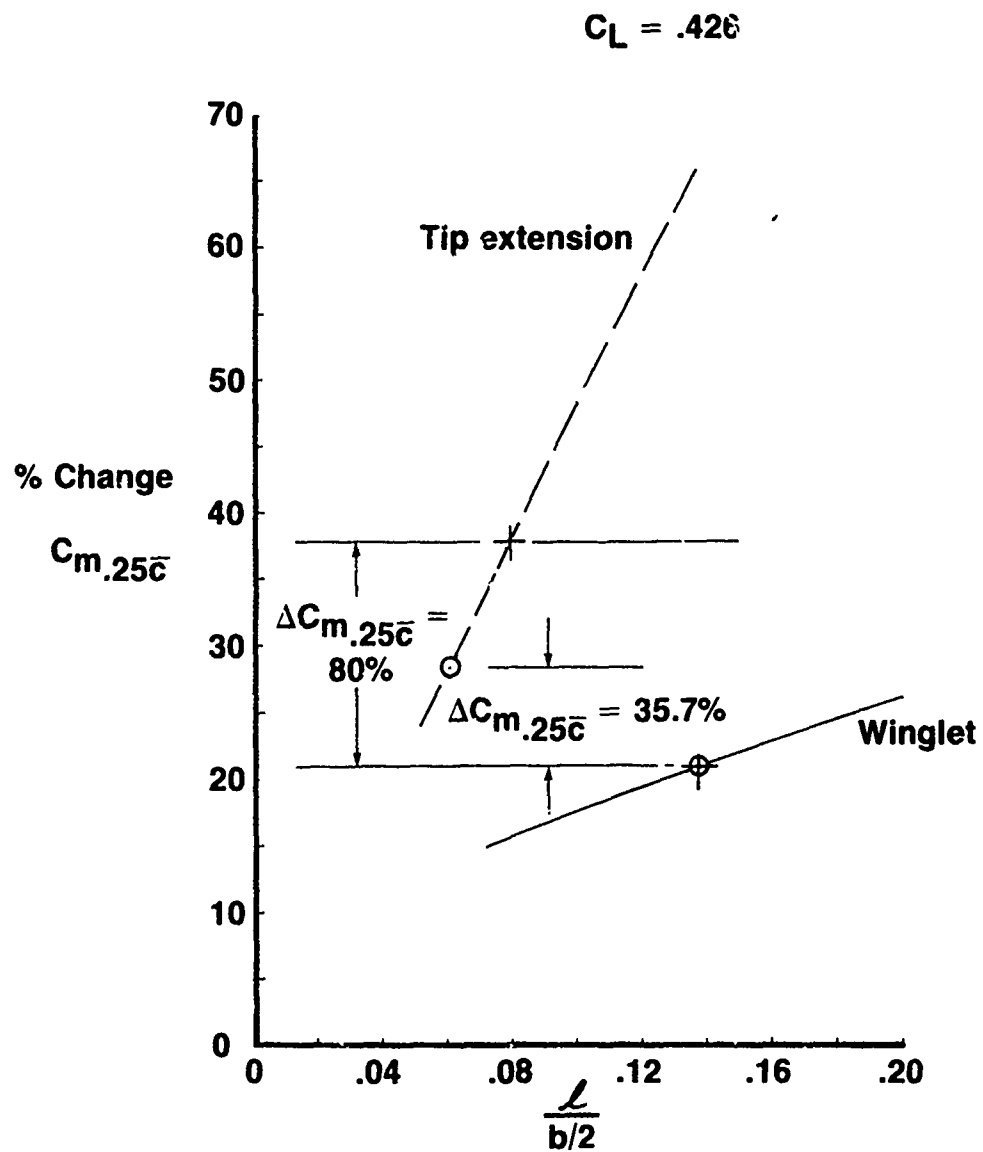


Figure 61.— Comparison of Pitching Moment Increment Between Winglets and Tip Extensions

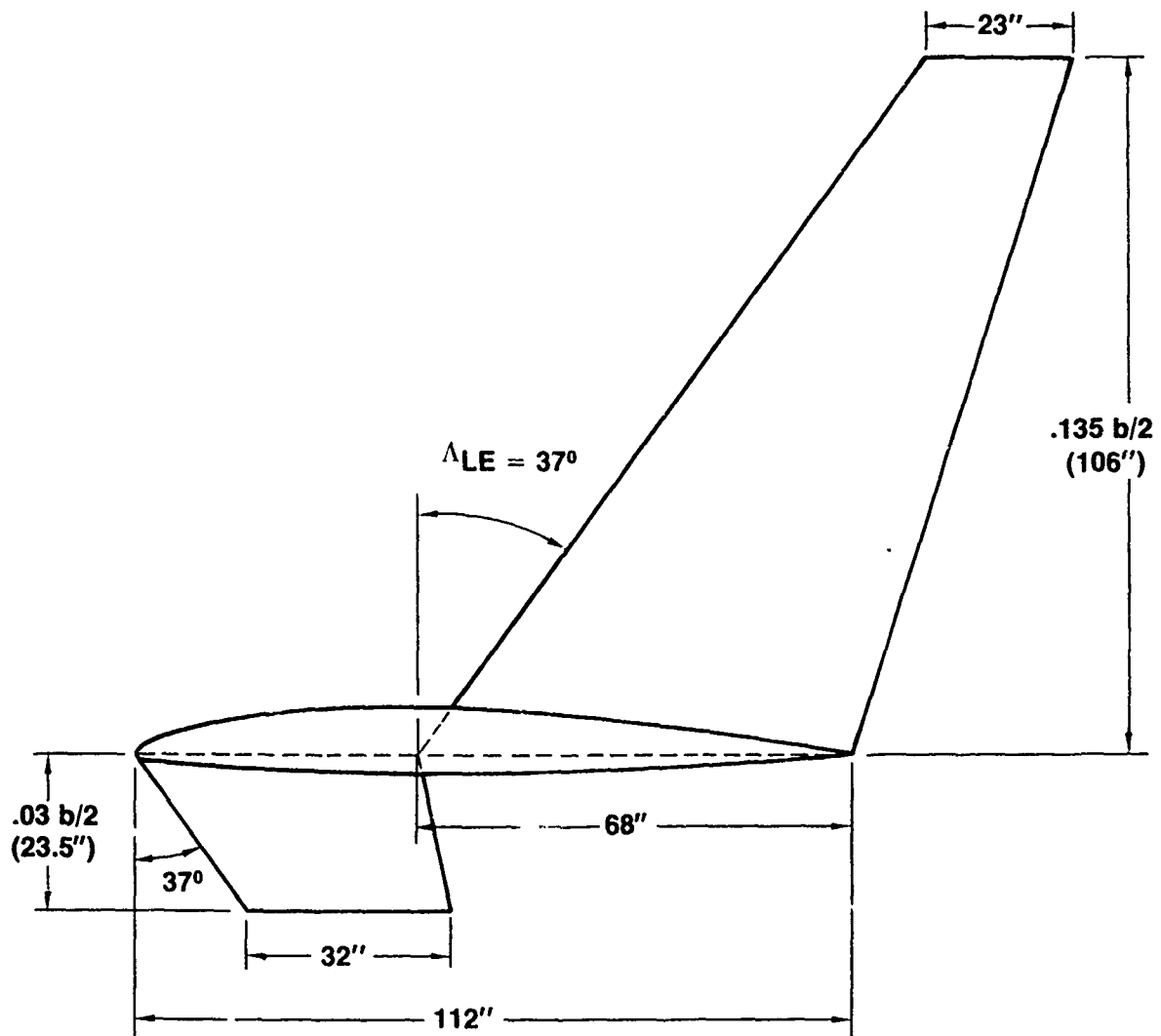
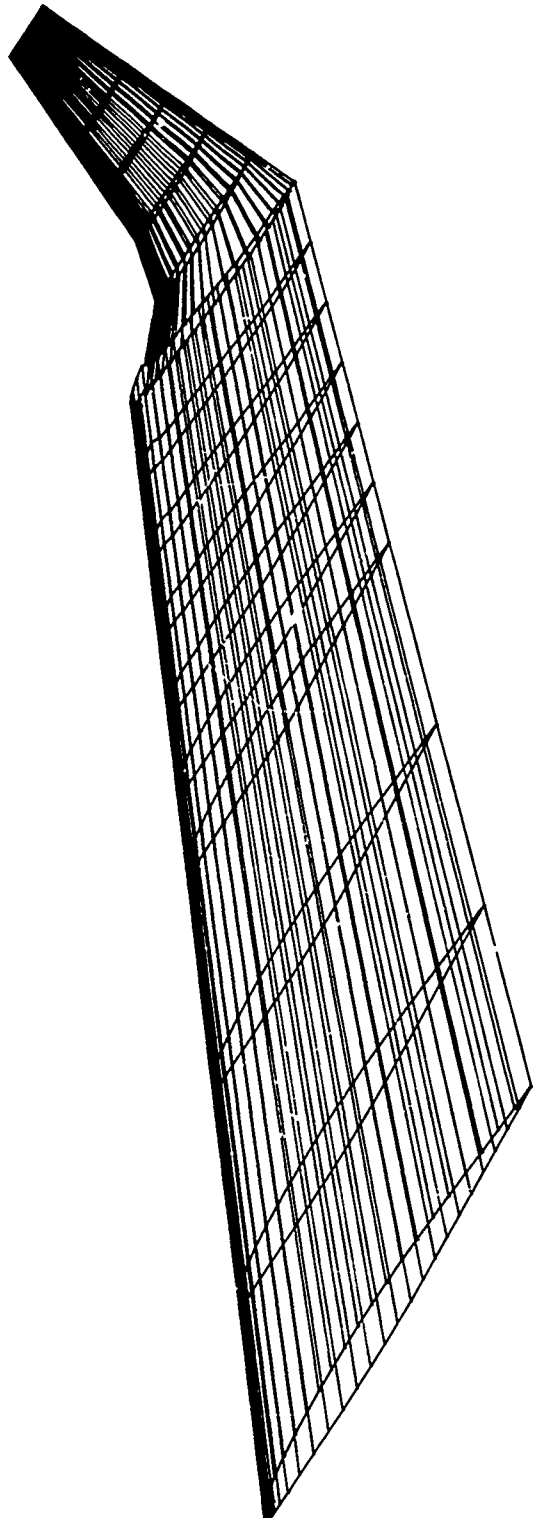
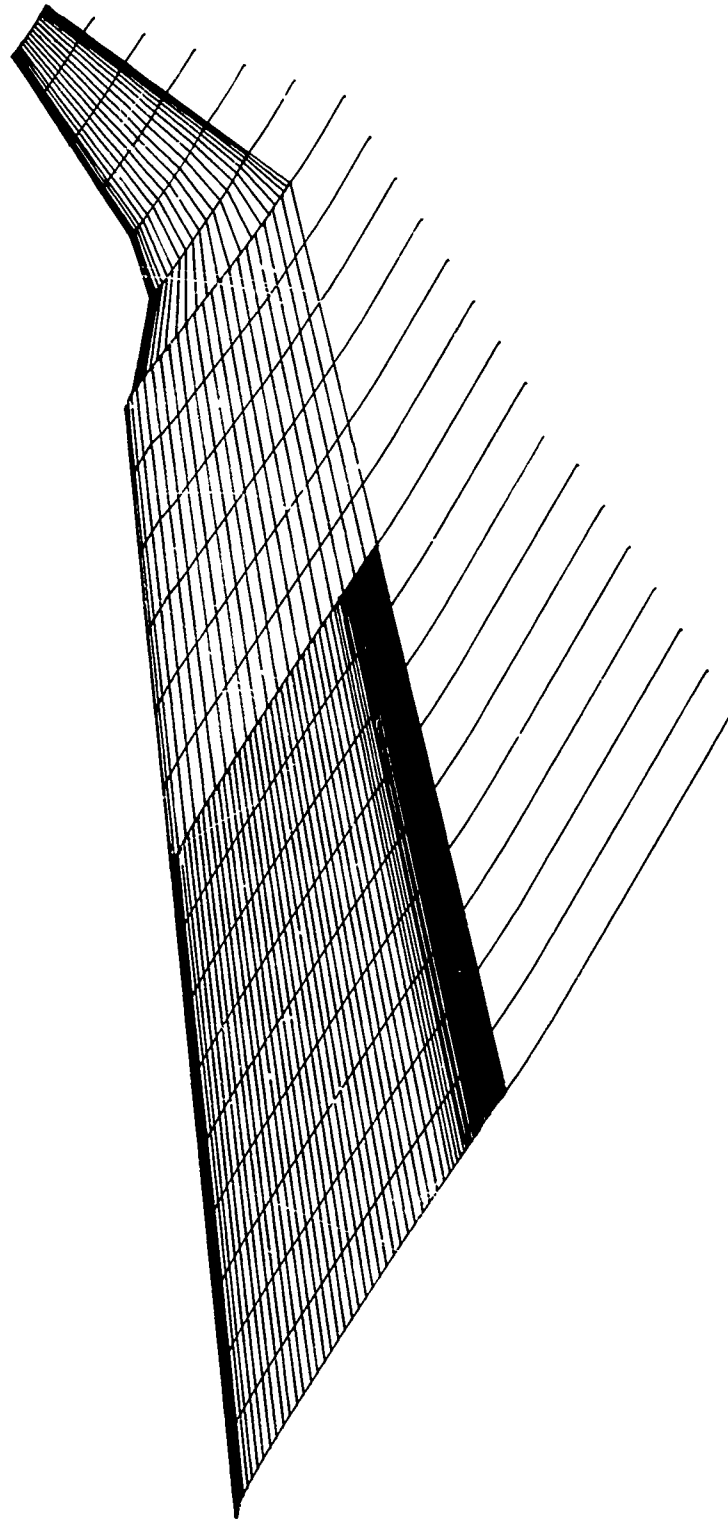


Figure 62.—Upper and Lower Winglets Analyzed in TEA-230



a (Source Singularities)
Figure 63. -- TEA-230 Modeling of Winglet and Outboard J Portion of Wing



b (Vortex Singularities)
Figure 63. — (Concluded)

Wing press. dist. at $M = .70$, $C_L \approx .5$
 $\eta_{wing} = .975$

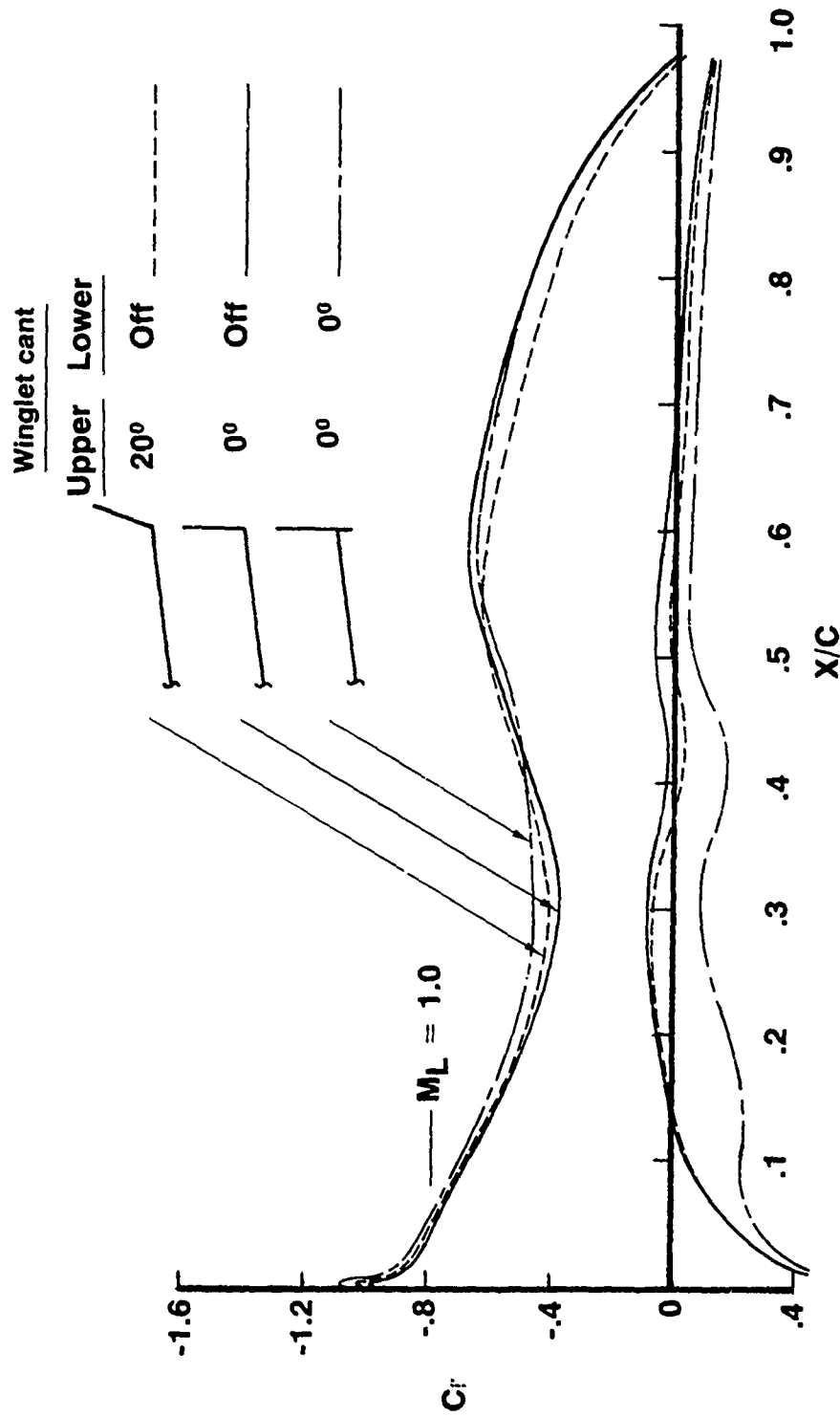


Figure 64.— Effect of Cant and Lower Winglet on Wing Pressure Distribution

Upper winglet press. dist. at $M = .70$, $C_L \approx .5$

$\eta_{\text{winglet}} = .083$

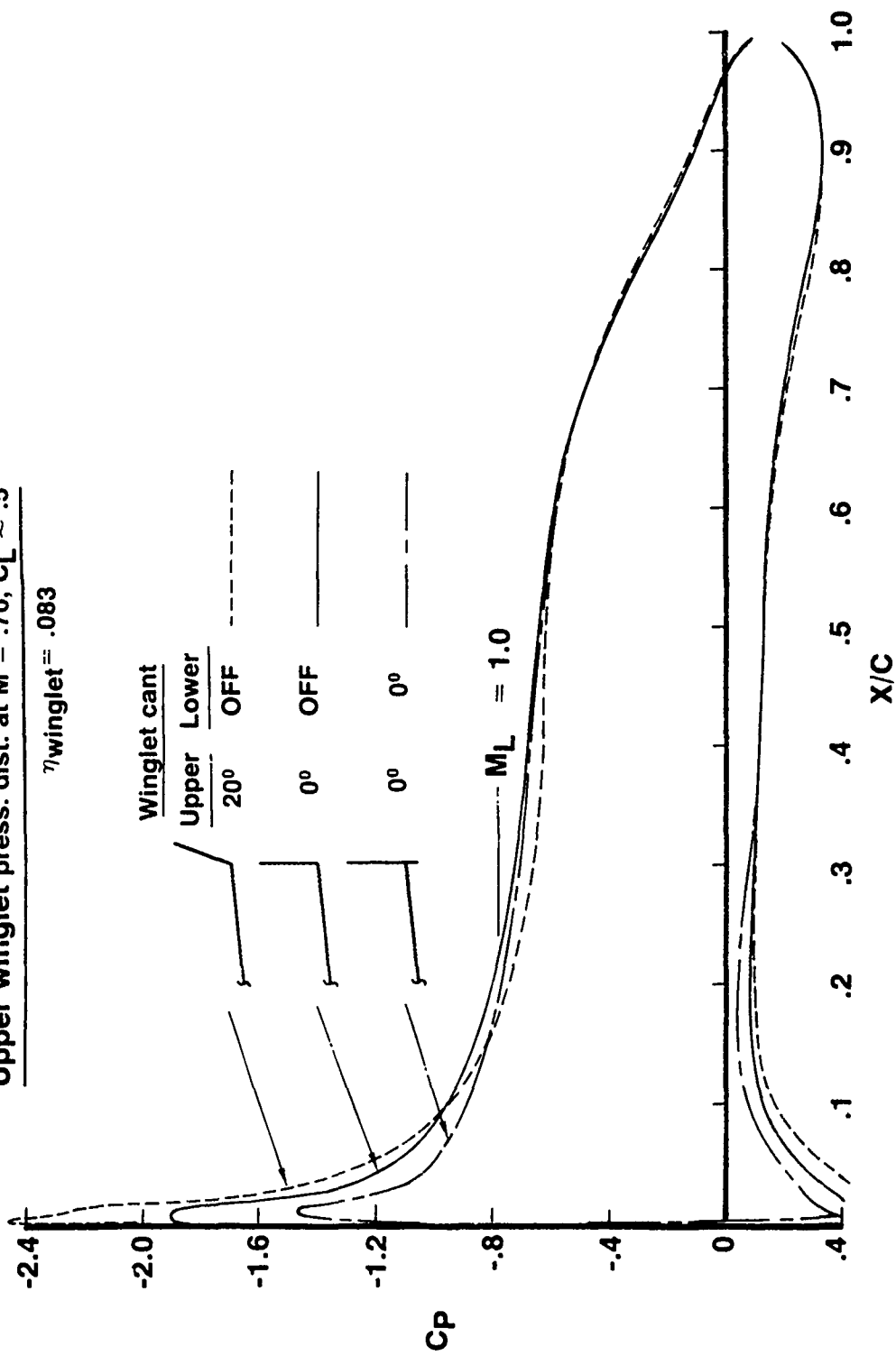


Figure 65.—Effect of Cant and Lower Winglet on Upper Winglet Pressure Distribution

Strap = 4823 in²
S_{total} = 5215.22 in²
AR_{trap} = 2.33
λ_{trap} = .338

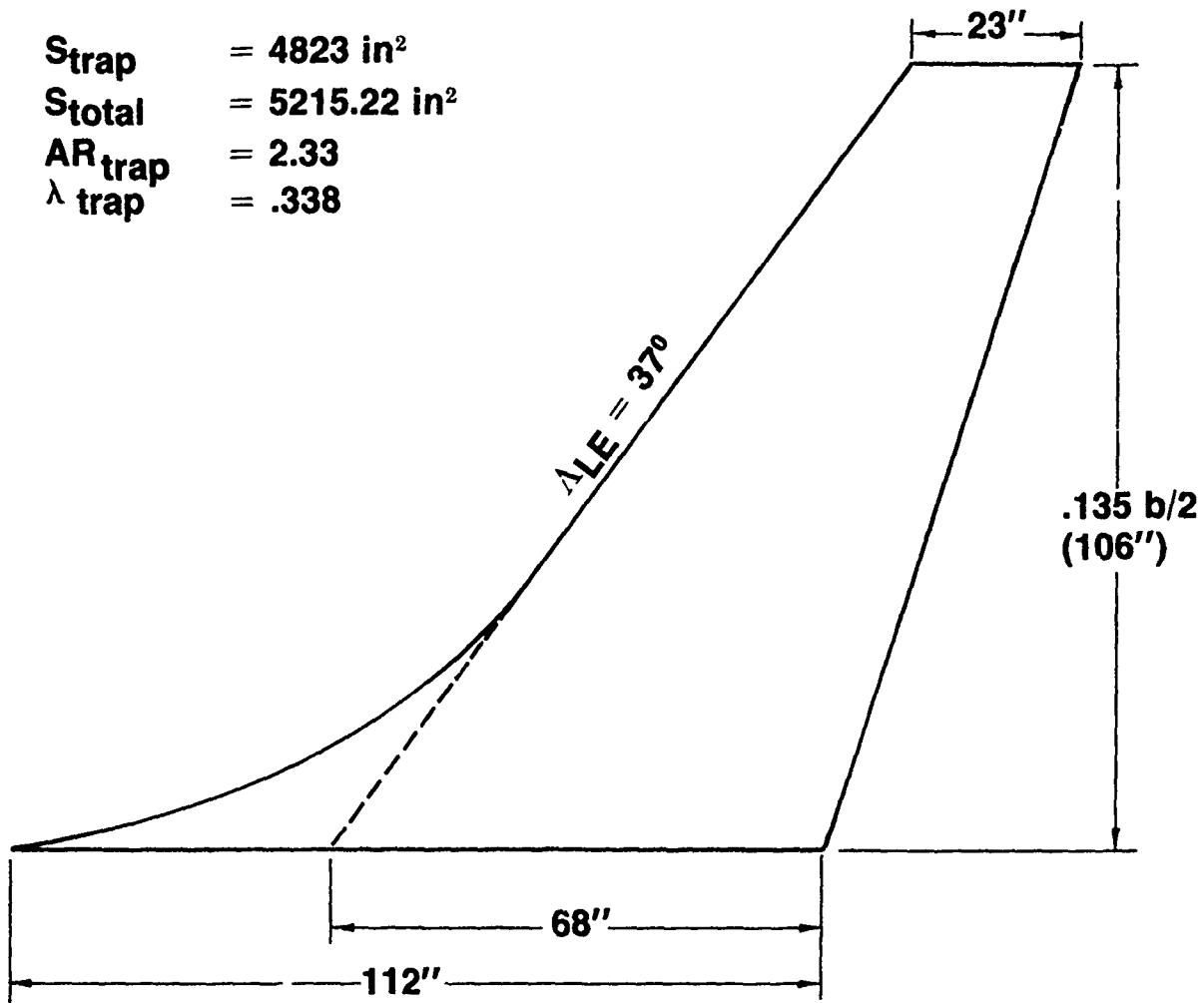
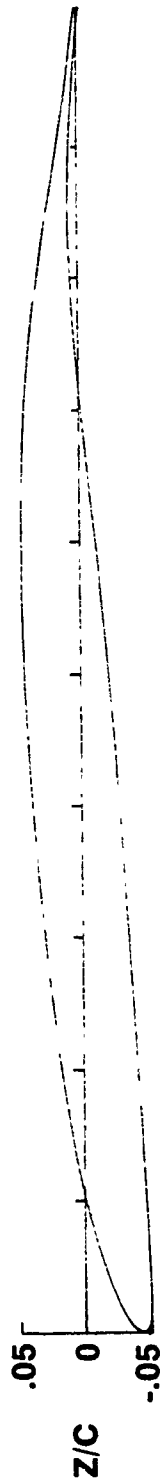


Figure 66.—Final Selected KC-135 Winglet Platform

$\eta = .417 \sim 1.0$



$\eta = .20$



$\eta = 0$

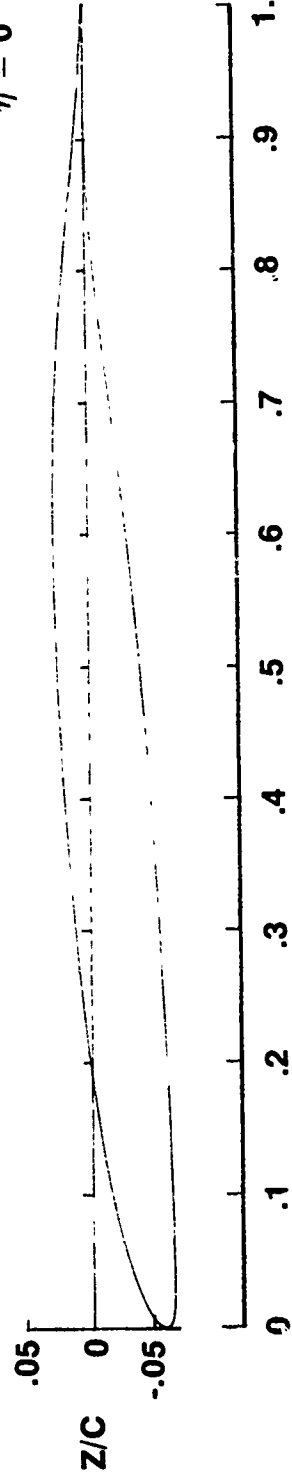


Figure 67. — Streamwise Airfoil Sections of Winglet Designed for KC-135

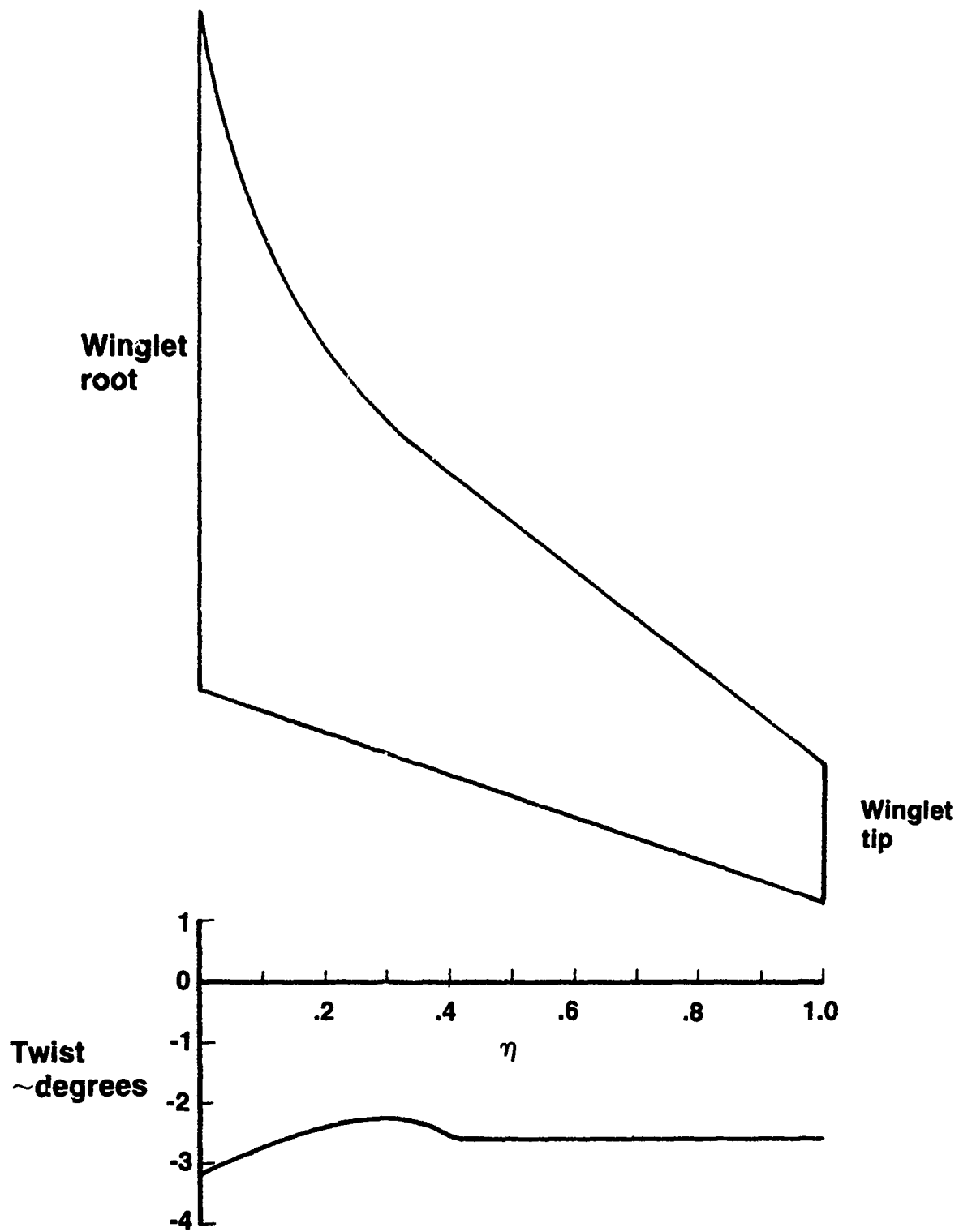


Figure 68.— Twist Distribution of KC-135 Winglet

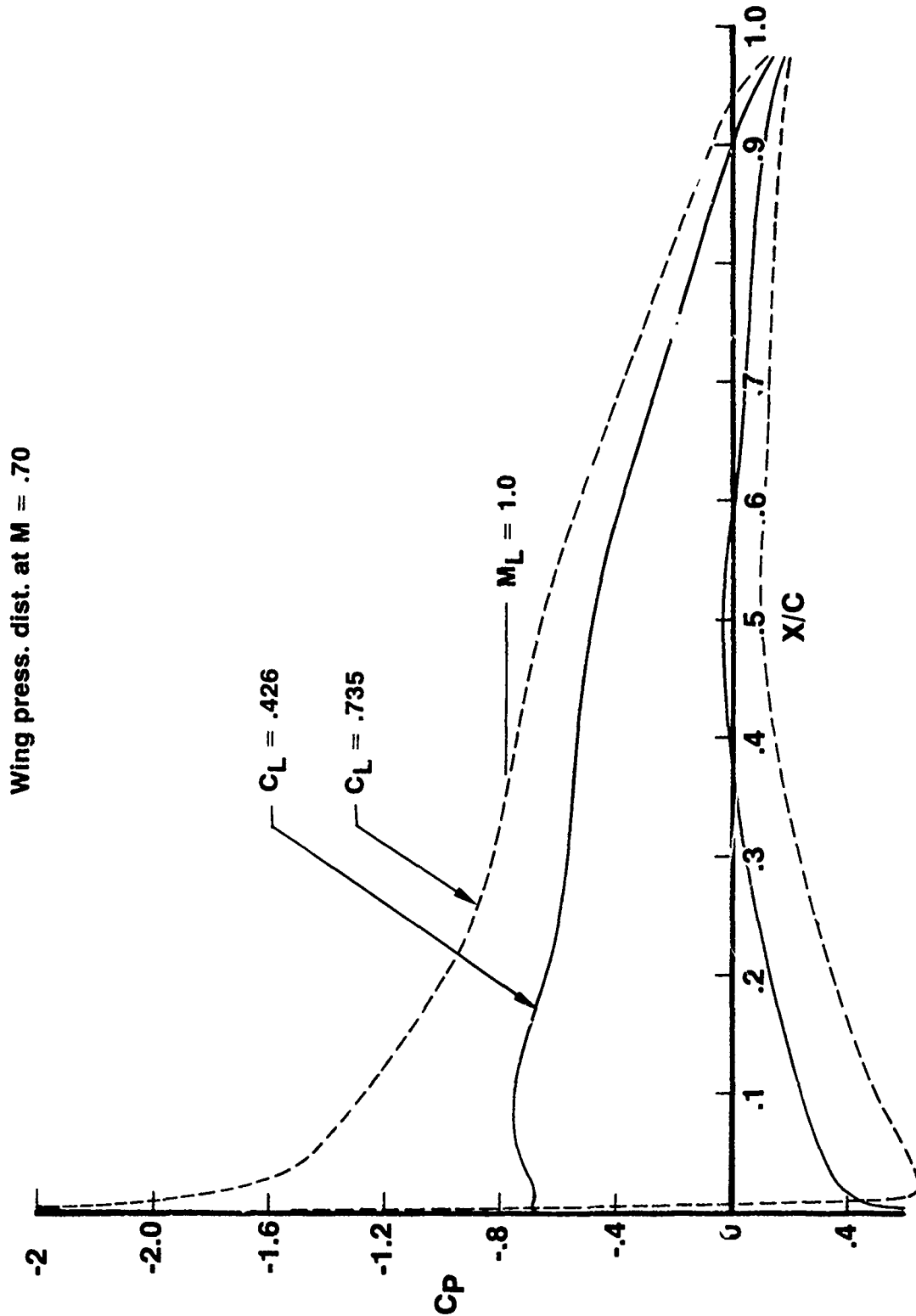
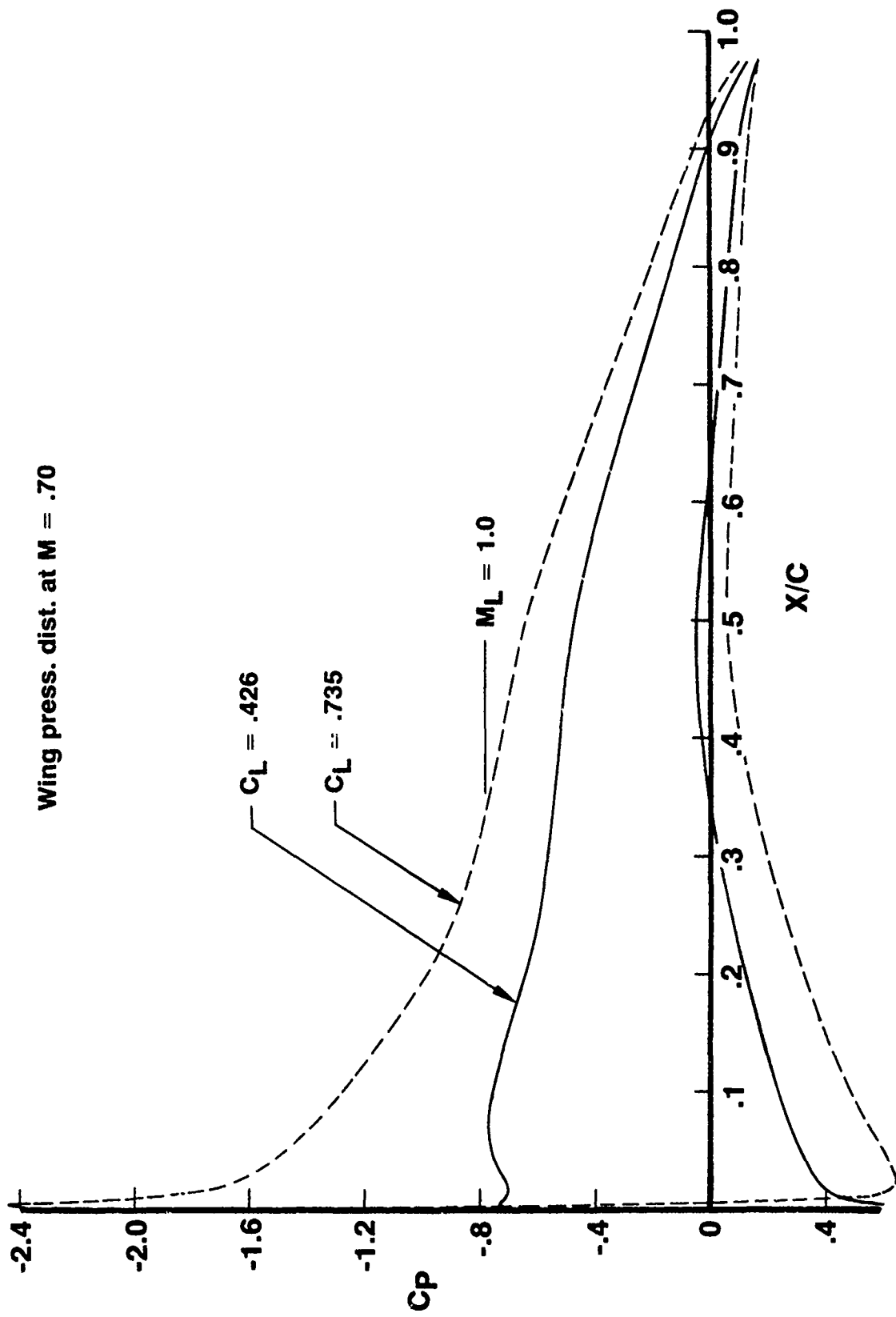
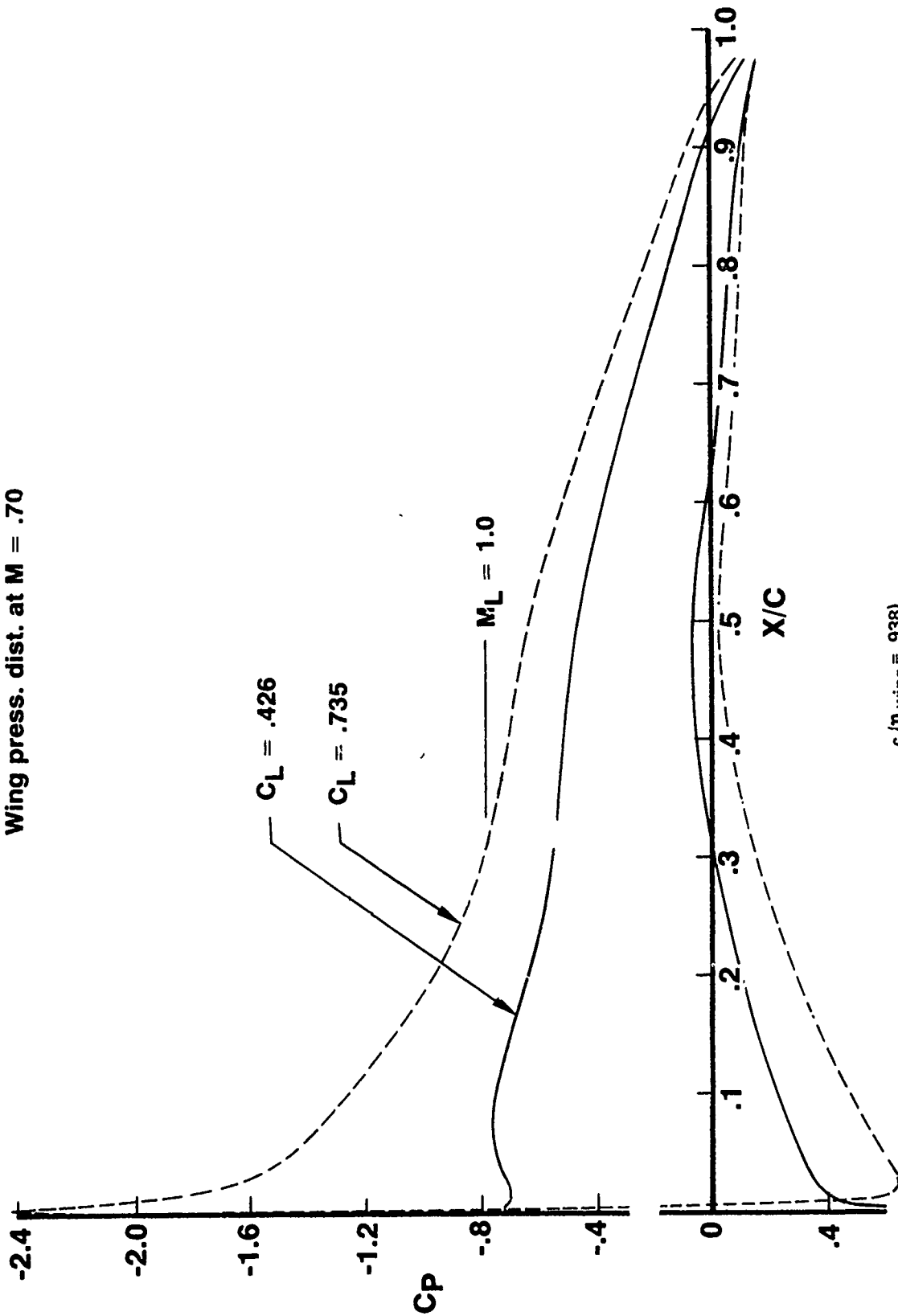


Figure 69. — Outboard Wing Pressure Distributions on KC-135 With Designed Winglet Installed
 a ($\eta_{wing} = .869$ & $.892$)



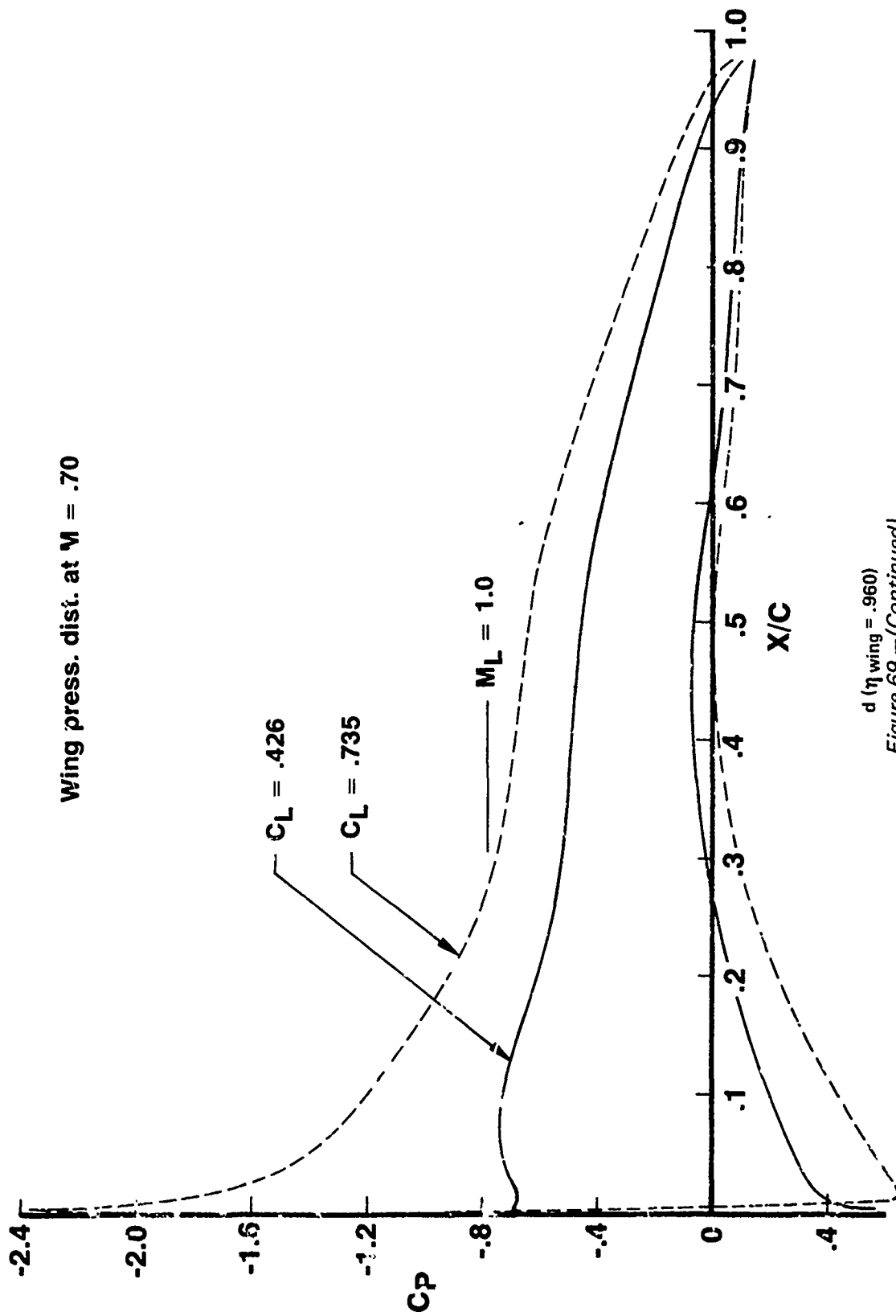
b (η wing = .915)
Figure 69.—(Continued)

Wing press. dist. at $M = .70$



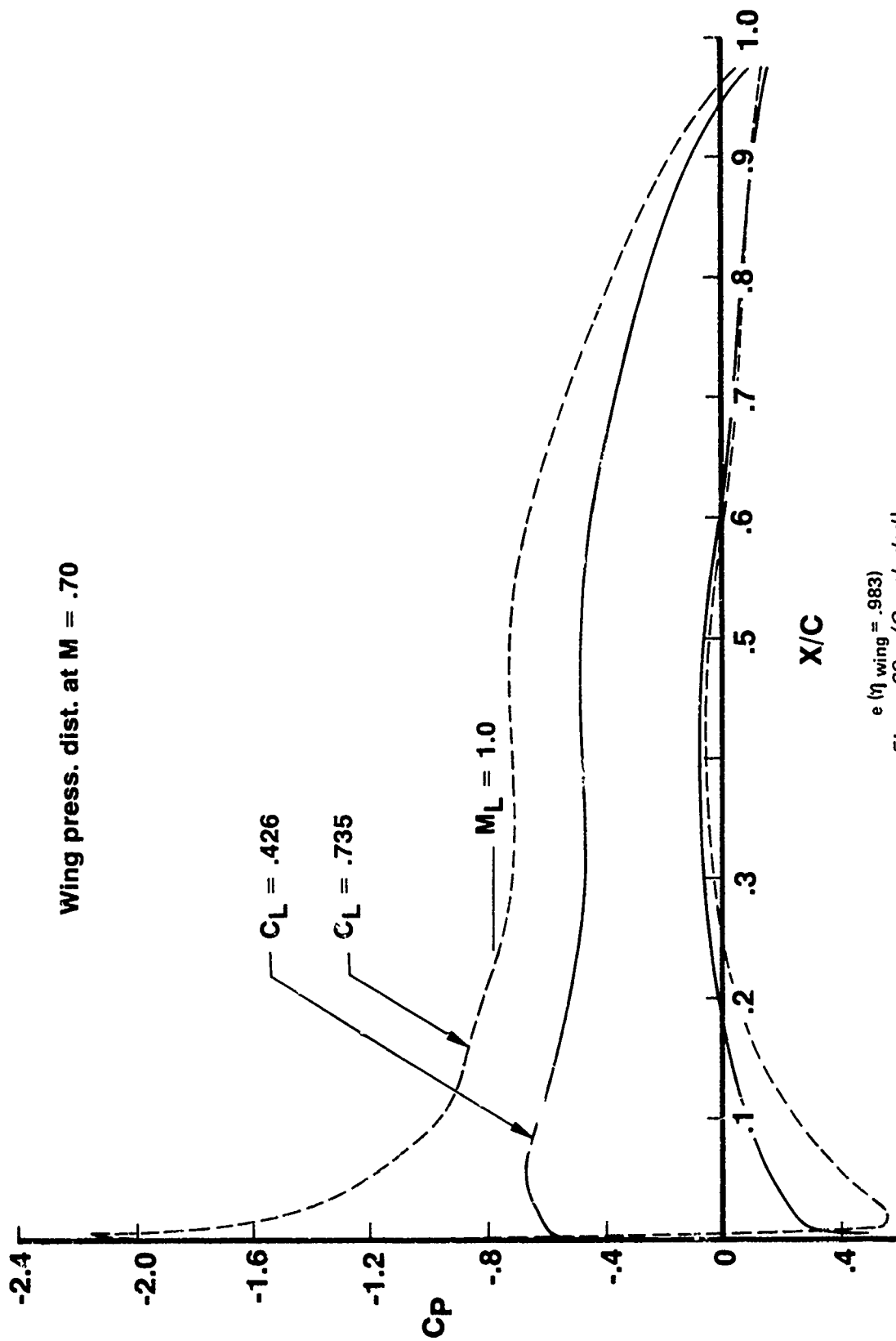
c ($\eta_{wing} = .938$)
Figure 69. — (Continued)

Wing press. dist. at $M = .70$



d ($\eta_{wing} = .960$)

Figure 69. -- (Continued)



$e(\eta)_{wing} = .983$
Figure 69. — (Concluded)

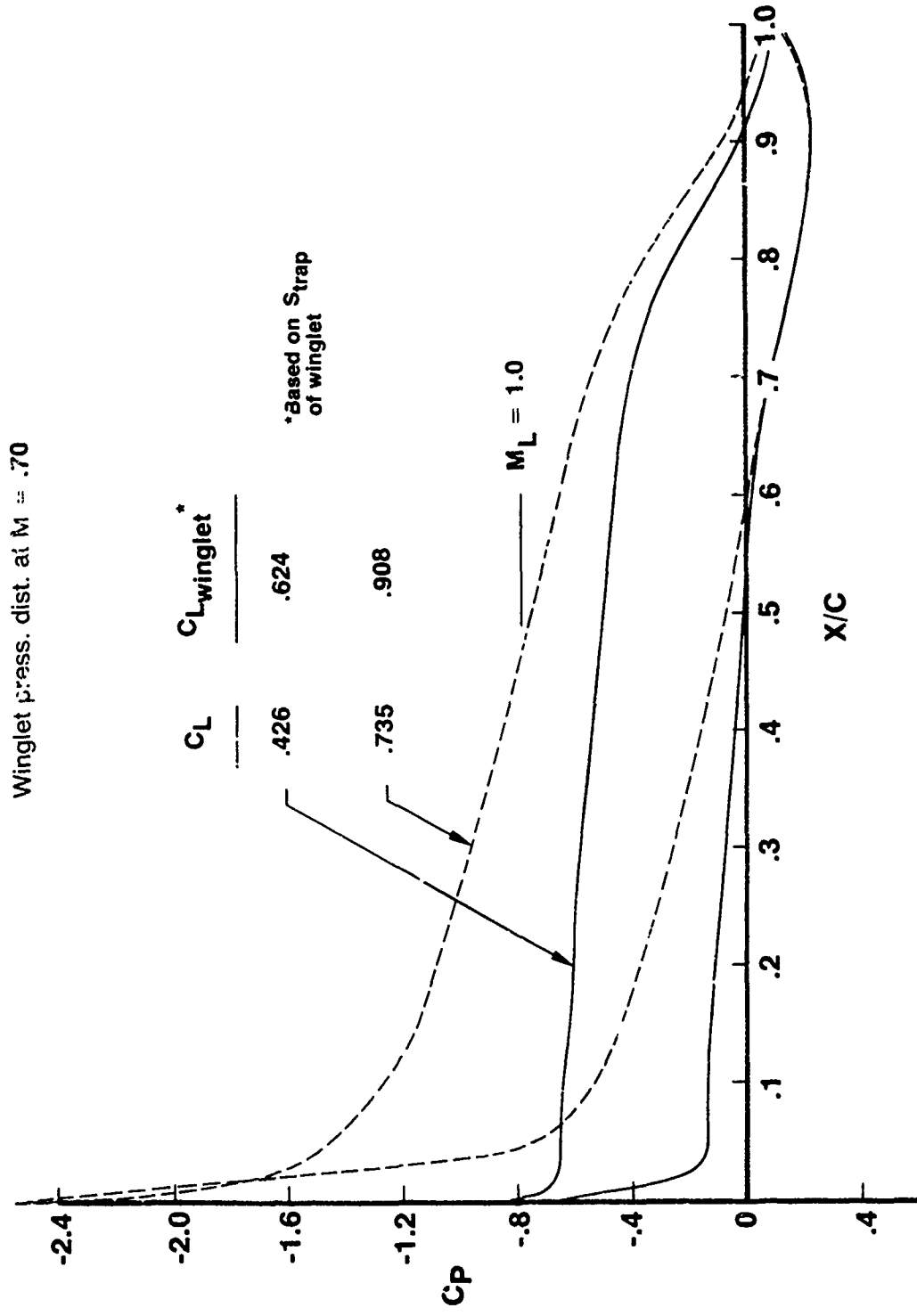
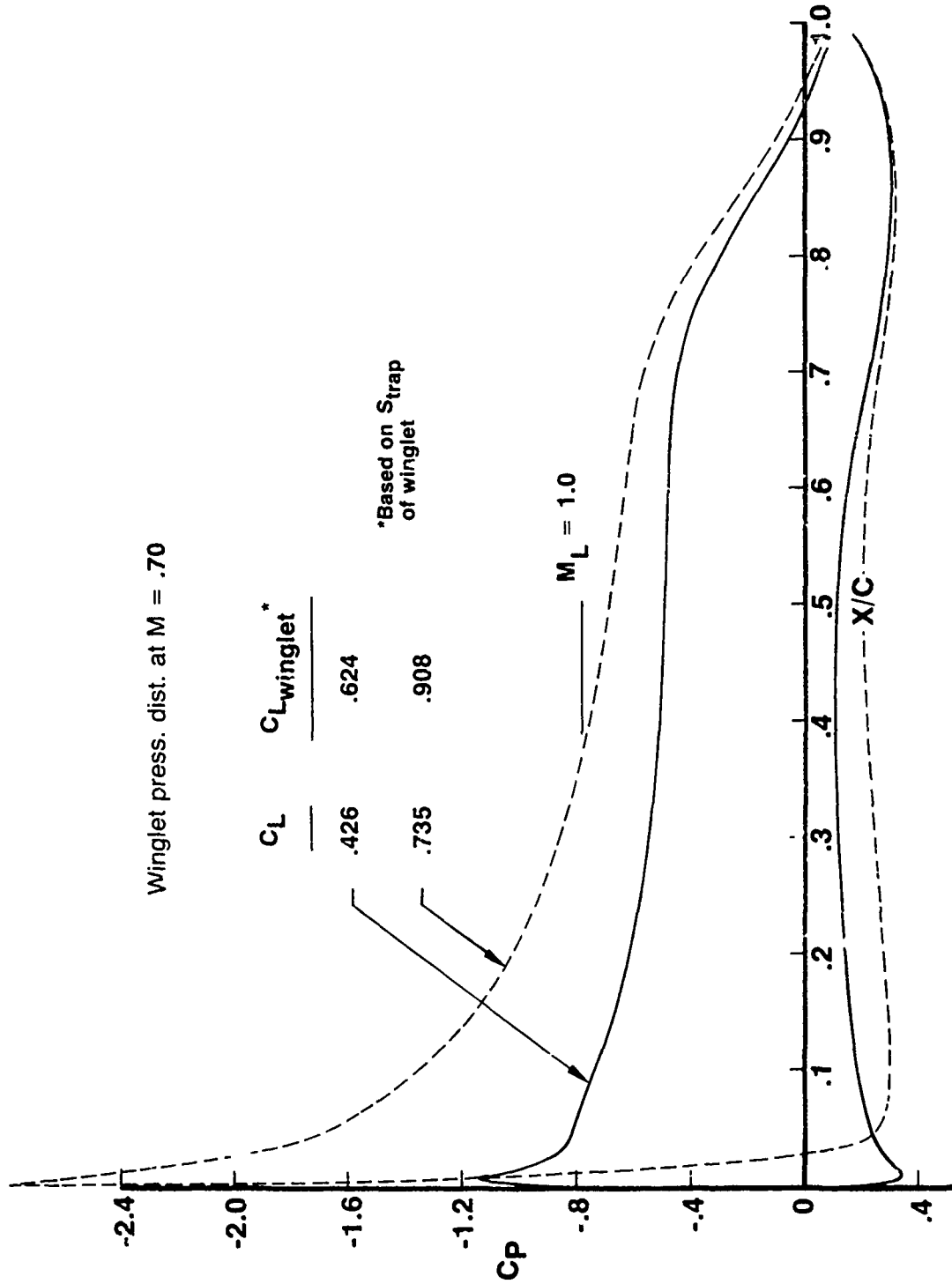
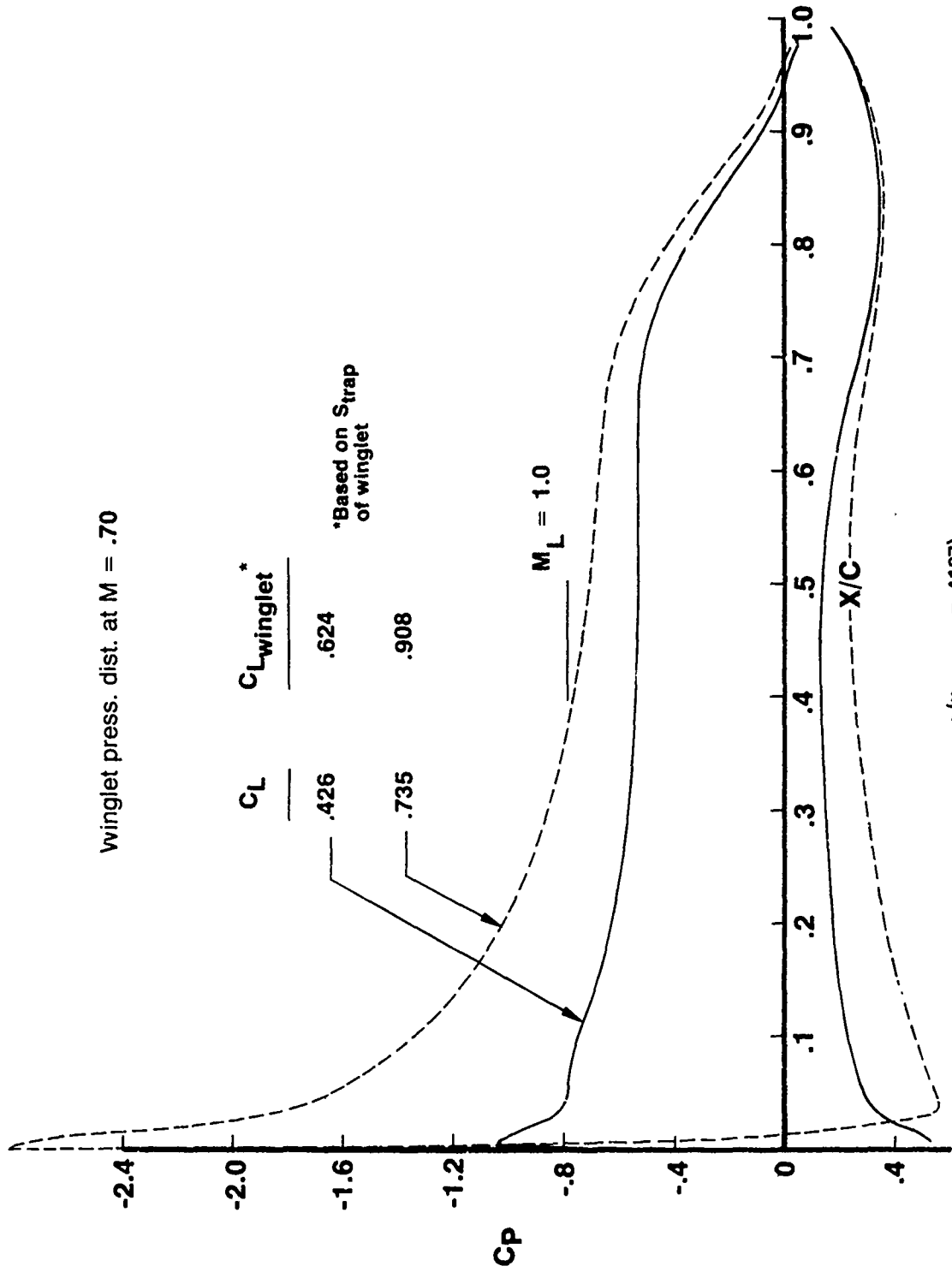


Figure 70.—Pressure Distributions on Winglet Designed for $k = .135$ Wing
 a ($\eta_{winglet} = .0833$)



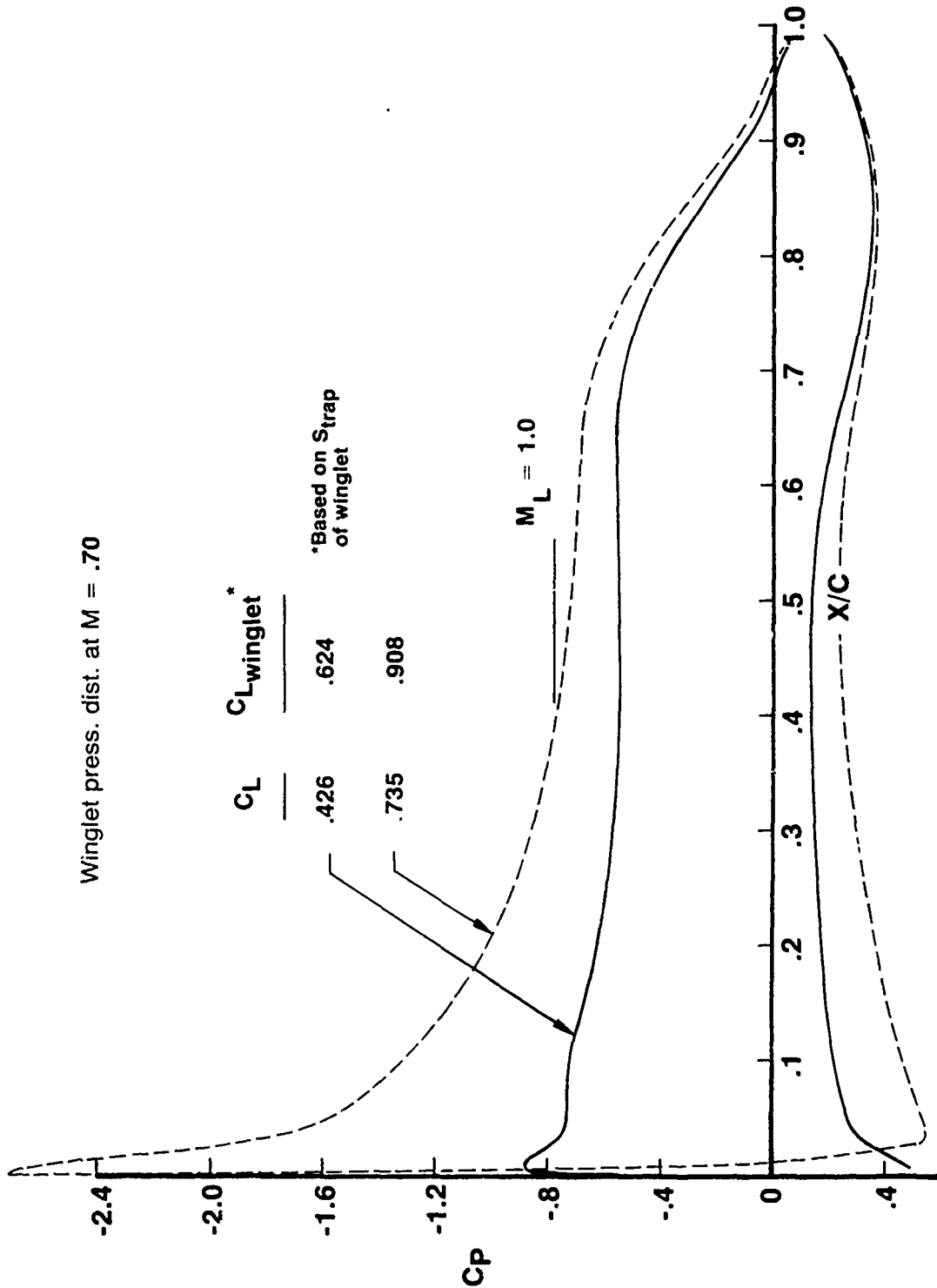
b ($\eta_{winglet} = .25$)
Figure 70.—(Continued)

winglet press. dist. at $M = .70$

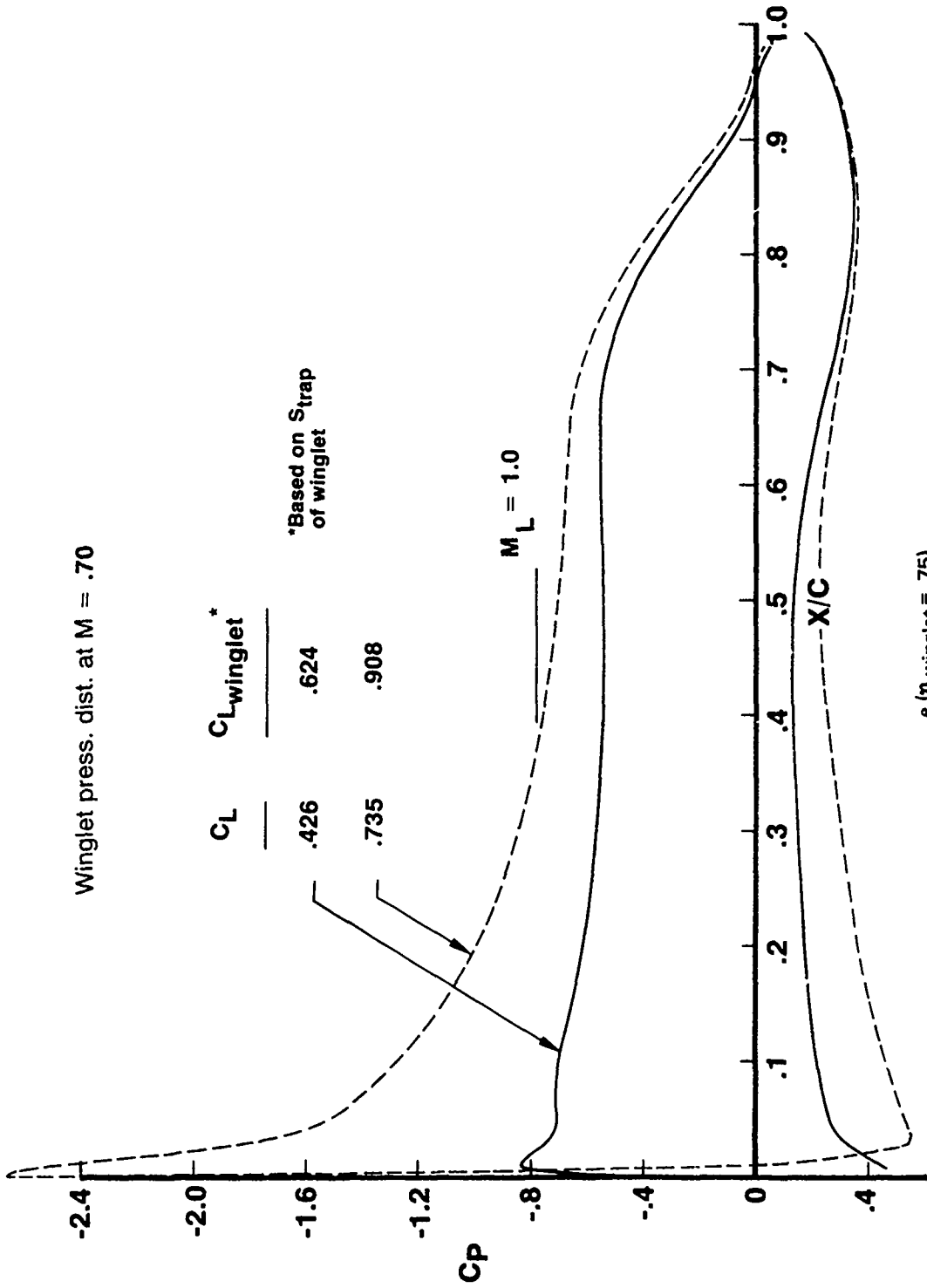


$c(\eta_{winglet} = .4167)$
Figure 70. — (Continued)

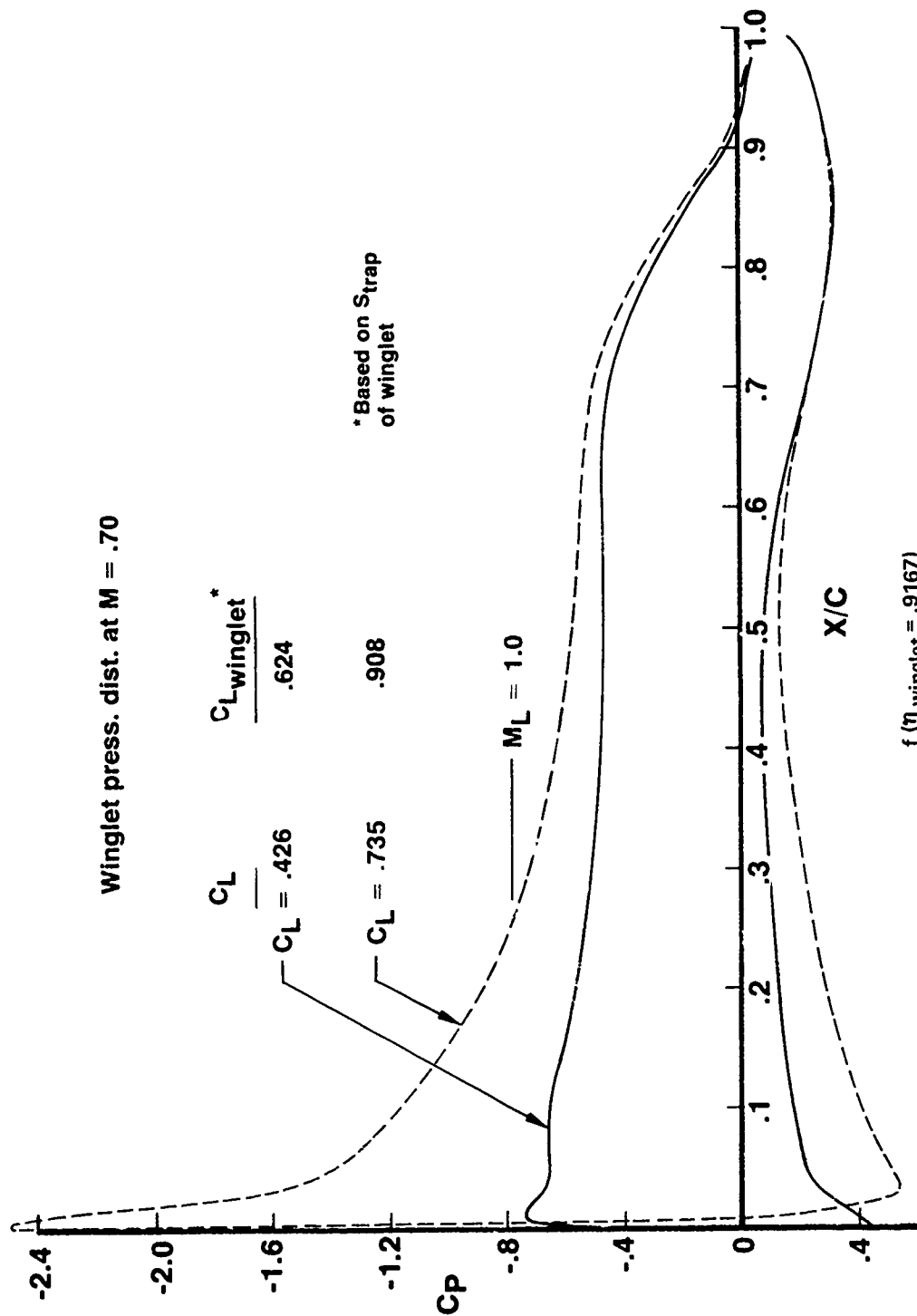
Winglet press. dist. at $M = .70$



d ($\eta_{\text{winglet}} = .5833$)
Figure 70.—(Continued)



e ($\eta_{winglet} = .75$)
Figure 70.--(Continued)



$f(\eta_{winglet} = .9167)$
Figure 70.—(Concluded)

Table 1.—Summary of Winglet Effects on the KC-135 and C-141

	KC-135 $C_L = 0.426$	C-141 $C_L = 0.55$
ΔC_{D_i}	-0.0011	-0.00135
$\Delta C_{D_p \text{ winglets}}$	0.0002	0.0002
$\Delta C_{D_p \text{ wing}}$	-0.00034	-0.00044
$\Delta C_{D_i} + \Delta C_{D_p \text{ winglets}} + \Delta C_{D_p \text{ wing}}$	-0.00124	-0.00159
$C_{D \text{ airplane}}$	0.0241	0.0285
$\frac{\Delta C_{D_i} + \Delta C_{D_p \text{ winglet}} + \Delta C_{D_p \text{ wing}}}{C_{D \text{ airplane}}} \times 100$	5.1%	5.6%
$\Delta C_{m_{.25\bar{c}}}$	-0.013	-0.01
% increase in root bending moment	4.2%	1.9%

Table 2.—Wing and Winglet Design Conditions

Cond. No.	Type	G. W. (Lb)	h (Ft)	V _e (KTS)	Mach No.	n (g)	α (Deg)	ψ (Deg)	α Gust (Deg)
1	Symmetric	245 000	Sea Level	253	0.38	2.5	15.425	--	--
2	Symmetric	297 000	29 000	350	0.95	2.0	7.903	--	--
3	Symmetric	297 000	Sea Level	248	0.375	2.0	15.394	--	--
	Antisymmetric - Over yaw	297 000	Sea Level	248	0.375	1.0	7.289	14.4	--
4	Antisymmetric - Over yaw	297 000	29 000	350	0.95	1.0	3.793	5.1	--
5	Symmetric - Side gust	297 000	Sea Level	201	0.304	1.0	11.26	--	10.84
6	Symmetric - Side gust	297 000	24 000	350	0.85	1.0	3.105	--	4.84

Table 3.—Ultimate Load Factors

Winglet	Nacelles	
	Outboard	Inboard
11g down	9g down	7g down
8g up	6g up	4g up
± 4g lateral	± 3g lateral	± 3g lateral
± 3g longitudinal	thrust	thrust

Table 4.—KC-135A Winglet Spanwise Loads

Cond	Ve KTS	h Ft	Gr Wt: Lb	n	c. g.	UE Ft/Sec
1.0	253.0	0.0	245 000.	2.5	0.16 \bar{c}	0.0

η	ULT Shear (Lb) x 10 ³	ULT Moment (in-Lb) x 10 ⁶	ULT Torsion (in-Lb) x 10 ⁶	ULT MP	ULT TP
1.000	0.000	0.000	0.000	0.000	0.000
0.900	0.247	0.001	-0.001	0.002	0.000
0.700	1.687	0.022	-0.013	0.025	0.000
0.500	3.767	0.080	-0.046	0.092	0.000
0.300	6.316	0.187	-0.109	0.216	0.000
0.100	9.407	0.353	0.206	0.409	0.000
0.000	11.229	0.463	-0.270	0.536	0.000

Note: UE: Sidestep velocity
 ULT MP: Ultimate moment perpendicular to load reference axis
 ULT TP: Ultimate torsion parallel to load reference axis

Table 5.—KC-135A Winglet Spanwise Loads

Cond	Ve KTS	h Ft	Gr Wt Lb	n	c. g.	UE Ft/Sec
2.0	350.0	29 000.0	297 000.	2.0	0.16 \bar{c}	0.0

η	ULT Shear (Lb) $\times 10^3$	ULT Moment (In-Lb) $\times 10^6$	ULT Torsion (In-Lb) $\times 10^6$	ULT MP	ULT TP
1.000	0.000	0.000	0.000	0.000	0.000
0.900	0.374	0.002	-0.001	0.002	0.000
0.700	2.353	0.031	-0.018	0.036	0.000
0.500	4.997	0.109	-0.063	0.126	0.000
0.300	7.996	0.247	-0.144	0.285	0.000
0.100	11.357	0.452	-0.264	0.523	0.000
0.000	13.299	0.582	-0.340	0.674	0.000

Note:

UE: Side gust velocity

ULT MP: Ultimate moment perpendicular
to load reference axis

Ult TP: Ultimate torsion parallel to
load reference axis

Table 6.—KC-135A Winglet Spanwise Combined Loads
(Yaw + Induced Effects)

Cond	Ve KTS	h Ft	Gr Wt Lb	n	c. g.	UE Ft/Sec
3.0	248.0	0.0	297 000.	1.0	0.21 \bar{c}	0.0

η	ULT Shear (Lb) x 10 ³	ULT Moment (In-Lb) x 10 ⁶	ULT Torsion (In-Lb) x 10 ⁶	ULT MP	ULT TP
1.000	-0.000	-0.000	-0.000	-0.000	-0.000
0.900	0.504	0.002	-0.001	0.003	-0.000
0.700	2.468	0.033	-0.019	0.038	-0.000
0.500	5.167	0.114	-0.066	0.132	-0.000
0.300	8.393	0.257	-0.150	0.297	0.000
0.100	12.060	0.473	-0.276	0.548	0.000
0.000	14.026	0.612	-0.357	0.708	0.000

Note:

UE: Side gust velocity

ULT MP: Ultimate moment perpendicular
to load reference axis

ULT TP: Ultimate torsion parallel to
load reference axis

Table 7. -KC-135A Winglet Spanwise Combined Loads
(Yaw + Induced Effects)

Cond	Ve KTS	h Ft	Gr Wt Lb	n	c. g.	UE Ft/Sec
4.0	350.0	29 000.0	297 000.	1.0	0.21 \bar{c}	0.0

η	ULT Shear (Lb) $\times 10^3$	ULT Moment (In-Lb) $\times 10^6$	ULT Torsion (In-Lb) $\times 10^6$	ULT MP	ULT TP
1.000	-0.000	-0.000	-0.000	-0.000	-0.000
0.900	0.505	0.003	-0.001	0.003	-0.000
0.700	2.689	0.036	-0.021	0.042	-0.000
0.500	5.535	0.123	-0.072	0.142	0.000
0.300	8.785	0.274	-0.160	0.318	0.000
0.100	12.223	0.497	-0.290	0.575	0.000
0.000	13.838	0.635	-0.371	0.735	0.000

Note:

UE: Side gust velocity

ULT MP: Ultimate moment perpendicular
to load reference axis

ULT TP: Ultimate torsion parallel to
load reference axis

Table 8.—KC-135A Winglet Spanwise Combined Loads
(Gust + Induced Effects)

Cond	Ve KTS	h Ft	Gr Wt Lb	n	c. g.	UE Ft/Sec
5.0	201.0	0.0	297 000.	1.0	0.21 \bar{c}	65.

η	ULT Shear (Lb) x 10 ³	ULT Moment (In-Lb) x 10 ⁶	ULT Torsion (In-Lb) x 10 ⁶	ULT MP	ULT TP
1.000	-0.000	-0.000	-0.000	-0.000	-0.000
0.900	0.303	0.002	-0.001	0.002	-0.000
0.700	1.584	0.021	-0.012	0.024	-0.000
0.500	3.365	0.073	-0.043	0.085	-0.000
0.300	5.516	0.167	-0.098	0.194	0.000
0.100	8.018	0.311	-0.181	0.360	0.000
0.000	9.406	0.403	-0.235	0.466	0.000

Note:

UE: Side gust velocity

ULT MP: Ultimate moment perpendicular
to load reference axis

ULT TP: Ultimate torsion parallel to
load reference axis

Table 9.—KC-135A Winglet Spanwise Combined Loads
(Gust + Induced Effects)

Cond	Ve KTS	h Ft	Gr Wt Lb	n	c. g.	UE Ft/Sec
6.0	350.0	24 000.0	297 000.	1.0	0.21 \bar{c}	50.

η	ULT Shear (Lb) $\times 10^3$	ULT Moment (In-Lb) $\times 10^6$	ULT Torsion (In-Lb) $\times 10^6$	ULT MP	ULT TP
1.000	-0.000	-0.000	-0.000	-0.000	-0.000
0.900	0.475	0.002	-0.001	0.003	-0.000
0.700	2.525	0.034	-0.020	0.039	-0.000
0.500	5.181	0.115	-0.067	0.133	0.000
0.300	8.215	0.257	-0.150	0.297	0.000
0.100	11.375	0.464	-0.271	0.538	0.000
0.000	12.785	0.592	-0.346	0.686	0.000

Note:

UE: Side gust velocity

ULT MP: Ultimate moment perpendicular
to load reference axis

ULT TP: Ultimate torsion parallel to
load reference axis

Table 10.—Wing-Root Bending Moments (Ultimate)

Cond. No.	Type	G. W. (Lb)	h (Ft)	V _e (KTS)	Mach No.	n (g)	Basic Airplane Ultimate WRBM (In-Lb x 10 ⁶)	Airplane + Winglets Ultimate WRBM (In-Lb x 10 ⁶)	% WRBM Increase
1	Symmetric	245 000	Sea Level	253	0.38	2.5	72.834	74.244	1.9
2	Symmetric	297 000	29 000	350	0.95	2.0	79.118	79.662	0.7
3	Symmetric	297 000	Sea Level	248	0.375	2.0	78.211	79.242	1.3

Table 11.—Wing Loads and Deflections

Flight Condition No. 1

G. W. = 245 000 Lb.

ALT. = Sea Level

V_e = 253 Kts

M = 0.38

n = 2.5 g

c. g. 16% MAC

Basic Airplane

η	Lift DIST. (Lb/In)	Shear (Lb x 10 ³)	EA MOM (In-Lb x 10 ⁶)	EA TOR (In-Lb x 10 ⁶)	EA DEFL (In)	LOCAL α (Deg)
0.05	0.54	150.	52.7	-10.3	0.0	15.22
0.15	0.52	118.	43.4	- 4.36	0.84	14.95
0.25	0.49	100.	35.4	- 1.24	2.65	14.6
0.35	0.45	88.	27.4	- 0.65	6.01	14.05
0.45	0.42	83.	19.2	0.19	11.6	13.37
0.55	0.39	67.	12.6	- 0.37	19.6	12.59
0.65	0.36	46.	7.8	- 0.76	30.2	11.69
0.75	0.31	35.	3.6	0.33	43.5	10.91
0.85	0.24	19.	1.2	0.18	59.4	10.45
0.95	0.17	5.6	0.1	0.003	76.7	10.26

Basic Airplane + Winglets

η	Lift DIST. (Lb/In)	Shear (Lb x 10 ³)	EA MOM (In-Lb x 10 ⁶)	EA TOR (In-Lb x 10 ⁶)	EA DEFL (In)	LOCAL α (Deg)
0.05	0.54	150.	53.6	-10.5	0.0	15.22
0.15	0.52	118.	44.3	- 4.4	0.85	14.96
0.25	0.49	100.	36.3	- 1.17	2.7	14.6
0.35	0.45	88.7	28.2	- 0.54	6.1	14.08
0.45	0.42	83.9	19.9	0.25	11.9	13.41
0.55	0.39	67.5	13.22	- 0.28	20.1	12.64
0.65	0.36	46.4	8.39	- 0.67	31.	11.75
0.75	0.31	56.2	4.1	0.43	44.9	10.96
0.85	0.24	19.9	1.6	0.28	61.5	10.45
0.95	0.18	6.0	0.4	0.13	80.13	10.17

Note: EA MOM: Moment along elastic axis
 EA TOR: Torsion along elastic axis
 EA DEFL: Deflection along elastic axis
 LOCAL α : Local angle of attack of wing with respect to freestream

Table 12.—Wing Loads and Deflections

Flight Condition No. 2

G. W. = 297 000 Lb.
 ALT. = 29 000 Ft.
 V_e = 350 Kts
 M = 0.95
 n = 2.0 g
 c. g. = 21% MAC

Basic Airplane

η	Lift DIST. (Lb/In)	Shear (Lb x 10 ³)	EA MOM (In-Lb x 10 ⁶)	EA TOR (In-Lb x 10 ⁶)	EA DEFL (In)	LOCAL α (Deg)
0.05	0.63	183.	57.1	-20.36	0.0	7.6
0.15	0.6	141.9	46.6	-11.4	0.95	7.1
0.25	0.55	113.8	36.5	-6.	2.98	6.6
0.35	0.5	92.8	26.99	-3.7	6.64	5.8
0.45	0.44	80.2	17.95	-1.66	12.6	4.96
0.55	0.38	60.2	11.18	-1.13	20.8	4.06
0.65	0.33	39.2	6.66	0.94	31.2	3.14
0.75	0.37	29.5	2.92	0.27	44.1	2.43
0.85	0.2	15.2	0.94	0.18	59.	2.04
0.95	0.13	4.4	0.07	0.02	75.1	1.9

Basic Airplane + Winglets

η	Lift DIST. (Lb/In)	Shear (Lb x 10 ³)	EA MOM (In-Lb x 10 ⁶)	EA TOR (In-Lb x 10 ⁶)	EA DEFL (In)	LOCAL α (Deg)
0.05	0.63	183.	57.4	-20.4	0.0	7.63
0.15	0.6	141.9	46.9	-11.38	0.95	7.13
0.25	0.55	113.7	36.9	-5.94	3.	6.58
0.35	0.5	92.7	27.34	-3.6	6.7	5.83
0.45	0.44	80.	18.32	-1.58	12.7	4.96
0.55	0.38	60.	11.57	-1.05	21.	4.05
0.65	0.33	39.	7.07	-0.85	31.6	3.11
0.75	0.37	29.4	3.33	0.38	44.8	2.36
0.85	0.2	15.3	1.35	0.29	60.3	1.91
0.95	0.135	4.4	0.43	0.19	77.5	1.66

Note: EA MOM: Moment along elastic axis
 EA TOR: Torsion along elastic axis
 EA DEFL: Deflection along elastic axis
 LOCAL α : Local Angle of attack of wing with respect to freestream

Table 13.—Wing Loads Deflections

Flight Condition No. 3

G. W. = 297 000 Lb.
 ALT. = Sea Level
 V_e = 248 Kts
 M = 0.375
 n = 2.0 g
 c. g. = 21% MAC

Basic Airplane

η	Lift DIST. (Lb/In)	Shear (Lb x 10 ³)	EA MOM (In-Lb x 10 ⁶)	EA TOR (In-Lb x 10 ⁶)	EA DEFL (In)	LOCAL α (Deg)
0.05	0.51	164.	56.6	-11.01	0.0	15.2
0.15	0.5	131.8	46.23	- 4.15	0.9	14.9
0.25	0.47	111.2	37.	- 0.81	2.84	14.52
0.35	0.43	96.1	28.14	- 0.16	6.4	13.95
0.45	0.4	86.7	19.54	0.35	12.24	13.25
0.55	0.37	68.7	12.68	- 0.17	20.54	12.47
0.65	0.34	47.3	7.71	- 0.54	31.46	11.6
0.75	0.29	35.1	3.58	0.3	45.03	10.84
0.85	0.23	18.7	1.19	0.16	61.11	10.36
0.95	0.16	5.5	0.11	0.002	78.61	10.16

Basic Airplane + Winglets

η	Lift DIST. (Lb/In)	Shear (Lb x 10 ³)	EA MOM (In-Lb x 10 ⁶)	EA TOR (In-Lb x 10 ⁶)	EA DEFL (In)	LOCAL α (Deg)
0.05	0.51	164.	57.2	-11.2	0.0	15.2
0.15	0.5	132.	46.9	- 4.2	0.91	14.9
0.25	0.47	111.6	37.6	- 0.77	2.9	14.5
0.35	0.43	96.4	28.7	- 0.1	6.5	13.97
0.45	0.4	87.1	20.1	0.42	12.4	13.25
0.55	0.37	69.1	13.2	- 0.1	20.9	12.45
0.65	0.34	47.8	8.2	- 0.47	32.1	11.55
0.75	0.29	35.7	4.	0.4	46.1	10.74
0.85	0.23	19.3	1.56	0.26	62.9	10.2
0.95	0.17	5.8	0.4	0.13	81.6	9.9

Note: EA MOM: Moment along elastic axis
 EA TOR: Torsion along elastic axis
 EA DEFL: Deflection along elastic axis
 LOCAL α : Local angle of attack of wing with respect to freestream

Table 14.—Winglet to Wingtip Loading

Load Condition Per reference (1) 	Rear spar up-bending moment (in-lb)	Front spar up-bending moment (in-lb)	Rear spar tension (lb)	Aux. spar compression (lb)	Rear spar down- bending moment (in-lb)	Aux. spar down- bending moment (in-lb)	Rear spar compression (lb)	Aux. spar tension (lb)
No. 1 Sym. Flight Condition (same loading on each wing)	185 200	370 400	4799	18 274	-	-	-	-
No. 2 Sym. Flight Condition (same loading on each wing)	232 800	465 600	6380	22 339	-	-	-	-
No. 3 Overyaw Condition (one wing)	244 800	489 600	6675	23 506	-	-	-	-
No. 3A Overyaw Condition (other wing) 	-	-	-	-	38 400	76 800	1227	3428
No. 4 Overyaw Condition (one wing) 	254 000	508 000	7232	23 837	-	-	-	-
No. 4A Overyaw Condition (other wing)	73 200	146 400	2197	6 652	-	-	-	-
No. 5 Gust Condition (one wing)	161 200	322 400	4325	15 612	-	-	-	-
No. 5A Gust Condition (other wing)	-	-	-	-	26 000	52 000	706	2407
No. 6 Gust Condition (one wing)	236 800	473 600	6792	22 134	-	-	-	-
No. 6A Gust Condition (other wing)	90 400	180 800	2636	8 354	-	-	-	-

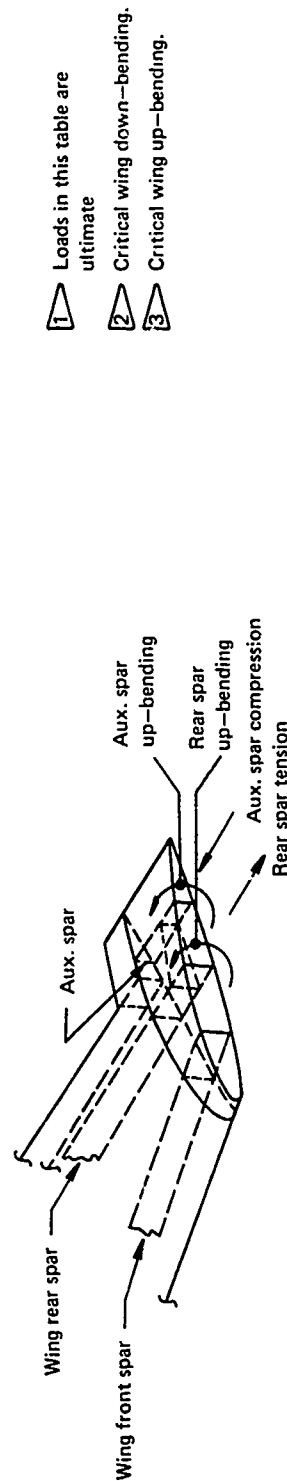


Table 15.— Model Constrained Reactions @ W.S. 948.744

Wing Up-Bending

Wing Down-Bending

Respective axis
reactions (lb)

Respective axis
reactions (lb)

NODE	x	y	z	x	y	z
8	-3392	60 221	-4348	502	-8808	-659
9	837	32 863	4361	-181	-5141	-659
108	3131	-17 970	-4361	-491	2999	659
109	-7854	-60 189	4348	1135	8971	-659

Table 16.— Model Nodal Deflections

NODE	Wing Up-Bending			Wing Down-Bending		
	Respective axis deflection (in.)					
	x	y	z	x	y	z
1	0.346	-0.314	-0.940	-0.050	0.045	0.143
2	0.156	-0.225	-0.878	-0.022	0.033	0.133
3	0.045	-0.079	-0.532	-0.006	0.012	0.081
4	0.139	-0.235	-0.225	-0.020	0.033	0.035
5	0.095	-0.135	-0.332	-0.014	0.020	0.051
6	0.044	-0.118	-0.060	-0.006	0.017	0.009
7	0.001	-0.044	-0.165	0	0.007	0.025
8	0	0	0	0	0	0
9	0	0	0	0	0	0
101	0.090	-0.038	-0.939	-0.011	0.003	0.143
102	0.045	0.144	-0.379	-0.005	-0.023	0.133
103	0.013	0.129	-0.532	-0.002	-0.019	0.081
104	0.041	-0.100	-0.225	-0.005	0.013	0.035
105	-0.001	0.061	-0.334	0.001	-0.010	0.051
106	-0.028	0.047	-0.060	0.004	-0.008	0.009
107	0.029	0.087	-0.165	-0.004	-0.013	0.025
108	0	0	0	0	0	0
109	0	0	0	0	0	0
301	0.004	-0.205	0.369	-0.001	0.029	-0.056
302	-0.070	-0.128	0.369	0.011	0.017	-0.056

Table 17.-- Model Chord Loads and Stresses

Element	Wing Up--Bending		Wing Down--Bending		Element	Wing Up--Bending		Wing Down--Bending	
	Chord load	Chord stress	Chord load	Chord stress		Chord load	Chord stress	Chord load	Chord stress
	+(ten) -(comp)	+(ten) -(comp)	+(ten) -(comp)	+(ten) -(comp)		+(ten) -(comp)	+(ten) -(comp)	+(ten) -(comp)	+(ten) -(comp)
	(Lb)	(PSI)	(Lb)	(PSI)		(Lb)	(PSI)	(Lb)	(PSI)
20	-101 959	-49 256	15 311	7 397	123	-9 042	-13 297	1354	1991
21	- 39 120	-55 099	5 814	8 189	124	5 436	7 153	- 759	- 998
22	32 711	43 041	- 4 864	-6 400	125	15 234	17 653	-2361	-1651
23	1 222	1 797	193	- 284	126	19 978	27 747	-2990	-4153
24	8 687	11 430	- 1 236	- 1 627	127	-6 401	-15 612	970	2365
25	- 14 099	- 9 859	2 107	1 474	128	22 625	41 897	-3695	-6843
26	- 13 818	-19 191	2 120	2 944	129	55 564	80 528	-8278	-11997
27	4 775	11 646	- 725	-1 768	130	0	0	0	0
28	- 64 346	-105 485	9 439	15 474	310	-15 984	-11 100	2374	1649
29	- 28 299	-37 732	4 446	5 929	311	1 032	2 517	- 171	- 417
30	0	0	0	0	312	21 205	10 244	-3231	-1561
31	1 958	1 088	- 293	- 163	313	-9 678	-23 606	1449	3533
32	13	15	- 2	- 2	314	32	47	- 5	- 7
33	- 1 086	- 835	153	118					
34	- 1 142	- 1 586	165	229					
35	14	23	- 2	- 3					
36	1 032	688	- 142	- 95					
37	41	27	- 6	- 4					
38	0	0	0	0					
39	0	0	0	0					
120	80 801	39 035	-12 276	-5 930					
121	37 526	52 852	- 5 801	-8 171					
122	- 10 515	-13 836	1 657	2 181					

Table 18.— Model Panel Maximum Shear Stresses and Shear Flow

Element	Wing Up-Bending		Wing Down-Bending	
	Max. shear stress	Max. shear flow	Max. shear stress	Max. shear flow
	(PSI)	(Lb/In)	(PSI)	(Lb/In)
50	5886	918	879	137
51	2993	464	473	73
52	4750	323	700	48
53	8330	3748	1264	569
54	12399	1934	1890	295
55	4848	756	742	116
56	35921	5604	5442	849
58	8018	1251	1211	189
59	5374	838	212	127
60	6627	331	957	48
61	538	27	77	4
62	16004	1024	2423	155
63	0	0	0	0
64	18721	1198	2833	181
150	1367	213	223	35
151	6843	1060	1017	157
152	3448	221	546	35
320	9034	1807	1365	273
321	35180	1794	5316	271
70	10854	(1)	1598	(1)
170	9998	(1)	1527	(1)
330	8023	(1)	1186	(1)
331	8068	(1)	1175	(1)
332	8524	(1)	1279	(1)
333	16392	(1)	2400	(1)

Note: (1) Shear flow is not computed for the triangular membranes

Table 19.—Weight Summary

Airplane "Delta" Weight:		Weight ~ Lb.
Ex	2992 wingtip instl. "0" degree incidence	92
Ex	2993 wing modification	+ 204
Ex	2994 fin assembly	<u>296</u>
Total airplane "delta" weight		<u>+ 592</u>

Airplane "Kit" Weight:		
Ex	2992 wing tip instl 0, +2, -2 degrees incidence	167
Ex	2993 wing modification	364
Ex	2994 fin assembly	<u>296</u>
Total airplane "kit" weight		<u>827</u>

Table 20.—Weights Breakdown of Production Winglet Modification

<u>Item</u>	<u>Qty</u>	<u>Weight ~ Lb.</u>
Ex 2991 winglet delta weight per airplane	—	+ 591.866
Ex 2991 winglet delta weight per side	1	295.933
Ex 2992 wing—fin inst'l (0° incidence)	1	+ 46.155
Dorsal ass'y	1	6.502
Fin—wing—root fillet ass'y	1	3.269
Wing tip cap ass'y	1	25.261
Fin ass'y attach bolts	8	3.321
Incidence blocks	2	7.802
Ex 2993 wing modification delta wt.	1	+ 101.953
Additions:	—	+ 181.983
Front spar ass'y (w.s. 960 --- → w.b.l. 780)	1	6.828
Rear spar ass'y (w.s. 960 --- → w.b.l. 780)	1	17.514
Auxiliary spar ass'y (w.s. 960 --- → w.b.l. 780)	1	29.319
Rib ass'y (w.b.l. 785.6)	1	7.492
Rib ass'y (w.b.l. 780.0)	1	19.969
Rib ass'y (w.s. 960.0)	1	24.407
Trailing edge ass'y	1	13.730
Leading edge ass'y	1	1.267
Interspar skin ass'y	1	50.506
Fuel vent scoop panel ass'y	1	9.226
Access door ass'y	1	1.725
Deletions	—	— 80.030
5-73119-1 Wing tip inst'l	1	— 60.320
5-89854-1 Wing rib inst'l (w.s. 960)	1	— 19.710
Salvaged items:	—	---
50-3389-1 Transmitter inst'l (Type C-2 compass)	1	---
50-2670 Plenum ass'y		
50-2669-1 Duct ass'y	Vent ass'y	1
87955-2-24 Light ass'y		
63-1504 Grommet	Navigation	1
90-4074-1 Inst'l parts	light ass'y	1
Ex 2994 wing fin ass'y	1	147.825
Leading edge ass'y	1	37.391
Trailing edge ass'y	1	37.886
Fin tip ass'y	1	4.279
Torque box ass'y	1	68.269

Table 21.—Weights Breakdown of Prototype Winglet Modification

<u>Item</u>	<u>Qty</u>	<u>Weight ~ Lb.</u>
"Kit" weight per airplane	—	826.652
"Kit" weight per side	—	413.326
Ex 2992 wing fin inst'l (Winglet)	—	46.155
Aluminum sheet	—	4.382
Aluminum extrusion/machined alum.	—	9.669
Steel bolts	—	3.321
Fiberglass	—	24.078
Attach hardware	—	4.276
Misc. (aero smoother)	—	0.429
Ex 2992 wing fin inst'l additional parts	—	37.363
Additional parts include those required when the incidence angle is changed (fairings, incidence blocks, attach bolts)		
Aluminum extrusion/machined alum	—	15.605
Fiberglass	—	13.571
Steel bolts	—	6.641
Attach hardware	—	1.546
Ex 2993 wing modification	—	181.983
Aluminum sheet	—	93.527
Aluminum extrusion/machined alum.	—	75.214
Magnesium sheet	—	1.230
Steel	—	3.904
Attach hardware	—	5.450
Aluminum honeycome core	—	0.280
Fiberglass	—	0.330
Misc.	—	2.048
Ex 2994 wing fin	—	147.825
Aluminum sheet	—	18.699
Aluminum extrusion/machined alum.	—	65.083
Fiberglass	—	52.443
Attach hardware	—	11.356
Misc.	—	0.244

Table 22.— Fuel Condition

Tank	% Full	Weight (Lb)
Forward body	49.50	18 661.0
Aft body	77.15	31 982.0
Upper deck	1.41	200.0
Center wing	69.45	33 000.0
Inboard mains	91.33	27 166.0
Outboard mains	90.77	24 398.0
Outboard reserves	99.77	5 642.0
Total Fuel 141 049.0 Lb		
Gr Wt = O.W. E. + Fuel = 245 351 Lb		

Table 23.— Analysis Configurations

Conf No	Alt (KFT)	Symm	Asymm	Winglet Wt (Lb)	Winglet CG	Winglet Freq (CPS)
1	29.0/21.5	X		0.0	—	—
2			X	0.0	—	—
3		X		141.3	NOM	RIGID
4				141.3	NOM	RIGID
5		X		200.0	NOM	RIGID
6		X		300.0	NOM	RIGID
7				200.0	NOM	RIGID
8				300.0	NOM	RIGID
9		X		141.3	15 in. FWD	RIGID
10		X		141.3	15 in. AFT	RIGID
11			X	141.3	15 in. FWD	RIGID
12			X	141.3	15 in. AFT	RIGID
13	21.5	X		141.3	NOM	5.0
14	21.5	X		141.3	NOM	10.0
15	21.5		X	141.3	NOM	5.0
16	21.5		X	141.3	NOM	10.0

Table 24.—Weight Comparison of Three (3) Winglet Design Concepts

Components	Design concept		
	Aluminum baseline	Advanced metallic	Advanced composite
Covers Lb.	81	39	46
Spar assembly and terminal fittings lb.	45	42	44
Rib assembly or h/c core lb.	17	23	18
Total weight lb.	143	104	108

Table 25.—Relative Cost of Winglet Design Concepts

Program	Design concepts		
	Aluminum baseline	Advanced metallic	Advanced composite
Prototype	1.00	0.60	0.40
Production	1.00	0.73	0.82

Table 26.—KC-135A Performance Improvement for Installing Winglets

MAXIMUM RANGE CRUISE FLIGHT CONDITION

	$W/\delta \times 10^{-6}$ Lb	Mach	L/D^*	ML/D^*	TSFC [*] / θ LB/Hr-Lb	RF ^{**} NM
KC-135A (Basic)	910 000	0.77	17.8	13.7	1.050	8065
KC-135A with winglets	965 000	0.774	19.2	14.9	1.054	8720
Percent change relative to KC-135A			+ 7.8%	+ 8.4%	-0.3%	+ 8.1%

* Based on a gross weight of 210 000 lb.

** Avg range factor over the complete gross weight range (max weight to OEW)

99% max range + climbing cruise correction + 5% service tolerance on fuel

flow + bleed and power extraction

Table 27.—Summary of Equal Area Tip Extension
Geometry Variations

Length, ℓ	$\frac{\ell}{b/2}$	L.E.	λ
45.6 in.	0.058	37°	0.889
64.6 in.	0.083	58.8°	0.246
80.7 in.	0.103	51.5°	0.328
106.0 in.	0.135	42.7°	0.333

Table 28.— Summary of Tip Extension to Winglet Performance Comparisons

Case	Condition	$\frac{\Delta C_{Di} \text{ winglet}}{\Delta C_{Di} \text{ Tip Ext.}}$	$\frac{\Delta C_{mx} \text{ Tip Ext.}}{\Delta C_{mx} \text{ winglet}}$	$\frac{\Delta C_{m.25} \text{ Tip Ext.}}{\Delta C_{m.25} \text{ winglets}}$
1	Constant induced drag improvement, $C_{Di} = -14\%$	1.0	1.31	1.80
2	Constant increase in wing-root bending moment, $C_{mx} = +4.2\%$	1.23	1.0	1.36

APPENDIX A

COMPUTER PROGRAMS USED FOR ANALYSIS AND DESIGN OF WINGLETS

Four computer programs, TEA-372, TEA-242, TEA-230, and TEA-200 were used for the analysis and design of wing/winglet configurations in three-dimensional flow. The KC-135 and C-141 study, the entire parameter study, and the final winglet design were completed with TEA-372. A separate side study was made with TEA-230 to help understand the effects of winglet cant and lower surface winglets on interference. TEA-242 used the spanload from TEA-230 and calculated the induced drag. The chordwise pressure distributions from TEA-230 were used in TEA-200 to calculate the boundary-layer growth and profile drag. TEA-372 is an incompressible, potential flow program in which each lifting surface (wing and winglet) is represented by a multihorseshoe vortex lattice. This lattice is generally placed along the camber line, and there is no simulation of the thickness. A typical lattice for a wing/winglet configuration is shown in figure A.1. The dashed outline shows the wing/winglet planforms. The strengths of individual vortex elements are determined by satisfying tangency boundary conditions at specific points on the camber surface. These boundary point locations are shown as small signs in figure A.1. Note also that the presence of the fuselage was not simulated. Instead, the wing camber surface was simply extended inboard to the plane of symmetry. Lift, induced drag, and moments for the configuration are obtained by a vector summation of the net force (and force x moment arm) acting on each vortex element.

This program can be used as both an analysis and a design tool. In the design mode, part of the configuration can be held in a fixed position while other parts are allowed to move about some nominal position. The program determines the locations of the movable parts which will give minimum induced drag for the total configuration. In other words, it is an induced drag optimizer.

The optimization capability is especially applicable to the wing/winglet problem. The existing wing geometry must obviously be maintained, but freedom exists to twist and camber the winglet as required to minimize drag. Two types of winglet design (optimization) runs were made during the course of this contract. In the first type, only the section twist was allowed to vary across the winglet to find the point of minimum C_{D_i} . In the second type, both the twist and camber of the winglet sections were allowed to vary. These two design runs give the same minimum C_{D_i} , since C_{D_i} is a function of the spanwise loading and not the manner in which that load is distributed over the chord at a given spanwise station.

The first type of design run was made in cases where the camber line shape was not of any particular interest. The only item of interest was minimum C_{D_i} and the program would apply whatever twist was necessary to the input sections to obtain the span load distribution for minimum induced drag. This type of run was made throughout the parameter study.

The second type of design run was made in cases where not only was minimum C_{D_i} of

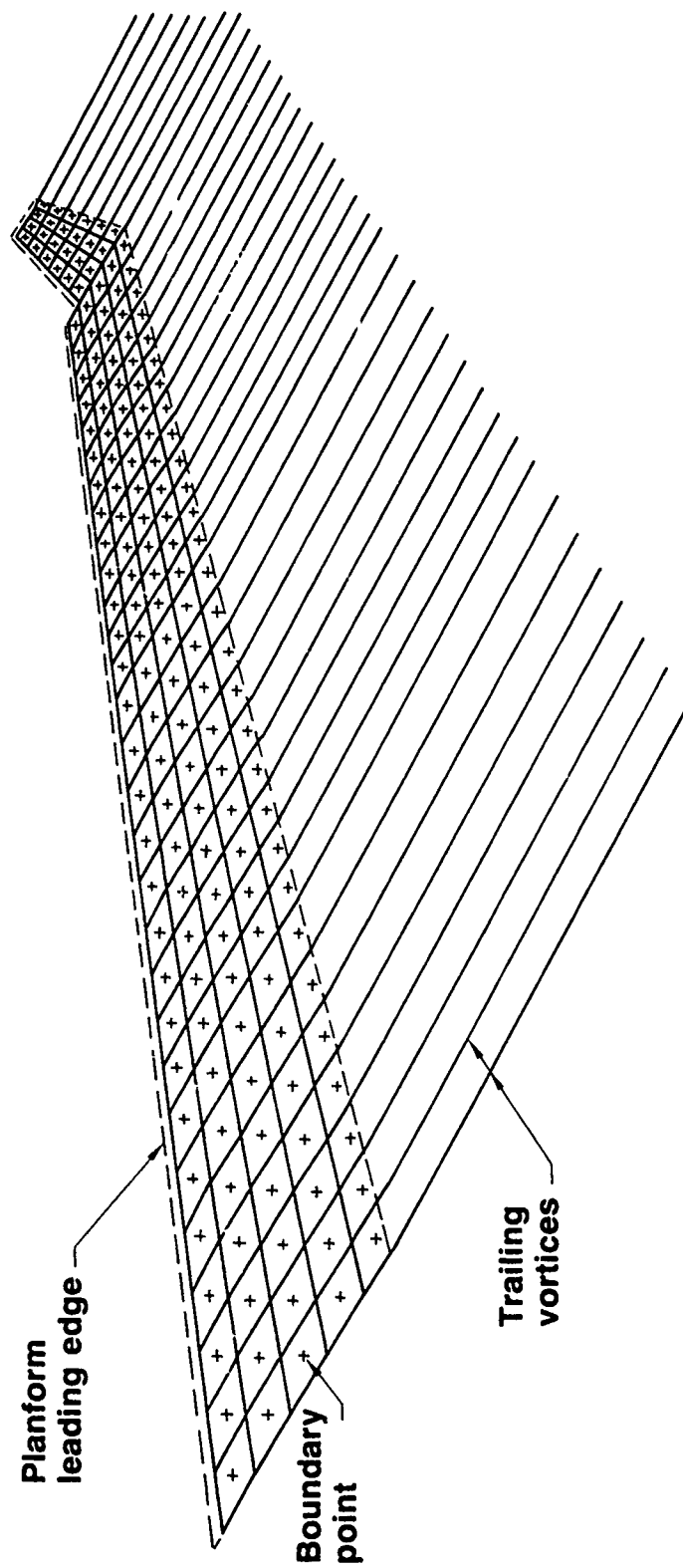


Figure A-1.— Typical Representation of Wing and Winglet in TEA-372 by a Multihorseshoe Vortex Lattice

interest, but also a specific chordwise loading was desired for good performance in supercritical flow. This type of run was made to design the final winglet once the desired planform and cant angle had been chosen.

The input camber line definition for the winglet is of importance when making an analysis run. In this type of run, all of the input geometry is fixed, and no attempt can be made to optimize C_{D_i} . Throughout the discussions in this report, an "analysis" run means one in which all geometry is fixed. A "design" run means one in which the winglet is allowed to move about some nominal position in order to find the point of minimum C_{D_i} .

The vortex-lattice method of calculating induced drag tends to give answers which are somewhat low (3%) for most near-planar configurations. Induced drag curves plotted later in the report are based on values directly from TEA-372. Even though their absolute magnitudes may be low, increments obtained from these curves should be fairly accurate.

Force and moment coefficients presented from TEA-372 include lift (C_L), induced drag (C_{D_i}), pitching moment ($C_{m_{zsc}}$), and rolling moment for half of the configuration (C_{m_x}). The latter two coefficients are both nondimensionalized by wing reference area and mean aerodynamic chord. C_{m_x} is considered in this report as indicative of wing-root bending moment.

TEA-230 is a subsonic potential flow program which can analyze arbitrary configurations with thickness. Source panel and vortex lattices are distributed over the configuration to simulate thickness and lifting effects, respectively. Singularity strengths are determined by solving a set of linear algebraic equations which express exact tangency boundary conditions. Force and moment calculations are made only on source panel singularity surfaces. They are based on the integration of pressures where the pressure is assumed constant over a given panel.

The computer program TEA-242 is an induced drag program which is used to design and analyze span loadings. The theoretical development of the program uses the concept of the Trefftz plane and a distribution of singularities to model the flow. TEA-242 features a general, non-planar geometry capability, an optimization option for computing the load distribution for minimum induced drag, and an analysis option to calculate the induced drag produced by arbitrary span loads. For the optimization option, the lift force, bending moment and pitching moment can be constrained to specific values and the program will calculate the optimum span load for the minimum induced drag. For the analysis option, the program calculates the lift coefficient, wing bending moment, induced drag efficiency factor, and the induced drag.

TEA-200 is a computer program which calculates the two-dimensional boundary-layer growth on a surface with a known pressure distribution. This program uses Curles method to calculate the laminar boundary-layer growth. The transition analysis uses a

combination of Schlichting-Ulrich and Granville methods and the turbulent boundary-layer is calculated by the Nash-Hicks method. The momentum thickness, displacement thickness, shape factor, local skin friction, and profile drag are calculated for specified pressure distributions.

APPENDIX B

MATERIAL COSTS

Material	Cost
Fiberglass cloth	\$ 2.66/yd.
Graphite Epoxy Tape	97.46/lb.
0.020 x 2024-T3 clad	1.05/lb
0.040 x 2024-T3 clad	.60/lb
0.020 x 2024-0 bare	1.11/lb
0.025 x 7075-T6 bare	0.94/lb.
0.5 x 7075-T6 bare	.88/lb.
3 x 4 in. 7075-T61.	1.44/lb.
6 x 8 in. & 6 x 5 in.	1.31/lb.
Extruded "H" Section 7075-T6	1.25/lb.
Alum. Honeycomb 3.1 lb.	10.09/ft. ²
Alum. Honeycomb 8.1 lb.	47.55/ft. ²
Nomex Honeycomb	30.00/ft. ²
Titanium 6Al-4V 1/4 in. thick	35.13/ft. ²
Titanium 6Al-4V 1.5 in. thick	88.44/ft. ²
Adhesive (0.03 psf)	21.35/lb.
Adhesive (0.06 psf)	12.95/lb.
Adhesive (0.08 psf)	11.31/lb.

REFERENCES

1. Butler T. G. and Michel, D., "NASTRAN- A Summary of the Functions and Capabilities of the NASA Structural Analysis Computer System", NASA SP-260, 1971.
2. *Wing Stress Unit*, "Wing Stress Analysis, KC-135," Boeing Document D-16810, Nov. 9. 1956.
3. *Stress Unit*, "Vertical Tail Stress Analysis, C-135A and C-135B", Boeing Document D6-7564, March 1962.
4. Munk, M. M., "The Minimum Induced Drag of Aerofoils", NACA Report 121, 1921.
5. Dodson, R., "Design and Analysis of Winglets for Military Aircraft-Preliminary Program Plan for Winglet Flight Demonstration on the KC-135A Tanker Aircraft", Boeing Document D3-9936-1, Nov. 14, 1975.